PB83-114546

Proceedings of the Seminar on the Impact of GATE on Large-Scale Numerical Modeling of the Atmosphere and Ocean Held at Woods Hole, Massachusetts, August 20-29, 1979

(U.S.) National Research Council
Washington, DC

Prepared for

National Science Foundation
Washington, DC

Jun 80

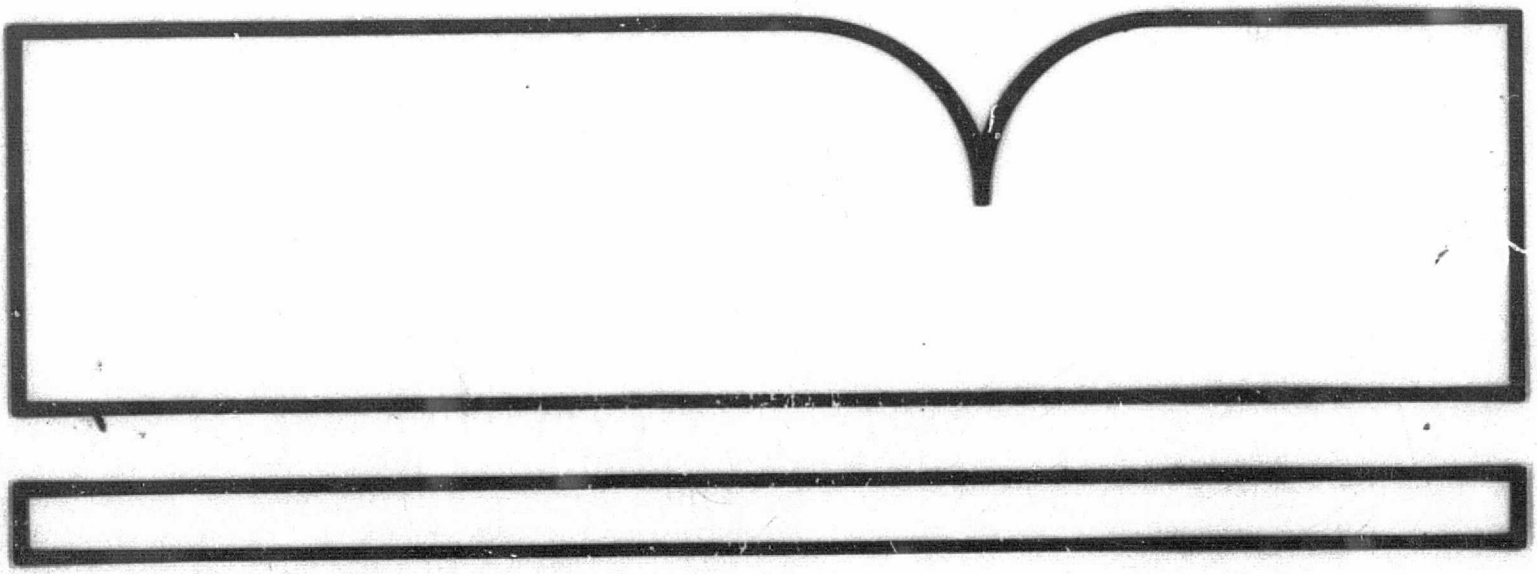

Proceedings of the Seminar on The Impact of GATE on Large-Scale Numerical Modeling of the Atmosphere and Ocean

Woods Hole, Massachusetts
August 20–29, 1979

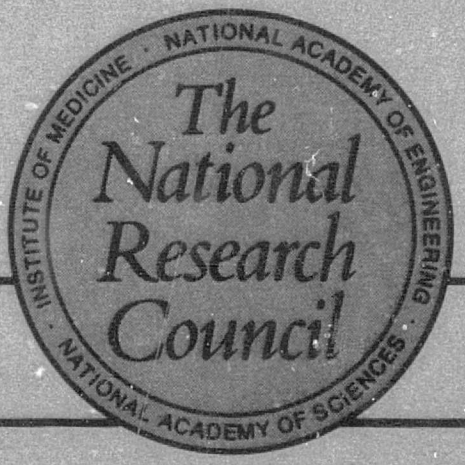

GATE Panel

U.S. Committee for the Global Atmospheric Research Program

Assembly of Mathematical and Physical Sciences

50272-101

REPORT DOCUMENTATION PAGE	1. REPORT NO.	2.	3. Recipient's Accession No. PB83 114546

4. Title and Subtitle
Proceedings of the Seminar on the Impact of GATE on Large-Scale Numerical Modeling of the Atmosphere and Ocean

5. Report Date
June 1980

6.

7. Author(s)
GATE Panel

8. Performing Organization Rept. No.

9. Performing Organization Name and Address
National Research Council
U.S. Committee for the Global Atmospheric Research Program
2101 Constitution Avenue NW
Washington, D.C. 20418

10. Project/Task/Work Unit No.

11. Contract(C) or Grant(G) No.
(C) NSF-C310 T.O.No.197
(G)

12. Sponsoring Organization Name and Address
National Aeronautics and Space Administration, National Oceanic and Atmospheric Administration, and National Science Foundation

13. Type of Report & Period Covered
Final

14.

15. Supplementary Notes
Proceedings of a seminar held at Woods Hole, Massachusetts, August 20-29, 1979

16. Abstract (Limit: 200 words)

The document records the proceedings of a seminar that dealt with the impact on large-scale numerical atmospheric and oceanic modeling by the GARP Atlantic Tropical Experiment, which took place in the summer of 1974. The seminar brought together data analysts, theoreticians and numerical modelers doing research using the GATE data. The sessions included topics of large-scale tropical circulations, air-sea interaction, diagnostic studies of cumulus convection and related topics, theoretical concepts of tropical circulation, parameterization studies, and large-scale model studies. The report contains abstracts of the presentations given at the seminar and presents some 20 principal findings.

17. Document Analysis a. Descriptors
atmospheric sciences, tropical meteorology, tropical oceanography, numerical modeling, air-sea interaction, tropical circulation, parameterization

b. Identifiers/Open-Ended Terms
GATE, FGGE, GARP

c. COSATI Field/Group

18. Availability Statement: This report has been approved for public sale; its distribution is unlimited	19. Security Class (This Report) Unclassified	21. No. of Pages 276
	20. Security Class (This Page) Unclassified	22. Price

(See ANSI-Z39.18) See Instructions on Reverse OPTIONAL FORM 272 (4-77) (Formerly N7IS-35) Department of Commer

Proceedings of the Seminar on The Impact of GATE on Large-Scale Numerical Modeling of the Atmosphere and Ocean

Woods Hole, Massachusetts
August 20–29, 1979

GATE Panel
U.S. Committee for the Global Atmospheric Research Program
Assembly of Mathematical and Physical Sciences
National Research Council

NATIONAL ACADEMY OF SCIENCES
Washington, D.C. 1980

NOTICE: The project that is the subject of this report was approved by the Governing Board of the National Research Council, whose members are drawn from the Councils of the National Academy of Sciences, the National Academy of Engineering, and the Institute of Medicine. The members of the Committee responsible for this report were chosen for their special competences and with regard for appropriate balance.

This report has been reviewed by a group other than the authors according to procedures approved by a Report Review Committee consisting of members of the National Academy of Sciences, the National Academy of Engineering, and the Institute of Medicine.

The material reported by the following authors was based wholly, or in part, on work supported by the Division of Atmospheric Sciences, National Science Foundation, under the indicated grants:

J. Charney, ATM-7620070.A01
S. Cox, ATM-7805743.A01
S. Esbensen, ATM-7818805*
W. Frank, ATM-7910606*
M. Garstang, ATM-7421701.A05*
W. Gray, ATM-7801640.A01*
R. Houze, ATM-7816359.A01*
R. Johnson, ATM-7811633.A01
Y. Ogura, ATM-7811642.A01*
K. Ooyama, National Center for Atmospheric Research†
D. Randall, ATM-7910844
R. Reed, ATM-7906105
D. Rodenhuis, ATM-7601201.A02*
S. Soong, ATM-7811642.A01*
D. Stevens, ATM-7826764*
C. Warner, ATM-7421701.A05*
E. Zipser, National Center for Atmospheric Research†

*These grants were jointly funded by the National Science Foundation and the U.S. GATE Project Office, National Oceanic and Atmospheric Administration.

†The National Center for Atmospheric Research is sponsored by the National Science Foundation.

The U.S. Committee for the Global Atmospheric Research Program and its GATE Panel sponsored this seminar through the support provided by the National Science Foundation, the National Oceanic and Atmospheric Administration, and the National Aeronautics and Space Administration under NSF Contract C130, Task Order 197. Any opinions, findings, and conclusions or recommendations expressed in this publication are those of the author(s) and do not necessarily reflect the views of the National Science Foundation, the National Oceanic and Atmospheric Administration, or the National Aeronautics and Space Administration.

Available from
U.S. Committee for the Global
Atmospheric Research Program
2101 Constitution Avenue
Washington, D.C. 20418

U.S. Committee for the Global Atmospheric Research Program

Verner E. Suomi, University of Wisconsin, *Chairman*
Francis P. Bretherton, National Center for Atmospheric Research, *Vice Chairman*
Richard A. Anthes, Pennsylvania State University
D. James Baker, Jr., University of Washington
T. N. Krishnamurti, Florida State University
John B. Kutzbach, University of Wisconsin
Richard S. Lindzen, Harvard University
Syukuro Manabe, National Oceanic and Atmospheric Administration
Norman A. Phillips, National Oceanic and Atmospheric Administration
Richard J. Reed, University of Washington
Peter B. Rhines, Woods Hole Oceanographic Institution
John M. Wallace, University of Washington

John S. Perry, National Research Council, *Executive Scientist*
Thomas H. R. O'Neill, National Research Council, *Executive Secretary*
Fred D. White, National Research Council, *Consultant*

LIAISON WITH FEDERAL AGENCIES

Eugene W. Bierly, National Science Foundation
Rex Fleming, National Oceanic and Atmospheric Administration
Elbert Friday, Department of Defense
Robert A. Schiffer, National Aeronautics and Space Administration

GARP Atlantic Tropical Experiment (GATE) Panel

Richard J. Reed, University of Washington, *Chairman*
Robert Burpee, National Oceanic and Atmospheric Administration
Stephen K. Cox, Colorado State University
Joshua Z. Holland, National Oceanic and Atmospheric Administration
George Philander, Princeton University
Wayne Schubert, Colorado State University
Joanne Simpson, National Aeronautics and Space Administration

Organizing Committee for the Seminar on the Impact of GATE on Large-Scale Numerical Modeling of the Atmosphere and Ocean

Richard J. Reed, University of Washington, *Chairman*
Bruce Albrecht, Pennsylvania State University
Richard A. Anthes, Pennsylvania State University
Robert Burpee, National Oceanic and Atmospheric Administration
George Philander, National Oceanic and Atmospheric Administration
Wayne Schubert, Colorado State University
Joanne Simpson, National Aeronautics and Space Administration

Foreword

The tropics cover half of the earth and what have been called the equatorial tropics about half of that region. Most of this quarter of the earth (71 percent) is ocean, and the land is mainly tropical jungle. Thus, although this region can be considered as the boiler of the giant atmospheric heat engine, "it has been recognized for some time that the meteorology of the tropical oceans constitutes one of the weakest links in our understanding of the general circulation of the atmosphere and, therefore, in our ability to model weather and climate. Routine synoptic data have never been adequate to define the mesoscale motions, and what detailed knowledge exists has been gained from special observational experiment."*

Satellite views of this region, especially those from geostationary altitude, show that much of the disturbed weather occurs in "cloud clusters" --the name given to the regions of organized deep convection that dominate the heat release in this region. These cloud clusters are very large in terms of individual convective cells but are small on the scale of the entire globe. Their dimensions are much smaller than the grid spacing of a typical numerical model used to simulate the general circulation (general circulation model or GCM) and thus the important contribution of these subgrid scale motions must be "parameterized" to be included realistically. Also, tests with these GCM's show that the behavior of the tropics has a profound influence on the weather at higher latitudes since a significant amount of the energy is transmitted from the equatorial region to higher latitudes.

The main purpose of the GARP Atlantic Tropical Experiment is to better understand the mechanism or mechanisms by which deep cumulus convection is organized by the synoptic or large-scale motions and how the resulting convective activity affects the synoptic motions that can be treated in the models. If we were to learn that synoptic-scale motions are unimportant in the organization of convective activity in the equatorial tropics, the task of extended weather prediction would be considerably more difficult and its cost significantly higher.

The data-collection stage of this massive international experiment was completed five years ago. Since that time scientists have completed much

*U.S. Committee for GARP, 1971: *Plan for U.S. Participation in the GARP Atlantic Tropical Experiment*.

of their analysis. The report of this workshop is the initial attempt at a synthesis of a physical understanding, but it is only the beginning. This synthesis must now be further validated not only with other data collected during GATE but also with data from other parts of the earth as well. This will soon be possible with the excellent data collected during the Global Weather Experiment in which a major effort was made to observe the entire earth, with special emphasis on the tropics.

Five years is a very short time from the beginning of the field experiment to the synthesis of results. This rapid progress was achieved because of careful planning, high-quality observations, excellent data management, and dedicated efforts by the scientists. The first results reported here are not yet definitive but do show clearly the potential of GATE.

On behalf of the U.S. Committee for the Global Atmospheric Research Program, I wish to express our gratitude to Richard J. Reed, Chairman of the GATE Panel, and to all those who continue to add to GATE's successes.

Verner E. Suomi, *Chairman*
U.S. Committee for the Global
Atmospheric Research Program

Preface

This document reports the proceedings of a seminar held at the National Academy of Sciences Summer Study Center, Woods Hole, Massachusetts, August 20-29, 1979. The seminar was arranged by the GATE Panel of the U.S. Committee for the Global Atmospheric Research Program for the purpose of evaluating the impact of GATE on large-scale modeling of the atmosphere and ocean. An earlier workshop assessing the progress of GATE research, sponsored by the GATE Panel, was held at the National Center for Atmospheric Research (NCAR) in Boulder, Colorado, during the summer of 1977. At that time, much of the data analysis was in a preliminary stage, and the focus was necessarily on descriptive aspects of the research. Although some results of numerical modeling experiments were presented at the workshop, it was still too early to evaluate the significance of the observational findings for the development of improved large-scale models of the atmosphere and ocean. It remained for this later meeting to attempt a first evaluation.

In order to make a proper assessment, the organizers felt that it was desirable to bring together data analysts, theoreticians, and numerical modelers in a setting that would be conducive to an effective exchange of information and ideas. Thus it was decided to hold a seminar in which invited speakers were given assigned topics and in which equal time was allotted to presentation and discussion of results. Also, it was decided to restrict the number of participants to the size that could be accommodated in a typical seminar room. Regrettably, this decision precluded the direct participation of many workers who have made substantial contributions to GATE research. These workers should know that their contributions did not go unrecognized in the seminar. It is hoped that the extended summaries of the papers presented at the seminar and the report following each paper concerning the main items of discussion will allow those who could not attend to be adequately informed of the outcome.

The GATE Panel wishes to express its thanks to all those who contributed to the success of the seminar: to the organizers for their efforts in arranging the sessions and preparing the summary; to the rapporteurs for recording the highlights of the discussions; to John S. Perry and Thomas H. R. O'Neill of the GARP Committee staff for their valuable help in the planning, implementation, and documentation of the meeting; and to Doris Bouadjemi and Theresa Fisher of the GARP Committee staff for their untiring secretarial assistance during the course of the seminar.

Dr. O'Neill's contributions to the organization of the meeting were much in evidence despite the illness that prevented him from being present.

Richard J. Reed, *Chairman*
GATE Panel

Contents

1. Introduction

The GARP Atlantic Tropical Experiment (GATE) took place in the summer of 1974. A series of articles in the *Bulletin of the American Meteorological Society* (Vol. 55, No. 7, July 1974, pp. 711-744) gives details about the participants and the observing programs.

The central objectives of GATE were

1. To provide a means of estimating the effects of smaller tropical weather systems on the large-scale (synoptic-scale) circulation;
2. To facilitate the development of numerical modeling and prediction methods.

To refresh the memory of the reader of this report, the following three facts should be kept in mind:

1. The GATE field phase was divided into three phases of about three weeks each.
2. The GATE scientific program was divided into five subprograms held together by the "Central Program." They were the Synoptic-Scale subprogram; the Convection subprogram; the Radiation subprogram; the Oceanographic subprogram; and the Boundary-Layer subprogram. A *Report of U.S. Central Program Workshop*, held July 25-August 12, 1977, is available from the National Center for Atmospheric Research.
3. Four scales were defined for GATE, namely,
   The A scale (10^3 to 10^4 km) = the synoptic scale;
   The B scale (10^2 to 10^3 km) = the cloud-cluster scale;
   The C scale (10 to 10^2 km) = the mesoscale;
   The D scale (1 to 10 km) = the cumulus scale.

The observing systems for the experiments were designed to gather data relevant to these scales of phenomena. For example, the A-scale array consisted of a network of ships in the Atlantic and land stations in Africa, South America, Central America, and the Caribbean that were capable of defining synoptic-scale systems.

The central objective of the GATE was to gather observational data that would be suitable for studying the interaction of convective-scale motions with large or synoptic scales and that would lead eventually to improved models for predicting large-scale atmospheric motions. The Woods Hole

Seminar was convened to evaluate the progress that has been made in advancing this goal. In evaluating progress, it must be kept in mind that the experimental plan did not specify a step-by-step procedure for translating observational findings into superior numerical models within a fixed time frame. Rather, the plan was to gather a unique set of data that, when fully analyzed and digested, would lead to a deeper understanding of tropical weather processes. It was hoped that this understanding would give rise to physical insights that would aid in the development of improved large-scale models. The attainment of such insights cannot be programmed or even promised. They must be obtained from the processes that in general govern the erratic and unpredictable growth of scientific knowledge.

When viewed in this context, the progress made during the five years that have elapsed since the field phase of GATE has been highly gratifying. An unprecedented definition of the large-scale tropical motions and associated fields of cumulus and mesoscale convection has been obtained for a substantial portion of the tropics. The data have stimulated a variety of diagnostic studies that already have contributed to a better understanding of physical processes in the tropical atmosphere. Numerical-modeling efforts have moved forward, testing the ability of present models to predict the large-scale motions and providing soon a gridded GATE data set that should prove of great value in future diagnostic and prognostic studies.

A more detailed account of the accomplishments of the past five years is found in the chapters that follow. Chapters 2 and 3 give the principal findings of the seminar and summaries of the six sessions that were held. Extended summaries of the papers presented in the sessions and main items of discussion appear in Chapters 4 to 9.

2. Principal Findings of the Seminar

Specific, principal conclusions of the seminar follow. These conclusions are listed in the order in which the subjects were discussed during the seminar. The order is not meant to indicate the relative importance of the conclusions.

1. GATE data have refined and reinforced pre-GATE knowledge of easterly waves and, in particular, have provided a much clearer picture of the relation of convective activity and precipitation to the waves. While the structure and characteristics of the waves have been examined in the A/B array for all three phases and for a wider area in Phase III, they still remain to be examined in other areas during Phases I and II.
2. The diurnal variations of vertical motion, deep convection, and precipitation that had been observed in other tropical oceanic regions prior to GATE were also present in the GATE area. These diurnal variations have been examined far more quantitatively than had been possible previously. The cause of the variations is still not understood although radiative forcing has been suggested.
3. Considerable progress has been made in defining the mean state over much of the GATE area; however, a complete definition of the mean state has not been achieved because of the difficulties involved in comparing observations of temperature and humidity measured by different radiosonde systems. Much has been learned about the differences between these systems, but further efforts to account for these differences are needed with the GATE observations. These efforts should be of considerable interest for FGGE.
4. Techniques to estimate rainfall from satellite data have been developed with GATE data. These techniques provide much-needed estimates of rainfall over the oceans where surface observations of rainfall are lacking.
5. Thermal anomalies in the ocean associated with squall lines and cloud clusters over the B-scale area were of insufficient amplitude to have significant feedback effects on these systems.
6. Large-scale seasonal sea-surface-temperature changes are significant throughout the tropics. Because of the importance of advection and low-frequency waves, parameterization of these changes is impossible.
7. Modeling efforts aimed at the seasonal response of the upper ocean will be facilitated by the availability of the GATE data set as a case study. (The data will be displayed in the GATE Oceanographic Atlas.)

8. Radar, aircraft, and satellite data have been used to obtain a unique description of the mesoscale squall and nonsquall systems that occurred during GATE. These mesoscale features have been shown to account for a significant fraction of the precipitation and vertical mass transfer that was associated with the passage of easterly waves. Quantifying the effect that these systems have on the large scale is of utmost importance. B-scale data may be useful in increasing our understanding of the scale interaction problem. In general, however,a more complete theoretical understanding of the dynamics and thermodynamics of these systems is needed.

9. Extensive cloud updraft and downdraft statistics were obtained from aircraft penetrations of convective systems. Mass transport in downdrafts was one half to three fourths that in updrafts.

10. Radar statistics of convective elements have been generated and show a log-normal distribution. The physical explanation for this distribution and its possible implications to parameterization should be further studied.

11. Aircraft and tethered-balloon measurements have greatly increased our understanding of the undisturbed and disturbed boundary layers. The undisturbed structure is similar to the daytime boundary layer over land. Aircraft missions that probed the boundary layer for several hours in undisturbed conditions detected mesoscale features; the importance and origin of these mesoscale features is still unclear. There is a well-defined transformation of the boundary layer from undisturbed to disturbed that is caused by the downdrafts associated with convective systems. A period of several hours was required for the recovery of the boundary layer to an undisturbed state. The interaction of the boundary layer and the mesoscale systems that disturb the boundary layer needs to be further investigated if the mesoscale systems are to be completely understood.

12. Diagnostic budget studies of cumulus convection have been an important tool for increasing our understanding of how convection alters the thermodynamic structure of the large-scale environment. Physically reasonable mass fluxes have been obtained from these diagnostic studies by using more-sophisticated cloud models. The impact that these models might have on prognostic results has not been determined. Further diagnostic studies may be useful in increasing our understanding of how convection alters the large-scale momentum and vorticity fields.

13. The radiative profiles obtained for GATE clearly show the importance of clouds in modulating the radiative budget of the atmosphere. Variations in cloudiness result in horizontal gradients of the radiative divergence. Furthermore, substantial day-night differences between clear and cloud regions were also observed. The role that these radiational differences might have on the dynamics of the tropical atmosphere should be evaluated.

14. From the theoretical standpoint, many of the basic questions of tropical meteorology still remain unanswered. A combination of the insights gained from the analysis of GATE data and creative thought are needed for making further headway.

15. The large-scale controls on the cloud population and precipitation, documented by the analysis of GATE data, encourage efforts to parameterize cumulus convection.

16. The diagnosis and parameterization of convective effects in the heat and moisture budget equations have advanced to a mature state. Pioneering attempts have been undertaken to understand convective effects in the vorticity and momentum equations, and this important problem should attract considerable future interest.

17. Models that simulate the detailed life cycles of whole populations of clouds have begun to appear. Since they allow for large-scale forcing mechanisms to be externally specified, such models are powerful tools in the effort to understand how large-scale processes control a cloud ensemble.

18. Linear models have been useful in studying the growth and structure of easterly waves. These indicate that the waves have their origin in barotropic instability associated with the midtropospheric easterly jet over Africa. Dry models reproduce the low-level structure well. Moist models yield qualitatively correct upper-level structure as well, but the features are too weak. Nonlinear models will be needed to handle better the effects of latent heat release.

19. Analyses utilizing four-dimensional data assimilation for the GATE period are progressing well. These analyses have great potential for future studies of tropical circulations and their interactions with extratropical systems.

20. Limited-area models show considerable skill in predicting easterly waves, but some deficiencies remain. Continued use of the GATE data may prove useful in resolving these deficiencies.

3. Summary of Seminar Sessions

Sessions were held on the following topics: large-scale tropical circulations, air-sea interaction, diagnostic studies of cumulus convection and related topics, theoretical concepts of tropical circulation, parameterization studies, and large-scale modeling studies.

The organizers have prepared the following summaries of the findings that emerged from the papers presented in their respective sessions.

3.1 LARGE-SCALE TROPICAL CIRCULATIONS

Daily and phase mean wind analyses near the surface and in the upper troposphere have been completed for the entire GATE region for all three phases of the experiment, and large-scale analyses of wind, temperature, and moisture have been prepared at mandatory pressure levels throughout the troposphere for Phase III. The mean meridional structure has been defined in western Africa, the eastern Atlantic, and the Caribbean for each phase. In addition, sea-surface temperature analyses have been produced on a daily basis for all the oceanic region, and 6-hourly values of rainfall estimated from infrared satellite images have been prepared for a limited area. A synthesis of all of these analyses indicates that the intertropical convergence zone (ITCZ) is the main contributor on a large scale to upward vertical motion in the subcloud layer since the deep convective clouds and precipitation patterns are oriented in an east-west direction near 10° N. Preliminary results from energy and vorticity budgets based on the radiosonde data averaged for Phase III were presented.

Easterly waves with wavelengths of approximately 2500 km and periods of 3.5 days were the most important synoptic-scale features. During Phase III, when these waves were at a maximum amplitude throughout the troposphere, their structure and energetics were observed over both the eastern Atlantic and western Africa. In both regions, these waves clearly modulate the cloud coverage and the precipitation patterns such that the rainfall observed slightly to the west of the trough is roughly two to three times greater than that measured near the ridge. The waves are generated as a result of barotropic instability of the midtropospheric easterly jet in eastern and central Africa but continue to develop in western Africa largely as a result of latent heat release in deep convective clouds and

in the eastern Atlantic through barotropic processes. On the average, the waves weaken as they propagate across the Atlantic to the west of the A/B array. North of 10° N, the maximum rainfall associated with the waves occurs in a region with relatively low humidity. This implies that some form of cumulus parameterization is needed in order to model the precipitation patterns of these waves properly.

The detailed structure of the waves has been determined for Phase III in the A/B array, where budgets of mass, heat, and moisture for the total tropospheric column are in reasonable agreement. The moisture budget indicates that there is a strong correlation between moisture convergence and precipitation.

Moisture budget studies computed with several different analysis methods for A/B-array data consistently diagnose more rainfall than was estimated by radar in the B array. This imbalance may be the result of difficulties in estimating the large-scale mean moisture advection in the budget studies, or perhaps the surface evaporation or radar rainfall estimates are less accurate than believed. Total tropospheric condensation computed from the moisture budget agrees rather well with net condensation obtained from the dry static energy budget. There is, however, a lag of 4 to 6 hours between the computed condensation and the radar observed precipitation. This lag may be accounted for by storage of liquid water in the atmosphere. On the scale of the A/B array, there is little correlation between net tropospheric temperature change and latent heat release. Apparently, the released latent heat is rapidly dispersed to larger scales.

Diurnal variations of vertical motion and deep convective activity have been clearly shown during all three phases. In both disturbed and suppressed regions of the ITCZ in the A/B array, there is a morning maximum and early evening minimum of vertical motion that appears to be part of the diurnally varying meridional circulation between the ITCZ and the trade-wind stratocumulus and dust region to the north. In addition, diurnal variations of vertical motion with a similar phase are observed on the cloud-cluster scale. These variations of the ITCZ and cloud clusters may possibly be related to day-night differences in tropospheric radiational cooling.

In the A/B array, the 850-mbar vertical motion on the large scale is forced by a combination of the ITCZ, easterly waves, diurnal variations of the ITCZ and cloud clusters, convective feedback in the cluster regions, and frictional convergence. The ITCZ is clearly the dominant forcing mechanism.

3.2 AIR-SEA INTERACTION

Fluctuations of the sea-surface temperature (SST) occur over a spectrum of frequencies and have an amplitude that increases with increasing period. On time scales of a month or less, variability in the C-scale area has an amplitude of the order of 0.5°C and is primarily associated with diurnal oscillations and fluctuations with a period of 3 to 4 days. Entrainment of cold water into the mixed layer is unimportant because (1) the stability of the tropical thermocline is exceptionally high; (2) the wind stress is too weak to generate surface currents large enough to induce a dynamic instability and mixing across the bottom of the mixed layer; (3) rainfall during the passage of a squall lowers the salinity of the surface waters,

thus increasing the static stability of the upper ocean, and hence countering the effectiveness of mechanical stirring associated with increased wind speeds.

On time scales of the order of a month or less, sea-surface temperature changes within a few degrees latitude of the equator are primarily associated with propagating waves and with wind-induced upwelling. Fluctuations are particularly energetic and have an amplitude of several degrees Celsius, at periods of 30 days (because of an instability of surface currents) and 14 days, and 3 to 5 days (because the wind forcing is energetic at these periods).

SST fluctuations are large throughout the tropics on time scales longer than a month. This variability is not local and cannot be simulated by means of one-dimensional models because it is associated with a horizontal redistribution of heat in the upper ocean. This occurs when the large-scale slope of the thermocline changes in (dynamical) response to large-scale changes in the wind stress. For example, the zonal slope of the equatorial thermocline--downwards from east to west--is observed to fluctuate in phase with the seasonally varying zonal wind stress so that a large amount of heat is redistributed zonally and seasonally in the equatorial Atlantic. There is a similar latitudinal redistribution of heat. A three-dimensional model that resolves equatorial waves and currents is necessary to simulate this low-frequency variability.

3.3 DIAGNOSTIC STUDIES OF CUMULUS CONVECTION AND RELATED TOPICS

Although convection in the GATE area is strongly modulated by the passage of large-scale easterly waves, it is also organized on horizontal scales significantly smaller than the scale of the waves. On the smallest scale, isolated cumulus are observed, although frequently these cumulus clump together in groups. Often these groups are in the form of lines, which are associated with mesoscale squall and nonsquall systems, the latter being by far the more frequent. On any given day, these various convective features may appear in a general region of the wave in a somewhat complicated pattern.

Although the overall picture of the GATE convection is complicated, the individual components of this cloudiness have been studied in some detail. Radar observations of the cumulus convection indicate that isolated cells as well as cells that are in groups have areas, durations, and heights that appear to be log normally distributed. These results are consistent with radar statistics obtained in other tropical regions. Many updraft and downdraft statistics were also obtained from aircraft penetrations of convective elements. Radar and aircraft observations have been used to give a much clearer description of the mesoscale systems that frequented the GATE area. Systems observed during the experiment were classified into squalls and nonsqualls, with the former having a significantly greater propagation speed than the latter. Although the more frequent nonsquall systems are generally weaker than the squall systems, both systems have a number of similarities and appear to maintain themselves by the formation of new cells along the leading edge of the system. These systems have convective-scale (1-10 km) updrafts and

downdrafts with the downdrafts transporting approximately one half to three fourths as much mass as updrafts. Both the squall and nonsquall systems have large regions of stratiform precipitation in an associated anvil region. This is a significant feature of these systems, and the precipitation associated with these anvil regions has been estimated to account for 40 percent of the observed GATE rainfall. This rainfall appears to be associated with a mesoscale updraft in the anvil and a mesoscale downdraft below the anvil. Latent heat effects and radiation have been postulated as possible mechanisms for maintaining this circulation. Although a much clearer description of the dynamic and thermodynamic structure of these systems was obtained with the GATE observations, a complete theoretical understanding of them has not been obtained. Since a significant fraction of the total vertical mass transfer in a wave system may be associated with the mesoscale systems, a more complete understanding of the latter will be essential in determining their importance to the large-scale dynamics.

In general, the air flowing into convective elements and systems has its origin below cloud base. Consequently, temperature and moisture in the lowest layers of the atmosphere can significantly affect the thermodynamics and hence the dynamics of the convective elements. Aircraft, ship, and tethered-balloon observations have been used to study the boundary layer for both undisturbed and disturbed conditions. Under undisturbed conditions, the boundary layer has a structure that is similar to the structure found in other oceanic regions and over land during the day. This structure consists of a subcloud layer, where water vapor mixing ratio and potential temperature are approximately constant with height. This mixed layer is capped by a transition layer in which potential temperature increases with height and mixing ratio decreases with height. The vertical flux profiles of heat and moisture, the budget of turbulence kinetic energy, and the scale of the vertical velocity eddies associated with this structure are similar to those observed over land. Diurnal variations are much weaker than those over land although there is evidence that the boundary layer is most unstable in early morning. A very definite, although yet unexplained, mesoscale organization in the moisture field was also observed during undisturbed periods of GATE. In disturbed conditions, the boundary-layer structure may be altered significantly. For light rain conditions, evaporation gives a cooling in the subcloud layer, with little change in the moist static energy. In situations of moderate and heavy rainfall, mass transports associated with convective-scale downdrafts result in a cooling and drying of the boundary layer and a significant decrease in its depth. This structure recovers to the undisturbed state over a period of several hours. This relatively long recovery period appears to be due to the light winds observed during GATE and the subsidence associated with mesoscale downdrafts. This long recovery period has important implications concerning the ability of the boundary layer to support convection in the wake of a disturbance. Simple mixed-layer models appear to provide an adequate description of the undisturbed mixed layer and the recovery of the mixed layer from disturbed conditions.

The effect of convection on the large-scale heat, moisture, and momentum budgets was diagnosed using the GATE rawinsonde network. The residuals that are obtained from these budgets have been interpreted using simple

cloud models. Although the original diagnostic studies included only updrafts, more recent studies have considered the effect of cloud lifetimes, convective-scale downdrafts, and mesoscale updrafts and downdrafts. These more complicated models have diagnosed mass fluxes that are physically more reasonable than those obtained using only simple updrafts. The heat budgets obtained from B-scale data may eventually be useful in establishing the contribution that mesoscale features make to the large-scale heat and moisture budgets. Although the diagnostic studies of cumulus convection have significantly increased our understanding of how the convection may alter the heat and moisture budgets, these studies cannot indicate how the various cloud model formulations affect the behavior of a prognostic model through the cumulus parameterization.

Radiative processes also affect the heat budget of the tropical atmosphere. The principal modulation of this heat budget is due to variations in cloudiness. Satellite-determined cloudiness was used to obtain cloud distributions for the purpose of obtaining radiative profiles for the GATE area. The radiative profiles obtained indicate that previous estimates of radiative divergence in the tropics may be inadequate because of the vertical structure induced by clouds and the 10- to 12-m continuum cooling. Averaged over the entire day, these radiative profiles show horizontal gradients in the radiative heating due to horizontal gradients in cloudiness. However, day-night differences between clear and cloudy regions are much larger than the horizontal differences obtained for the average over the entire day. In the GATE area, horizontal differences are significantly greater in the N-S direction than in the E-W direction. If the total tropospheric divergence (TTD) of the radiative flux is averaged over a number of days for the GATE area, it is found that the TTD varies only by 6 W m^{-2} for a 5-day mean and 3 W m^{-2} for a 10-day mean. Dust transported from the African continent has also been shown to have a potentially important effect on the radiative characteristics of the atmosphere.

3.4 THEORETICAL CONCEPTS

Various areas of tropical dynamics were discussed. Hurricane formation and the reasoning that led to the formulation of the CISK hypothesis were reviewed. Frictional convergence was regarded as playing an important role in CISK only in the problem of the growth of the prehurricane depression, not in the development of weak depressions or waves. The hypothesis that the location of the ITCZ is governed by the combined effects of Ekman pumping and static stability was also reviewed, and greater credence was given to the idea that the position of the ITCZ is determined by the SST. An instability mechanism was described whereby movement of the ITCZ away from the equator produces relatively cold SST's at the equator, thus maintaining the displaced position. It was mentioned that many of the most important questions of tropical meteorology remain unanswered. Examples discussed were the maintenance of tropical waves as they cross the Atlantic, in particular, the role of cumulus convection in their maintenance; the origin of the occasional hurricanes that form from the easterly waves or other weak disturbances; the interaction of Hadley-scale circulations with the synoptic scales; and the development of mesoscale circulations and their interaction with the synoptic scale.

The interaction of the internal waves with the moisture or convective fields was reviewed. Mention was made of the concept of overreflection as an alternative, but related, view of the mechanism of wave instability. The importance of cumulus friction in the wave dynamics was stressed. Because of the friction, wave amplitude is relatively insensitive to the precipitation or heating rate. Without cumulus friction, temperature changes in the waves would be much larger than observed. It seems possible that the waves are maintained in an approximately neutral state by the balance between cumulus heating and cumulus friction. It has been found that CISK always exists for internal gravity waves with time and space scales of squalls and clusters.

3.5 PARAMETERIZATION

One speaker investigated how the convective activity within the A/B array was modulated by traveling easterly waves and the surface confluence line. It was found that, although easterly waves were identifiable in all three phases, the waves were not as vertically coupled in Phase I and were quite weak in Phase II. The precipitation pattern was oriented southwest-northeast in Phases I and II, whereas it was widely spread in Phase III. Phase II precipitation was notably smaller than that in the other phases. In Phase III, the surface confluence line was strongly modulated by the waves, whereas it hardly moved in Phases I and II. Several individual cases show that two types of precipitation and cloudiness occur: one associated with shallow ascent in the southerly flow south of the surface confluence line and the other associated with deeper ascent to the north.

The vorticity budgets in tropical regions were discussed. This vertical distribution of apparent vorticity source for each of the Reed wave categories was presented. Good agreement was found between this apparent source and the parameterized source computed using a single-cloud model. The parameterized source computed using a spectral-cloud model was much less satisfactory.

The possibility of significant horizontal vorticity transport by cumulus convection was examined. This was envisaged to occur through the action of the cloud-scale convergence on a vortex couplet, which has been produced by the vertical advection and twisting of an originally horizontal vortex tube.

The vorticity budget for a 100-day period in the Marshall Islands area was presented. This budget is not dominated by the divergence term but indicates that all terms can be important. In addition, a large apparent vorticity sink at low levels is not found. In interpreting such budget studies, it was emphasized that it is important to distinguish between the budget of a composite and the composite of individual budgets.

A simple stochastic model of cumulus-cloud clumping was discussed. This represents a beginning attempt to understand mesoscale-cloud organization in the tropics.

Cumulus parameterization and its purpose was presented, and the history of tropical cyclone and wave modeling was reviewed. It was felt that the failure of early tropical cyclone models was due to their improper formulation of the fully nonlinear stage. This improper formulation involves simplification of the static stability field.

Experiments with cumulus parameterization theories using GATE data were discussed. Evidence in support of the quasi-equilibrium of the cloud work function was presented. Using this quasi-equilibrium, rainfall rates were produced that agreed remarkably well with radar observations. The vertical distribution of parameterized heating showed somewhat too much warming and drying in the lower troposphere. The cellular cloud model of Rodenhuis was discussed. This model is unique in that it computes (for a spectrum of cloud depths) not only the mass flux but also the fractional area of cloud.

Results were shown from what is essentially a two-dimensional cloud model with a domain large enough to include many clouds. In this model, one may specify large-scale forcing effects such as w, $\nabla \cdot \nabla\theta$, $\nabla \cdot \nabla\overline{q}$, and Q_R. This is a powerful tool for testing how such things as the shape of the $\overline{w}$ profile controls the cloud population. It is possible to find not only the adjustment time but also what is in quasi-equilibrium.

3.6 LARGE-SCALE MODELING

Several aspects of the tropical atmosphere as simulated by GFDL general circulation models were discussed. A deficiency of the 11-layer 2.4° gridpoint model was the unrealistic simulation of intense tropical cyclones during the summer season. At high levels over the storms, overly intense anticyclonic circulations marred the tropical circulation over the Pacific. These defects were eliminated in a 30-wave-number spectral model, although the reason is not known. Also the westward propagation of easterly waves over the western Pacific was better simulated by the spectral model.

The general circulation models contain Kelvin waves and mixed Rossby gravity waves as observed. Evidence of these waves was shown by space-time power-spectrum analyses.

The generation and maintenance of transient tropical planetary waves corresponding to Kelvin and mixed Rossby-gravity waves were investigated in the model by eliminating possible physical processes responsible for their growth. First, the zonal variation of sea-surface temperature was removed. Then the effect of midlatitude disturbances was eliminated by setting these perturbations to zero. Finally, condensation heating, as simulated by the moist convective adjustment scheme, was eliminated. Latent heating alone was sufficient to excite these waves. In contrast to their negligible effect on Kelvin waves, midlatitude disturbances enhanced the mixed Rossby-gravity waves. While the midlatitude disturbances did not significantly alter the transient eddy kinetic energy near the equator, they did significantly increase the eddy kinetic energy in the subtropics.

A movie was shown that depicted the surface wind flow and precipitation over the tropics during the summer season. A pulsing of the precipitation centers was related to a modulation by traveling synoptic waves.

The sensitivity of a regional version of the British Meteorological Office's general circulation model to initial moisture conditions and to the parameterization of cumulus convection and cloud radiation interactions over the tropics was discussed. The thermodynamic structure, moisture, and precipitation forecasts were sensitive to the initial moisture

distribution for at least 50 days, particularly over the Sahara. In the relatively moist simulation, there was too much rain over the Sahara and the easterly flow south of the Sahara was too weak, a consequence of a too-weak temperature gradient. With drier, more realistic initial conditions, soil moisture over the Sahara did not increase, precipitation was much more realistic, and the easterly jet over Africa was better developed.

In 5-day forecasts with and without an interaction between clouds and radiation, the forecasts showed considerable differences. The interactions appeared to improve the forecasts of the waves emerging off Africa by weakening the waves over land and enhancing the waves as they moved over water. As a result of these changes, the intensity of the modeled waves was closer to the observed.

Some details of an 11-layer, limited-area model forecast over the GATE area were presented. The analysis scheme for these forecasts incorporates variational analysis and dynamic initialization techniques. Autocorrelation functions for the GATE data set were presented. The use of revised autocorrelations based on the GATE observations made a difference in the objective analysis.

The structure and energetics of the easterly waves as predicted by the model were presented. Composite analyses following a wave over a three-day period were made. The vertical velocity became upward as the wave trough approached, as observed, and the rainfall distributions were generally realistic. The temperature perturbations were somewhat too large. The energetics of the model waves showed some differences from diagnostic studies based on composited data, although observed differences in the energetics over land and water were reproduced by the model.

Two versions of GFDL four-dimensional objective analyses over the tropics during the GATE experiment were compared with each other and with subjective analyses of Dean and Sadler. The first set of analyses were produced in near real time; the second was run using a revised analysis scheme and the full GATE data set. The revised scheme utilizes a combination of dynamic assimilation and an optimal interpolation method. Although both objective schemes gave overall similar results, the more recent version showed a better resolution of easterly waves.

An important result of the analysis was a time-longitude diagram for the v-component of the wind at the 700-mbar level. This diagram revealed the westward propagation of waves that were similar to observed easterly waves.

The sensitivity of the GCM to subgrid-scale physics in simulating the climate over a one-month period was examined. Variations included simple and more sophisticated boundary-layer physics and formulation of the parameterization of cumulus clouds. In general, the results were insensitive to the various physics. There were some indications that variations in the cumulus parameterization had a greater impact than variations in the boundary-layer physics.

The growth and structure of easterly waves in primitive equation linear models was discussed. These models differ from nonlinear models in that the base state remains unchanged during the integration. After reviewing the early models of Rennick and Simmons, results from the recent 10-layer model of Mass were summarized. The growth rate of disturbances was sensitive to the shape of the mean zonal wind profile but not very sensitive

to latent heating. The perturbations grew by a conversion of zonal kinetic energy to eddy kinetic energy. The structure of the waves was quite similar to the structure of the waves determined by compositing data. Although latent heat release did not greatly affect the growth rate of the disturbances, it did increase the divergence perturbations in low levels and the amplitude of the perturbations aloft. The latter resulted from an increased vertical coupling of the disturbance above the jet level.

Research on the use of explicit rather than parameterized convection was summarized. Realistic model hurricanes have been produced in which condensation and evaporation effects are modeled explicitly. Explicit modeling of these effects requires prognostic equations for cloud and precipitation water. Although requiring more time than parameterized models, the use of explicit condensation/evaporation physics eliminates many arbitrary assumptions inherent in cumulus parameterization schemes.

Although the use of explicit modeling of convection may be desirable in models with horizontal resolution of 10 km or less, there is still a real need for parameterization of moist convective effects in larger-scale models. An outline of when cumulus parameterization is necessary was presented. Parameterization is a viable choice when (1) the horizontal grid is much larger than the dominant scale of convection and (2) the cumulus effects are related to the large-scale (resolvable) variables. If these conditions are met, the simplest scheme that adequately relates the cumulus effects to the large scale should be used. On the other hand, if the model grid size is of the same order or smaller than the convective scales, or if the details of the interactions are of primary interest, explicit models of convection become necessary.

4. Large-Scale Tropical Circulations

Organizer	R. Burpee
Speakers	R. Burpee
	R. Reed
	W. Frank
	W. Gray
Session Chairmen	M. Wallace
	R. Burpee
Rapporteurs	W. Frank
	T. Carlson

MEAN CHARACTERISTICS OF THE LARGE SCALE DURING GATE

Robert W. Burpee
NOAA National Hurricane and Experimental Meteorology Laboratory

The synoptic-scale subprogram of GATE has produced a set of observations that represents a significant step forward in terms of the quality and quantity of observations in the tropical region that includes the Atlantic, Africa, South America, and the Caribbean. The success of this data-gathering effort can be attributed to several factors: in particular, the special array of research ships in the tropical Atlantic, the enhanced network of observations over land, the availability of new observing tools that were used operationally for the first time during GATE, and greatly improved data archiving procedures. As a result of this effort, the final validated data sets included observations of the structure of the atmosphere in areas where the conventional network had few, if any observations. Thus, comprehensive analyses of the large-scale features of the GATE region became possible throughout the troposphere for the first time. In the five years since the field experiment, several research groups have already produced daily and phase mean analyses of many quantities observed during GATE, while analyses of some derived quantities, such as mean vertical motion, are still in progress at other institutions. This paper presents a summary of those analyses of the mean conditions during GATE that were completed prior to August 1979, with particular emphasis on Phase III.

While many of the major features of the mean wind field at the surface and in the upper troposphere were well known prior to GATE, relatively little was known about the mean atmospheric structure in the middle troposphere. Comparison of average maps for Phase III of GATE with mean maps for August and September from earlier years suggest that Phase III was a fairly typical period. The east-west oriented cloud maximum was located near 8-10° N over the central Atlantic and near 10-12° N over Africa. The mean surface wind field for Phase III [Figure 1(b)] shows that a large part of the oceanic region was influenced by the easterly trade winds of the northern and southern hemisphere, which were separated by a zone of confluence near 10° N. A col in the surface wind flow was located near 9° N, 32° W, not far from its position in other years. The southwest monsoon dominated the mean surface flow in western Africa from 5-20° N and extended westward from the African coast in the eastern Atlantic, where it encompassed most of the A/B ship array.

An objective analysis of the Phase III sea-surface temperatures (SST) by Krishnamurti *et al.* (1976) indicates that there is a maximum in the

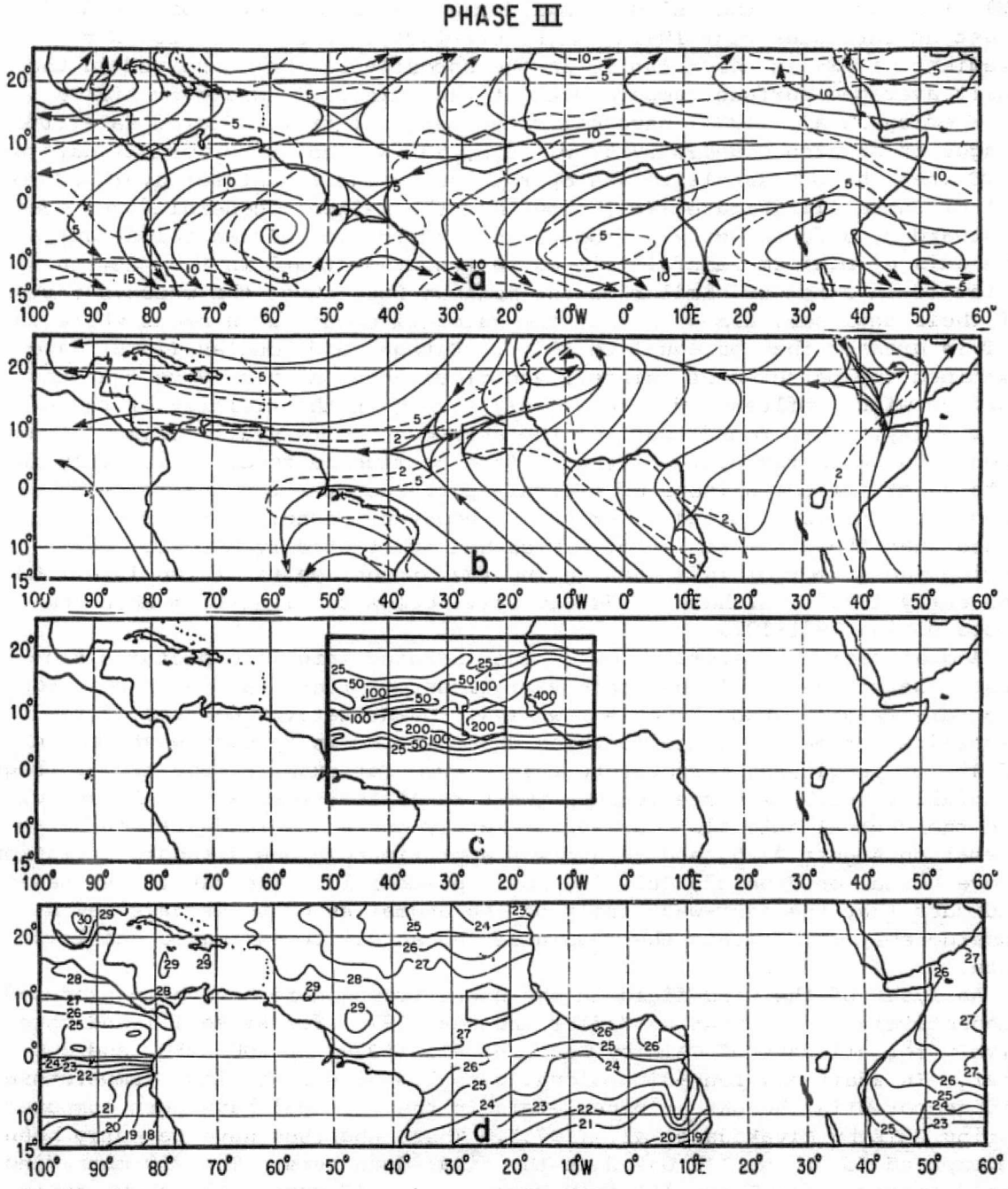

FIGURE 1 Phase III (a) Streamlines (solid) and isotachs in m sec^{-1} (dashed) at 250 mbar from Pasch *et al.* (1978); (b) surface streamlines (solid) and isotachs in m sec^{-1} (dashed) from Reynolds (1977); (c) total satellite estimated rainfall (mm) subjectively smoothed from Woodley *et al.* (1979); and (d) sea-surface temperature (°C) from Krishnamurti *et al.* (1976).

SST of about 27° C that slopes toward the west-southwest from the African coast at latitudes near 10-12° N [Figure 1(d)]. From 10 to 25° N the gradient of SST in the Atlantic is the opposite of that observed in the daily averaged surface temperatures at the same latitudes over Africa.

Woodley *et al.* (1979) have estimated rainfall from infrared satellite images in an area bounded by 5° W, 5° S, 50° W, and 22° N for all days of GATE when the SMS satellite was operational. Their analyses averaged for all of Phase III [Figure 1(c)] show that the rainfall generally decreases westward by a factor of 2-3 from western Africa to the central Atlantic. The axis of maximum rainfall slopes west-southwestward in the eastern Atlantic in a manner similar to the maximum SST. Over the oceanic region of their analyses, almost all of the rainfall occurred in areas where the SST is greater than or equal to 26° C. Estoque and Douglas (1978) have examined the patterns of rainfall and cloudiness on those days that the surface wind confluence was relatively strong in the vicinity of the A/B ship array. They found that, on the average, the rainfall maximum occurs about 100 km to the south of the surface confluence zone. Relatively few data exist for comparisons of rainfall patterns over the entire GATE region with rainfall during other years; however, Nicholson (1979) has indicated that the Sahel region of Africa had substantially more rainfall during the summer of 1974 than during the drought years of the late 1960's and early 1970's, although 1974 was still below the long-term mean computed during 1901-1975.

A qualitative interpretation of the infrared satellite pictures suggests that there are large-scale variations of precipitation in the tropics that are readily apparent on a few days. Quantitative analyses of the satellite-estimated rainfall, which was computed in an east-west domain of 45° of longitude, corroborate this view. For example, the area-averaged rainfall in each of three regions (western Africa, the eastern Atlantic, and the central Atlantic) was approximately one standard deviation below normal on August 4, 5, and 14 and was approximately one standard deviation above normal on June 27, July 18, and September 19. The satellite images indicate that the east-west scale of the anomalies on these days may be considerably larger than the domain of the satellite-estimated rainfall data.

Analyses of the wind field in the upper troposphere have been produced subjectively at 250 mbar by Sadler and Oda (1978) for Phase III and objectively for all days of GATE by Pasch *et al.* (1978) at 200, 250, and 300 mbar. In addition, four-dimensional global analyses of wind, temperature, and geopotential height at nine levels in the vertical have been computed during GATE by Miyakoda *et al.* (1976). These analyses have recently been recomputed for Phase III based on the final data sets. The 250-mbar wind field averaged for Phase III from Pasch *et al.* [Figure 1(a)] shows anticyclonic circulations over Saudi Arabia and Mexico, the mid-Atlantic trough, and a zone of diffluence near 10° N in the eastern Atlantic and Africa that is located approximately above the phase mean rainfall maximum.

Meridional cross sections of zonal wind in the eastern Atlantic and western Africa, based on operational data, were presented by Burpee and Dugdale (1975). The major features of these cross sections are the mid-tropospheric easterly wind maximum located near 17° N and 650 mbar and upper tropospheric easterlies with a maximum near 5° N and 200 mbar.

These cross sections revealed that there were rather small differences in the zonal wind between Africa (7.5° W) and the eastern Atlantic (23.5° W) except just above the surface, where the southwesterly monsoon penetrated considerably farther north over Africa. There were also relatively minor differences from Phase I to Phase III in the mean zonal wind profiles, particularly in the middle and lower tropopshere, although there was a slight weakening of the easterlies above 300 mbar during this time. The final validated data sets corroborate these preliminary findings [Figures 2(a) and 2(e)]. As a result of the large horizontal shear of the mean zonal wind on the equatorial side of the midtropospheric easterly wind maximum, the gradient of absolute vorticity changes sign. This is a necessary condition for barotropic instability. Reed *et al.* (1977) have shown that the horizontal shear near 10° N is somewhat stronger in the eastern Atlantic than over Africa. As pointed out by Burpee and Dugdale, it had been expected that the horizontal shear near 600-700 mbar would be weaker in the oceanic region, based on the reversal of the surface temperature gradient from Africa to the eastern Atlantic and thermal wind arguments. Apparently warm air, advected westward from Africa just above the surface layer, maintains a temperature gradient in the lower troposphere of the eastern Atlantic that is quite similar in magnitude to that observed in western Africa. Since the thermal wind accounts for approximately the same vertical shear of the zonal wind in both regions, the stronger horizontal shear in the middle troposphere of the eastern Atlantic must be accounted for by the stronger cyclonic shear of the surface wind in the oceanic area. The zonal wind cross section for Phase III in the western Caribbean is shown in Figure 2(g) for comparison. The horizontal shear of the mean zonal wind is considerably weaker in this region and does not satisfy the necessary condition for barotropic instability.

North-south cross sections of the mean meridional wind at 7.5 and 23.5° W for Phase III are shown in Figures 2(b) and 2(f). These figures indicate that the meridional wind term of the divergence contributes to strong convergence close to the surface and strong divergence about 200-250 mbar near 10° N. Computations of divergence (not presented) show that there are also regions of convergence and divergence in the midtroposphere that have not been observed in other regions. As a result of this pattern of divergence, the GATE area is characterized by maximum upward motion near 600-700 mbar [Figure 2(h)] rather than in the upper troposphere as is observed in the western Pacific and Caribbean.

Phase III temperature deviations computed relative to the equator and averaged from 10° E to 31° W are shown in Figure 2(c). The largest positive temperature deviations occur at 850 mbar near 20-24° N. At the latitudes near the maxima of rainfall and upward motion, the temperature deviations are slightly positive from the surface to about 700 mbar and negative above that level. It had been hoped to show temperature deviations at 23.5° W based directly on nighttime temperature observations of the A/B ships corrected for biases following the method suggested by Reeves and MacKechnie (1979), but final bias corrections are not yet available. The highest mean relative humidities along 23.5° W [Figure 2(d)] occur at the same latitude as the maxima of rainfall and upward vertical motion.

The thermodynamic and moisture structure of the lower and middle troposphere of the A/B array is distinctly different from that observed in the

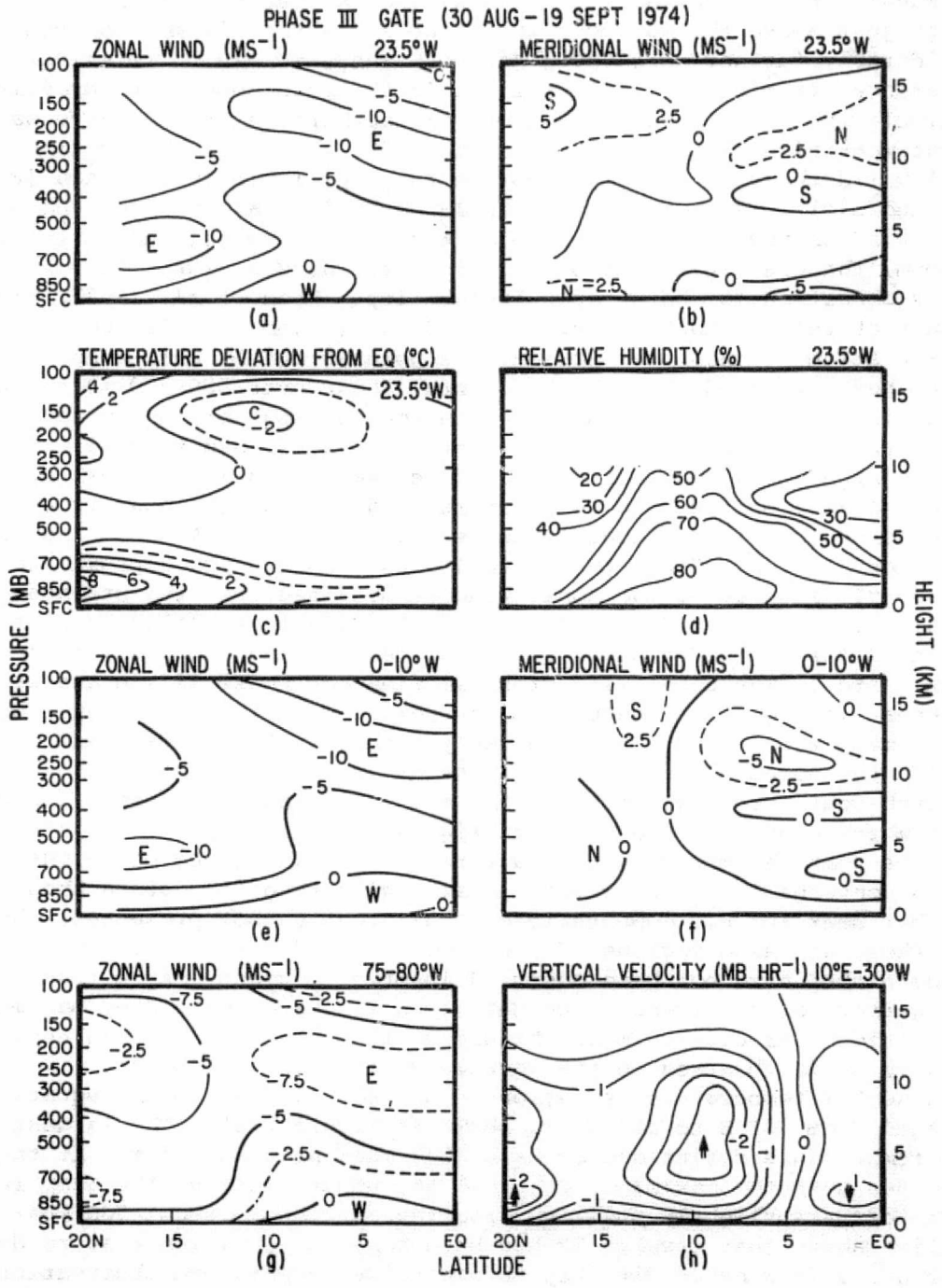

FIGURE 2 Meridional cross sections at key longitudes during Phase III. (c) has been reproduced from Reed *et al.* (1977) and (h) from R. J. Reed (University of Washington, personal communication).

western Pacific and Caribbean. The A/B area is colder in the lower troposphere than in the other regions, and it is more moist in the levels from 850 to 550 mbar (W. M. Gray, Colorado State University, personal communication).

Research is still continuing on the mean structure of the largest scales during GATE. Subjective analyses of the wind field in Phases I and II and budget studies on the A scale for all three phases are in progress.

REFERENCES

Burpee, R. W., and G. Dugdale (1975). A summary of weather systems affecting western Africa and the eastern Atlantic during GATE. GATE Report No. 16, ICSU/WMO, Geneva, Switzerland, pp. 2.1-2.42.

Estoque, M. A., and M. Douglas (1978). Structure of the intertropical convergence zone over the GATE area. *Tellus 30*, 55-61.

Krishnamurti, T. N., V. Wong, H. L. Pan, G. V. Dam, and D. McClellan (1976). Sea-surface temperatures for GATE. Report 76-3, Dept. of Meteorol., Fla. State U., Tallahassee, Fla.

Miyakoda, K., L. Umscheid, D. H. Lee, J. Sirutis, R. Lusen, and F. Pratte (1976). The near-real-time, global, four-dimensional analysis experiment during the GATE period, Part I. *J. Atmos. Sci. 33*, 561-591.

Nicholson, S. E. (1979). Revised rainfall series for the west African subtropics. *Mon. Wea. Rev. 107*, 620-623.

Pasch, R., T. N. Krishnamurti, and C. Depradine (1978). An atlas of the motion field over the GATE area, Part II (250 mbs). Report No. 78-3, Dept. of Meteorol., Fla. State U., Tallahassee, Fla. (There are also additional atlases for 200 and 300 mbar; all three atlases are available on microfilm from World Data Center-A, Asheville, North Carolina.)

Reed, R. J., D. C. Norquist, and E. E. Recker (1977). The structure and properties of African wave disturbances as observed during Phase III of GATE. *Mon. Wea. Rev. 105*, 317-333.

Reeves, R. W., and W. T. MacKechnie (1979). A method for estimating temperature and height biases in GATE. Unpublished manuscript, Center for Environmental Assessment Services, NOAA, Washington, D.C.

Reynolds, R. (1977). Large-scale (A-scale) mean features of the GATE atmosphere during Phase III. Met.0.20 Tech. Note No. II/105, U.K. Meteorol. Office, Bracknell, England.

Sadler, J. C., and L. K. Oda (1978). The synoptic (A) scale circulations during the third phase of GATE, 20 August-23 September 1974. Dept. of Meteorol., U. of Hawaii, Honolulu, Hawaii.

Woodley, W. L., C. G. Griffith, J. S. Griffin, and S. C. Stromatt (1979). Satellite-estimated rainfall in GATE. Submitted to *J. Appl. Meteorol.*

THE STRUCTURE OF EASTERLY WAVES DURING GATE

Robert W. Burpee
NOAA National Hurricane and Experimental Meteorology Laboratory

During a typical summer season, synoptic-scale easterly wave disturbances are observed propagating westward across the Atlantic Ocean from late May to mid-October with an average wavelength of approximately 2500 km and an average period and speed of 3.5 days and 8.0 m sec^{-1}, respectively. Of the 45-50 easterly waves that cross the African coast during the summer, 4 or 5 intensify and become named tropical cyclones in the Atlantic region. Normally these disturbances develop into tropical cyclones only during August, September, and early October, and it is quite rare for these waves to be the source of tropical cyclones during the remaining months that they are observed. While it is more difficult to track these systems in the eastern Pacific, where satellite images are usually the only source of information, the National Hurricane Center estimates that about 60 percent of the tropical cyclones that form in that area are linked to wave disturbances that were first observed over Africa. The obviously important role that these disturbances play in initiating tropical cyclones resulted in many studies of the structure of these waves with the conventional observing network prior to GATE, for example, Riehl (1954) in the Caribbean and Carlson (1969a; 1969b) and Burpee (1972; 1974) in western Africa. The extensive data base obtained during GATE has presented an excellent opportunity to re-examine the structure of the waves and to determine how these waves organize deep convection in far greater detail than had been possible previously.

Most of the studies of the structure of the waves during GATE have concentrated on Phase III, when the waves were particularly well developed, and in the longitudes from 10° E to 31° W in the eastern Atlantic and western Africa, where radiosonde observations were relatively plentiful. Reed *et al.* (1977) tracked the vorticity centers of the waves at 700 mbar and defined the wave structure by compositing the observations relative to the 700-mbar wave trough at the mean latitude of the disturbance paths, which was at about 12° N. They divided each wave into eight categories in the east-west direction. At the reference latitude, category 4 represents the 700-mbar trough, category 8 marks the 700-mbar ridge, and categories 2 and 6 are the maximum northerly and southerly wind components, respectively. The intermediate regions of the waves are designated by categories 1, 3, 5, and 7. The composited streamline fields with the mean flow removed are shown for the surface, 700 mbar, and 200 mbar in Figures 1(a), 1(b), and 1(c). The perturbation surface wind field composited for

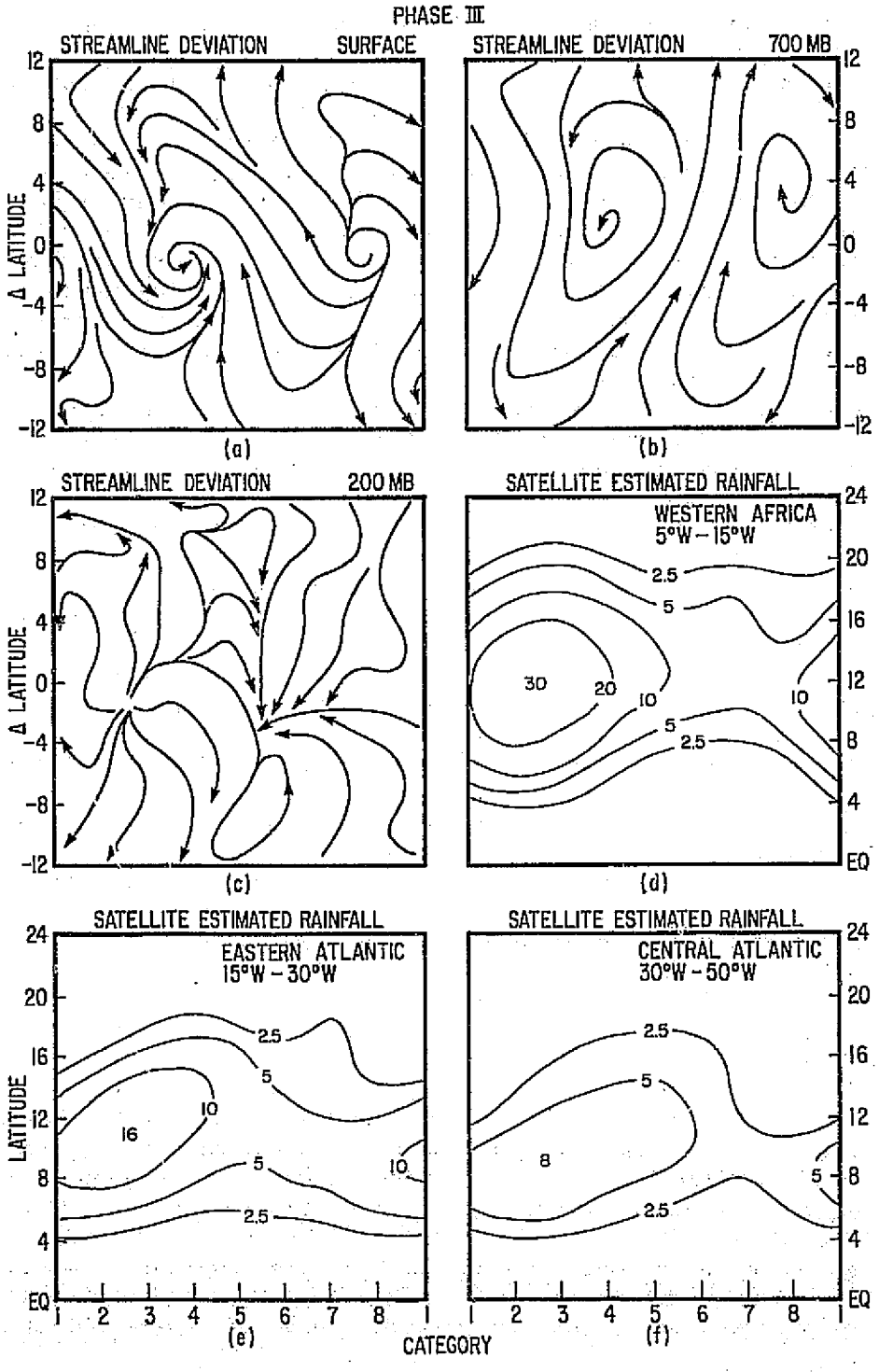

FIGURE 1 Streamline deviations in (a), (b), and (c) are composited from 10° E to 31° W (reproduced from Reed *et al.*, 1977). Zero Δ latitude is approximately 12° N.

the eastern Atlantic and western Africa shows one cyclonic and one anticyclonic center near the reference latitude. In western Africa, Carlson (1969b) and Burpee (1974) had previously noted two cyclonic and two anticyclonic circulation centers in the surface wind field. The more northerly ciruclation centers were located in a relatively cloud-free region along the southern edge of the Sahara, while the second, more southerly, pair of centers was nearer to the latitude of maximum convective activity. The 700-mbar perturbation streamline analyses show a single cyclonic and anticyclonic circulation center that is located nearly vertically above the surface centers. At this level, the trough and ridge axes slope from southwest to northeast on the south side of the circulation center, which is also the region of cyclonic shear on the south side of the midtropospheric easterly jet. The slope of the wave features, therefore, indicates a southward flux of easterly momentum away from the jet maximum. The perturbation flow at 200 mbar reveals a region of strong diffluence to the west of the 700-mbar trough and strong confluence to the west of the 700-mbar ridge.

A vertical cross section of the meridional wind at the reference latitude [Figure 2(a)] shows that the maximum amplitude of about 5 m sec^{-1} occurs near 700 mbar. Below 700 mbar the wave features are nearly vertical, but above this level the meridional wind pattern tilts toward the west. Secondary maxima with a nearly opposite phase to the maxima in the lower troposphere are located near 200 mbar. The zonal wind component also undergoes substantial fluctuations, with the maximum amplitude of the zonal wind, 3 m sec^{-1}, located near 700 mbar. Westerly winds and southerly winds are positively correlated in the middle troposphere, as is implied by the southwest-northeast tilt of the wave features.

The temperature anomalies [Figure 2(b)] show a cold core below 700 mbar in the trough that is overlain by a warm anomaly in the middle troposphere. A second area of cold anomalies occurs near 150 mbar. The vertical cross section of moisture at the reference latitude shows that, above the surface layer, the highest relative humidities are located in the same region as the southerly winds and the lowest humidities are observed where there are northerlies [Figure 2(c)]. Near 300 mbar the pattern is reversed so that the highest relative humidities are above the relative dryness at lower levels.

The divergence pattern [Figure 2(d)] features strong convergence near the surface and strong divergence around 200-250 mbar, with the maximum values to the west of the 700-mbar trough. In the middle troposphere there are two additional regions of convergence and divergence. The corresponding cross section of vertical motion [Figure 2(e)] shows that the largest values of upward motion are about 5 mbar h^{-1} (1-2 cm sec^{-1}) and occur near 700 mbar, slightly to the west of the low-level trough. In a study of easterly waves in the western Pacific, Reed and Recker (1971) had determined previously that the maximum value of upward motion was near 400 mbar.

In a study of satellite observed cloudiness, Payne and McGarry (1977) found that convective clusters tended to form in nearly equal amounts in each of the eight wave categories but determined that larger and longer-lived clusters tended to be located just to the west of the 700-mbar trough axis, with the result that a higher percentage of convective cloud

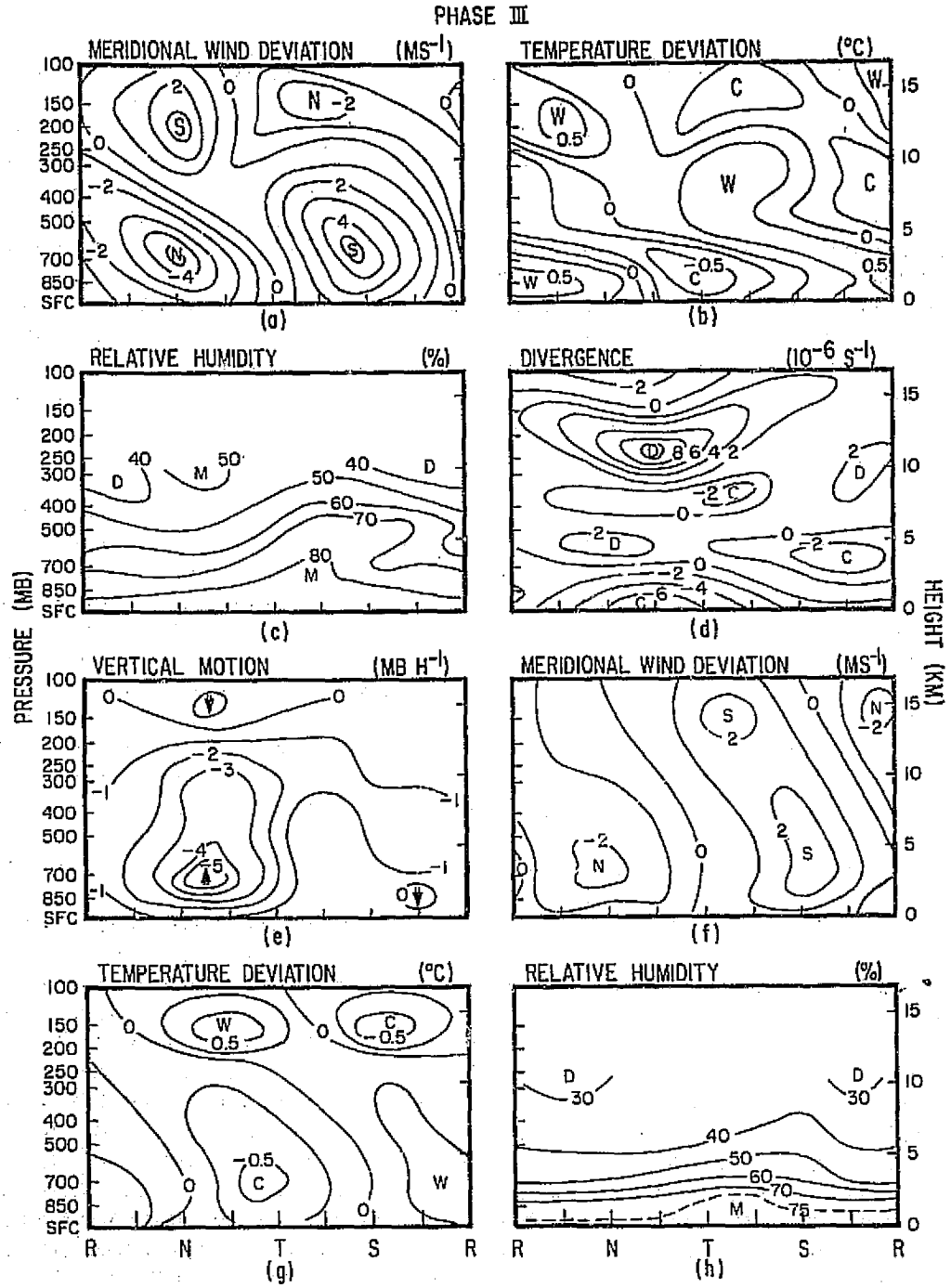

FIGURE 2 East-west cross sections of composited waves near latitude of maximum wave amplitude. Latitude is approximately 12° N in (a), (b), (c), (d), and (e) for longitudes from 10° E to 31° W (reproduced from Reed *et al.*, 1977) and 16° N in (f), (g), and (h) for the Caribbean region. R, N, T, and S refer, respectively, to the ridge, northerly wind maximum, trough, and southerly wind maximum.

cover occurred in that region than near the ridge. Aspliden *et al.* (1976) and Payne and McGarry used infrared satellite pictures to track the west African squall lines and related the origin and decay of the squall lines to wave features. In a sample of 46 squall lines that had an average lifetime of 10 h, Payne and McGarry found that most of the squall lines formed a few hundred kilometers west of the wave trough (near categories 2 and 3 of the composite wave) and propagated westward faster than the synoptic-scale waves. On the average, the squall lines decayed about 300 km west of their origin in a coordinate system moving with the wave. In Figures 2(c) and 2(e), the wave structure in the preferred region of squall development is characterized by relatively strong upward motion and rather dry air located just above the surface layer. Reed (1978) has composited rainfall relative to the waves in western Africa and found that maximum rainfall of 15 mm day^{-1} is observed to the west of the wave trough near 10° N, while rainfall near the ridge at the same latitude is slightly greater than 5 mm day^{-1}.

The structure of the waves summarized above is valid for longitudes from 10° E to 31° W. Thompson *et al.* (1979) have determined the detailed structure of the waves at the center of the B-scale ship array. Elsewhere in the GATE region, the waves have somewhat different characteristics. It is known from studies of upper-air data from the early 1960's that the waves typically form in eastern Africa near the Sudan at latitudes of 10-15° N and that barotropic instability is the likely energy source (Burpee, 1972; Mass, 1978). Initially, the waves are confined to a vertical layer near 600-700 mbar on the equatorward side of the midtropospheric easterly jet and do not appear to organize convective activity. As the waves propagate westward across Africa, they gradually enter a region that is more conducive for deep convection (Carlson, 1969a; 1969b) and the vertical depth of the troposphere influenced by the waves increases as they approach the west African coast (Burpee, 1972; Mass, 1978).

Burpee and Dugdale (1975) noted that the wave structure was generally fairly similar in western Africa and the eastern Atlantic; however, Reed *et al.* (1977) stated that the wavelength and period changed from average values of 2700 km and 3.7 days over land to 2200 km and 3.2 days over the ocean. In addition, there was a tendency for the wave features to tilt more in the horizontal and for the 700-mbar meridional wind amplitude to be larger in the eastern Atlantic. Over land, the upward vertical motion occurred at higher levels and the convection also appared to be deeper. Burpee has composited the satellite estimated rainfall computed by Woodley *et al.* (1979) relative to the waves in western Africa and the eastern and central Atlantic [Figures 1(d), 1(e), and 1(f)]. In each region during Phase III, the waves clearly modulate the rainfall with maximum values located to the west of the 700-mbar trough over Africa but occurring near the trough in the central Atlantic. The total rainfall decreases from western Africa westward, and, consequently, at the latitude of maximum precipitation, the difference between maximum and minimum wave associated rainfall is about 25 mm day^{-1} over western Africa and only 5 mm day^{-1} in the central Atlantic. Note that the maximum satellite estimated rainfall in Figure 1(d) is about double that shown by Reed (1978) from the composite raingauge data for western Africa. The satellite composite is based on a narrower longitude band that is more influenced by the high rainfall totals

in the southwest corner of the African bulge, and the satellite estimation method has a tendency to overestimate the rainfall north of 10° N.

The wave circulation centers typically move slightly north of west as they propagate westward. In the Caribbean, the meridional wind amplitude, averaged for August and September on days without tropical cyclones, has a maximum value slightly less than 3 m sec^{-1} near 700 mbar and 16° N [Figure 2(f)]. The wave features tilt eastward with height up to 700 mbar and then tilt westward, whereas an eastward tilt throughout the entire troposphere had been described earlier by Riehl (1954). Temperatures are relatively cool near the trough in the lower troposphere and warm in the upper troposphere above 200 mbar [Figure 2(g)]. The relative humidities near 16° N in the Caribbean are generally somewhat lower than those at the latitude of maximum wave amplitude over Africa (12° N). The highest values of relative humidity are observed to the east of the wave trough [Figure 2(h)].

In general, those waves that do not develop into tropical cyclones weaken as they travel across the Atlantic and have less of an effect on the patterns of precipitation over the ocean than over land. Comparison of composite results form June and July, when these waves rarely become tropical cyclones, with results for August and September indicates the waves are much weaker in June and July and have relatively little influence in organizing convective activity. The meridional wind amplitude during these months is about half of that observed later in the summer, and the waves extend through a relatively small depth of the troposphere.

REFERENCES

Aspliden, C. I., Y. Tourre, and J. B. Sabine (1976). Some climatological aspects of West African disturbance lines during GATE. *Mon. Wea. Rev. 104*, 1029-1035.

Burpee, R. W. (1972). The origin and structure of easterly waves in the lower troposphere of North Africa. *J. Atmos. Sci. 29*, 77-90.

Burpee, R. W. (1974). Characteristics of North African easterly waves during the summers of 1968 and 1969. *J. Atmos. Sci. 31*, 1556-1570.

Burpee, R. W., and G. Dugdale (1975). A summary of weather systems affecting western Africa and the eastern Atlantic during GATE. GATE Report No. 16, ICSU/WMO, Geneva, Switzerland, pp. 2.1-2.42.

Carlson, T. N. (1969a). Synoptic histories of three African disturbances that developed into Atlantic hurricanes. *Mon. Wea. Rev. 97*, 256-276.

Carlson, T. N. (1969b). Some remarks on African disturbances and their progress over the tropical Atlantic. *Mon. Wea. Rev. 97*, 716-726.

Mass, C. (1978). A numerical and observational study of African wave disturbances. Ph.D. thesis, Dept. of Atmos. Sci., U. of Washington, 278 pp.

Payne, S. W., and M. McGarry (1977). The relationship of satellite-inferred convective activity to easterly waves over West Africa and the adjacent ocean during Phase III of GATE. *Mon. Wea. Rev. 105*, 413-420.

Reed, R. J. (1978). The structure and behavior of easterly waves over West Africa and the Atlantic. *Meteorology over the Tropical Oceans*, Royal Meteorol. Soc., Bracknell, U.K., pp. 57-71.

Reed, R. J., and E. E. Recker (1971). Structure and properties of synoptic-scale wave disturbances in the equatorial western Pacific. *J. Atmos. Sci. 28*, 1117-1133.

Reed, R. J., D. C. Norquist, and E. E. Recker (1977). The structure and properties of African wave disturbances as observed during Phase III of GATE. *Mon. Wea. Rev. 105*, 317-333.

Riehl, H. (1954). *Tropical Meteorology*, McGraw-Hill, New York, 392 pp.

Thompson, R. M., S. W. Payne, E. E. Recker, and R. J. Reed (1979). Structure and properties of synoptic-scale wave disturbances in the Intertropical Convergence Zone of the Eastern Atlantic. *J. Atmos. Sci. 36*, 53-72.

Woodley, W. L., C. G. Griffith, J. S. Griffin, and S. C. Stromatt (1979). Satellite-estimated rainfall in GATE. Submitted to *J. Appl. Meteorol.*

DISCUSSION
W. Frank, *Rapporteur*

The easterly waves were observed to have larger wind amplitudes and to extend through a greater depth of the troposphere in Phase III than in Phases I and II. The greater vertical extent of the waves during Phase III appears to be related to the presence of a thermodynamic structure that is more favorable for deep convection. In the oceanic region, the 1-2°C increase in sea-surface temperature at latitudes of 10-20° N from Phase I to Phase III appears to be an important factor in the stronger amplitude of the waves during Phase III.

It was observed particularly at latitudes from 10 to 20° N that the maximum wave precipitation occurred during relatively dry parts of the waves. This may have resulted from a tendency to undersample water vapor in the cloud lines during the most active parts of the wave and the cumulative effect of moistening, which resulted in maximum humidities after convection had ended.

Vincent showed some early results of a mean-state analysis indicating substantial logitudinal variations in vertical motion and temperature at 11° N. He also presented estimates of latent heat release determined from a Kuo-type scheme that were about a factor of 2 larger than satellite-derived rainfall estimates in some areas. The latter point raised questions since it was generally agreed that long-term satellite rainfall estimates agreed well with radar, gauge, and budget results.

Reed showed a recent latitudinal cross section of vertical motion over W. Africa. Maximum upward motion near 9° N between subsidence zones to the north and south were indicated. Near 20° N there was upward motion from the surface to about 300 mbar in the vicinity of the surface trough. The latter feature was discussed at some length since the ascending motion did not coincide with observed precipitation and since the adiabatic cooling associated with this deep upward motior would be difficult to balance in a sensible heat budget. It was noted that extremely dry air in the lower troposphere in this region prevents significant precipitation despite strong convection, and radiative absorption by dust was proposed as a possible additional heat source to balance adiabatic cooling.

ENERGETICS AND HEAT AND MOISTURE BUDGETS OF EASTERLY WAVES

Richard J. Reed
University of Washington

I. INTRODUCTION

The identification of the synoptic-scale wave disturbances that occurred during the GARP Atlantic Tropical Experiment (GATE) and the elucidation of their structure and properties are essential to the central objective of studying the interaction of cumulus convection with features of the large-scale circulation. Studies of the synoptic-scale disturbances have ranged from purely descriptive studies of their structure (Burpee, 1975; Reed *et al.*, 1977) to budget studies that seek to establish the roles of various physical processes in maintaining the balances of mass, heat, and moisture (Thompson *et al.*, 1979); vorticity (Shapiro, 1978; Stevens, 1979); momentum (Stevens, 1979); and kinetic energy (Norquist *et al.*, 1977). Taken collectively, these studies provide an unusually complete and detailed definition of the disturbance characteristics and hence provide numerical modelers with an excellent means of judging the performance of their models in simulating tropical weather systems.

This paper is concerned only with the mass, moisture, heat, and kinetic energy budgets, since other participants in the seminar will discuss the general structure and behavior of the waves and their momentum and vorticity budgets. The results presented are taken mostly from the aforementioned papers of Norquist *et al.* (1977) and Thompson *et al.* (1979). The reader is referred to these papers for a detailed discussion of the methodology employed and for the pertinent equations. Here we will concentrate on the results, giving only enough background to make them understandable.

All results are for Phase III (August 30-September 19) when the wave disturbances were best developed. Mass, moisture, and heat budgets apply to the B-scale area. Measurements were made at 3-h intervals, and each set of measurements was assigned to one of eight wave sectors or categories: the sectors centered about the trough and ridge axes (categories 4 and 8), the axes of maximum northerly and southerly wind components (categories 2 and 6), and the four intermediate sectors (categories 1, 3, 5, and 7). Categorization is based on the 700-mbar meridional wind component at the center of the B-scale network. The 3-h measurements are based on fitted values of the meteorological variables. At least-squares linear fit in time and a quadratic fit in sapce were employed.

Surface-sensible heat flux and evaporation are derived from the bulk aerodynamic method applied to shipboard measurements of temperature,

humidity, and wind. Precipitation amounts are obtained from Hudlow's hourly estimates, based on radar measurements. Radiative flux divergences are taken from the work of S. K. Cox and K. T. Griffith (Colorado State University) and surface radiative fluxes from shipboard observations.

Kinetic energy budgets are determined separately for land and ocean areas. The areas are bounded by latitudes 1° S and 26° N and longitudes 10° E and 31° W and have a common boundary at 15° W. A basically similar method of compositing is employed as that described above.

II. RESULTS

A. *Mass Budget*

This budget is shown because of its crucial role in later budgets. Only the vertical part of the mass circulation ($\omega = dp/dt$) is displayed (Figure 1). The figure depicts the average vertical velocity over the B-scale area as a function of height and wave position. *R*, *N*, *T*, and *S* refer to the ridge, northerly wind, trough, and southerly wind regions of the wave, respectively. Since the waves averaged about 3½ days in period and 2500 km in wavelength, the abscissa can be regarded as either a time or space axis of these dimensions.

From the figure, it is apparent that the motion is almost always upward, net subsidence taking place only at upper levels in the ridge region. Strongest upward mass flux of nearly 200 mbar per day (about 2 cm sec^{-1}) occurs somewhat ahead of the trough at the 700-mbar level. The level of maximum is much lower than in western Pacific systems (Reed and Recker, 1971).

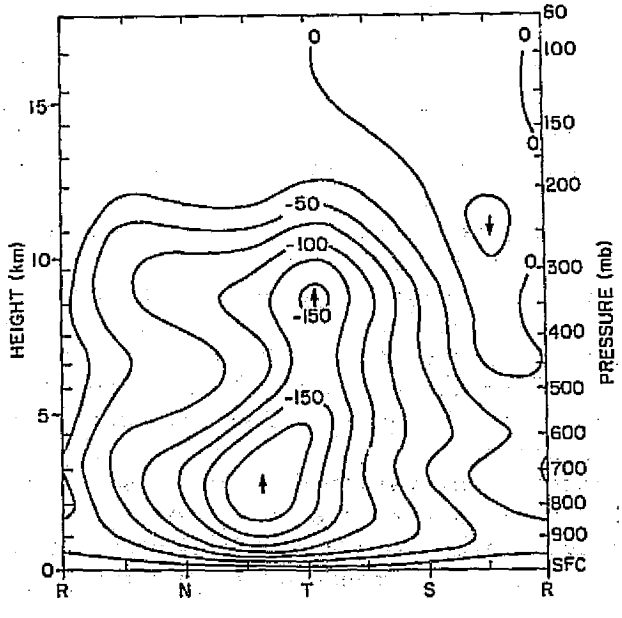

FIGURE 1 Vertical cross section of vertical velocity (dp/dt). Units: 10^{-5} mbar sec^{-1} (approximately mbar day^{-1}) R, ridge axis; T, trough axis.

TABLE 1 Moisture Budget for B-Scale Area (mm Day^{-1})

Wave Category	A_q	= $-D_q$	$-P_0$	$+E_0$	+Residual
1	2.4	7.2	- 3.5	2.8	-4.1
2 (Northerly)	1.0	13.3	-15.0	3.4	-0.7
3	2.3	21.0	-18.5	3.8	-4.0
4 (Trough)	3.6	22.6	-23.4	4.1	0.3
5	-1.0	12.0	-20.3	4.3	3.0
6 (Southerly)	-3.5	3.5	- 7.3	4.3	-4.0
7	-2.1	0.9	- 6.8	4.2	-0.4
8 (Ridge)	-2.7	0.1	- 4.9	3.7	-1.6
MEAN	0.0	10.1	-12.5	3.8	-1.4

B. Moisture Budget (Table 1)

The appropriate equation is represented symbolically at the top of the table. All terms apply to the total atmospheric column. The following definitions are used: A_q, storage or accumulation rate of water vapor; D_q, horizontal divergence of water vapor; P_0, precipitation rate; E_0, surface evaporation rate.

In the phase mean, the precipitation rate (12.5 mm day^{-1}) is almost exactly balanced by the sum of the horizontal moisture convergence (10.1 mm day^{-1}) and the evaporation (3.8 mm day^{-1}). Thus in the GATE Intertropical Convergence Zone (ITCZ) nearly three times as much moisture is imported from the surrounding atmosphere as is supplied from the ocean surface. The cause of the residual is not known. It could simply reflect the errors of measurement.

The wave produces a sizable modulation of most terms in the budget. The variations in moisture convergence and precipitation rate are especially large. A lesser fluctuation occurs in the moisture storage, and still lesser in the evaporation, which is controlled almost entirely by the wind speed. Residuals are generally small and vary erratically.

C. Sensible Heat Budget (Table 2)

Additional definitions are: A_S, storage rate of sensible heat (dry static energy); D_S, horizontal divergence of dry static energy; L, latent heat of condensation; S_0, surface sensible heat flux; Q_R, radiative flux divergence or heating. From the table, it is apparent that in the mean the condensation heating is balanced mainly by the sum of the net horizontal outflow of dry static energy and the radiative cooling, the latter being about half of the former. The surface flux is relatively small, and the residual is essentially zero. The principal wave modulation of the budget occurs in the heat outflow and condensation heating terms.

TABLE 2 Sensible Heat Budget for B-Scale Area (W m^{-2})

Wave Category	A_S =	$-D_S$	$+LP_0$	$+S_0$	$+Q_R$	+Residual
1	28	-148	101	14	- 95	156
2 (Northerly)	-62	-307	431	21	-139	- 68
3	27	-439	532	26	-116	24
4 (Trough)	-26	-573	670	30	-114	- 39
5	2	-366	582	30	-126	-118
6 (Southerly)	25	-179	211	25	-122	90
7	12	- 49	196	20	-118	- 37
8 (Ridge)	- 6	- 1	141	17	-143	- 20
MEAN	0	-258	358	23	-122	- 1

D. Total Heat Budget (Table 3)

This is the moist static energy (h) budget obtained by multiplying Table 1 by L and summing with Table 2. In the mean, the horizontal import is small, indicating that generally air of slightly higher moist static energy converges into the area at low levels than diverges from it aloft. Surface evaporation and, to a lesser extent, sensible heat transfer from the ocean also supply moist static energy to the column. The compensating loss is by radiative cooling. An unexplained negative residual is required for balance. The wave modulation is somewhat erratic. Generally it shows largest import and storage in advance of the wave trough and largest energy supply from the ocean in the vicinity of the trough.

By considering the total heat budget for thin layers, it is possible to determine the vertical distribution of heating by eddy (cumulus) transport and, by integration from the surface, the vertical distribution of

TABLE 3 Total Heat Budget for B-Scale Area (W m^{-2})

Wave Category	A_h =	$-D_h$	$+S_0$	$+LE_0$	$+Q_R$	+Residual
1	97	59	14	79	- 95	40
2 (Northerly)	-32	76	21	97	-139	-87
3	93	164	26	108	-116	-89
4 (Trough)	77	77	30	114	-114	-30
5	-27	-22	30	121	-126	-30
6 (Southerly)	-77	-78	25	122	-122	-24
7	-48	-22	20	119	-118	-47
8 (Ridge)	-83	0	17	95	-143	-52
MEAN	0	32	23	107	-122	-40

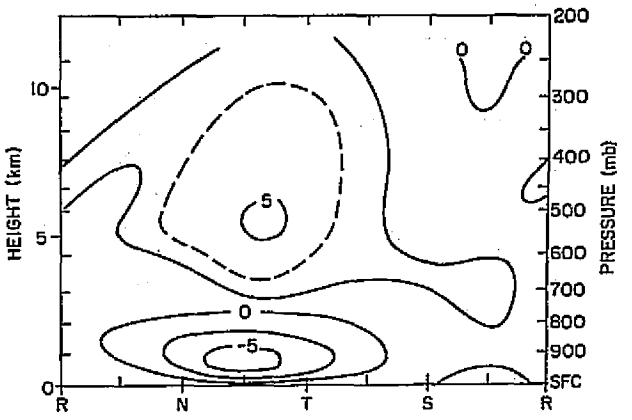

FIGURE 2 Vertical distribution of cumulus heating as function of wave position. Units: 10^{-2} W kg^{-1} (or approximately °C day^{-1}).

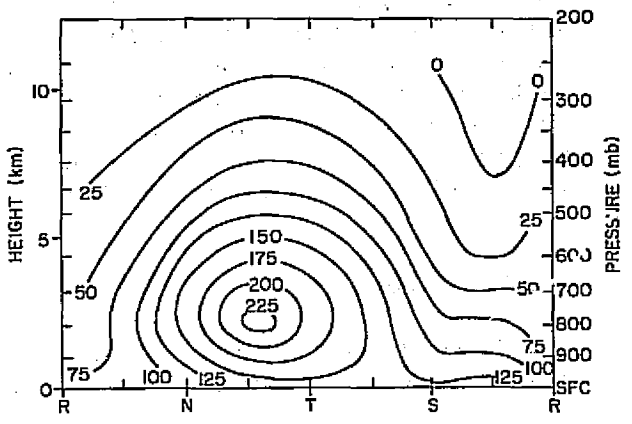

FIGURE 3 Vertical eddy flux of total heat or moist static energy as function of wave position. Units: W m^{-2}.

the eddy heat flux. These are shown for different wave categories in Figures 2 and 3. Below 800 mbar, in the convectively active part of the wave, a cooling is indicated. Here the large-scale flow supplies energy that is carried aloft by the convection. The energy is deposited at upper levels, resulting in widespread heating that has its largest magnitude at the 500-mbar level. Correspondingly, the maximum vertical eddy flux occurs ahead of the wave trough at 800 mbar.

E. Surface Energy Budget (Table 4)

Newly defined symbols are R_0, net incoming radiation (solar plus infrared) at the surface, and G, net downward heat flux at the surface (radiative and turbulent) obtained as a residual. According to the measurements, in the mean the net incoming radiative energy is utilized primarily for evaporation and secondarily for sensible heat transfer to the atmosphere (Bowen ratio of 0.21). Heat flux into the ocean is essentially zero. Because of errors of measurement, it is possible that the latter flux is positive as in adjoining regions, where insolation is greater than

TABLE 4 Surface Energy Budget for B-Scale Area (W m^{-2})

Wave Category	R_0	=	LE_0	$+S_0$	$+G$
1	174		79	14	81
2 (Northerly)	95		97	21	-23
3	55		108	26	-79
4 (Trough)	104		114	30	-40
5	121		121	30	-30
6 (Southerly)	123		122	25	-24
7	192		119	20	53
8 (Ridge)	170		95	17	58
MEAN	129		107	23	- 1

in the ITCZ, but it is almost certainly smaller than in these regions. There is a substantial modulation of the surface energy budget with wave passage. Above, average net incoming radiation in the ridge is associated with temporary heat storage in the ocean. Below, average radiation in the trough is associated conversely with a return energy flux to the atmosphere. Sensible and latent heat fluxes also contribute to the oceanic fluctuations being larger in the vicinity of the troughs than the ridges.

F. Wave Energetics

These are given in Figure 4, which employs the familiar Lorenz energy diagram. Numerical estimates are taken from Norquist *et al.* (1977) and

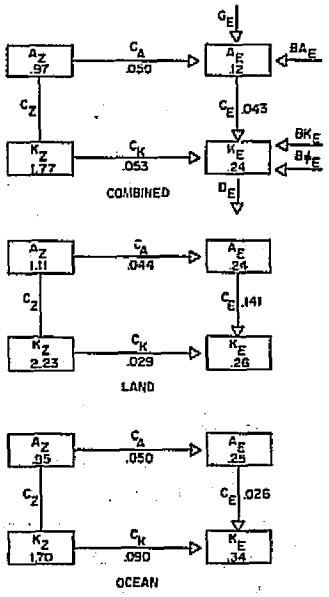

FIGURE 4 Partitioned energies (10 J m^{-2}) and energy conversion rates (W m^{-2}) for West Africa (top) and eastern Atlantic (bottom). Symbols are defined in text.

are based on the Quick Look Data Set. Measurements now in progress, using superior analytical techniques and final validated data, fail to reveal any important differences from these early results. Quantities appearing in the diagram are A_Z and A_E, the zonal and eddy available potential energies; K_Z and K_E, the zonal and eddy kinetic energies; and C_A, C_E, and C_K, the conversion rates from A_Z to A_E, A_E to K_E, and K_Z to K_E, respectively.

Our principal object here is to note the processes responsible for the generation and maintenance of the wave or eddy kinetic energy. Perhaps surprising are the large differences in the conversion rates between land and ocean regions. Over land the eddy kinetic energy is maintained largely by the conversion from eddy available potential energy, C_E. The conversion from zonal kinetic energy, C_K, makes a much lesser contribution. Over the ocean the roles are reversed. In both regions, the conversion of zonal to eddy available potential energy is intermediate in size.

Our present conclusion is that the waves over Africa owe their origin in part to dry baroclinic and barotropic processes connected with the instability of the midtropospheric jet stream that forms south of the Sahara in summer. However, condensation heating produced by cumulus convection also plays a major role in their formation, supplying eddy available potential energy as in tropical Pacific disturbances (Nitta, 1972). Over the eastern Atlantic, condensation heating no longer is a major contributor to the wave growth, and the waves draw their kinetic energy from the zonal current. They are at this stage in a declining phase.

Theoretical and modeling studies (Rennick, 1976; Pedgley and Krishnamurti, 1976; Walker and Rowntree, 1977; Mass, 1978) give quite varied pictures of the energetics of the easterly waves. Evidently a correct simulation of the wave energetics poses a formidable problem for numerical modelers.

REFERENCES

Burpee, R. W. (1975). Some features of synoptic-scale waves based on compositing analysis of GATE data. *Mon. Wea. Rev. 103*, 921-925.

Mass, C. (1978). *A Numerical and Observational Study of African Wave Disturbances*, Ph.D. thesis, U. of Washington, Seattle.

Nitta, T. (1972). Energy budget of wave disturbances over the Marshall Islands during the years 1956 and 1958. *J. Meteorol. Soc. Jpn. 50*, 71-84.

Norquist, D. C., E. E. Recker, and R. J. Reed (1977). The energetics of African wave disturbances as observed during Phase III of GATE. *Mon. Wea. Rev. 105*, 334-342.

Pedgley, D. E., and T. N. Krishnamurti (1976). Structure and behavior of a monsoon cyclone over West Africa. *Mon. Wea. Rev. 104*, 149-167.

Reed, R. J., and E. E. Recker (1971). Structure and properties of synoptic-scale disturbances in the equatorial western Pacific. *J. Atmos. Sci. 28*, 1117-1133.

Reed, R. J., D. C. Norquist, and E. E. Recker (1977). The structure and properties of African wave disturbances as observed during Phase III of GATE. *Mon. Wea. Rev. 105*, 317-333.

Rennick, M. A. (1976). The generation of African waves. *J. Atmos. Sci. 33*, 1955-1969.

Shapiro, L. J. (1978). The vorticity budget of a composite African tropical wave disturbance. *Mon. Wea. Rev. 106*, 806-817.

Stevens, D. E. (1979). Vorticity, momentum, and divergence budgets of synoptic-scale wave disturbances in the tropical eastern Atlantic. *Mon. Wea. Rev.* (to be published).

Thompson, R. M., Jr., S. W. Payne, E. E. Recker, and R. J. Reed (1979). Structure and properties of synoptic-scale wave disturbances in the Intertropical Convergence Zone of the eastern Atlantic. *J. Atmos. Sci. 36*, 53-72.

Walker, J., and P. R. Rowntree (1977). The effect of soil moisture on circulation and rainfall in a tropical model. *Quart. J. R. Meteorol. Soc. 103*, 29-46.

DISCUSSION
W. Frank, *Rapporteur*

The most recent analyses of the easterly waves in the A/B array generally supported earlier findings for western Africa and the eastern Atlantic. The good agreement between the moisture budgets and radar precipitation estimates was emphasized.

With respect to wave energetics it was noted that convective systems in the A/B array seemed to contain much larger amounts of relatively shallow convection (tops below 400-500 mbar) than has been indicated in intensifying systems elsewhere.

The high percentage of shallow clouds may be related to differences in the production of eddy kinetic energy between western Africa and the eastern Atlantic. In western Africa, where deep cumulonimbus activity occurs more frequently than in the eastern Atlantic, the baroclinic conversion of eddy potential energy to eddy kinetic energy is relatively large, while in the A/B array, where shallow convection is far more prominent, the conversion from eddy potential energy to eddy kinetic energy is relatively small. It was also noted that the lack of significant baroclinic energy conversion on the wave scale over the eastern Atlantic does not preclude the possibility of significant kinetic energy generation of this kind on smaller scales within the wave.

INDIVIDUAL TIME PERIOD A/B ARRAY BUDGET ANALYSIS

William M. Frank
University of Virginia

INTRODUCTION

The GATE rawinsonde data set is used to analyze vertically integrated budgets of dry static energy (s) and moisture (q) for the A/B area at each rawinsonde observation time during the three phases. Net condensation is derived as a residual in each budget and compared with master-array radar rainfall. Relationships between the mean tropospheric temperature and latent heat release are explored, and diurnal variations of temperature and precipitation are determined.

DATA AND ANALYSIS

Rawinsonde data were taken from the GATE-processed and -validated data tapes, and data flagged as suspicious by Center for Environmental Assessment Services (CEAS) were eliminated. Phase III radiation data from Cox and Griffith (1978; 1979) were extrapolated to Phases I and II using radar rainfall data (Frank, 1979). Radar precipitation values are from Hudlow and Patterson (1978).

Divergences were computed by fitting wind data from the seven USSR ships and the VANGUARD to a plane of least squares. Less accurate B-array winds were used only in advection computations.

Temperature and moisture observations were analyzed as deviations from individual ship phase means to remove persistent biases. Small corrections for solar heating errors were applied in the analyses of the diurnal cycle and the net tropospheric temperature.

The dry static energy and water vapor budget equations are

$$\frac{\partial \bar{s}}{\partial t} + \overline{\vec{\nabla} \cdot \vec{v}s} + \frac{\partial \overline{s\omega}}{\partial p} = Q_R + \frac{L}{c_p}(c - e),$$

$$\frac{L}{c_p}\left(\frac{\partial \bar{q}}{\partial t} + \overline{\vec{\nabla} \cdot \vec{v}q} + \frac{\partial \overline{q\omega}}{\partial p}\right) = \frac{-L}{c_p}(c - e).$$

The vertical fluxes were assumed to be zero at 100 mbar, and surface fluxes were obtained by the bulk aerodynamic method.

MEAN BUDGETS

Table 1 compares time-averaged moisture budget results of Frank (1979), Thompson *et al.* (1979), and Dewart and Gray (1979) with radar rainfall (Hudlow and Patterson, 1978). Each budget study used different computational procedures, but agreement was good. All the budgets diagnosed more rainfall than was estimated by the radar--perhaps because of inability to resolve fully the large-scale mean moisture advection.

Time series of condensation derived from the Phase III dry static energy budget were compared with radar rainfall estimates. Despite the difference in sampling areas, the two methods produced similar profiles during most major convective episodes. There was a mean lag of about 4-6 h between the estimates (Table 2), which seemed to result from storage of liquid water (Frank, 1979). Distinctions between condensation and precipitation are important when estimating latent heat release.

NET TROPOSPHERIC TEMPERATURE

Deviation temperatures from B-array ships were used to analyze variations in the net temperature of the surface--100-mbar layer ($\overline{\Delta T_B}$). Temperatures corrected to remove assumed solar radiation errors are written $\overline{\Delta T_B}(c)$. Mean diurnal variations of these temperatures for all of GATE are shown in Figure 1a, along with the net Phase III radiational cooling. Maximum temperatures occurred near 1200 local time (LT). The troposphere warmed

TABLE 1 GATE Precipitation Estimates (g cm^{-2} day^{-1})

	Total Required/ Measured Rainfall	- Storage	Horizontal Moisture Convergence	Surface Evaporation
All GATE				
Dewart and Gray (A/B area)	1.53	0	1.06	0.47
This study (A/B area)[a]	1.41[a]	0.03	1.00	0.38[a]
This study (A/B area)	1.36	0.04	0.95	0.37
Radar (master array)	1.02	--	--	--
Phase III				
Thompson *et al.* (B-scale area)	1.33	0	0.95	0.38
This study (A/B area)	1.35	0.03	0.91	0.41
Radar (master array)	1.12	--	--	--

[a]Includes data from 21 GMT July 30, 1974, to 18 GMT August 2, 1974

TABLE 2 Lag Time between s-Budget A/B-Scale Condensation and Master-Array Radar-Observed Precipitation

Day	Time of s-Budget Condensation Maximum[a]	Time of Radar Rainfall Maximum (Hour Ending)	Peak Lag (Hours)[b]
183	06 GMT	14 GMT	8
188[c]	09	17	8
194	18	19	1
224[c]	06	10	4
245	09	17	8
247	12	21	9
255[c]	09	14	5
256[c]	12	18	6
259[c]	03	6	3
Mean			5.8
In situ Mean[c]			5.2

[a]Time of maximum is defined as the time when the condensation/rainfall either (a) "plateaus" (increases to a value within 75% of the event maximum but fails to increase by more than 1°C in the next 6 h) or (b) "peaks" (obtains a clear maximum event value that is not preceded by a plateau).
[b]Time at which s-budget condensation reached peak or plateau minus time of radar peak/plateau.
[c]Convection developed locally (*in situ*) within master array.

rapidly in the morning hours beginning before sunrise and cooled more slowly from local noon through about 03 LT (Figure 1b).

The temperature budget may be written:

$$\frac{\partial \overline{\Delta T_B}}{\partial t} + \overrightarrow{\overline{v}} \cdot \overrightarrow{\nabla} (\overline{\Delta T_B}) - \overline{Q_R} = \left[\overline{\omega (\Gamma_d - \Gamma)}\right] + \left[\overline{\frac{L}{c_p} (c - e)}\right] = Q_v,$$

where $\overline{Q_R}$ and $(L/c_p)(c - e)$ are the net heating of the column due to radiation and latent heating, respectively, and the brackets denote averages from the surface to 100 mbar. The bracketed terms ($= Q_v$) are the net warming due to vertical processes (vertical advection, moist convection). Figure 1c shows that Q_v was maximum during the morning and dropped to near zero in the afternoon. This was a very regular phenomenon (Frank, 1979), which also occurs elsewhere in the tropics and at higher latitudes (Foltz and Gray, 1979). It results from a large-scale diurnal circulation process--perhaps the S-1 solar tide. It is not closely related to latent heat release, which showed a mean diurnal variation during GATE (Figure 1d) but which was heavily concentrated in sporadic episodes.

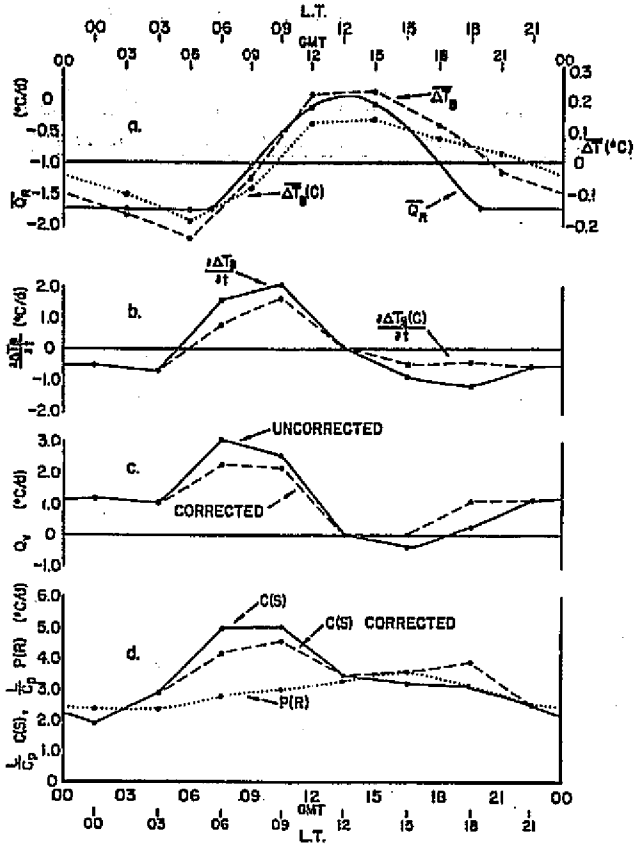

FIGURE 1 Diurnal variations of a, Radiative heating ($\overline{Q_R}$), net tropospheric temperature ($\overline{\Delta T_B}$), and net temperature corrected for solar radiation-induced error, [$\overline{\Delta T_B}(c)$]. b, Time rates of change of ΔT_B and $\overline{\Delta T_B}(c)$. c, Vertical process warming (Q_V) computed with $\overline{\Delta T_B}$ (uncorrected) and $\overline{\Delta T_B}(c)$ (corrected). d, Latent heat release due to s-budget condensation [$c(s)$], s-budget condensation computed using $\overline{\Delta T_B}(c)$ (corrected), radar precipitation [$P(R)$].

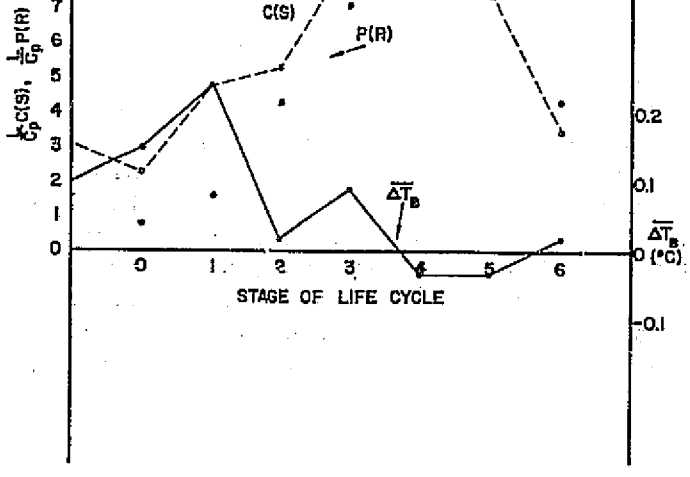

FIGURE 2 s-Budget condensation heating, radar rainfall estimated heating, and net temperature during composite convective-system life cycle. Stages are at approximately 3-h intervals. Maximum rain at stage 4.

WARMING DUE TO LATENT HEAT RELEASE

Figure 2 compares $\overline{\Delta T_B}$ with budget condensation and radar rainfall during the life cycle of a composite of GATE convective systems (Frank, 1978). Except for a small peak near the beginning there was no net increase in tropospheric temperature despite the large increase in latent heat release. Correlations between temperature changes and latent heat release were small and negative during GATE. These and related results imply that storage of sensible heat in the tropical troposphere is very small on the time and space scales of mesoscale convective systems. Released latent heat must be rapidly dispersed to larger scales.

CONCLUSIONS

The GATE rawinsonde data set is of sufficient quality to allow various quantitative analyses of the A/B area at individual observation times. In this study budgets of moisture and dry static energy were compared with radar rainfall showing a systematic lag believed to result from storage of liquid water. The net temperature of the troposphere on the B scale was found to undergo a regular dirunal cycle out of phase with solar heating alone. Latent heat release was found to have little effect on net temperatures on resolvable time and space scales.

REFERENCES

Cox, S. K., and K. T. Griffith (1978). Tropospheric radiative divergence during Phase III of the GARP Atlantic Tropical Experiment (GATE). Atmospheric Science Paper #291, Colorado State University, Ft. Collins, Colo., 166 pp.

Cox, S. K., and K. T. Griffith (1979). Estimates of radiative divergence during Phase III of the GARP Atlantic Tropical Experiment, Part II: Analysis of Phase III results. *J. Atmos. Sci. 36*, 586-601.

Dewart, J. M., and W. M. Gray (1979). Diurnal variability in the GATE region. To be submitted.

Foltz, G. S., and W. M. Gray (1979). Diurnal variation of the troposphere's energy balance. *J. Atmos. Sci.*, to be published.

Frank, W. M. (1978). The life cycle of GATE convective systems. *J. Atmos. Sci. 35*, 1256-1264.

Frank, W. M. (1979). Individual time period analyses of the GATE A/B area. Submitted to *Mon. Wea. Rev.*

Hudlow, M. D., and V. L. Patterson (1978). GATE radar rainfall atlas. NOAA Special Report, Center for Environmental Assessment Services, August, 162 pp.

Thompson, R. M., S. W. Payne, E. E. Recker, and R. J. Reed (1979). Structure and properties of synoptic scale wave disturbances in the intertropical convergence zone of the eastern Atlantic. *J. Atmos. Sci. 36*, 53-72.

DISCUSSION
T. Carlson, *Rapporteur*

The discussion centered around the implications prompted by Figure 2, which implies that the condensation rate and net tropospheric warming on the A/B scale were not well correlated in large convective clusters. The question was raised why one needs to account for cloud and condensation on the A/B scale if tropospheric warming is not produced by large clusters in the array. A distinction was then drawn between condensation heating (Q) and the rate of atmospheric warming ($\partial T/\partial t$). It was also asked where the tremendous amount of heat released goes if it does not warm the system. Gray postulated that the heat was quickly dispersed, and the discussion became concerned with mechanisms for affecting this heat dispersal. It was also suggested that warming might occur on scales well below that of the A/B scale array over which the measurements were made. It was generally felt, however, that the atmosphere responded to the heating, first by a slight warming but later by motions that fully compensated for the warming, resulting in no net temperature change. The only lasting effect would then have been those motions induced by the heat release and by a change in atmospheric stability, since a net warming actually did occur in the upper troposphere and a net cooling occurred in the lower troposphere.

Additional discussion was related to the apparent lag between condensation and precipitation, the latter following the former by some 4-6 h. Also, it was pointed out that the moisture convergence was not always confined to the boundary layer but sometimes extended fairly uniformly over the lowest 300 mbar, as is seen in western ocean convective systems. It was suggested that the amount of liquid water storage might account for the delay but that the amount mentioned might be too large. In regard to the lag between precipitation and moisture convergence it was also noted that some precipitation peaks exactly coincided with maxima in the moisture convergence (with no lag involved); such episodes, however, generally involved relatively small fluctuations in precipitation.

Finally, a point was raised by some individuals that the question of heat sources and sinks cannot be resolved without a full atmopsheric model and without knowledge of the surface heating.

TROPICAL ANALYSIS OF LIKELY SIGNIFICANCE FOR LARGE-SCALE NUMERICAL MODELING

William M. Gray
Colorado State University

The following discussion synthesizes some of the observational and modeling analysis results that have been accomplished in recent years on the author's project that he believes to be of significance for the large-scale numerical modeling of the tropical atmosphere.

CONDENSATION-INDUCED TEMPERATURE CHANGE

Cumulus convection brings about no significant net tropospheric temperature change at the time and place it occurs. Rain-area upper-tropospheric temperature increase is typically balanced by a lower-tropospheric temperature decrease. This upper-level warming and lower-level cooling can result in a net tropospheric thickness increase and slight lowering of surface pressure by virtue of the ($\delta P/P$) coefficient influence on pressure thickness

$$\Delta Z = \frac{R}{g} \int_{P_1}^{P_2} T \frac{\delta P}{P} .$$

Such slight surface-pressure drops without consequent net tropospheric warming act to maintain the tropical disturbance. The primary influence of cumulus convection in the typical disturbance is thus one not of net temperature increase but rather of rearranging the temperature in the vertical (see Frank, 1978; Grube, 1979).

The detectable temperature change occurring in the tropical atmosphere in both convective and nonconvective regions is primarily a result of response to diurnal variations in tropospheric radiational energy loss and not to direct condensation-induced temperature change (see Grube, 1979; Dewart, 1978).

Recent studies at Colorado State University of wind-pressure adjustment by W. Schubert, P. Silva Dias, and W. Fingerhut indicate that at tropical locations where f and Z_r are small (for mesoscale or smaller-scale motion) the mass field adjusts to the winds. In general, temperature increase on the mesoscale or smaller scale occurs only when the mass field sinks and warms in adjustment response to a stronger momentum field. Temperature increase does not occur directly from the large condensation energy

releases in individual cumulus elements. Such local energy releases as occur with penetrative cumulus convection produce gravity waves, which rapidly disperse away any local accumulated temperature increases that the convection may have brought about. Thus, in a general sense, the influence of cloud convection on mesoscale temperature increase appears to be primarily that of the convective cloud's role in altering the momentum field and a consequent mass adjustment to such altered momentum fields. This has a large implication in regard to previous cumulus condensation heating ideas such as CISK and wave-CISK and quasi-wind-pressure balance assumptions. It appears that tropical modeling efforts should concentrate less on ways of parameterizing cumulus heating and more on the influences of cumulus momentum alteration and wind-pressure imbalances. We must also sort out the up versus down gradient ways of the cumulus mixing process. In the boundary layer and at the tropopause, Cb vertical mixing appears to be primarily an up-gradient process, and in the intermediate levels a down-gradient process.

LARGE DIURNAL CYCLE IN TROPICAL DISTURBANCE VERTICAL MOTION

A very large and quite unexpected diurnal cycle in oceanic tropical disturbance vertical motion is being detected, as indicated in Figure 1. This large diurnal morning maximum and evening minimum in vertical motion appears to be primarily a result of day versus night difference in tropospheric radiational cooling with a 3-6 h lag time (see papers of Gray and Jacobson, 1977; Fingerhut, 1978; McBride and Gray, 1978; Dewart, 1978; Frank, 1978; and Grube, 1979).

LARGE DIURNAL CYCLE IN TROPOSPHERIC SUBSIDENCE WARMING

A large diurnal cycle in tropospheric mass subsidence is, apparently, continually occurring throughout the tropics with 00-12 LT subsidence being 2-3 times larger than 12-24 LT subsidence. This morning subsidence maximum and evening minimum is a pervasive feature of the tropical atmosphere. It is independent of the diurnal characteristics of the local rainfall patterns. This subsidence cycle is primarily a result of day versus night differences (with a 3-6 h time lag) in tropospheric radiational cooling, which appears to manifest itself in one or a combination of three basic physical processes:

1. Large morning subsidence surrounding cloud cluster convection in response to the cluster's morning maximum of deep convection,
2. Larger morning sinking motion in Intertropical Convergence Zone (ITCZ) subtropical zones and anticyclones in response to larger diurnal morning versus weaker evening Hadley and Walker cell circulation variations; and
3. Larger morning-weaker evening subsidence due to a global diurnal tide driven by day versus night differences in net tropospheric radiational cooling (see papers by Foltz, 1976; Foltz and Gray, 1979, for more discussion).

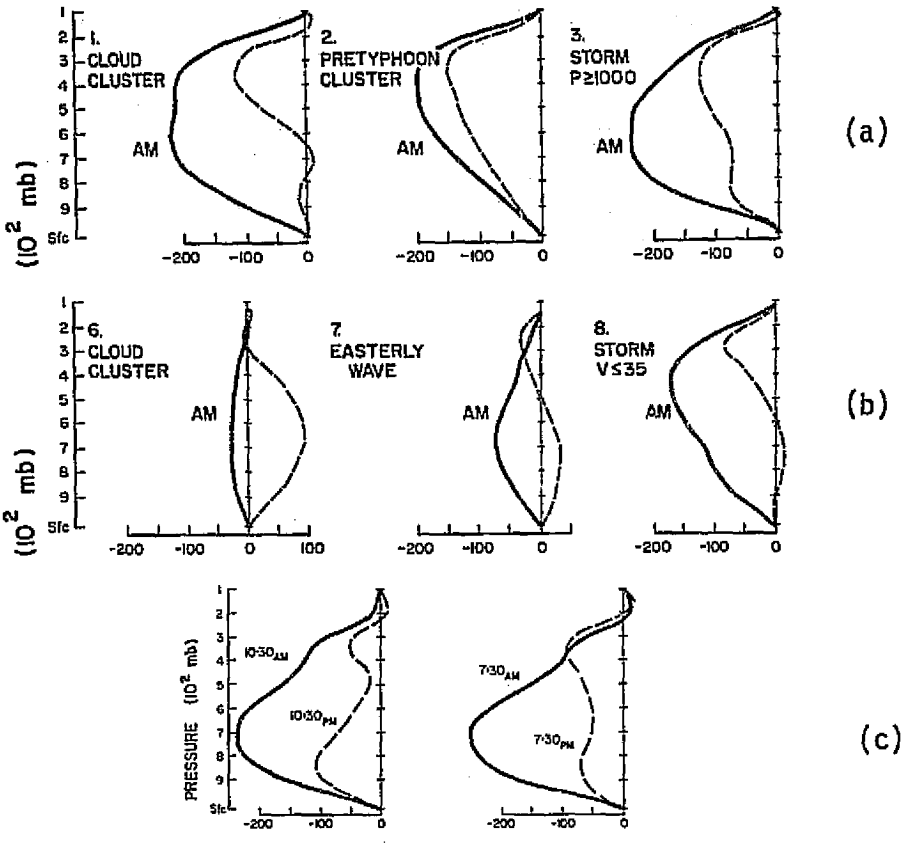

FIGURE 1 Morning versus evening mean vertical motion (r = 0-3° radius) in mbar/day for various tropical weather systems in (a) the western Pacific; (b) the western Atlantic; and (c) the A/B array for the 10 most convectively active days in GATE.

The importance of accounting for this large diurnal subsidence cycle in numerical models should be discussed.

IMPLICATIONS FOR THE MODELING OF TROPICAL CYCLONE FORMATION

Several numerical modelers have simulated the intensification process of tropical cyclones. These modeling efforts have not dealt with the question of cyclone genesis, however. Note in Table 1 how weak the typical tropical disturbance is in comparison with the initial cyclone strength assumed by the numerical modelers for their intensification experiments. The transformation of a disturbance to a cyclone has yet to be realistically modeled. Why? The author believes that this is due, for example, to lack of incorporation of basic physical processes necessary for genesis such as Cb cloud-induced momentum, enhanced evaporation due to downdrafts, and large-scale horizontal eddy influence of the environment. The physical importance of such processes has yet to be realized and generally tested.

TABLE 1 Recent Numerical Modeling Papers on Tropical Cyclone Intensification and Their Assumed Initial Lower-Tropospheric Cyclone Strength[a]

Modelers	Assumed Initial Maximum Wind Velocity and Radius of Maximum Wind		Vortex Vorticity Inside the Radius of Maximum Winds	Type of Vortex
	($m\ sec^{-1}$)	(km)	($10^{-6}\ sec^{-1}$)	
Kuo (1965)	10	141	142	Symmetrical
Yamasaki (1968)	4.7	100	94	Symmetrical
Ooyama (1969)	10	50	400	Symmetrical
Miller (1969)	10	200	100	Real vortex
Rosenthal (1970)	7	250	56	Symmetrical
Sundqvist (1970)	15	200	150	Symmetrical
Carrier (1971)	21	50	840	Symmetrical
Anthes *et al.* (1971a,b)	18	240	150	Asymmetrical
Anthes (1972)	18	240	150	Asymmetrical
Mathur (1972)	15	200	150	Asymmetrical
Harrison (1973)	~10	~120[b]	~170	Asymmetrical
Kurihara and Tuleya (1974)	12	200	120	Symmetrical
Ceselski (1974)	17	~100-150	~200	Real vortex
Kurihara (1975)	12	200	120	Symmetrical
Anthes (1977)	18	240	150	Symmetrical
Rosenthal (1978)	7.2	220	65	Symmetrical

Typical pre-cyclone cloud cluster vorticity is ~10-15 × $10^{-6}\ sec^{-1}$.

[a] From Gray (1979).
[b] Estimated from initial height field.

Most of the cyclone intensification models have been based on the CISK idea. This theory appears to offer an approximate explanation for the later-stage and inner-core region intensification of already developed cyclones but does not appear to be applicable for the early-stage cyclone formation and growth (see papers of Gray, 1977, 1979; McBride, 1979, for more discussion).

Only a small fraction (10-20 percent) of the mass converging into the disturbance results from boundary layer (~ surface to 900 mbar) frictional processes. Frictional veering over all oceanic regions averages but 10-15°. In tropical disturbances and at all stages of cyclone development there is a large down-pressure-gradient flow above and within the boundary layer that is not frictionally driven. Even in the hurricane stage, about 50 percent of the mass inflow at 4° radius occurs above 900 mbar. There is thus substantially more mass inflow into tropical disturbances and cyclones than can be explained from boundary-layer frictional processes.

Moist-static energy, h, can increase or decrease in the typical tropical disturbance through transfer from the sea by latent and sensible exchange, E_S, by radiation, R, or through horizontal transport on the boundaries, $\vec{V} \cdot \vec{\nabla}h$. Estimates of E_S and R for the inner 4° radius of tropical systems indicate that $E_S + R$ is slightly positive in weak disturbances but strongly positive in hurricanes, where large sea-surface energy input occurs. Steady-state, $\partial h/\partial t = 0$, hurricanes export large amounts of energy. They accomplish this through radial export of potential energy in their upper-level outflows. Idealized h budgets for the steady-state cloud cluster and hurricane are portrayed in Figure 2.

It is seen that the usual vertical circulations through the organized tropical weather system or cyclone typically produce an energy depletion of the system. The tropical system maintains itself only through energy received from the ocean (this is not true of GATE, in which surface energy flux is significantly less than in the western oceans). It is observed that most tropical systems weaken or die when this ocean energy source is cut off.

Thus, the transverse circulation of the tropical disturbance and cyclone is typically acting to decrease the energy of the system. Any process that acts to reduce this mean circulation is likely to lead to energy accumulation within the system and intensity increase. Conversely, any process leading to an enhancement of the radial circulation will lead to energy loss and system weakening. This idea is quite at variance with the long-held and prevailing view that increase in intensity of the mean radial circulation is positively related to increased intensity. Cumulus parameterization schemes that show energy accumulation depending on the magnitude of the mean upward circulation appear invalid. Intense and intensifying cyclones do not show stronger transverse circulations than do weak and filling systems. It should also be realized that frictional dissipation is a slowly acting process and that the momentum field of the tropical system will be only slowly influenced by a temporary lessening of the transverse circulation's cross-contour flow. A major portion

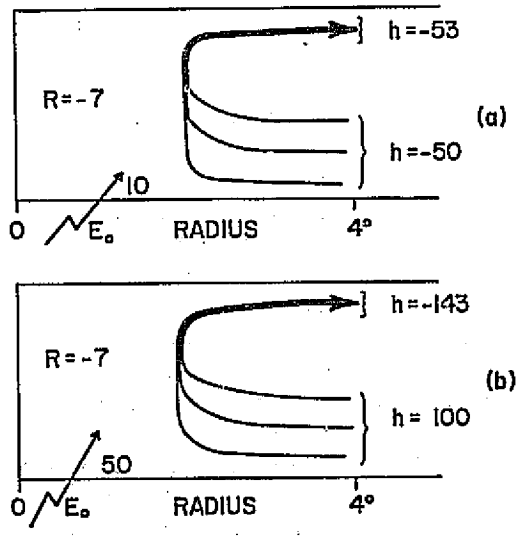

FIGURE 2 Schematic representation of the typical h budget within 4° radius (a) of the steady-state western ocean cloud cluster and (b) of the steady-state hurricane. Units are arbitrary.

of the hurricane's inward horizontal angular momentum flux necessary to balance friction is accomplished in the upper troposphere at large radius ($r > 4°$) through standing eddy processes that are independent of the cyclone's transverse circulation (see Frank, 1977; Gray, 1979; McBride, 1979).

It is the large-scale (radius 4-8°) lower (900 mbar) and upper (200 mbar) tropospheric vorticity differences that best distinguish between tropical disturbances that develop into cyclones from those that do not. Other parameters such as moisture, cloudiness, lapse-rate stability, vertical motion (if above 100 mbar/day for r = 0-3° area) show almost no distinguishing power for specifying the tropical disturbances that develop into cyclones from those that do not. It appears that what is needed for cyclone genesis is a favorable large-scale environment and not the specific characteristics of the disturbance itself. This favorable large-scale upper- and lower-tropospheric environment is hypothesized to be necessary for the establishment of more organized Cb cloud and squall lines with more active updrafts and downdrafts and for more favorable angular momentum advection into the systems. Tropical cyclone genesis and early growth appear to be fundamentally related to small-scale torque spin-up due to Cb updrafts and downdrafts. Such Cb momentum influences should likely be incorporated in cyclone genesis models. It appears that tropospheric temperature increases necessary for cyclone genesis are not a result of enhanced water vapor convergence and condensation due to an increase of the transverse circulation into the incipient disturbance but rather to a sinking warming response of the cyclone's mass field to supergradient wind fields established by the special small-scale action of Cb updrafts and downdrafts in a favorable vertical shear environment [see Gray, 1979; McBride, 1979; and Fingerhut's (1979) recent numerical modeling results].

Our recent observational and numerical modeling results are also indicating that latent and sensible heat transfer from the ocean (as calculated from the h budget) are considerably larger--by factors of 2-3--than that specified by the bulk formula. This is believed a consequence of the bulk formula's not accounting for the effects of Cb downdrafts on surface-wind increase and drying.

LARGE-SCALE FORCING MECHANISMS OF OCEANIC TROPICAL CONVECTION

We have attempted to estimate the relative magnitudes of the various summertime large-scale low-level (850 mbar) forcing mechanism in the GATE region and for the western Atlantic (15-30° N) and western Pacific (5-20° N). These are shown in Table 2. More discussion is contained in the report by McBride and Gray (1978). There are a number of conclusions that can be drawn from these results.

The major contribution to the net convergence of tropical weather systems in GATE and the western Pacific area comes from ITCZ forcing. The overwhelming role played by diurnal variation of the Hadley-Walker cell circulations and of the cloud cluster and its surrounding region circulations must be realized. This large diurnal contribution has yet to be fully documented and appreciated. Its possible significant ramifications

TABLE 2 Estimated Typical Magnitude of Various Large-Scale 850-mbar Vertical Motion Forcing Components (mbar/Day)

Magnitude of Lower Tropospheric Vertical (~850 mbar) Motion in a Convective Weather System	=	(A) ITCZ Forcing	+	(B) Diurnal Modulation of ITCZ Forcing	+	(C) Easterly Wave Forcing	+	(D) Frictional Convergence	+	(E) Cluster Scale Diurnal Modulation	+	(F) Convective Feedback in Cluster Region
Region	Term	(1)		(2)		(3)		(4)		(5)		(6)
				AM/PM				Trough/ Ridge		AM/PM		
Western Pacific		-30		0		∓20		-7		∓60		-20
Western Atlantic		+10		± 5		∓15		-4		∓40		-25
GATE		-80		∓45		∓30		-3		∓30		-40

for cumulus parameterization and large-scale modeling has yet to be investigated.

Another point that needs to be discussed is the relative role of easterly waves as a large-scale forcing mechanism. GATE was a region (downwind from West Africa) of especially strong waves and significant wave modulation of convection. But GATE rainfall also occurred without significant wave passage. Observational studies in other oceanic regions where wave forcing is weaker than in GATE indicate a weaker wave modulation to convection. It must be realized that very heavy and long-lasting oceanic rainfall often occurs over low-latitude oceanic regions because of ITCZ variations and without apparent easterly wave association.

It is time that the magnitude of the typical tropical wave forcing of convection be seen in comparison with other major forcing mechanisms. Easterly waves are only one of a number of important large-scale forcing mechanisms.

Our observational analysis also indicates that boundary-layer frictional convergence plays only a minor role in the large-scale forcing of organized tropical convection. Boundary-layer convergence associated with easterly waves also is typically quite small. Thus, the important roles previously ascribed to the physical processes associated with the so-called CISK and wave-CISK hypotheses appear to overly exaggerate the role that low-level frictionally driven convergence plays in tropical-weather-system dynamics.

DISCUSSION

It appears that tropical modeling efforts have (because of lack of observations) suffered from too much deduction and not enough induction. We are only beginning to observe the tropical atmosphere in enough detail to learn of some of its important physical processes. Much more empirical information must still be gathered. It is questionable to what extent a realistic physical synthesis necessary for successful tropical modeling

can be accomplished at this time. I like a passage from one of Jacob Bronowski's books:

> Until a science has passed through a long stage of observation and trial, it cannot develop a system of ordering its observations; and it is mere presumption to try to fit it with so ambitious an order as Newton's [i.e., PE modeling].

Has tropical meteorology passed through a long enough observation and trial period?

REFERENCES OF AUTHOR'S PROJECT PAPERS

Dewart, J. M. (1978). The diurnal variability in the GATE region. Dept. of Atmos. Sci. Paper No. 298, Colo. State U., Ft. Collins, Colo., 80 pp.

Fingerhut, W. A. (1978). A numerical model of a diurnally varying tropical cloud cluster disturbance. *Mon. Wea. Rev. 106*, 255-264.

Fingerhut, W. A. (1979). Modeling studies of tropical cyclone genesis. Forthcoming Ph.D. Thesis, Dept. of Atmos. Sci., Colo. State U., Ft. Collins, Colo.

Foltz, G. S. (1976). Diurnal variation of the tropospheric energy budget. Dept. of Atmos. Sci. Paper No. 262, Colo. State U., Ft. Collins, Colo., 141 pp.

Foltz, G. S., and W. M. Gray (1979). Diurnal variation of the troposphere's energy balance. *J. Atmos. Sci.* to be published.

Frank, W. M. (1977). The structure and energetics of the tropical cyclone, Paper II: Dynamics and energetics. *Mon. Wea. Rev. 105*, 1136-1150.

Frank, W. M. (1978). Diagnostic analyses of the GATE A/B scale area at individual time periods. Dept. Atmos. Sci. Paper No. 297, Colo. State U., Ft. Collins, Colo., 102 pp.

Gray, W. M. (1977). Tropical disturbance to cyclone transformation. Paper prepared for the 11th Tech. Conf. on Hurricanes and Tropical Meteorology, Dec. 13-16, Miami Beach, Fla., pp. 27-34.

Gray, W. M. (1979). Hurricanes: their formation, structure and likely role in the tropical circulation, in *Meteorology Over the Tropical Oceans*, supplement to *Quart. J. R. Meteorol. Soc. 105*, 155-218.

Gray, W. M., and R. J. Jacobson, Jr. (1977). Diurnal variation of deep cumulus convection. *Mon. Wea. Rev. 105*, 1171-1188.

Grube, P. G. (1979). Convection induced temperature change in GATE. Dept. of Atmos. Sci. Paper No. 305, Colo. State U., Ft. Collins, Colo., 128 pp.

McBride, J. L., and W. M. Gray (1978). Mass divergence and vertical velocity in tropical weather systems, Part I: Diurnal variation; Part II: Large scale controls on convection. Dept. Atmos. Sci. Paper No. 299, Colo. State U., Ft. Collins, Colo., 109 pp.

McBride, J. L. (1979). Observational analysis of tropical cyclone formation. Dept. of Atmos. Sci. Paper No. 308, Colo. State U., Ft. Collins, Colo., 230 pp.

DISCUSSION
T. Carlson, *Rapporteur*

The discussion centered primarily on two issues: (1) the mechanisms by which convective disturbances (i.e., cloud clusters) are able to grow into vortical disturbances (i.e., tropical cyclones) from an initial weak state and (2) the nature of the diurnal oscillations in the precipitation and the vertical motion patterns that are possibly radiationally forced. One of the five topics Gray discussed, that tropical disturbances intensify by external forcing because of eddy import of momentum at high levels and by vertical momentum rearrangement of momentum between high and low levels in cumulonimbus up and downdrafts, was questioned, especially on the latter point. Gray conceded that he was unsure exactly how such cumulonimbus momentum exchanges occur; but studies of several convective systems seemed to support the physical concept that convective clusters developed into tropical cyclones only in those regions where the large-scale vorticity was more cyclonic than normal in the lower troposphere and more anticyclonic than normal in the upper troposphere. He suggested that the formation of the upper anticyclone was to a large extent independent of the convective system itself and is set up by environmental flow conditions. He was asked how intensification of cyclones would occur if there was a retardation in radial circulation (as Gray hypothesizes). He showed observational data that indicate that an eddy import (advection) of vorticity rather than additional convergence associated with an increased radial circulation were responsible for the spin-up of the system and the balancing of the increased winds against frictional dissipation.

The diurnal forcing of vertical motion was discussed at some length. The likely role of radiational forcing as an explanation of this diurnal forcing on the cluster scale, ITCZ scale, continent-ocean scale, and tidal scale was made. Gray suggested that numerical modeling must account for all these effects and that, just as waves modulated convection, diurnal oscillations strongly modulate the wave convection. This modulation is stronger in the vertical motions than in the precipitation record. Gray was questioned with regard to the physical mechanisms for producing the observed diurnally forced vertical velocity oscillation since the radiational mechanism might not be able to account for the observed vertical motions. Rather, it was suggested that the radiation might act as a trigger for the latent heating that would further augment the vertical motions. Gray disagreed with the hypothesis, however, since the diurnal variations in rainfall are small in comparison with the diurnal variations in vertical motion.

5. Air-Sea Interactions

Organizer ..... G. Philander

Speakers ..... G. Philander
D. Halpern
C. Rooth

Session Chairman ..... G. Philander

Rapporteurs ..... D. Halpern
G. Philander

VARIABILITY OF SEA-SURFACE TEMPERATURES IN LOW LATITUDES

George Philander
NOAA Geophysical Fluid Dynamics Laboratory/Princeton University

Local thermodynamical processes determine the sea-surface temperature over most of the oceans, but not in the tropics. In the western equatorial Atlantic Ocean, for example, the local flux of heat from the atmosphere to the ocean has a secondary effect on the seasonal variation of the rate of heat storage (Merle, 1979). There, changes in heat storage (and hence sea-surface temperature) are caused primarily by vertical excursions of the thermocline. These movements of the thermocline are part of the dynamical response of the ocean to variable winds. To understand the variability of sea-surface temperature in low latitudes, it is necessary to understand this dynamical response of the ocean.

The prevailing winds in the tropics are from the east so that the warm surface waters accumulate along the western coasts of ocean basins. Hence, the thermocline slopes downward from east to west, and cold water is exposed along the eastern coasts of tropical oceans. (In the tropical Atlantic Ocean the sea-surface temperature along the western coast can be 5°C higher than along the eastern coast.) A sudden intensification of the easterly winds will, after an adjustment time T say, cause the east-west slope of the thermocline (and hence the zonal temperature gradient) to be more pronounced. Hence, if the winds vary only on time scales long compared with T, then the ocean is always in equilibrium with the wind--it has no memory on these time scales--and the sea-surface temperature gradient is directly proportional to the zonal wind stress. If, on the other hand, the winds fluctuate on a time scale short compared with T then the ocean is never in an adjusted state and the response is primarily wavelike. In the latter case, undulations (waves) propagate along the thermocline, whose large-scale slope is determined by the mean winds (Philander, 1979).

An estimate for the adjustment time T of the ocean can be obtained from the vorticity equation

$$\left(\nabla^2 - \frac{1}{\lambda_2}\right) \psi_t + \beta\psi_x = \text{forcing}, \qquad (1)$$

where λ is the radius of deformation, t denotes time, x longitude, β the latitudinal derivative of the Coriolis parameter, and ψ the stream function, which is related to the depth of the thermocline. Equation (1) describes the response of an idealized linear ocean to forcing. If

dispersive effects (associated with the Laplacian operator) are neglected, then the first two terms in Eq. (1) define a time scale T, where

$$T = L/\beta\lambda^2. \qquad (2)$$

For time scales long compared with T, the first term in Eq. (1) is unimportant, so that the only time dependence is implicit, through the variable forcing function. Hence T is in fact the adjustment time T discussed earlier. (The adjustment of the ocean is effected by Rossby waves. T is the time it takes a Rossby wave to propagate a distance L from the eastern coast; an equilibrium Sverdrup balance is established in the wake of these waves.) Veronis and Stommel (1956) first pointed out that according to Eq. (2) large-scale changes (in the slope of the thermocline, for example) in the north Atlantic Ocean occur on the time scale of decades. (This is one reason for the success of one-dimensional mixed-layer models that neglect the dynamical response of the ocean.) However, the radius of deformation is inversely proportional to the Coriolis parameter f:

$$\lambda^2 = gh/f^2.$$

Hence the value of T decreases with decreasing latitude and may be short near the equator (Lighthill, 1969). In the tropics, however, there are intense zonal currents such as the North Equatorial Countercurrent that must be taken into account. Furthermore, Eq. (1) breaks down within about 5° latitude of the equator because equatorially trapped waves are possible there. Analysis of a modified version of Eq. (1), valid in the neighborhood of the equator, reveals that the adjustment time of the equatorial oceans is proportional to the time it takes planetary waves to propagate across the basin (Cane and Sarachik, 1977). For the equatorial Atlantic Ocean, the adjustment time is estimated to be of the order of 100 days. Winds that vary on a time scale much longer than this can induce oceanic changes on a basinwide scale, such as changes in the large-scale zonal slope of the equatorial thermocline.

One of the principal results from the GATE oceanographic program is that seasonal changes in the slope of the thermocline in the western equatorial Atlantic are proportional to, and occur practically in phase with, the seasonal changes in the zonal windstress (Katz *et al.*, 1977). The response of the equatorial Atlantic to seasonally varying winds is apparently an equilibrium one. Associated with the seasonal changes in the slope of the thermocline is a considerable redistribution of heat. Part of this redistribution is zonal: when the thermocline becomes shallow in the western equatorial Atlantic, it deepens in the eastern equatorial Atlantic. This gives rise to a seasonal suppression of upwelling along the coast of the Gulf of Guinea even though the local winds are always favorable for upwelling there (Philander, 1979). Because of the vertical movements of the thermocline, there is also a seasonal convergence and divergence of heat from the equatorial band (5° N to 5° S) (Merle, 1979). At this stage it is unclear how this latitudinal redistribution of heat affects the sea-surface temperature poleward of 5° latitude.

On time scales of the order of, and smaller than, 100 days, variability of the equatorial sea-surface temperature is due to a number of processes

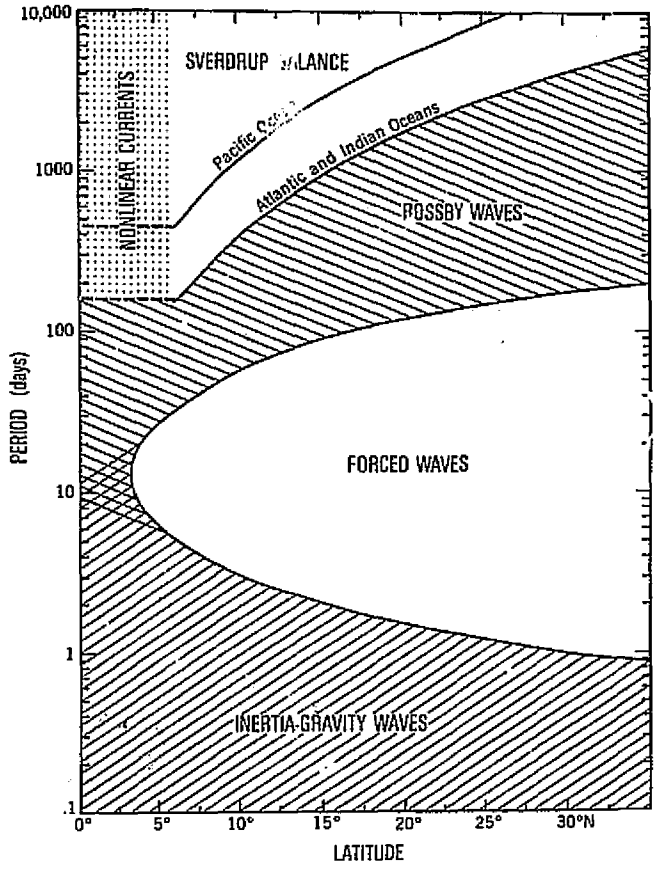

FIGURE 1 Dispersion diagram for linear low-latitude wave modes.

that include propagating waves that cause displacements of the thermocline; wind-induced upwelling, which is efficient in the neighborhood of the equator; advection by local wind-generated currents that transport warm water eastward or cold water westward; and instabilities of currents, which are important at periods of a month and two weeks. The amplitude of variability on time scales short compared with 100 days is perhaps more difficult to simulate than the low-frequency variability, but it also has a smaller amplitude.

Figure 1 shows the time scales, as a function of latitude, in which different physical processes dominate the oceanic response.

REFERENCES

Cane, M., and E. Sarachik (1977). *J. Marine Res. 34*, 395.
Katz, E., and collaborators (1977). *J. Marine Res. 35*, 293.
Lighthill, M. J. (1969). *Phil. Trans. R. Soc. 265*, 45.
Merle, J. (1979). Seasonal heat budget in the equatorial Atlantic ocean. *J. Phys. Oceanog.* (in press).
Philander, S. G. A. (1979). Variability of the tropical oceans. *Dyn. Ocean Atmos.* (in press).
Veronis, G., and H. Stommel (1956). *J. Marine Res. 15*, 43.

DISCUSSION
D. Halpern, *Rapporteur*

There are basically two reasons why one-dimensional mixed-layer models are much less successful in low than in high latitudes: the fluctuating component of the wind is much weaker in low latitudes so that there is less wind stirring of the mixed layer in the tropics; the stratification of the tropical thermocline is extremely strong and this inhibits the entrainment of cold, deep water into the mixed layer. In low latitudes it is relatively easy to redistribute the heat in the mixed layer horizontally by changing the slope of the thermocline. This, and not entrainment, is the primary cause of changes in the heat content of the upper ocean.

The arguments presented in this paper are valid only on time scales short compared with the diffusive time scale, which is of the order of a century.

A number of fascinating and important results from the GATE Oceanographic programming have been described in a cursory manner because of the limited space available here. For further details, the reader is referred to the special GATE issue of the oceanographic journal, *Deep Sea Research*, which is scheduled for publication in 1980.

REVIEW OF THE GATE C-SCALE OCEANOGRAPHIC EXPERIMENT

David Halpern
NOAA Pacific Marine Environmental Laboratory

INTRODUCTION

One objective of the GATE C-Scale Oceanographic Experiment was to describe the response of the upper-ocean current and temperature fields to variable atmospheric forcing. Wind-generated entrainment at the bottom of the oceanic mixed layer, internal gravity waves breaking in the top of the thermocline, horizontal advection of lower-temperature water, upwelling of cold water, evaporative cooling, and a positive sensible heat flux are factors likely to contribute to a lowering of sea-surface temperature and, consequently, a stabilization of the tropical atmosphere.

Wind, radiation, precipitation, temperature, salinity, and current measurements were made from ships and moored buoys throughout an approximate 100 km × 150 km region centered at about 8°45' N, 23° W during Phase III of GATE. The GATE C-Scale Oceanographic Experiment was located near the northern boundary of the North Equatorial Countercurrent. Surface current speeds were about 0.40 m sec^{-1} eastward and 0.10 m sec^{-1} northward, the thickness of the mixed layer was about 30 m (determined as the uppermost depth at which the vertical gradient of temperature was $\geq 0.1°C\ m^{-1}$), the temperature gradient in the thermocline between 30 m and 90 m was 0.2°C m^{-1}, and the mean position of the Intertropical Convergence Zone (ITCZ) was about 25-50 km north of the C-scale region. The average sea-surface temperatures during Phase II and Phase III were equal to within 0.2°C. Virtually all of the 0.35°C standard deviation of the 0.4-m temperature measurements was produced by 3-4 day and 1-day period surface-heat-flux variations which had *e*-folding depths of about 7 m (Reed and Lewis, 1979). The winds during Phase III were low, never exceeding 10 m sec^{-1} at 10-m height.

OCEANIC RESPONSE TO WIND-FORCING

The mean ± standard deviation of the east-west (u; positive eastward) and north-south (v; positive northward) wind compoments (referenced to 10-m height assuming a log profile) measured at 5-m height at the E3 buoy moored near the center of the C-scale region were 3.0 ± 1.8 m sec^{-1} and 2.3 ± 2.7 m sec^{-1}, respectively. Mean ± standard deviation values of hourly east (τ_x^o) and north (τ_y^o) components of the wind stress (computed from the square law and a drag coefficient of 1.3×10^{-3}) were

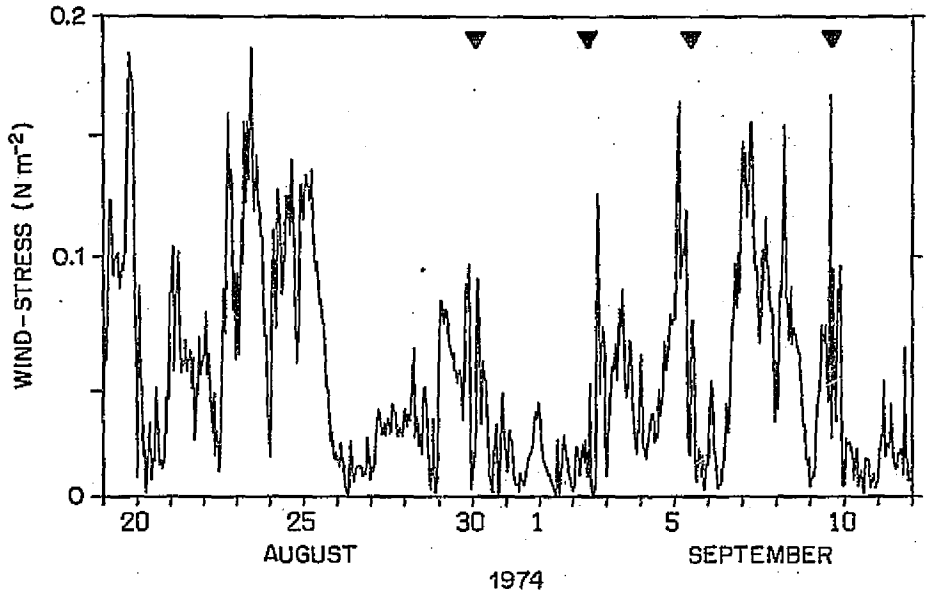

FIGURE 1 Hourly values of the magnitude of the surface wind-stress. Solid triangles represent times of large 6-hourly average rainfall rate.

$(3.0 \pm 3.1) \times 10^{-2}$ N m^{-2} and $(2.8 \pm 4.0) \times 10^{-2}$ N m^{-2}, respectively. Time variations of the wind-stress magnitude, $|\tau^{\circ}|$ are shown in Figure 1.

Wind-Driven Mean Horizontal Current

Halpern (1980) used a linearized, stationary, horizontally inviscid model to show that 20 percent of the mean transport in the 30-m-thick mixed layer of the North Equatorial Countercurrent was wind-driven and 80 percent was geostrophic. The 24-day mean profiles of the east and north current components determined from the E3 moored current measurements at four depths between 7.6 m and 27.5 m were $u(z) = 0.32z + 0.39$ and $v(z) = -0.33z + 0.11$, where z is the depth, positive upward. Assuming that the mean profiles were representative of the current structure throughout the mixed layer, the total eastward and northward transports

$$\left[\int_{-30\ \mathrm{m}}^{0} (u,v)\,dz\right]$$

per unit width of longitude and latitude were 10.3 m^2 sec^{-1} and 4.8 m^2 sec^{-1}, respectively. The mean east and north components of the Ekman transport ($\tau^{\circ}_{y}/\rho f$, $\tau^{\circ}_{x}/\rho f$; f, the Coriolis parameter, is equal to 2.2×10^{-5} rad sec^{-1} at the center of the C-scale array and ρ is the density) were 1.3 m^2 sec^{-1}, respectively, indicating that the wind-driven transports were 15 and 30 percent of the corresponding components of the total transport. The east and north components of the geostrophic transport computed

from the model were 9.1 m^2 sec^{-1} and 6.2 m^2 sec^{-1}, respectively. Insufficient hydrographic data were obtained during GATE to compute the baroclinic geostrophic current components of the North Equatorial Countercurrent. If the mean u and v components recorded at about 30 km northeast of E3 for 19.3 days at 51-m depth (Käse *et al.*, 1978) represented the depth-independent geostrophic current in the mixed layer, then the observed east and north geostrophic transports were 8.9 m^2 sec^{-1}, and 2.3 m^2 sec^{-1}, respectively. The mean east- and north-component Ekman transports computed from the model were M_{xe} = 1.4 m^2 sec^{-1} and M_{ye} = -2.5 m^2 sec^{-1}. The mean east- and north-component Ekman transports computed from the mean wind stress,

$$\frac{\tau_y^\circ}{\rho f} , \frac{\tau_x^\circ}{\rho f} ; f = 2.2 \times 10^{-5} \text{ rad sec}^{-1} ,$$

directed normal and toward the right in the northern hemisphere, were 1.3 m^2 sec^{-1} and -1.4 m^2 sec^{-1}, respectively. The remarkably excellent agreement between the computed and observed east components of the Ekman transport and the agreement within 60 percent between the north component indicated that, to first order, the mean flow in the mixed layer of the North Equatorial Countercurrent consisted of Ekman and geostrophic currents. The mean wind-driven (Ekman) transport was approximately 20 percent of the total transport.

Wind-Generated Mean Vertical Current

For linearized stationary motion without horizontal viscous stresses, the horizontal divergence of the transport within the Ekman layer, $\text{div}_H \vec{M}_e$, is given by

$$\text{div}_H \vec{M}_e = \frac{\text{curl}_z \vec{\tau}^\circ - \beta M_{ye}}{f} ,$$

where β is the northward rate of increase of the Coriolis parameter, M_{ye} is the north component of the Ekman mass transport, and $\text{curl}_z \vec{\tau}^\circ$ is the curl of the surface wind stress. x and y are positive toward east and north. With zero vertical motion at the sea surface, $\text{div}_H \vec{M}_e$ represents the vertical velocity at the bottom of the Ekman layer. A typical value of the Phase III mean wind-stress curl was 1×10^{-7} N m^{-3} (Perkins, 1979). With $\beta = 2.6 \times 10^{-11}$ m^{-1} sec^{-1} and $M_{ye} = -1.4 \times 10^3$ kg m^{-1} sec^{-1}, then $\beta M_{ye} = -3.6 \times 10^{-8}$ N m^{-3} and the mean upward advective velocity per unit mass at the bottom of the mixed layer associated with Ekman pumping was about 6×10^{-6} m sec^{-1}.

Wind-Generated Inertial Currents

It is fairly well established that inertial oscillations observed in the surface mixed layer in midlatitudes are generated by storms. In the GATE C-scale region, where wind speeds were relatively low and where the inertial

period was equivalent to the time scale of synoptic disturbances in the atmosphere that have periods of 3-5 days (Reed *et al.*, 1977), inertial motions were resonantly generated by wind fluctuations. Käse and Olbers (1979) found significant correlation between inertial oscillations recorded in the mixed layer from F1 moored current measurements and inertial oscillations simulated from the observed wind-stress and a time-dependent Ekman model with a constant eddy-viscosity coefficient, A_z, of 3×10^{-3} m^2 sec^{-1}. Halpern (in preparation) found a slightly larger value, $A_z \sim 1 \times 10^{-2}$ m^2 sec^{-1}, by assuming the vertical shear of the inertial motion in the mixed layer was maintained by the wind stress. Käse and Olbers (1979) determined an average downward speed, $3 \times 10 \times$ m^2 sec^{-1}, of propagation of inertial wave energy through the thermocline from the time lags of the first maximum in the correlations between F1 current measurements at different depths. Using time series of D2 and D3 current profiles, Perkins and Van Leer (1977) computed a similar value of the vertical group velocity. Then the downward kinetic energy flux of the inertial motion was about 0.7×10^{-3} W m^{-2} (Perkins and Van Leer, 1977; Käse and Olbers, 1979), indicating that about 20 percent of the surface input of low-frequency wind energy was lost to the thermocline region by inertial wave motion. Using observed upper-ocean stratification and wind-stress spectrum, Käse (1978) theoretically determined a transfer of 1×10^{-3} W m^{-2} from the wind to the first few inertial-internal wave modes.

Wind-Generated Mixed-Layer Deepening

The Pollard, Rhines, and Thompson (1973) theoretical model of the local response of the surface layer of the ocean to the transient wind-stress predicts that after one-half inertial period the thickness of the mixed layer reaches its maximum value, given by

$$h_{max} = 1.7 \left(\frac{\tau^o}{\rho f N} \right)^{\frac{1}{2}} ,$$

where N is the Brunt-Väisälä frequency at the top of the pycnocline. With $N = 3.5 \times 10^{-2}$ rad sec^{-1} and $|\tau^o| = 1.5 \times 10^{-1}$ N m^{-2} corresponding to the maximum 3-hour averaged wind stress occurring during the disturbed conditions of August 22, the computed maximum wind-induced depth of the mixed layer is 23 m, which is less than the measured mixed-layer depth. In agreement with the theoretical result, the E3 moored temperature records (Halpern, in preparation) and the temperature and salinity measurements recorded at the *Meteor* and *Planet* (Peters, 1978) did not show evidence of wind-induced entrainment of cold water from the thermocline into the mixed layer. Peters (1978) found that a Niiler-Kraus (1977) type of one-dimensional mixed-layer model was inadequate to simulate time variations of near-surface temperature and salinity. Apparently the wind stress was too weak to generate mixed-layer currents large enough to induce a dynamic instability across the bottom of the mixed layer (see, e.g., Halpern, 1974). With $N = 3.5 \times 10^{-2}$ rad sec^{-1}, the shear corresponding to a Richardson number of 1/4 would be about 7×10^{-2} sec^{-1}, a value not found in the E3 moored fine-structure measurements.

Although the shear was *a priori* expected to be larger across the bottom of the mixed layer, the shears in the upper thermocline determined from Perkins and Van Leer's (1977) D2 measurements and from J. Simpson's (University of Wales, Bangor, personal communication, 1976) microstructure measurements were similar to the mixed-layer observations.

Wind-Generated High-Frequency Internal Waves

The 2-5 cph fluctuations that Käse and Clarke (1978) observed in the upper 30 m of the thermocline from Fl temperature and *Quadra* conductivity-temperature-depth (CTD) data were internal gravity waves with an average rms amplitude of 1-2 dbars. These frequencies were 2-5 octaves lower than the local Brunt-Väisälä frequency, and 2 cph was equal to the N value of the largest constant N layer, the Sabinin (1966) resonance layer, which occurred between 150 and 600 m. Käse and Clarke (1978) simulated the high-frequency spectral peak with a stationary homogeneous Heaviside wind stress and the measured stratification to indicate that, perhaps, the high-frequency fluctuations were wind-generated. Correlation of the time variations between the energy of the 2-5 cph band and the wind-stress field might provide observational evidence of wind-generated high-frequency internal waves. On several occasions Proni *et al.* (1978) observed ~3.5-km-wide packets of ~400-m wavelength, ~900-sec period, long-crested internal waves from acoustic-scattering measurements recorded while the *Iselin* was under way. If the nonstationary character of the Eulerian-measured internal waves was produced because the waves formed into packets, then the internal waves observed by Käse and Clarke (1978) and Proni *et al.* (1978) were probably the same.

EXPERIMENTAL DESIGN

The experimental design of the GATE C-Scale Oceanographic Experiment was primarily determined by the positions of the GATE meteorological ships *Dallas*, *Meteor*, *Planet*, and *Quadra* and by the available oceanographic resources such as the roving ships *Discovery* and *Iselin* and the D, E, and F nested triangular arrays of moored wind, current, and temperature measurements. The low-latitude location of the C-Scale Experiment in the North Equatorial Countercurrent near the ITCZ presented additional problems for interpretation of the data because most theories of mixed-layer development neglect lateral advection, because the variability of the surface wind and precipitation had relatively small horizontal scales and because the durations of increased wind speed were a small fraction of the inertial period.

Given the initial constraints imposed by the meteorological program and by hypotheses of prominant physical processes occurring in the tropical upper ocean, there is general agreement even after 5-years hindsight that the oceanographic program was well designed. Perhaps a much smaller separation between the C-scale meteorological ships, where high-quality upper-ocean salinity profile measurements were recorded every 3 hours, would have allowed correlation studies of patches of rainfall-produced

low-salinity water moving through the mixed layer (see, e.g., Siedler and Zenk, 1975). If 100 percent success had been achieved for the moored current measurements, then perhaps upper-ocean heat-budget studies might have been accomplished. In future studies made in approximately the same region, the number of different moorings and current meters should be minimized; a longer observational period is required to estimate the contribution of lateral advection as a factor of large-scale sea-surface temperature variations; the emphasis on frontal zones, eddies, and mesoscale (50-100 km) variations can be relaxed; repeated areal density surveys of closely spaced stations should be made to estimate the variations of the baroclinic geostrophic current; and, because the curl of the wind stress was positive north of 8° N and negative south of 8° N, an ~25-km spacing between wind measurement is required.

SUMMARY

The objective of the GATE C-Scale Oceanographic Experiment was to describe the interaction between the ocean and atmosphere as a necessary preliminary step toward the goal of developing three-dimensional models of the coupled tropical ocean and atmosphere. Several results of the C-Scale Oceanographic Experiment were as follows:

1. The mean wind-driven (Ekman) transport was confined to the 30-m-thick mixed layer and represented about 20 percent of the total transport.
2. The mixed-layer eddy viscosity generated by the wind was (3-10) × 10^{-3} m^2 sec^{-1}.
3. The wind-generated mean upward current at the bottom of the mixed layer was about 6 × 10^{-6} m^2 sec^{-1}.
4. Wind-driven inertial waves transfer 20 percent of the wind energy to the thermocline.
5. Wind events did not produce mixed-layer deepening or entrainment at the bottom of the mixed layer.
6. Internal waves at 2-5 cph found near the top of the thermocline were probably generated by the wind, and the spectral properties of upper-ocean internal waves differed considerably from deep-water internal waves.

In conclusion, the results indicate that the observational objective was successfully achieved and the development of models containing the observed characteristics of the coupled ocean and atmosphere, such as advection and divergence in the mixed layer, has begun (see e.g., Worthem and Mellor, 1979).

ACKNOWLEDGMENTS

I am extremely grateful to my GATE colleagues for advice, assistance, and preprints of unpublished manuscripts. My GATE studies were supported by NOAA's GATE Office and by NOAA's Environmental Research Laboratories, and this support is gratefully acknowledged. Contribution No. 414 of the NOAA Pacific Marine Environmental Laboratory.

REFERENCES

Halpern, D. (1974). Observations of the deepening of the wind-mixed layer in the northeast Pacific Ocean. *J. Phys. Oceanog. 4*, 454-466.

Halpern, D. (1980). Variability of near-surface currents in the Atlantic North Equatorial Countercurrent during GATE, *J. Phys. Oceanog.* (in press).

Käse, R. H. (1978). Calculations of the energy transfer by the wind to near-inertial internal waves. *Deep-Sea Res. 26*, 227-232.

Käse, R. H., and R. A. Clarke (1978). High frequency internal waves in the upper thermocline during GATE. *Deep-Sea Res. 25*, 815-826.

Käse, R. H., and D. J. Olbers (1979). Wind-driven inertial waves observed during Phase III of GATE. Submitted to *Deep-Sea Res.*

Käse, R., H. Peters, G. Siedler, and W. Zenk (1978). A compilation of current temperature, and conductivity data from moorings F1 and F2 in the GATE C-area. *"Meteor" Forsch. A20*, 13-48.

Niiler, P. P., and E. B. Kraus (1977). One-dimensional modes of the upper ocean. In *Modelling and Prediction of the Upper Layers of the Ocean*, E. B. Kraus, ed., Pergamon Press, New York, pp. 143-172.

Perkins, H. (1979). Low-frequency meteorological forcing of the tropical Atlantic Ocean under the ITCZ during GATE. Submitted to *Deep-Sea Res.*

Perkins, H., and J. Van Leer (1977). Simultaneous current-temperature profiles in the equatorial countercurrent. *J. Phys. Oceanog. 7*, 264-271.

Peters, H. (1978). On the variability of the near-surface oceanic layer in the Intertropical Convergence Zone. *Oceanol. Acta 1*, 305-314.

Pollard, R. T., P. B. Rhines, and R. O. R. Y. Thompson (1973). The deepening of the wind-mixed layer. *Geophys. Fluid Dynam. 3*, 381-404.

Proni, J. R., F. Ostapoff, and R. L. Sellers (1978). Acoustic observations of high-frequency, near-surface internal wave groups in the deep ocean during GATE. *Deep-Sea Res. 25*, 299-307.

Reed, R. J., and R. M. Lewis (1979). Response of upper ocean temperatures to diurnal and synoptic-scale variations of meteorological parameters in the GATE B-Scale area. Submitted to *Deep-Sea Res.*

Reed, R. J., D. C. Norquist, and E. E. Recker (1977). The structure and properties of African wave disturbances as observed during Phase III of GATE. *Mon. Wea. Rev. 105*, 317-330.

Sabinin, K. D. (1966). Connection of short-period internal waves with the vertical density gradient in the sea. *Izv. Atmos. Ocean. Phys., Eng. Ed. 2*, 872-882.

Siedler, G., and W. Zenk (1975). Variations of temperature, salinity and currents in the mixed layer and the thermocline (preliminary results). In *Preliminary Scientific Results of the GARP Atlantic Tropical Experiment, 2*. GATE Report 14, World Meteorological Organization, Geneva, pp. 372-378.

Worthem, S., and G. Mellor (1979). Turbulence closure model applied to the upper tropical ocean. Submitted to *Deep-Sea Res.*

DISCUSSION
D. Philander, *Rapporteur*

The first rough calculations showed a net heat flux from the atmosphere into the ocean in the C-scale area, but if the final radiation data are used it emerges that there was a zero flux into the ocean. Why did upwelling associated with the curl of the wind stress not cause a cooling of the mixed layer? The wind-induced divergence can have two effects: it can cause entrainment of cold water across isotherms into the mixed layer, or it can raise the isotherms and decrease the depth (and heat content) of the mixed layer. During Phase III there was practically no entrainment; the thermocline moved upward. Because this thermocline is strongly stratified, its vertical displacement is hardly observable over a period of a few weeks but is noticeable over a period of a few months. See the discussion at the end of Rooth's paper, which follows.

Before GATE, it was hoped that salinity measurements in the upper ocean would give an estimate of the rainfall over the B- and C-scale areas. Unfortunately, the spatial resolution of measurements were inadequate to trace the advection of freshwater puddles through the C-scale area. Hence, rainfall estimates are not possible with high spatial or temporal resolution, but gross estimates, for the entire B-scale area for the third phase of GATE, are consistent with estimates by meteorologists. (See Rooth's paper.)

UPPER-OCEAN RESPONSE ON B/C SCALE IN GATE

C. Rooth
University of Miami

Contrary to the situation in the equatorial A-scale work, where the waveguide characteristics of the experimental region has provided a focusing principle for a vigorous analysis effort, as well as a follow-up effort to plan new experiments, the B/C scale interpretation effort is rather diffuse and, to a large extent, still incomplete. Most of the participants have had unexpected data-processing problems and have become involved with other field experiments while the GATE analysis progressed, which means that the GATE work is becoming an element in the progression of investigations by each individual, rather than a coherent group venture. The shortly expected appearance of the GATE Atlas, and of a special issue of *Deep-Sea Research*, devoted to papers on GATE results is expected to activate the general interpretation efforts. A general impression of the degree of stability of the large-scale hydrographic situation is gained from Figures 1 and 2, which show mean conditions for each phase, for the upper 200-m temperature field, and for phases 1 and 3 for the salinity in the upper 300 m. The most striking feature is perhaps the relaxation of the cold ridge just south of the equator, but a significant decrease in mixed layer thickness in the B-region is also apparent, along with a substantial freshening of the surface waters there. Lest these pictures be taken as zonally representative for the day-to-day structure, we must consider the topography snapshot in Figure 3 (Figures 1-3 are from the preliminary data report from the ORSTOM data center at Brest), which indicates the presence in phase 1 of a substantial eddy feature. The three-dimensional structure of this feature, which may be associated with the topography of the Sierra Leone Bank has been discussed in detail by Tyabin and Sleptsov-Shevlevich (1975). The development of a fresh surface layer and its short-term variability due to combination of advection and local rainfall are illustrated in Figure 4. A halocline of this magnitude presents a very effective barrier against short-term entrainment cooling. The combination of salinity and temperature gradient at the bottom of the mixed layer generates a very powerful internal wave duct, allowing a very energetic high-frequency internal gravity wave spectrum. In addition, the inertial frequency band was shown by profiler measurements to exhibit a short vertical wavelength shear structure, with subcritical Ri values associated with evanescent step structures in the stratification. Because the spectral gap between f and N is several octaves wider here than in typical high-latitude internal wave observations, these data

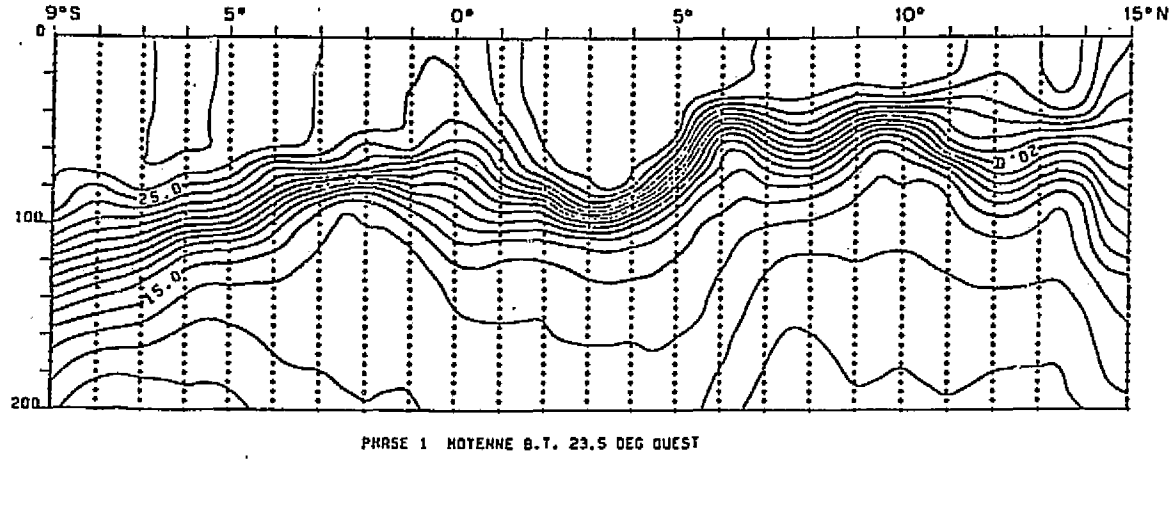

PHASE 1 MOYENNE B.T. 23.5 DEG OUEST

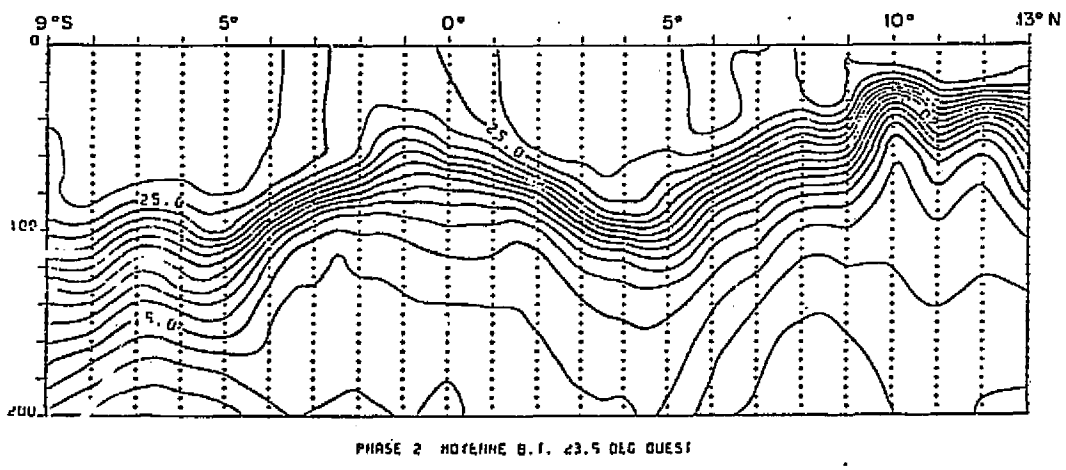

PHASE 2 MOYENNE B.T. 23.5 DEG OUEST

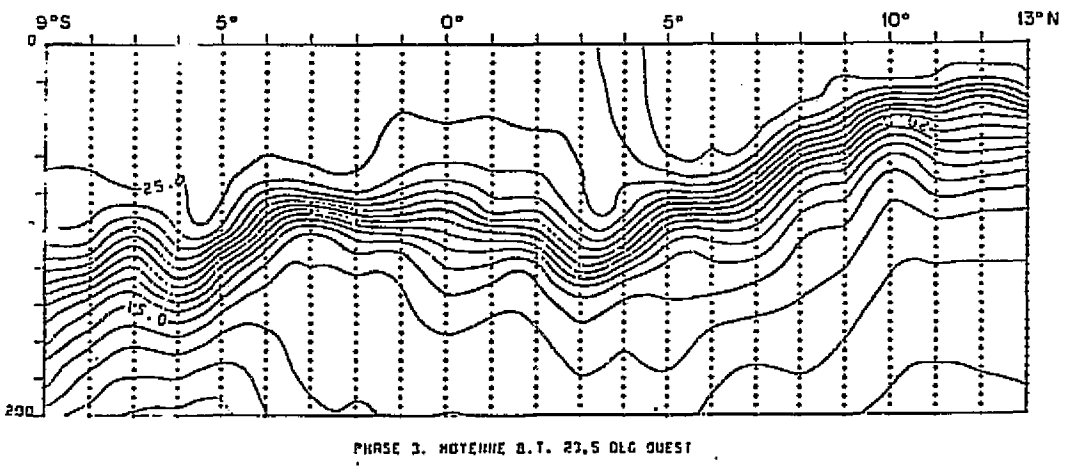

PHASE 3. MOYENNE B.T. 23,5 DEG OUEST

FIGURE 1 Average T at 23½° W for each phase of GATE (ORSTOM/Brest).

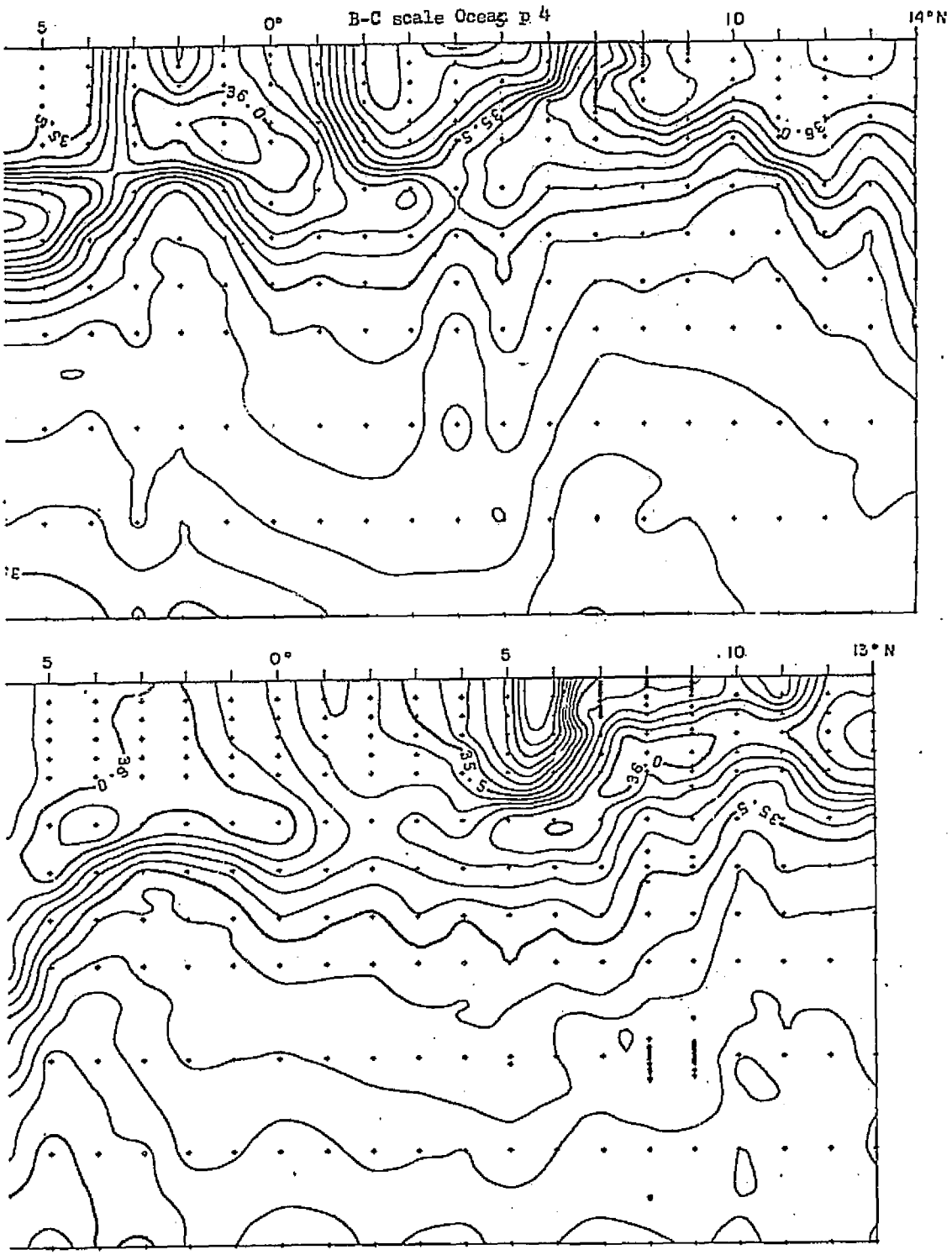

FIGURE 2. Mean salinity at 23½° W for Phases I (top) and III (bottom) of GATE.

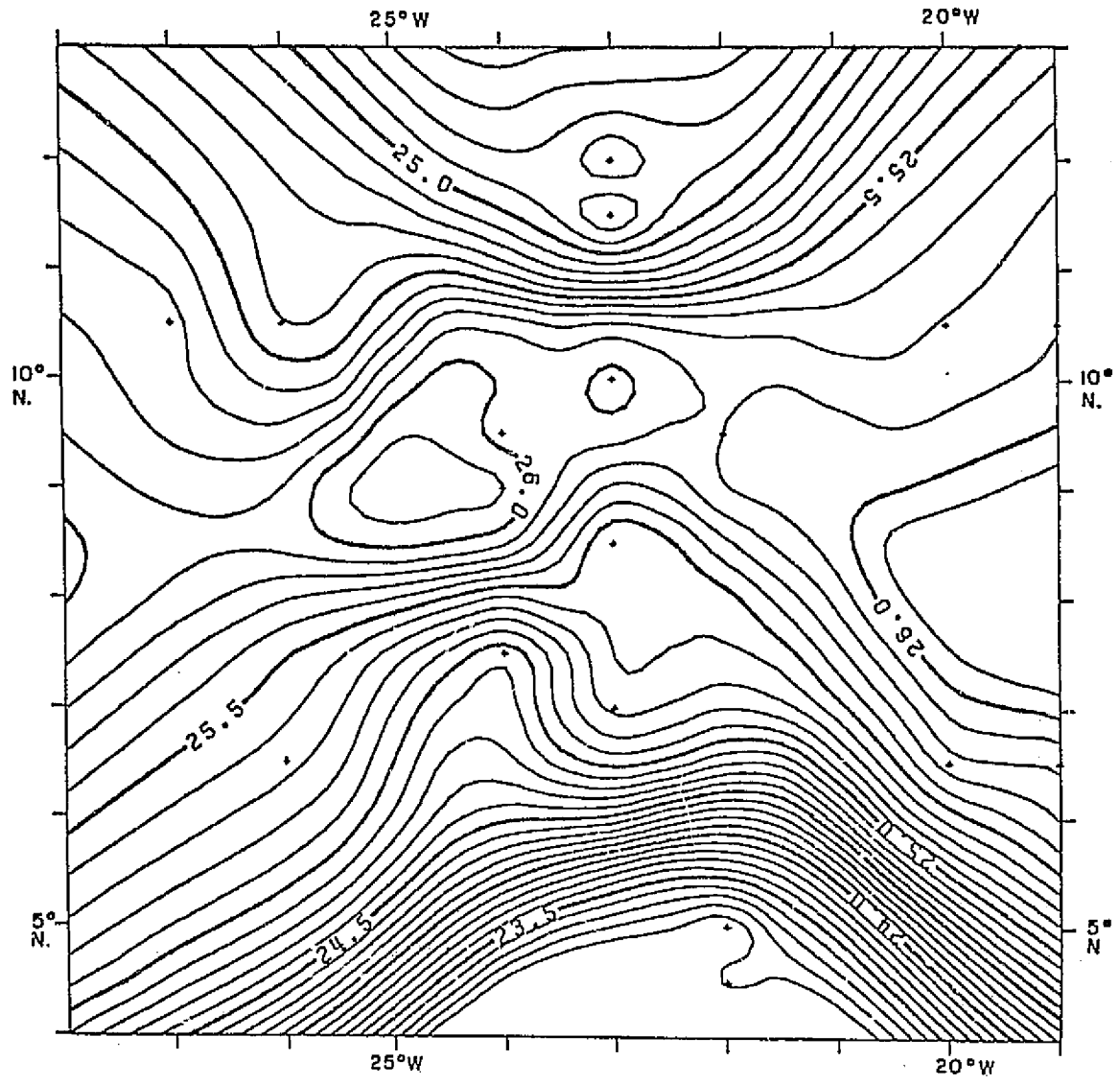

FIGURE 3 Sigma-*T* at 50 m in B array on July 10, 1974. The peak topography of the Sierra Leone Bank lies between 22° and 23° W, and extends roughly from 8° to 11° N.

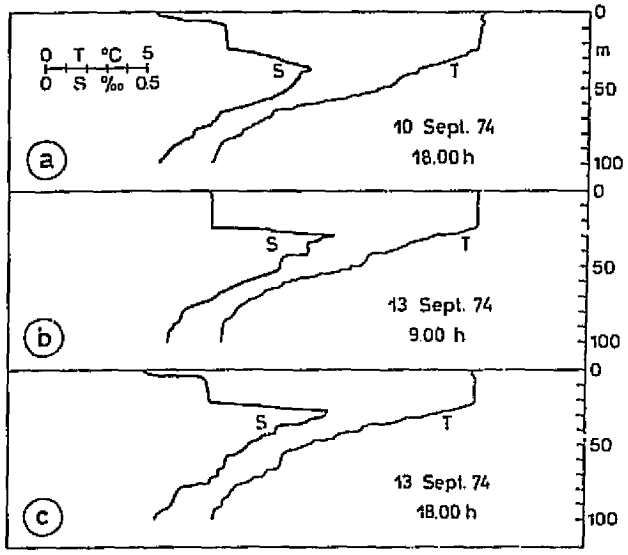

FIGURE 4 Short-term variability of upper-ocean conditions in the zone of low surface salinity. One half per mille salinity anomaly is at the temperatures involved here equivalent to 2-3°C in its buoyancy effects. (From Siedler and Zenk, 1975.)

should ultimately contribute significantly to our understanding of the near-surface turbulence parameterization problem.

REFERENCES

Siedler, G., and W. Zenk (1975). Variations of temperature, salinity and currents in the mixed layer and the thermocline (preliminary results). Preliminary Scientific Results of the GARP Atlantic Tropical Experiment, Vol. II. ICSU/WMO, GATE Report No. 14, pp. 372-378.

Tyabin, N. I., and B. A. Sleptsov-Shevlevich (1975). On reality of existence of sporadic large scale eddy formations in the ocean. Preliminary Scientific Results of the GARP Atlantic Tropical Experiment, Vol. II. ICSU/WMO, GATE Report No. 14, pp. 328-343.

DISCUSSION

D. Halpern, *Rapporteur*

The decrease in salinity of the upper ocean in the B-scale area between Phases I and III is consistent with rainfall estimates, provided there was no entrainment of highly saline water into the upper ocean. A lack of entrainment is consistent with the heat budget of the upper ocean. (See Halpern's paper, immediately preceding.)

Although the ITCZ is usually found over warm water, its presence in a given region could lead to a reduction in sea-surface temperature because of wind stirring of the upper ocean. The rainfall deposited on the ocean surface could prevent this, however. This fresh rainwater, which overlies the more saline ocean water, increases the stability of the upper ocean and thus inhibits vertical mixing. Hence the sea-surface temperature below the ITCZ will remain warm because of the precipitation.

These were considerable large-scale changes in the structure of the thermocline in the A/B-scale area during GATE. These changes must be related to the variable winds. Further analyses of GATE data to investigate this relation should prove fruitful.

6. Diagnostic Studies of Cumulus Convection and Related Topics

Organizers ..... B. Albrecht
J. Simpson

Topics	Speakers	Session Chairmen	Rapporteurs
6.1 Organization and Structure of Cumulus Elements	C. Warner R. Lopez	R. Houze	T. Carlson
6.2 Mesoscale Convective Elements	E. Zipser R. Houze	R. Johnson	A. Betts
6.3 Budget Studies of Cumulus Convection	R. Johnson S. Esbensen D. Stevens	A. Betts B. Albrecht	T. Nitta S. Lord M. Rennick
6.4 Radiative Processes	S. Cox	B. Albrecht	M. Rennick
6.5 Boundary-Layer Processes	M. LeMone M. Garstang	E. Zipser	E. Esbenson

A CASE STUDY OF THE ORGANIZATIONS OF CUMULUS CONVECTION: GATE DAY 245

Charles Warner
University of Virginia

THE LARGE SCALE

For Phase III of GATE, the streamline upper-air analyses of Dean (1978) feature mesoscale cyclones to levels as great as 400 mbar, spaced at intervals of roughly 800 km along low-level zones of confluence (ZC). The cyclones alternate with neutral points (with wind speeds approaching zero). For the period 1200 GMT day 244 (September 1, 1974) to 1200 GMT day 246, dashed lines heading generally northwestward in Figure 1 (top) show tracks of cyclones at 850 mbar. For 00 and 1200 GMT day 245 and 00 GMT day 246, solid lines linking the cyclones show the ZC at 850 mbar. A cusp in the ZC appeared with cyclone B at 00 and 1200 GMT day 245; also an anticyclone X. Cyclone B made a loop to the south during the middle of day 245; the ZC west of it penetrated southward, and heavy precipitation fell in the GATE area. At this time cyclone C was close to B, to the northeast. As cyclone A moved westward, D appeared at 18 Z between A and B. After 1800 GMT day 245, as convection near cyclone B dissipated, a break in the ZC appeared between B and C, with southerly flow.

Cyclone B was the only one followed completely across Dean's analysis area. It nearly lost its identity in the A/B array: as shown in Table 1, it was discerned only at the 850-mbar level at 00 GMT day 245. Convection in the GATE area accompanied renewed intensification of cyclone B. The table shows the life history of cyclones A, B, C, and D. In general, cyclones originated at 850-700 mbar and dissipated last at the lowest levels.

For 1200 GMT 245, the vertical structure is shown in Figure 1 (bottom). Cyclone C was off Africa; it sloped southward from the surface to 700 mbar. Cyclone B sloped approximately southward to 500 mbar. Cyclone A reached only 850 mbar. Zones of confluence linked the three cyclones at the surface and 850 mbar. A zone of confluence linked C and B at 700 mbar. A similar feature appeared to extend south-southwestward from B at 500 mbar. West of cyclone B, the ZC extended relatively far southward at 850 mbar. Later it returned northward as cyclone D appeared.

The ZC at 700 mbar has been widely recognized as the trough line of a 700-mbar wave. Features of the composite wave disturbance of Reed *et al.* (1977; Figure 2) may be related to analyzed fields around cyclone B at 22.5° W in Figure 1 (bottom). Differences between the analyzed and composite fields may have been related to cumulus convection.

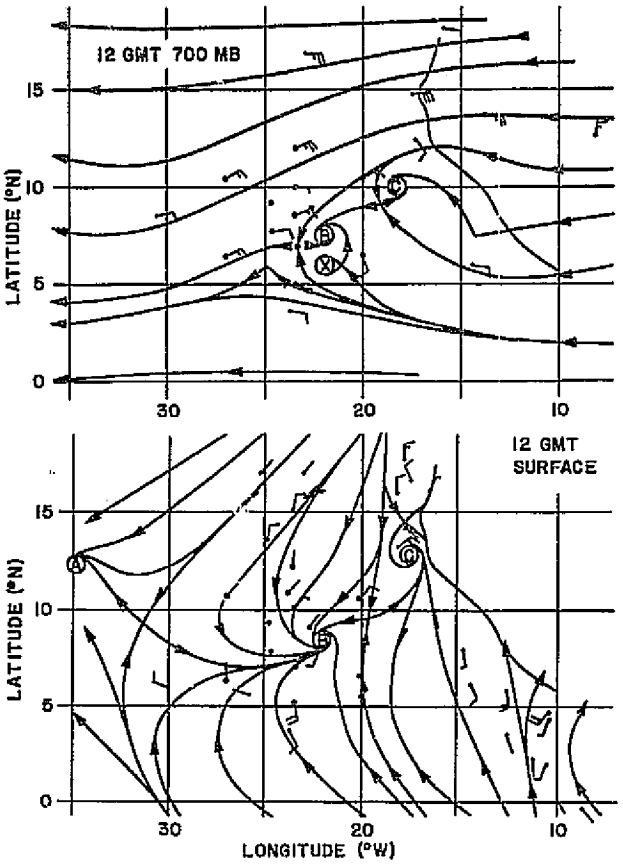

FIGURE 1 Plan views of the GATE area, with the coast of Africa at top right and dots showing the A/B hexagon. Bottom: Surface streamline analysis for 1200 GMT September 2, 1974 (day 245), from Dean (1978). Top: 700-mbar streamline analysis for 1200 GMT day 245, from Dean (1978).

Clouds were detected by satellite near the cyclones, as shown by the hand-drawn contours of infrared brightness in Figure 1 (bottom). Northwest of cyclone B were bands oriented across cyclonically curving northeasterly low-level flow. Details of these are given below. It is not yet known how the cloud clusters were related to the large-scale patterns of flow, except that unstable stratification and low-level convergence were necessary for growth, and divergence at 250 mbar followed from deep clouds.

CLOUD LINES NORTHWEST OF CYCLONE B

From Mower *et al.* (1979), Figure 2 shows a 700-mbar streamline analysis for 1200 GMT day 245, superimposed on radar echoes. This analysis omits cyclone B at 7.8° N 21.9° W, shown in Figure 1 (bottom) and in Figure 9 of Mower (1977). The speeds plotted imply that the analysis is simplified. Aligned east-west across the C-scale triangle is the southern of two lines of echoes, which were penetrated by aircraft patrolling northward and southward along the short line *x-x*. The northern line first appeared at roughly 1145 at 9.7° N 22.8° W, as an irregular group of cumulus clouds reaching altitude 3 km. It is not visible in Figure 2.

TABLE 1 Vertical Extent of Cyclones A to D

Time	Date	Levels of Appearance			
		Surface	850 mbar	700 mbar	500 mbar
18 Z	August 30		A	A	A
00	August 31, day 243		A	A	A
06		A	A	A	A
12		A	AB	A	A
18		A	AB	A	A
00	September 1, day 244	A	ABC	ARC	A C
06		A	ABC	ABC	BC
12		A	ABC	ABC	BC
18		A	ABC	ABC	BC
00	September 2, day 245	A	ABC	A C	C
06		ABC	ABC	BC	BC
12		ABC	ABC	BC	B
18		BCD	BCD	BCD	B D
00	September 3, day 246	BCD	BCD	B D	D
06		BCD	BCD	B D	B D
12		BCD	BCD	B D	B D
18		B D	B D	B D	
00	September 4, day 247	B D	B D	B D	
06		B D	B D	B D	
12		B	B	B	
18		B	B	B	

The southern line moved southward at 6 m sec^{-1} at the same speed as a gust front discontinuity (of as much as 5 m sec^{-1} at 970 mbar) in northerly wind ($-v$). Behind the gust front, the pseudo-equivalent potential temperature θ_E dipped as much as 7 K below ambient in the lowest 30 mbar, with density increases of about 0.25 percent. Above this layer, relative flow had a southerly component. The lines propagated by new growth at their leading edges.

Derived by photogrammetry from the US-C130 aircraft flying at altitude 4 km and from the Electra at 1 km, Figure 3 shows a cross section for 1200 GMT longitude 22.85° W through the cloud lines, S to the right and N to the left. From the leading edge of line S, cumulus increased in height, to 12 (±1) km at a distance of 20 km behind the leading edge. About 6.5 km wide, this tower was 4 km higher than a column of radar echo seen from the ship *Quadra*. The C130 penetrated this tower; there were small cumulus north of it, then more rain and an extensive overhang roughly 2 km thick. On top of the overhang were active cumulus towers only about 2 km wide. Convection persisting in the overhang may have been due to greater radiative cooling at the top as opposed to the base of the overhang: the relatively small width of the towers implies relatively shallow overturning. Fragmentary stratus was common above 4.4 km (600 mbar); this corresponds to a level of nondivergence on the A/B scale at 12 Z, seen on a plot at right of Figure 3, by W. M. Frank.

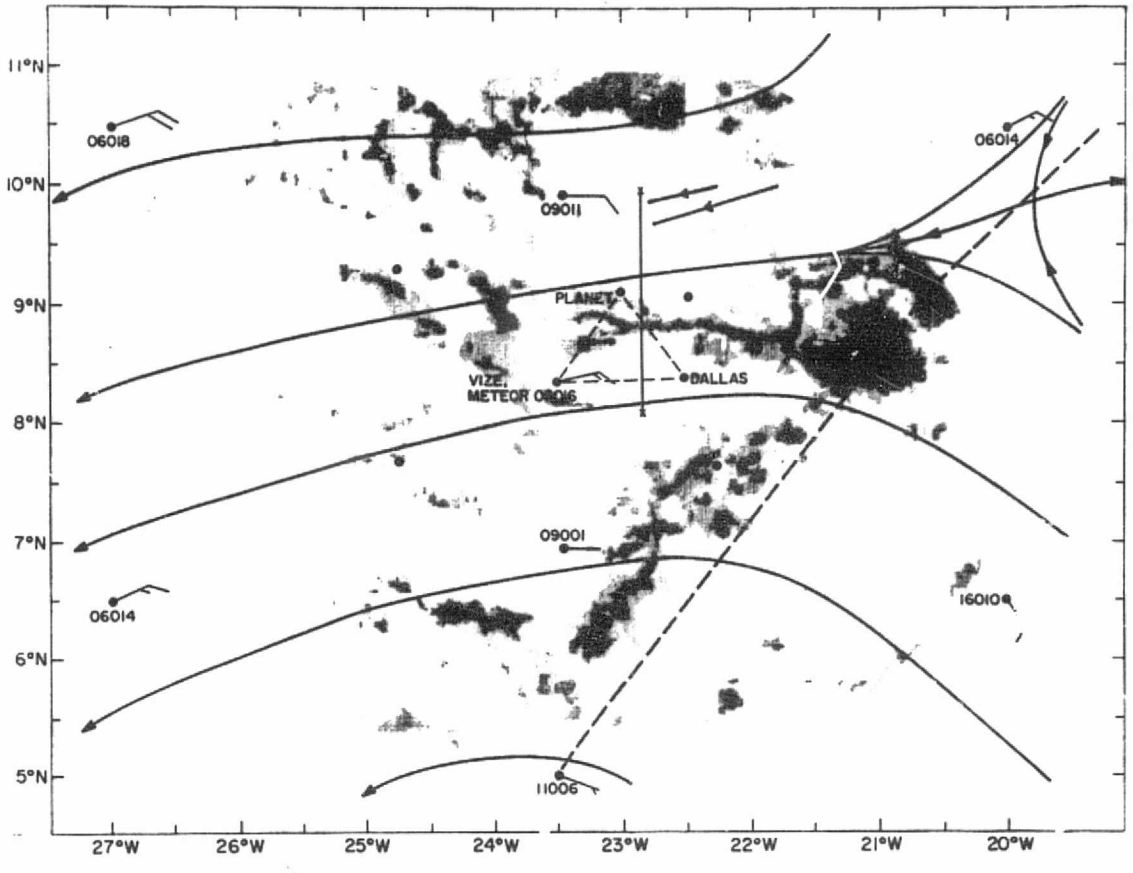

FIGURE 2 700-mbar streamline analysis superimposed on composite radar echoes from the *Oceanographer*, *Researcher*, *Gillis*, and *Quadra* for 1200 GMT. The gray shades correspond to rainfall rates of 0.05, 2.0 and 14 mm h^{-1}. The vertical line denotes the aircraft tracks during 1130 to 1500 GMT. The C-scale ship triangle is indicated (from Mower *et al.*, 1979). Two short straight lines with arrows have been added to the figure. The lower and longer shows the track of the Electra flying in from Dakar, over the interval 1154:30 to 1207:30 GMT. At 1154:30 the Electra was descending toward altitude 1 km and had just encountered relatively dry air at altitude 1.8 km. This persisted through line N, which was encountered at 1207:30, in its incipient stage. The upper short line shows the track of the DC-6 flying in from Dakar, over the interval 1213 to 1222:30 GMT. Flying at altitude 340 m, at 1213 the DC-6 first encountered relatively dry air. It turned on to the patrol line at 1222:30. The relatively dry air was associated with relatively strong northeasterly winds in each case. It appeared to be continuous between the two aircraft traverses and is interpreted as a downdraft related to the mesoscale precipitation feature at about 10.7° N. It appears that this aircraft initiated line N.

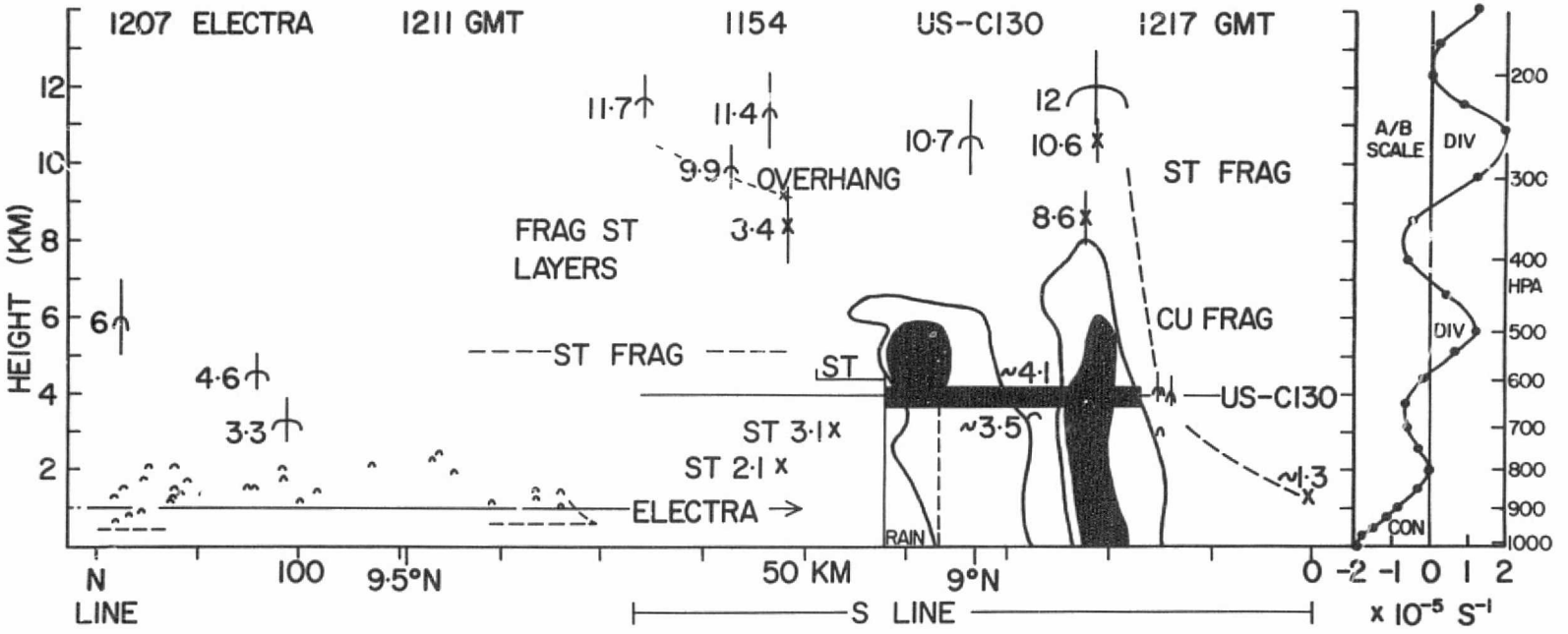

FIGURE 3 Cross section showing clouds near 22.85° W at about 1200 GMT, September 2. Line S had a leading edge of low cumulus at 8.7° N (at 0 on kilometer scale). An overhang of high cloud around 2 km thick reached a position 70 km further north. Caps of cumulus towers are drawn to scale (with vertical exaggeration ×3.7). Short verticals show height uncertainties. In line S, contoured profiles of two radar echoes are from Mower *et al.* (1979). The US-C130 met cloud and rain, as shown by shading along its track at 4 km. Dense stratus based at 4.4 km protruded 7 km north of the rain. The Electra flew at 1 km through line N at its incipient stage. Bases of low cumulus were at 400 to 610 m. Line N formed near the tower to 6 km. At right is a profile of A/B-scale divergence at 1200 GMT by W. M. Frank.

THE BEGINNINGS OF LINE N

At 1207 GMT line N consisted of many small cumulus based at 400 to 610 m, with a tower to 6 km (Figure 3). Two other towers to 4.6 and 3.3 km were 0.3° to the west. No line organization was apparent from the Electra. At 1226:40, 1231:20, and 1236:40, the DC-6 flew southward, then northward, then southward below a distinct line at 9.63° N, based at 350 m. These

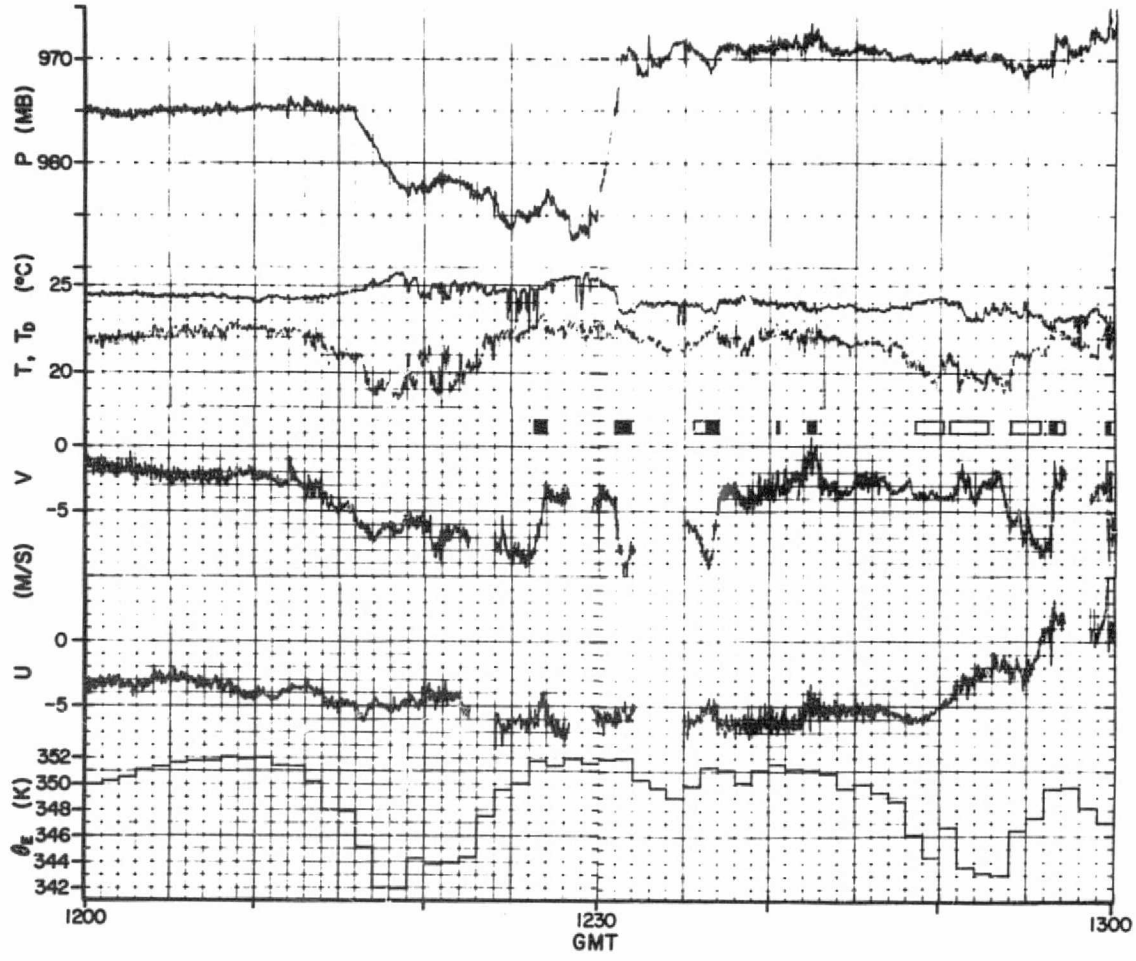

FIGURE 4 1200 to 1300 GMT, September 2. Traces of pressure (P), temperature (T), dew point (T_D), and wind components (v) and (u) from NCAR microfilm data for the DC-6 aircraft at altitudes from about 330 to 400 m. Shaded boxing along a central strip shows passage near cloud base. Open boxing shows rain. At the bottom are 1-min averages of θ_E. The DC-6 flew in from the east-northeast, from Dakar, until 1222:30. Then it turned southward; winds are not plotted during turns. Line N was penetrated at 1226:40, 1231:20, and 1236:40 flying, respectively, southward, then northward, then southward. Continuing southward after this loop, line S was reached at 1256:30.

passes are shown by shading in a central strip of the time-series plots of DC-6 data in Figure 4. Rain (open boxing) was encountered at the later two times. From 1235 the DC-6 flew consistently southward, encountering line S at 1256:30. Figure 4 shows how after 1213 the DC-6 at 340 m encountered a strong northeasterly current with $\theta_E \sim 344$ K (also see Figure 2). The Electra at 1 km found air of $\theta_E \sim 341$ K extending far east-northeastward toward the mesoscale precipitation feature visible in Figure 2 at 10.7° N. This air of low θ_E is interpreted as a downdraft originating (near altitude 1.8 km) in the clouds to the north and is held responsible for initiating line N.

Once initiated, the lines appear to have been self-maintaining, with rainy downdrafts and local (one-dimensional) convergence of 10^{-3} sec^{-1}. The ratio of A/B-scale to local low-level convergence, 2×10^{-5} to 10^{-3} sec^{-1}, is of the same order as the fractional coverage at cloud base of cloudy updrafts assessed from the aircraft films, 0.05.

CONCLUSIONS

Mesoscale precipitation features were related to mesoscale and large-scale patterns of flow. Many details of these relationships remain to be discovered. While it is becoming clear that convection follows from unstable stratification and low-level convergence, it remains to relate quantitatively large-scale convergence and transports related to cumulus drafts and to rain.

REFERENCES

Dean, G. A. (1978). Atlas of GATE synoptic analyses, Phase III. Florida State U., Tallahassee, Fla., 32 pp.

Mower, R. N. (1977). Case study of convection lines during GATE. Atmos. Sci. Paper No. 271, Colorado State U., Fort Collins, Colo., 92 pp.

Mower, R. N., G. L. Austin, A. K. Betts, C. Gautier, R. Grossman, J. Kelley, F. Marks, and D. W. Martin (1979). A case study of GATE convective activity. *Atmosphere-Ocean 17*, 46-59.

Reed, R. J., D. C. Norquist, and E. E. Recker (1977). The structure and properties of African wave disturbances as observed during Phase III of GATE. *Mon. Wea. Rev. 105*, 317-333.

DISCUSSION

T. Carlson, *Rapporteur*

Initial discussion centered around the various analyses presented by Warner for this case study. Although Warner clearly stated that Dean's analyses contained some inherent deficiencies, some details in the flow patterns, particularly the numerous vortices drawn, were questioned by several participants because of the paucity of rawinsonde data in some areas of the maps. The analyses and particularly the satellite photographs

corresponding to the streamline maps aroused considerable interest. Reed pointed out that his own analyses differed from those presented by Warner; the presentation of this apparent discrepancy underscored the subjectivity of such analyses and the real complexity of mesoscale flow patterns. The satellite photographs, it was pointed out, were typical examples in that they strikingly resembled some of the larger-scale cloud effects noted in earlier talks. The classic distribution of cloudiness near the ITCZ, modulated by an easterly wave that was passing through the A/B ship array, was recognizable--also a diurnal fluctuation in cloud amount. Although these features were evident on the photographs, the relationship between mesoscale flow patterns and convection was far from obvious.

Later discussion concerned the nature of middle-level outflow and the significance of the divergence profile shown on the right side of Figure 3. The divergence at 500 mbar was called to attention, and it was suggested that this feature might reflect an outflow at 500 mbar in response to diurnal forcing of the ITCZ. It was questioned whether the divergence profile derived from mean A/B-scale data represented that near the squall line. It was felt that this case was quite typical and probably exhibited a typical divergence profile. The role of cold air from a mesoscale precipitation feature to the north was discussed as a possible triggering mechanism for one of the lines of convection.

STATISTICS AND STRUCTURE OF THE CUMULUS CLOUD FIELD

Raúl E. López
NOAA, National Hurricane and Experimental Meteorology Laboratory

INTRODUCTION

When a cloud cluster is observed with a radar, a wide variety of shower scales is apparent. Among the many small showers, mesoscale regions of convective precipitation can be observed. In some cases, large areas completely covered by radar echoes approach the subsynoptic scale. Even within each scale the variation in size is very large. This nonuniformity is not only present in the horizontal dimension but in the height, duration, and reflectivity of the echoes as well. The purpose of this paper is to review the efforts that have been made to characterize and describe this seemingly chaotic field of showers in a coherent way.

SHOWER STATISTICS

Before the GATE radar data were available, López (1976) studied the radar echo populations of tropical disturbances in the northwest Atlantic. It was found that the low-level horizontal area, height, and duration of echoes followed very skewed frequency distributions, which could be described by the log-normal probability law. Simultaneously and independently, Biondini (1976) found a similar distribution for south Florida showers. The same characteristically skewed distributions were found for echo populations in many parts of the world in a review of most of the published echo-population data (Lopez, 1977a). Even populations of clear-air convective plumes can be described by the log-normal, as well as the incipient fair-weather cumuli that form in association with them (López, 1977b).

As soon as the radar data on microfilm from GATE became available, Houze and Cheng (1977) made a broad survey of the convective echo populations present at midday during the three phases of the experiment. Although in all three phases the distributions retained their typical log normality, the parameters of the distributions changed slightly in response to differences in the characteristics of the convection as summer progressed.

Also, using the *Oceanographer* microfilm radar data, Nasim (1977) analyzed all the echoes of a Phase II disturbance that appeared on the radarscope during the passage of the system. He tracked each of the echoes from the origin to dissipation. The distributions proved log normal for maximum echo area and duration.

Obasi (1974), and Betts *et al.* (1976). According to Payne and McGarry (1977), squall clusters are identifiable in the GATE infrared satellite imagery by their "explosive growth, high brightness and distinct and general convex shaped leading edge." The speed of this leading edge averaged 16 m sec^{-1}, or about twice the speed of propagation of synoptic-scale waves (Reed *et al.*, 1977), while the nonsquall clusters tended to retrograde slightly with respect to the large-scale waves.

STUDIES OF SQUALL CLUSTERS

Case studies of squall clusters observed in GATE have been made by Reed (1975), Houze (1977), Zipser (1977), and Fortune (1979). These studies show that the squall clusters in GATE had the classical structure described by Hamilton and Archbold (1945) and Zipser (1969), in which a leading, arc-shaped line of active, heavily precipitating cumulonimbus elements was followed by a more lightly precipitating anvil cloud. GATE radar, aircraft, and satellite data have allowed the above authors to describe the structure of both the leading line and the trailing anvil regions in much more detail than had been possible in previous studies. For these details, the interested reader is referred to these papers. One of the most significant findings of these studies of GATE squall-line systems regards the anvil precipitation. It has been recognized since Hamilton and Archbold's (1945) work that the anvil cloud of a squall-line system covers an extensive region. For example, they noted that, while the leading line of cumulonimbus takes about 30 min to pass overhead, the trailing anvil cloud, described as overcast altostratus with a base at an altitude of 3-4 km, takes 2-3 h to pass over. Prior to GATE, however, the *amount* of water falling from the anvil had not been determined. For the squall-line system that passed over the GATE area on September 4, 1974, GATE quantitative radar data showed that of the total rain that fell from the cluster as a whole, about 40 percent came from the anvil cloud (Houze, 1977). The implications of this finding will be discussed in subsequent sections.

STUDIES OF NONSQUALL CLUSTERS

Case studies of intense GATE nonsquall cloud clusters have been made by Zipser and Gautier (1978), Warner and Austin (1978), Leary and Houze (1979a), and Warner *et al.* (1979). These studies show (using radar data) that the deep convection in these clusters was organized on the mesoscale in a manner highly similar, in certain important respects, to the convection in squall-line clusters. Specifically, the precipitation in the nonsquall clusters was contained almost entirely in one or more mesoscale regions of continuous radar echo. Each such mesoscale feature (typically $\sim 10^4$–10^5 km^2 in area) was composed of two distinct regions, a *convective* region, enclosing a fluctuating pattern of deep, heavily precipitating cores, and a *stratiform* region, which consisted of lighter, horizontally uniform and slowly varying precipitation falling from a middle-level cloud base. Each mesoscale feature evolved through a characteristic life

cycle, composed of an *intensifying stage,* in which the convective region developed in a region of enhanced low-level convergence, a *mature stage,* in which the stratiform region developed adjacent to the convective region from the blending together of old diffuse cells from the convective region, and a *dissipating stage,* in which new cells ceased forming in the convective region but in which the stratiform region persisted for up to 8 h after the demise of the convective region.

The structure and life cycle of the mesoscale features in nonsquall clusters strikingly resemble those of the precipitation area in the squall-line cluster, which also is composed of a convective region (namely, its leading arc-shaped line) and a stratiform region (its trailing anvil region). These similarities suggest that the squall clusters are not so anomalous as might have been expected from their appearance in satellite imagery. Instead, they appear to be especially well-defined examples of a characteristic mesoscale organization of Intertropical Convergence Zone (ITCZ) convection. The similarity of the internal structure of squall and nonsquall clusters indicates that it may be possible to use rather similar cloud models to treat both squall and nonsquall convective systems.

STATISTICAL STUDIES OF GATE RADAR ECHO PATTERNS

The large amount of anvil precipitation falling as stratiform rain in squall clusters, and the further appearance of stratiform precipitation in nonsquall clusters, raises the question of whether this stratiform rain contributes substantially to the total precipitation in the ITCZ or is only important in specific cloud clusters. Since weather radars detect the regions of precipitation beneath the large cirrus shields of cloud clusters, as seen in satellite pictures, radar data are particularly useful for determining the average characteristics of precipitation patterns in the cloud-cluster-dominated ITCZ. Statistical studies of GATE radar echo patterns have been made by Houze and Cheng (1977), Lopez (1978), Warner and Austin (1978), and Cheng and Houze (1979). A variety of information on such characteristics as echo areas, heights, durations motions, number of high-intensity cores, and organization or echoes into lines has been obtained, and the reader is referred to these articles for details. The relative importance of stratiform precipitation is indicated by Cheng and Houze's (1979) result that while ~60 percent of the total rain in GATE can be directly associated with a spectrum of convective cells of various heights, the remainder of the rain, some 40 percent, falls as horizontally uniform rain in the stratiform regions of large mesoscale precipitation features in cloud clusters.

SUMMARY OF THE OBSERVED STRUCTURE OF CLOUD CLUSTERS

The large proportion of stratiform precipitation in cloud clusters suggests that, in addition to convective-scale updrafts and downdrafts, air motions on the scale of the stratiform rain areas may also be important in the dynamics of a cluster. To visualize the types of air motions

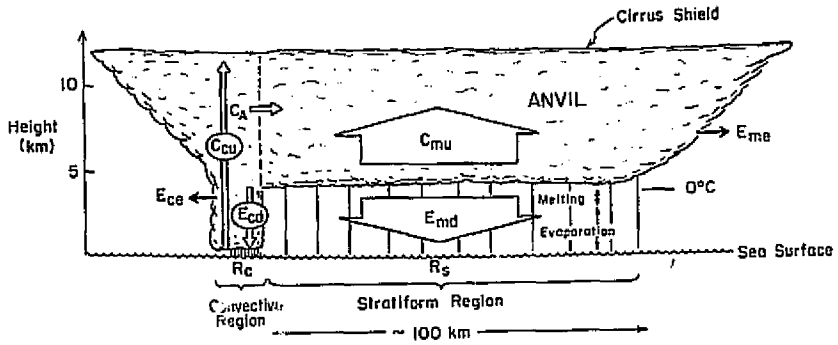

FIGURE 1 Schematic showing various components of a typical GATE cloud cluster. See text for details.

that may be involved, the structure of a typical cloud cluster, as observed in GATE, is summarized schematically in Figure 1. The figure is idealized in that it shows only one region of convective rain and one region of stratiform rain, when actually a cloud cluster can contain any number of regions of convective cells of various heights and more than one region of stratiform rain. The rain area in the diagram may be thought of as a bulk system in which the convective rain R_C is the sum of all of the convective rain produced in all the convective regions of a cloud cluster, and the stratiform rain (R_S) is the sum of all of the rain falling in stratiform precipitation regions throughout the cluster.

Two scales of updrafts and downdrafts are shown in Figure 1. *Convective-scale updrafts and downdrafts* (~1-10 km in horizontal dimension) occupy the convective rain region. These are the nonhydrostatic features usually associated with cumulus-scale convection. In the stratiform precipitation region, a *mesoscale downdraft* (~100 km in horizontal dimension) occupies the lower troposphere below the base of the precipitating anvil cloud. This type of downdraft appears to be a basically hydrostatic feature driven by cooling from the melting and evaporation of precipitation particles in the region of stratiform precipitation below the anvil. Zipser (1969) proposed that this type of downdraft occurred below squall-line anvil clouds, and Brown (1979) has simulated the occurrence of such a downdraft in a numerical model. GATE aircraft and synoptic data show that mesoscale downdrafts occurred in the stratiform precipitation regions of both squall and nonsquall clusters (Reed, 1975; Houze, 1977; Zipser, 1977; Zipser and Gautier, 1978; Leary and Houze, 1979a; Fortune, 1979). Vertical profiles of radar reflectivity in the stratiform precipitation region (Shupiatsky, *et al.*, 1975; Leary and Houze, 1979b) indicate that melting of precipitation particles provides strong cooling near the top of the mesoscale downdraft, possibly playing a role in its initiation, while evaporation provides cooling throughout the remainder of the layer of rainfall below the base of the anvil. Although there are few direct data to verify it, it is also possible that a *mesoscale updraft* (~100 km in horizontal dimension) occupies the anvil cloud itself, directly above the mesoscale downdraft. Such a feature occurred in Brown's (1979) numerical model. It is a hydrostatic circulation feature, thermally driven by condensation heating. Observations consistent with (but not proving the

existence of) such a mesoscale updraft in GATE cloud clusters include (a) the large amount of stratiform rain falling from anvils (Houze, 1977; Cheng and Houze, 1979); (b) divergent and anticyclonic 200-mbar level outflow centered in anvil cloud regions (Houze, 1977; Suchman and Martin, 1976; Leary, 1979; Fortune, 1979); (c) long persistent lifetimes of mesoscale rain areas after they reach their dissipating stage, in which they consist almost entirely of stratiform precipitation (Leary and Houze, 1979a); (d) indications that rimed ice particles (and, hence, liquid water and upward motion) existed in anvils; (e) average upward motion on the resolvable scale of rawinsonde data centered on the anvil cloud of a squall-line cluster (Ogura *et al.*, 1979).

IMPLICATIONS OF THE OBSERVED STRUCTURE OF CLOUD CLUSTERS FOR LARGE-SCALE MODELING

Possible implications for the incorporation of the effects of convection in cloud clusters into numerical models of large-scale flow patterns can be seen by considering the budget of condensed water in the idealized GATE cloud cluster in Figure 1. There are two sources of condensate for the cluster: C_{cu}, the mass of water condensed in convective-scale updrafts, and C_{mu}, the mass of water condensed in the mesoscale updraft. The disposition of C_{cu} and C_{mu} is indicated schematically in the figure and mathematically by

$$C_{cu} = R_c + E_{cd} + E_{ce} + C_A \tag{1}$$

and

$$C_{mu} + C_A = R_s + E_{md} + E_{me}, \tag{2}$$

where R_c is the part of C_{cu} that reaches the surface as precipitation in the convective rain region, E_{cd} is re-evaporated in convective downdrafts, E_{ce} is re-evaporated in the large-scale environment, and C_A is the portion of C_{cu} that is incorporated into the stratiform region, either by being detrained, that is, carried horizontally into the anvil cloud by air flowing out of convective cells, or by being left aloft by dying cells, which, upon ending their periods as active convective entities, blend into the anvil cloud. R_s is the total mass of water falling from the anvil cloud and reaching the surface as stratiform rain, E_{md} is the amount of water falling from the anvil cloud that is evaporated in the mesoscale downdraft, and E_{me} is moisture from the anvil cloud that is re-evaporated in the large-scale environment.

Equations (1) and (2) express the water budgets of the convective and stratiform regions, respectively, with sources of condensate on their left-hand sides and sinks on their right-hand sides. Since C_A is a sink for the convective region but a source for the stratiform region, it appears on the right of Eq. (1) and the left of Eq. (2). Here we focus on the stratiform region by considering Eq. (2).

The GATE observations, summarized in previous sections, indicate that the stratiform rain R_s is not small, either in specific cloud clusters

or on average. Furthermore, there is evidence of considerable mesoscale downdraft evaporation E_{md}. Consequently, the combined source in Eq. (2), $C_{mu} + C_A$, must also be large. A question that remains, though, is, what are the *relative* contributions of C_{mu} and C_A to this combined source?

Most previous diagnostic methods and parameterization schemes for determining the properties of tropical convection have either explicitly or implicitly assumed that

$$C_{mu} = 0. \tag{3}$$

Clearly, this is an extreme case, which deems *a priori* that mesoscale updrafts, which would give rise to a finite C_{mu}, do not exist. Instead, all the burden of supplying the sinks of condensed moisture in the stratiform region is placed on C_A, the only other source of condensate for this region. That is, all the sinks of condensate in the stratiform region are required to be supplied by water that was condensed externally to the stratiform region in convective cells.

Previous diagnostic and parameterization studies (except for the recent work of Johnson, 1979) have further assumed that

$$E_{md} = 0, \tag{4}$$

which specifies *a priori* that mesoscale downdrafts do not exist.

The requirements that mesoscale updrafts and downdrafts be zero, imposed by the assumptions Eqs. (3) and (4), prevent the role of mesoscale updrafts and downdrafts in large-scale fluxes of mass, heat, and other quantities to be diagnosed or parameterized. Instead, convective updrafts and downdrafts are required to account for fluxes actually accomplished by the mesoscale motions. If the mesoscale motions are significant, as is suggested by GATE observations, substantial errors may be made in diagnoses and parameterizations that do not include them.

Leary and Houze (1978; 1979c) calculated the contributions to large-scale mass and heat fluxes of an idealized cloud cluster of the type shown in Figure 1. They considered various water budgets, including cases in which C_{mu} and E_{md} were allowed to be nonzero. In these cases, the mesoscale updraft and downdraft were found to contribute significantly to the large-scale fluxes of mass and heat, and the vertical profiles of the fluxes were substantially different from those of the cases given by Eqs. (3) and (4).

CONCLUSIONS

Cloud clusters in GATE have been found to have a characteristic mesoscale organization, in which part of the precipitation from the cluster falls directly from deep convective cells and part falls as horizontally uniform rain from a stratiform anvil cloud. A mesoscale downdraft occurs in the stratiform precipitation region below the middle level base of the anvil cloud. Melting and evaporation of precipitation particles in the stratiform region cool the downdraft. A mesoscale updraft may occur in the anvil cloud, directly above the downdraft. The mesoscale updraft and downdraft

may contribute significant fluxes of mass and heat to the large-scale budgets of these quantities, and, hence, they may have to be taken into account along with convective-scale updrafts and downdrafts in assessing the role of tropical convection in models of large-scale circulation patterns.

ACKNOWLEDGMENT

This work is sponsored by the Global Atmospheric Research Program, Division of Atmospheric Sciences, National Science Foundation, and the GATE Project Office, National Oceanic and Atmospheric Administration, Grant ATM78-16859.

REFERENCES

Aspliden, C. I., Y. Tourre, and J. B. Savine (1976). Some climatological aspects of west African disturbance lines during GATE. *Mon. Wea. Rev. 104*, 1029-1035.

Betts, A. K., R. W. Grover, and M. W. Moncrieff (1976). Structure and motion of tropical squall-lines over Venezuela. *Quart. J. R. Meteorol. Soc. 102*, 395-404.

Brown, J. M. (1979). Mesoscale unsaturated downdrafts driven by rainfall evaporation: a numerical study. *J. Atmos. Sci. 36*, 313-338.

Cheng, C.-P., and R. A. Houze, Jr. (1979). The distribution of convective and mesoscale precipitation in GATE radar echo patterns. *Mon. Wea. Rev.*, to be published.

Fortune, M. (1979). Properties of African squall lines inferred from time-lapse satellite imagery. Submitted for publication in *Mon. Wea. Rev.*

Frank, N. L. (1970). Atlantic tropical systems of 1969. *Mon. Wea. Rev. 98*, 307-314.

GARP Report (1970). *The Planning of GARP Tropical Experiments*. Publ. Ser. No. 4, WMO, Geneva, 78 pp.

Hamilton, R. A., and J. W. Archbold (1945). Meteorology of Nigeria and adjacent territory. *Quart. J. R. Meteorol. Soc. 71*, 231-262.

Houze, R. A., Jr. (1977). Structure and dynamics of a tropical squall-line system. *Mon. Wea. Rev. 105*, 1540-1567.

Houze, R. A., Jr., and C.-P. Cheng (1977). Radar characteristics of tropical convection observed during GATE: Mean properties and trends over the summer season. *Mon. Wea. Rev. 105*, 964-980.

Johnson, R. H. (1979). A diagnostic model for cloud population properties that includes effects of convective-scale and mesoscale downdrafts. Submitted to *J. Atmos. Sci.*

Leary, C. A. (1979). Behavior of the wind field in the vicinity of a cloud cluster in the Intertropical Convergence Zone. *J. Atmos. Sci. 36*, 631-639.

Leary, C. A., and R. A. Houze, Jr. (1978). Mesoscale vertical air motions in intense tropical convection. *Preprints, Conf. on Cloud Phys. and Atmos. Meteorol. Soc.*, pp. 435-442.

Leary, C. A., and R. A. Houze, Jr. (1979a). The structure and evolution of convection in a tropical cloud cluster. *J. Atmos. Sci. 36*, 437-457.

Leary, C. A., and R. A. Houze, Jr. (1979b). Melting and evaporation of hydrometeors in precipitation from the anvil clouds of deep tropical convection. *J. Atmos. Sci. 36*, 669-679.

Leary, C. A., and R. A. Houze, Jr. (1979c). Cloud mass and heat fluxes over tropical oceans: the role of mesoscale motions in intense convective systems. In preparation.

López, R. E. (1978). Internal structure and development processes of C-scale aggregates of cumulus clouds. *Mon. Wea. Rev. 106*, 1488-1494.

Martin, D. W. (1975). Characteristics of West African and Atlantic cloud clusters based on satellite data. *GATE Rep. No. 14, Vol. 1*, WMO, Geneva, pp. 182-190.

Martin, D. W., and O. Karst (1969). A census of cloud systems over the tropical Pacific. *Studies in Atmospheric Energetics Based on Aerospace Probings, Ann. Report, 1968*, Space Science and Engineering Center, U. of Wisconsin.

Martin, D. W., and V. E. Suomi (1972). A satellite study of cloud clusters over the tropical North Atlantic Ocean. *Bull. Am. Meteorol. Soc. 53*, 135-156.

National Academy of Sciences (1971). *Plan for U.S. Participation in the GARP Atlantic Tropical Experiment*. Report of the Ad Hoc Tropical Task Group to the U.S. Committee for the Global Atmospheric Research Program, National Research Council, Washington, D.C., 25 pp.

Obasi, G. O. (1974). The environmental structure of the atmosphere near West African disturbance lines. Preprints Int. Tropical Meteorology Meeting, Nairobi, Kenya, Part II, Am. Meteorol. Soc., pp. 62-66.

Ogura, Y., Y.-C. Chen, J. Russell, and S.-T. Soong (1979). On the formation of organized convective systems observed over the eastern Atlantic. *Mon. Wea. Rev. 107*, 426-441.

Payne, S. W., and M. M. McGarry (1977). The relationship of satellite inferred convective activity to easterly waves over West Africa and the adjacent ocean during Phase III of GATE. *Mon. Wea. Rev. 105*, 413-420.

Reed, R. J. (1975). An example of a squall line in the B-scale network. *GATE Rep. No. 14, Vol. 1*, WMO, Geneva, pp. 217-222.

Reed, R. J., D. C. Norquist, and E. E. Recker (1977). The structure and properties of African wave disturbances as observed during Phase III of GATE. *Mon. Wea. Rev. 105*, 317-333.

Riehl, H., and J. S. Malkus (1958). On the heat balance in the equatorial trough zone. *Geophysica 6*, 503-538.

Shupiatsky, A. B., A. J. Korotov, V. D. Menshenin, R. S. Pastushkov, and M. Jovasevic (1975). Radar investigation of evolution of clouds in the Eastern Atlantic. *GATE Rep. No. 14, Vol. 1*, WMO, Geneva, pp. 177-187.

Suchman, D., and D. W. Martin (1976). Wind sets from SMS images: an assessment of quality for GATE. *J. Appl. Meteorol. 15*, 1265-1278.

Warner, C., and G. L. Austin (1978). Statistics of radar echoes on day 261 of GATE. *Mon. Wea. Rev. 106*, 983-994.

Warner, C., J. Simpson, G. van Helvoirt, D. W. Martin, D. Suchman, and G. L. Austin (1979). Deep convection on day 261 of GATE. Submitted to *Mon. Wea. Rev.*

Zipser, E. J. (1969). The role of organized unsaturated convective downdrafts in the structure and rapid decay of an equatorial disturbance. *J. Appl. Meteorol. 8*, 799-814.

Zipser, E. J. (1977). Mesoscale and convective-scale downdrafts as distinct components of squall-line circulation. *Mon. Wea. Rev. 105*, 1568-1589.

Zipser, E. J., and C. Gautier (1978). Mesoscale events within a GATE tropical depression. *Mon. Wea. Rev. 106*, 789-805.

DISCUSSION

A. Betts, *Rapporteur*

Results were presented (Ogura) showing that an Oklahoma squall line had a similar structure to squall lines in GATE: both the sloping updraft and downdraft, apparent conservation of u,v momentum from inflow through updraft to the outflow, and a heavy rain area moving with the system.

The discussion of the GATE squall and nonsquall mesosystems centered on the mechanism of maintenance of the radiative forcing of the thick upper-level stratiform cloud layer through the cooling of the layer at night, and the absorption of shortwave radiation during the daylight hours was discussed as a possible forcing mechanism. It was pointed out that the hydrostatic model of Brown (1979) produces explicit mesoscale ascent above mesoscale descent without radiative forcing. The observations show a sloping system on the mesoscale with condensation heating and freezing generally above the zones of melting and evaporation. The long lifetime of stratiform precipitation over ~100 km does indicate continual generation of new condensate.

Although both squall and nonsquall systems have broad similarities, it is not yet clear what differences exist in their dynamic structure, nor whether mesoscale and convective scale need be distinguished in parameterization schemes. More study of the mesoscale dynamics is needed. It is clear though that only a few mesoscale systems at most are responsible for the mass-transport diagnosed from the A/B-scale fields.

CLOUD POPULATION PROPERTIES DETERMINED BY DIAGNOSTIC MODELS

Richard H. Johnson
University of Wisconsin

This discussion will focus primarily on present achievements, expectations, and limitations of diagnostic studies that use large-scale heat and moisture budgets and simple models for moist convective elements to determine the collective properties of groups of convective clouds. These studies usually assume that within a large-scale area over which averages are defined there exists a statistically representative population of cumulus clouds that occupy a small fraction (~1 percent) of the total area. Moist convection on scales larger than the 1-10 km cumulus scale has until recently been neglected in diagnostic studies because of a lack of knowledge about its importance.

During the last decade, notably following the cumulus parameterization theories proposed by Ooyama (1971), Fraedrich (1973), and Arakawa and Schubert (1974), there have been numerous diagnostic studies of cumulus and larger-scale interactions. The approach of most has been to use large-scale rawinsonde observations to deduce properties of cloud populations. These studies have been extremely valuable in determining the nature of cumulus and larger-scale interactions as well as providing a means for testing cumulus parameterization theories. Alternative approaches involving the use of direct observations of clouds (e.g., number of clouds, cloud cover, and radar and satellite observations) and simple cloud models to determine the large-scale sources of heat and moisture have been developed (López, 1973; Fraedrich, 1976; Houze and Leary, 1976). The latter methods, if truly independent of the former, should provide a valuable check on the validity of results obtained from diagnostic models based on large-scale rawinsonde observations.

Mechanisms by which cumulus clouds modify large-scale temperature and moisture fields have been proposed by a number of authors. Yanai *et al.*, considered an ensemble of one-dimensional entraining cumuli classified according to the heights of cloud tops, where detrainment is assumed to occur in a thin layer. They arrived at the following forms of the heat and moisture budget equations:

$$Q_1 \left(\equiv \frac{\partial \overline{s}}{\partial t} + \nabla \cdot \overline{s\underset{\sim}{v}} + \frac{\partial}{\partial p} \overline{\omega s} \right) = -M_c \frac{\partial \tilde{s}}{\partial p} - Le + Q_R \,, \qquad (1)$$

$$Q_2 \left[\equiv -L \left(\frac{\partial \overline{q}}{\partial t} + \nabla \cdot \overline{q\underset{\sim}{v}} + \frac{\partial}{\partial p} \overline{\omega q} \right) \right] = LM_c \frac{\partial \tilde{q}}{\partial p} - L\delta \, (\tilde{q}^* - \tilde{q}) - Le \,, \qquad (2)$$

where $M_c = \sum_i m_i$ is the mass flux due to i cumulus clouds, m_i the mass flux in the ith cloud, e the rate of re-evaporation of cloud droplets, δ the mass detrainment rate, s the dry static energy $c_pT + gz$, q the specific humidity, overbar denotes a large-scale average, tilde denotes values in the between-cloud environment, asterisk refers to saturation value, and Q_R is the next radiative heating rate. The apparent heat source Q_1 (the net heating due to clouds + Q_R) is interpreted by Yanai *et al.* (1973) to be a result of environmental subsidence that compensates M_c and re-evaporation of cloud droplets. The apparent moisture sink Q_2 has a similar interpretation with an additional term involving the detrainment of water vapor from the tops of individual cumulus clouds. Yanai *et al.* (1973) developed a method to solve for the bulk cumulus mass flux M_c without having to determine the mass flux within each cloud m_i. An interpretation of large-scale modification by convection similar to that proposed by Yanai (1973) was also forwarded by Gray (1973).

It is stressed that the number and types of terms that exist on the right-hand side of Eqs. (1) and (2) for a particular diagnostic study and, hence, the interpretation of how cumulus clouds modify the large-scale environment are dependent on the type of cloud model that is used. More comment on this point will be made later.

In an alternative approach, Ogura and Cho (1973) and Nitta (1975) spectrally decomposed M_c into individual cloud-base mass flux contributions $m_B(\lambda)$ from clouds having different top heights or entrainment rates (after Arakawa and Schubert). Cumulus elements were treated as one-dimensional entraining plume updrafts with detrainment occurring at the level of thermodynamic equilibrium at the top of each cloud. These authors used a combined form of Eqs. (1) and (2) that gives an integral equation that can be directly solved for $m_B(\lambda)$. It was found that during undisturbed situations in the tropics shallow cumuli predominate, whereas during disturbed conditions both deep and shallow clouds are present. A modification of the above model by Johnson (1977) to take into account detrainment from the sides of clouds showed that the diagnosed M_c may be overestimated by as much as 20 percent because of neglect of cloud side detrainment.

Recent studies (Johnson, 1976; Nitta, 1977) have included effects of saturated cumulus downdrafts and shown, consistent with the earlier findings of Riehl and Malkus (1958), that their contributions to large-scale heat and moisture budgets are important in tropical disturbances. Similar conclusions for tropical cyclone convection were reached in a diagnostic study by Frank (1977). Effects of the life cycles of clouds on the diagnosed properties of cloud populations were examined by Soong and Ogura (1976) using a time-dependent, two-dimensional, axisymmetric cloud model. Cho (1977) has formulated a diagnostic model that includes explicitly the life-cycle effects of cumulus clouds, considering re-evaporation of cloud droplets to take place within the cloud during its life cycle [Le in Eqs. (1) and (2) is zero], and therefore allowing for both cumulus updrafts and downdrafts. Bulk or single cloud models for diagnosing the mass flux within nonprecipitating cumuli have been proposed by others (e.g., Betts, 1975; Esbensen, 1978).

Considering the variety of cloud models that exist in the above studies and the rather different diagnosed properties of cloud populations that

are obtained, the question arises: Which model is correct? The answer to this question is not simple. An accurate independent determination of cloud mass flux properties for the full spectrum of cloud sizes within tropical distrubances, even for the data-rich GATE region, is not achievable. Certainly, however, we can expect that some of the essential features of the cloud population characteristics can be determined. Perhaps then we can identify features of cloud models that need to be included to achieve a successful cumulus parameterization theory. For example, how important in convective and large-scale interactions are the life cycle effects of clouds, downdrafts, mesoscale structures, tropical squall lines, cumulonimbus overshooting effects, and ice-phase processes, for example.

Some of these questions have been addressed. Many of the studies noted above and others have demonstrated that life-cycle effects, e.g., detrainment from sides of clouds during and at the end of the life cycle, and in-cloud downdrafts, are of considerable importance. Cloud life-cycle effects have been diagnosed during undisturbed and disturbed periods of GATE by Cho *et al.* (1979) using the model of Cho (1977). The effects of downdrafts on the diagnosed properties of cumulus populations in the lower troposphere during disturbed situations have been found to be significant in several studies. In a study of tropical wave disturbances that occurred during GATE, Johnson (1978) has found using a diagnostic model that includes effects of convective-scale downdrafts that there is a minimum of shallow cumulus activity at a time when deep cumulus activity is a maximum. This result contrasts sharply with earlier studies that neglected cumulus downdrafts (e.g., Ogura and Cho, 1973) and found a distinct bimodal distribution of clouds (deep and shallow) during disturbed situations. Figure 1, taken from Nitta (1978), presents the distribution of cloud base mass flux according to detrainment pressure levels for Phase III of GATE (August 31-September 18, 1974) determined from Nitta's (1977) model. Note that unimodal distributions are prevalent with a dominance deep or shallow clouds. The reduction of shallow cumuli at times of maximum deep convection can probably be attributed to the stabilizing effects of strong downdrafts from deep clouds. These findings are at least qualitatively consistent with direct observations of cloudiness during GATE.

Cumulonimbus overshooting near the tropopause has been found to be of some importance in GATE as reported by several authors. Frank (1977) has noted that this phenomenon is a particular problem for diagnostic studies based on Arakawa-Schubert theory, since integration to obtain $m_B(\lambda)$ begins at the tropopause level. A full assessment of the impact of including refinements for overshooting as well as ice-phase processes is not yet complete.

Recognition of the importance of convection on scales intermediate to the cumulus and large scale has increased considerably since GATE. Data taken within the B array during the passage of disturbances indicate the frequent existence of convection organized on the mesoscale (~100 km). Cumulonimbus cells with associated mesoscale areas of horizontally uniform precipitation have been identified as common features of GATE cloud clusters by Leary and Houze (1979). Properties of the air within the more intense systems of this type, tropical squall lines, have been

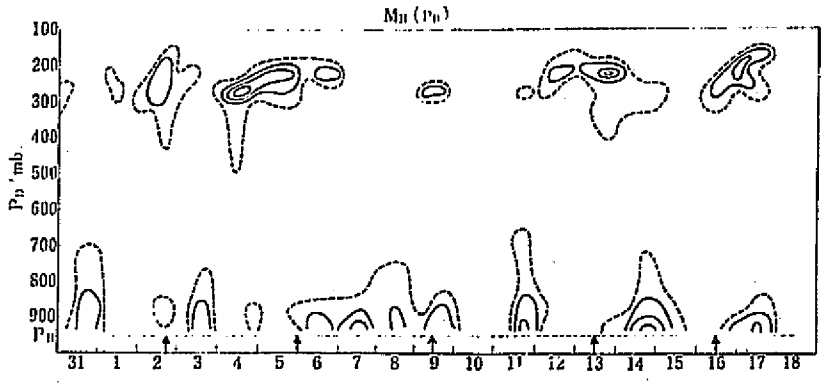

FIGURE 1 Time section of the cloud base mass flux as a function of the detrainment level for Phase III of GATE (from Nitta, 1978). Solid lines are isolines with intervals of 2 mbar h^{-1}. Arrows denote the time points when wave troughs pass the center of the B array.

examined by Houze (1977), Zipser (1977), and others. Zipser identified two distinct scales of downdrafts: convective-scale and mesoscale, the former nearly saturated and the latter often highly unsaturated. Given a sufficient number of systems having structures similar to the tropical squall line, though less intense, the effect on the large-scale circulation could be rather pronounced.

Some preliminary efforts to include effects of both cumulus-scale and mesoscale convection in diagnostic models have been made (Johnson, 1979; Houze *et al.*, 1979). Vertical motions associated with mesoscale systems (~10 cm/sec) are an order of magnitude less than those for cumulus clouds but an order of magnitude greater than the large-scale vertical motion. The fraction of the large-scale area occupied by mesoscale systems may be ~0.10 or 10 percent. The parameterization of mesoscale contributions to eddy transport terms such as $\overline{\omega' q'}$ in the same manner as cumulus-scale transports should in view of the above considerations be only a rough or first-order approximation. Nevertheless, with some justification, mesoscale systems have been included in simplified form.

With several simplifications Johnson (1979) has modeled mesoscale systems using a bulk or single mass flux model. Convective-scale updrafts and downdrafts are modeled using an entraining plume model. In the application of the model to GATE data it is assumed that all precipitation that occurs in mesoscale downdrafts is originally generated in cumulus updrafts. This assumption implies that mesoscale updraft motion is neglected. A parameterization is introduced to relate the fractional area occupied by mesoscale downdrafts to the fractional area occupied by cumulonimbus convection.

Results from an application of the model to African tropical wave disturbance composite data of Thompson *et al.* (1979) are shown in Figure 2. M_u is the cumulus updraft mass flux, M_d the cumulus downdraft mass

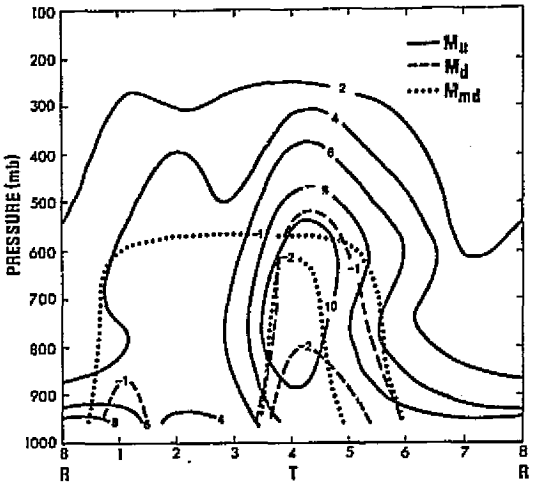

FIGURE 2 Cumulus updraft (M_u), downdraft (M_d), and mesoscale downdraft (M_{md}) mass fluxes for composite wave. T, wave trough; R, wave ridge; and numbers 1-8 refer to categories of composite wave (wavelength = 2500 km). Units: mbar h^{-1} (from Johnson, 1980).

flux, and M_{md} the mesoscale downdraft mass flux. Although M_u clearly predominates, both M_d and M_{md} are important. The associated downward transport of low-θ_e air below cloud base by downdrafts has been shown to be significant in the budget for water vapor in the subcloud layer.

Houze *et al.* (1979) have developed a diagnostic model that includes effects of both convective-scale and mesoscale updrafts and downdrafts based on the water budget of a convective cloud ensemble. Water condensed in cumulus updrafts may fall out as precipitation, re-evaporate in convective-scale downdrafts, re-evaporate in the large-scale environment, and also be incorporated into mesoscale anvil clouds. The disposition of water in each convective component is specified by means of model parameters. Importantly, their objective is to compare diagnosed collective properties by the conventional synoptic approach with those determined by an approach that uses radar observations of clouds. In the radar approach, the model clouds are constrained to produce the observed spectrum of convective and mesoscale precipitation. Application of their model to GATE data should provide valuable information concerning the importance of both cumulus and mesoscale convection in tropical disturbances.

The importance of a proper handling of both updraft and downdraft components of convective disturbances is illustrated in Figure 3. These results are for the wave trough region or the most convectively disturbed region of the Thompson *et al.* composite wave. The diagnosed total convective mass flux $M_c + M_{md}$ and environmental mass flux $\tilde{M}(=-\tilde{\omega})$ in the lower troposphere (below 500 mbar) depends to a considerable extent on whether cumulus and mesoscale downdrafts are included in the modeling of moist convective processes. Prognostic models that predict the height of the top of the mixed layer (e.g., Arakawa and Schubert, 1974) use an equation similar to

$$\frac{dz_i}{dt} = \frac{1}{\rho g}\,\tilde{M}_i - \frac{\widetilde{(s_v' w')}_i}{\Delta s_v}\,, \qquad (3)$$

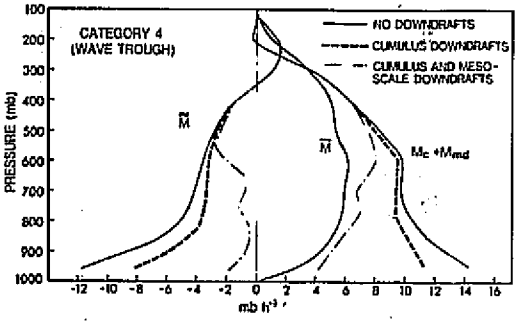

FIGURE 3 Environmental mass flux $\tilde{M}$ and net convective mass flux $M_c + M_{md}$ for category 4 of Thompson *et al.* (1979) composite wave for cases with and without downdrafts. $M_c = M_u + M_d$ and $\overline{M}$ = mean mass flux (from Johnson, 1980).

where z_i is the height of the mixed layer top, $\tilde{M}_i$ is the environmental subsidence at z_i, $(\overline{s_v' w'})_i$ is the buoyancy flux at z_i, and Δs_v is the jump in virtual static energy from z_i to cloud base. Figure 3 indicates that the contribution to a suppression of z_i by environmental subsidence $\tilde{M}_i$ in response to deep cumulus activity can be overestimated by a significant factor (6 for this study), depending on whether downdrafts are included in the cloud model. This result suggests that unless downdrafts are included in parameterization theories, predicted mixed layers in disturbed conditions will be too shallow. The fact that observed mixed layers during disturbed conditions are shallower than those observed during undisturbed conditions is probably not a result of enhanced environmental subsidence. This behavior is more likely due to a transformation of boundary-layer air following downdraft activity. In fact, for the composite wave it was found that $|\tilde{M}_i|$ is a minimum in the wave trough and a maximum in the ridge.

Considerable advances have been made in recent years in the diagnostic determination of properties of populations of cumulus clouds in large-scale tropical weather disturbances. Some authors (e.g., Cho, 1977) have developed formalisms for including explicitly effects of finite lifetimes of individual cumulus clouds in diagnostic models. Other diagnostic methods have been developed (e.g., Johnson, 1976; Nitta, 1977) that have included effects of cumulus updrafts and downdrafts and found both have an important influence on the diagnosed properties of cloud populations. More recent efforts have attempted to include effects of mesoscale convection in the diagnosis of convective transports.

The important point to be made regarding all the approaches discussed here is that diagnostic study results are cloud-model dependent. Ground-truth measurements for these types of studies are notably lacking, and even the alternative direct observational approaches (e.g., Houze and Leary, 1976) require application of cloud models. It will therefore be necessary to make a careful comparison of independent approaches before a satisfactory evaluation of the full range of cumulus- to large-scale interaction processes is achieved.

REFERENCES

Arakawa, A., and W. H. Schubert (1974). Interaction of a cumulus cloud ensemble with the large-scale environment, Part I. *J. Atmos. Sci. 31*, 647-701.

Betts, A. K. (1975). Parametric interpretation of trade-wind cumulus budget studies. *J. Atmos. Sci. 32*, 1934-1945.

Cho, H. R. (1977). Contribution of cumulus cloud life-cycle effects to the large-scale heat and moisture budget equations. *J. Atmos. Sci. 34*, 87-97.

Cho, H. R., R. Bloxam, and L. Cheng (1979). GATE A/B-scale budget analysis. *Atmosphere-Ocean 16*, 60-76.

Esbensen, S. (1978). Bulk thermodynamic properties of small tropical cumulus clouds. *J. Atmos. Sci. 35*, 836-847.

Fraedrich, K. (1973). On the parameterization of cumulus convection by lateral mixing and compensating subsidence. Part I. *J. Atmos. Sci. 30*, 408-413.

Fraedrich, K. (1976). A mass budget of an ensemble of transient cumulus clouds determined from direct cloud observations. *J. Atmos. Sci. 33*, 262-268.

Frank, W. (1977). Convective fluxes in tropical cyclones. *J. Atmos. Sci. 34*, 1554-1568.

Gray, W. M. (1973). Cumulus convection and larger scale circulations: I. Broadscale and mesoscale considerations. *Mon. Wea. Rev. 101*, 839-855.

Houze, R. A. (1977). Structure and dynamics of a tropical squall-line system. *Mon. Wea. Rev. 105*, 1540-1567.

Houze, R. A., and C. A. Leary (1976). Comparison of convective mass and heat transports in tropical easterly waves computed by two methods. *J. Atmos. Sci. 33*, 424-429.

Houze, R. A., C.-P. Cheng, C. A. Leary, and J. F. Gamache (1979). Cloud mass and heat fluxes over tropical oceans: Diagnosis from radar and synoptic data. Submitted to *J. Atmos. Sci.*

Johnson, R. H. (1976). The role of convective-scale precipitation downdrafts in cumulus and synoptic-scale interactions. *J. Atmos. Sci. 33*, 1890-1910.

Johnson, R. H. (1977). The effects of cloud detrainment on the diagnosed properties of cumulus populations. *J. Atmos. Sci. 34*, 359-366.

Johnson, R. H. (1978). Cumulus transports and their meridionally-varying response to large-scale forcing in an African tropical wave disturbance composite for Phase III of GATE. *J. Atmos. Sci. 35*, 484-494.

Johnson, R. H. (1980). Diagnosis of cumulus and mesoscale motions during Phase III of GATE. *J. Atmos. Sci.*, to be published.

Leary, C. A., and R. A. Houze (1979). The structure and evolution of convection in a tropical cloud cluster. *J. Atmos. Sci. 36*, 437-457.

López, R. E. (1973). Cumulus convection and larger-scale circulations: II. Small-scale considerations. *Mon. Wea. Rev. 101*, 856-870.

Nitta, T. (1975). Observational determination of cloud mass flux distributions. *J. Atmos. Sci. 32*, 73-91.

Nitta, T. (1977). Response of cumulus updraft and downdraft to GATE A/B-scale motion systems. *J. Atmos. Sci. 34*, 1163-1186.

Nitta, T. (1978). A diagnostic study of interaction of cumulus updrafts and downdrafts with large-scale motions in GATE. *J. Meteorol. Soc. Jpn. 56*, 232-242.

Ogura, Y., and H. R. Cho (1973). Diagnostic determination of cumulus cloud populations from observed large-scale variables. *J. Atmos. Sci. 30*, 1276-1286.

Ooyama, K. (1971). A theory on parameterization of cumulus convection. *J. Meteorol. Soc. Jpn. 49* (Special Issue), 744-756.

Riehl, H., and J. S. Malkus (1958). On the heat balance in the equatorial trough zone. *Geophysics 6*, 503-538.

Soong, S. T., and Y. Ogura (1976). A determination of the tradewind cumuli population using BOMEX data and an axisymmetric cloud model. *J. Atmos. Sci. 33*, 992-1007.

Thompson, R. M., S. Payne, E. Recker, and R. J. Reed (1979). Structure and properties of synoptic-scale wave disturbances in the Intertropical Convergence Zone of the eastern Atlantic. *J. Atmos. Sci. 36*, 53-72.

Yanai, M., S. Esbensen, and J.-H. Chu (1973). Determination of bulk properties of tropical cloud clusters from large-scale heat and moisture budgets. *J. Atmos. Sci. 30*, 611-627.

Zipser, E. J. (1977). Mesoscale and convective-scale downdrafts as distinct components of squall-line circulation. *Mon. Wea. Rev. 105*, 1568-1589.

DISCUSSION

T. Nitta and S. Lord, *Rapporteurs*

The discussion following Johnson's presentation can be divided into three general areas: (1) the influence of mesoscale systems on the sampling of large-scale fields by rawinsondes; (2) the relevance of diagnostic models for advancing the understanding of the impact of phenomena such as mesoscale convection on the large-scale circulation; and (3) the need for consideration of the relationships between the scale of phenomena and the grid scale of numerical models.

1. Since many cumulonimbus clouds occur in groups (see López's paper), it was argued that these clouds may entrain air that is not representative of the large-scale area. Furthermore, since mesoscale cloud systems may occupy a significant fraction of the large-scale area, it was argued that large-scale variables, e.g., those obtained from the GATE rawinsonde network, may not be the relevant quantities to use for large-scale diagnostic budget studies. It was suggested that the large-scale vertical wind shear can be an important factor determining the intensity of cumulus convection. To date, this fact has not been used in large-scale diagnostic budget studies.

It was pointed out that GATE rawinsonde appears to have been barely adequate to resolve mesoscale features and that this fact should be considered in the planning of future experiments.

2. The relevance of diagnostic modeling for the further improvement of our understanding of cumulus convection and its relationship to mesoscale and large-scale processes was discussed. Since the inclusion of additional physical processes, such as cumulus-scale and mesoscale downdrafts, requires an equal number of assumptions, is there any net gain in our understanding? Johnson's reply was that some diagnostic models included physically based assumptions and that these models could be useful.

3. It will be necessary to consider the relationships between scales of the phenomena being modeled to the model grid scales when parameterizing subgrid scale processes. For example, a model with sufficient resolution may explicitly resolve a mesoscale feature so that an implicit parameterization of this feature would not be needed.

Before the Esbensen/Ooyama talk, Anthes commented that the vertical distribution of cumulus heating is an important parameter for describing cumulus effects. Since the nature's complexity appears too great to be realistically simulated 1-D or 2-D cloud models, he suggested that empirical heating profiles derived from case studies may be used in parameterization schemes.

MESOSCALE CLOUD SYSTEMS AND THE INTERPRETATION OF LARGE-SCALE HEAT AND MOISTURE BUDGETS

Steven Esbensen
Oregon State University

INTRODUCTION

Heat and moisture budgets computed from observed variables on space scales larger than a few hundred kilometers have repeatedly demonstrated the importance of clouds for the maintenance of the temperatures and moisture structure of the Hadley circulation, easterly waves, and other large-scale tropical motion systems. An important discovery of the early 1970's (Yanai *et al.*, 1973) was that simple models of cumulus convection could be used to give plausible interpretations of the budget residuals from limited data sets of large-scale variables. These interpretations and their subsequent refinements by many authors have provided important guidance for the development of cloud parameterizations for large-scale dynamical models (e.g., Arakawa and Schubert, 1974) by identifying and estimating the importance of the mechanisms by which the large-scale systems and clouds may interact.

However, it is desirable to test these interpretations against real data sets. This is particularly true since diagnostic models have interpretated large-scale budget residuals entirely in terms of ensembles of noninteracting cumulus clouds. Mesoscale and cloud-cluster-scale circulations have generally been ignored. GATE was designed to provide an adequate data base for the improved understanding and modeling of interactions of these middle-scale disturbances with larger- and smaller-scale disturbances.

In the five years since the GATE observational period, considerable progress has been made. Using the unprecedented data coverage, the mass, heat, and moisture budgets of synoptic-scale features have been well established. The close relationship between the large-scale fields and the preferred location for the development of cloud clusters and squall lines has been established beyond reasonable doubt.

Based on the successes with the A-scale budgets, there is room for optimism that the study of interactions between synoptic-scale waves, mesoscale circulation systems, and cloud ensembles may be possible. This paper explores the potential of the GATE data set for the investigation of three-way interactions.

POTENTIAL OF THE GATE DATA SET

The unique aspect of the GATE set is a telescoping array of upper-air observing platforms, which took serial observations during the summer of 1974. The telescoping feature of the array is designed to allow the simultaneous observation of the Hadley circulation and monsoon structures, the traveling planetary- and synoptic-scale wave disturbances, and the circulations associated with cloud clusters and other mesoscale cloud features. The focal point of the array is an oceanic area in the northeastern Atlantic, approximately 1000 km southwest of Dakar. As the area is approached, the spatial density of the observation platforms increases. This upper-air network backed up by radar, satellites, and aircraft data provides unprecedented tropical data coverage.

The time and space scales of tropical disturbances in the GATE area are defined in Table 1. Assuming that the minimum spacing of observations needed to resolve a disturbance without compositing is one fourth of its characteristic space and time scales, we obtain the minimally adequate spacings shown in Table 2. These are compared with the actual spacings maintained during the observational program.

It is clear from Tables 1 and 2 that the wave-scale and cloud-cluster-scale phenomena have been adequately sampled in space and time. However, mesoscale phenomena have been significantly undersampled in space. And, of course, cloud-scale phenomena are not resolved in either space or time on a serial basis.

TABLE 1 Time and Space Scales of GATE Disturbances

Identifier	Space Scale (km)	Time Scale (min)	Phenomenon
A	≥ 10	$\geq 5 \cdot 10^3$	Synoptic-scale waves
B	10^2-10^3	10^2-10^3	Cloud clusters
C	10-10^2	10^2-10^3	Mesoscale circulations
D	1-10	1 -10^2	Cumulus clouds

TABLE 2 Adequate and Actual Spacings of Serial Upper-Air Observations in Eastern Atlantic GATE Arrays (Actual Spacings Shown in Parentheses)

Identifier	Space Interval (km)	Time Interval (h)
A	≥ 250 (400)	≥ 18 (6)
B	25-250 (150)	1/2-4 (3)
C	2.5-25 (100)	1/2-4 (3)
D	0.25-2.5 (N/A)	10^{-2}-1/2 (N/A)

We conclude from Tables 1 and 2 that quantitative studies of the interaction between waves, cloud-cluster-scale circulations, and combined mesoscale and cloud-scale (C/D) circulations are possible with the GATE upper-air data set provided that the observations are of sufficient quality and that the problem of spatial aliasing of mesoscale signals into A- and B-scale wavenumber domains can be overcome. As we will see in the next section, the data are of sufficient quality for A-scale budget studies. However, it is not yet clear that the high-frequency noise the B-scale wind fields identified by Ooyama and Esbensen (1977) can be overcome, although considerable progress has been made (Ooyama, National Center for Atmospheric Research, personal communication, 1979). Also, the problem of spatial aliasing of the C/D-scale signals has not been solved to date.

The interaction between large-scale (A-scale and larger) systems and smaller-scale phenomena may be described by the heat and moisture budget equations in their Reynolds averaged forms:

$$\underbrace{\frac{\partial}{\partial t}\rho\overline{s}^{A} \quad \nabla\cdot\rho\overline{\vec{v}}^{A}\overline{s}^{A} + \frac{\partial}{\partial z}\overline{\rho w}^{A}\overline{s}^{A}}_{\rho Q_1} + \underbrace{\frac{\partial}{\partial z}\overline{F}_R^{A}}_{-\rho Q_R} = -\frac{\partial}{\partial z}\overline{\rho w's'}^{A} + \overline{L(c-e)}^{A}, \tag{1}$$

$$\underbrace{\frac{\partial}{\partial t}\rho\overline{r}^{A} + \nabla\cdot\rho\overline{\vec{v}}^{A}\overline{r}^{A} + \frac{\partial}{\partial z}\rho\overline{w}^{A}\overline{r}^{A}}_{-\frac{\rho Q_2}{L}} = -\frac{\partial}{\partial z}\overline{\rho w'r'}^{A} - \overline{(c-e)}^{A}, \tag{2}$$

where s is the so-called dry static energy ($c_pT + gz$), r is the mixing ratio, and $-\frac{\partial}{\partial z}\overline{F_R}^{A}$ is the radiative heating term. The overbar denotes a horizontal space average over a typical A-scale area, and primes denote deviations from that average. Other symbols have conventional meanings. See Arakawa and Schubert (1974) for further details.

In studies of two-way interactions, the left-hand sides of Eqs. (1) and (2) are evaluated from A-scale observations. The right-hand side then contains the effects of all smaller-scale systems including those on the B, C, and D scales. Thus, we can learn about the statistical effects of small-scale convective systems without explicitly resolving them.

In studies of three-way interactions, the fluxes on the right-hand sides of Eqs. (1) and (2) can be further expanded to give

$$\overline{\rho w's'}^{A} = \left\{ \begin{array}{ccc} & & \overline{\rho w_A s_B}^{A} + \overline{\rho w_A s_{C/D}}^{A} \\ + \overline{\rho w_B s_A}^{A} & + \overline{\rho w_B s_B}^{A} & + \overline{\rho w_B s_{C/D}}^{A} \\ + \overline{\rho w_{C/D} s_A}^{A} & + \overline{\rho w_{C/D} s_B}^{A} & + \overline{\rho w_{C/D} s_{C/D}}^{A} \end{array} \right\}, \tag{3}$$

and

$$\overline{\rho w' r'}^{A} = \left\{ \begin{array}{c} \rho\overline{w_A r_B}^{A} + \rho\overline{w_A r_{C/D}}^{A} \\ + \rho\overline{w_B r_A}^{A} + \rho\overline{w_B r_B}^{A} + \rho\overline{w_B r_{C/D}}^{A} \\ + \rho\overline{w_{C/D} r_A}^{A} + \rho\overline{w_{C/D} r_B}^{A} + \rho\overline{w_{C/D} r_{C/D}}^{A} \end{array} \right\} , \tag{4}$$

where subscripts refer to signals in the A, B, and C/D wavenumber bands. Assuming for the present that cross-scale terms such as $\rho\overline{w_{C/D} s_A}^{A}$ are negligible, we may write Eqs. (3) and (4) as

$$\rho Q_1 - \rho Q_R = \frac{\partial}{\partial z} \rho\overline{w_B s_B}^{A} - \frac{\partial}{\partial z} \rho\overline{w_{C/D} s_{C/D}}^{A} + L\overline{(c-e)}^{A} , \tag{5}$$

and

$$-\frac{\rho Q_2}{L} = \frac{\partial}{\partial z} \rho\overline{w_B r_B}^{A} - \frac{\partial}{\partial z} \rho\overline{w_{C/D} r_{C/D}}^{A} - \overline{(c-e)}^{A} . \tag{6}$$

As in Eqs. (1) and (2), the left-hand sides of Eqs. (5) and (6) can be obtained from A-scale observations. However, using GATE data, it may also be possible to estimate the importance of interactions between waves and cloud-cluster-scale systems represented by the first terms on the right-hand sides of Eqs. (5) and (6) relative to the mesoscale and cloud-scale contributions. Although the quantitative analysis of this type of interaction is one of the goals of the GATE program, no definitive analysis exists. This problem remains a challenge for researchers using GATE data.

RESULTS OF GATE BUDGET STUDIES

A high-quality set of heat and moisture budgets has been obtained recently by Nitta (1978) and Thompson *et al.* (1979) in the vicinity of the eastern Atlantic Intertropical Convergence Zone (ITCZ) for all of Phase III. Frank (1978) has in addition computed the budgets for Phases I and II. Thompson *et al.* represent data from the A/B- and B-scale ship arrays (see Figure 1) with linear and quadratic polynomials that are fitted using a least-squares technique. In the studies by Frank and Nitta, data from the A/B ship array are fitted with linear polynomials. Although it is difficult to determine the exact nature of the spatial filtering that the least-squares fitting techniques impose on the data, it seems clear from Tables 1 and 2 that these budgets are representative of A-scale disturbances. The radiative component of the heat budgets has been evaluated in detail by Cox and Griffith (1979a; 1979b).

The above-mentioned studies have produced the following important conclusions concerning the effects of cloud systems on the large-scale heat conduct and moisture fields in the eastern Atlantic ITCZ region:

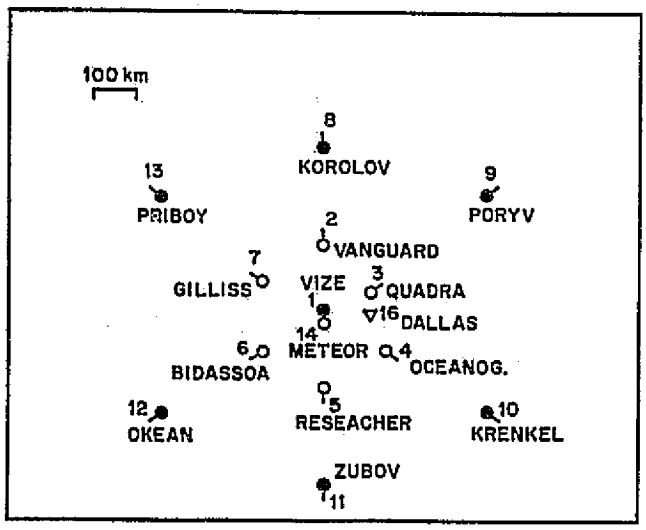

FIGURE 1 Relative positions of A/B-scale (solid circles) and B-scale (open circles) ships taking upper-air observations during Phase III. The nominal position of the *Vize* is 8.5° N and 23.5° W.

1. In the mean, cloud systems remove heat from the large-scale fields in the layer from the top of the boundary layer to about 800 mbar, while supplying heat aloft (Figure 2). This is in contrast to the western Pacific ITCZ region in which heat is supplied by cloud systems at nearly all levels.
2. The effects of cloud systems show a complex pattern with height in apparent response to the complex large-scale environment of the GATE area.

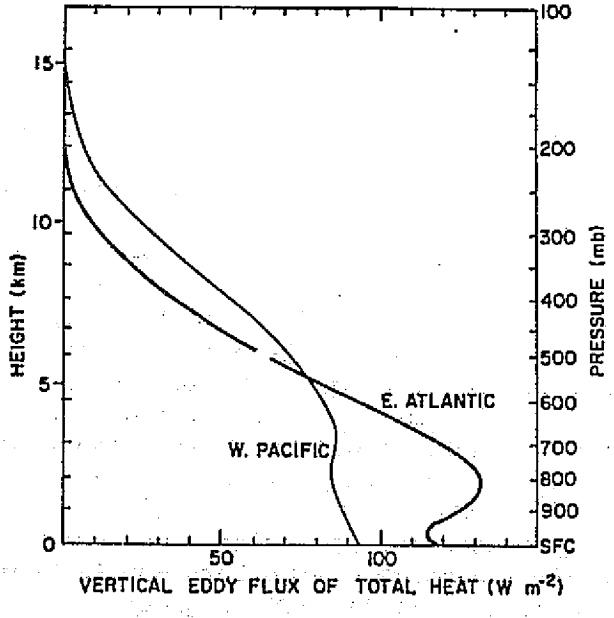

FIGURE 2 Variations with height of the vertical eddy flux of total heat ($C_pT + \phi + Lr$) for the B-scale GATE area and a similar size area in the Western Pacific ITCZ region. (Taken from Thompson *et al.*, 1979.)

3. The effects of cloud systems are strongly modulated by the passage of synoptic-scale disturbances (Figures 3 and 4).

4. Cloud systems in the vicinity of the ITCZ receive their moisture supply primarily (~70 percent) from large-scale moisture convergence, with evaporation playing a secondary role.

5. Small-scale cloud system effects on the radiative heating field are significant for the A-scale heat budgets (see paper by Cox in this volume).

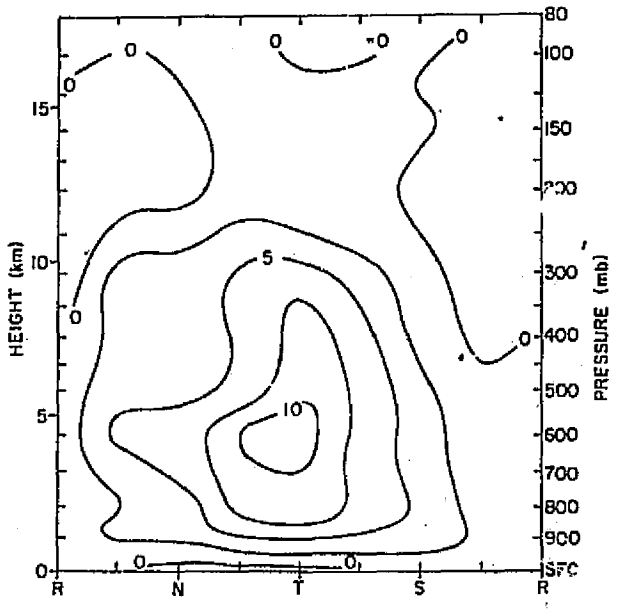

FIGURE 3 The apparent sensible heat source Q_1 as a function of wave position. Units: 10^{-2} W kg^{-1} (approximately equivalent to °C day^{-1}). (Taken from Thompson *et al.*, 1979.)

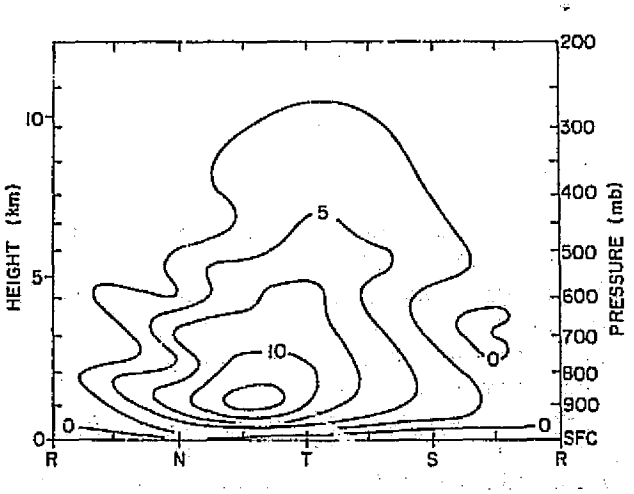

FIGURE 4 The apparent latent heat sink Q_2 as a function of wave position. Units: 10^{-2} W kg^{-1}. (Taken from Thompson *et al.*, 1979.)

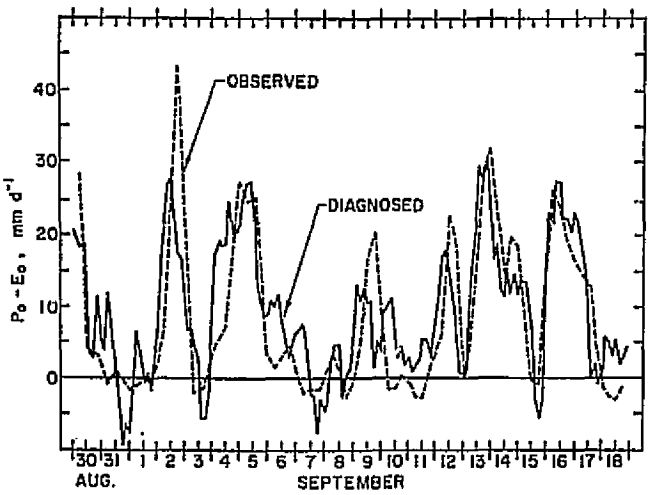

FIGURE 5 Time series for Phase III of diagnosed (solid) and observed (dashed) precipitation minus evaporation in the GATE B-scale area.

6. Precipitation minus evaporation estimates obtained by vertically integrating the A-scale moisture budget show good qualitative agreement with independent estimates from radar (Hudlow, 1977) and surface meteorological observations (Figure 5). This finding indicates that the storage of water substance in rapidly growing or decaying cloud systems is a second-order effect on the A-scale moisture field.

Additional A-scale budget analyses performed by Nitta (1977), Lord (1978), Johnson (1978), and Cho *et al.* (1979) are in essential agreement with the results of Nitta (1978), Thompson *et al.* (1979), and Frank (1978).

Although a definitive set of serial B-scale heat and moisture budgets has yet to be produced, some preliminary budgets of the subcloud layer and lower cloud layer by Drake (1977) using an A/B-scale array and by Brümmer (1977; 1978) using the C-scale array, indicate that first terms on the right-hand sides of Eqs. (5) and (6) may have appreciable magnitude. These studies found grid-scale values of $\rho w_B h_B$ to be an order of magnitude larger in disturbed conditions with significant cloud activity when compared with clear conditions.

CONCLUSIONS

The unprecedented data coverage during GATE has been used to produce high-quality heat and moisture budget analyses of synoptic-scale features in the vicinity of the ITCZ. The residuals from these budgets have revealed important information on the combined effects of cloud-cluster circulations, mesoscale circulations, and cumulus clouds on their large-scale environments.

However, definitive B-scale heat and moisture budgets have yet to be produced. The difficulty lies primarily in the spatial undersampling of mesoscale circulations, which leads to aliasing of the mesoscale features

into the larger-scale signals, and substantial high-frequency noise in the wind observations from the B-scale ship array. Overcoming these difficulties is a challenging task that must be accomplished before quantitative studies of the three-way interaction between synoptic-scale disturbances, cloud-cluster circulations, and smaller-scale cloud circulations can proceed.

REFERENCES

Arakawa, A., and W. H. Schubert (1974). Interaction of a cumulus cloud ensemble with the large-scale environment, Part I. *J. Atmos. Sci. 31*, 674-701.

Brümmer, B. (1977). Subcloud layer and lower cloud layer budget analysis. Report of the U.S. Workshop on the GATE Central Program, NCAR, Boulder, Colo., pp. 522-524.

Brümmer, B. (1978). Mass and energy budgets of a 1 km high atmosphere box over the GATE C-scale triangle during undisturbed and disturbed weather conditions. *J. Atmos. Sci. 35*, 997-1011.

Cho, H.-R., L. Cheng, and R. M. Bloxam (1979). The representation of cumulus cloud effects in the large-scale vorticity equation. *J. Atmos. Sci. 36*, 127-139.

Cox, S. K., and K. T. Griffith (1979a). Estimates of radiative divergence during Phase III of the GARP Atlantic Tropical Experiment: Part I. Methodology. *J. Atmos. Sci. 36*, 576-585.

Cox, S. K., and K. T. Griffith (1979b). Estimates of radiative divergence during Phase III of the GARP Atlantic Tropical Experiment: Part II. Analysis of Phase III results. *J. Atmos. Sci. 36*, 586-601.

Drake, J. (1977). Subcloud layer and lower cloud layer budget analysis. Report of the U.S. Workshop on the GATE Central Program, NCAR, Boulder, Colo., pp. 522-524.

Frank, W. M. (1978). Diagnostic analyses of the GATE A/B scale area at individual time periods. Atmos. Sci. Paper No. 297, Colorado State U., Fort Collins, Colo., 102 pp.

Hudlow, M. D. (1977). Precipitation climatology for three phases of GATE. Preprints of Second Conference on Hydrometeorology, Toronto, Canada, American Meteorological Society, Boston, Mass.

Johnson, R. H. (1978). Cumulus transports in a tropical wave composite for Phase III of GATE. *J. Atmos. Sci. 35*, 484-494.

Lord, S. J. (1978). Development and observational verification of a cumulus cloud parameterization. Ph.D. Thesis, U. of California, Los Angeles, 359 pp.

Nitta, Ts. (1977). Response of cumulus updraft and downdraft to GATE A/B-scale motion systems. *J. Atmos. Sci. 34*, 1163-1186.

Nitta, Ts. (1978). A diagnostic study of interaction of cumulus updrafts and downdrafts with large-scale motions in GATE. *J. Meteorol. Soc. Jpn. 56*, 232-242.

Ooyama, K., and S. Esbensen (1977). Rawinsonde data quality. Report of the U.S. Workshop on the GATE Central Program, NCAR, Boulder, Colo., pp. 131-163.

Thompson, R. M., Jr., S. W. Payne, E. E. Recker, and R. J. Reed (1979). Structure and properties of synoptic-scale wave disturbances in the intertropical convergence zone of the eastern Atlantic. *J. Atmos. Sci. 36*, 53-72.

Yanai, M., S. Esbensen, and J.-H. Chu (1973). Determination of bulk properties of tropical cloud clusters from large-scale heat and moisture budgets. *J. Atmos. Sci. 30*, 611-627.

DISCUSSION

T. Nitta and S. Lord, *Rapporteurs*

Most of the discussion was focused on expected results that will be obtained by using Ooyama's objective analysis. It was asked how the results will differ if Ooyama's scheme is used. Ooyama answered that results for the A scale would not be very different from the current results. For the B scale, however, no other analysis has been made, and Ooyama's results for this scale would be different from the results of a more traditional analysis. However, Ooyama did not conclude that the results would be necessarily better or more useful. Also he mentioned that it is hard to say how much we can understand real physical processes from these data because of the complexity of convective systems observed in GATE. There was a comment that different objective and subjective analyses might result in significantly different results especially for budget computations.

There was a question about the significant difference of amplitude of the Phase III mean vertical velocities computed from data taken at the six outer ships of the B-scale and A/B-scale ship arrays, respectively. Ooyama stated that with his analysis the results are nearly the same. It is true, however, that some observational biases have been found in the B-scale wind observations, but we cannot tell which data are wrong.

In general, the participants were very encouraged by Ooyama's results. It was stated by one of the participants that his analysis scheme might well be the ultimate objective analysis scheme. It was also felt that it was important that this data set be further investigated and utilized.

LARGE-SCALE VORTICITY AND MOMENTUM BUDGETS

Duane E. Stevens
Colorado State University

INTRODUCTION

Our ability to model and predict the development of large-scale tropical circulation systems depends on our theoretical understanding of how those motion systems actually behave, i.e., what dynamical principles govern their evolution. The midlatitude analogs are the quasi-geostrophic dynamics and baroclinic instability theory, which preceded the development of successful numerical weather-prediction models for synoptic-scale systems.

Since cumulus convection plays such an important role as a source of energy for tropical disturbances through its intense vertical circulation, it is reasonable to expect that convective-scale circulations will also affect the large-scale dynamic budgets (e.g., vorticity, momentum, and divergence) as well as the large-scale thermodynamic budgets (e.g., dry static energy and moisture). The common method for investigating the impact of the smaller-scale circulations has been to calculate the large-scale budgets from synoptic-scale observations, for example, as provided by surface and radiosonde measurements of the A/B- and B-scale ship arrays. Any residual imbalance is then identified with subsynoptic-scale circulations as an apparent source for the large-scale budget with the implicit assumption that data errors are negligible. Here we discuss the apparent sources of vorticity and momentum, which have been found to be a significant component of the large-scale budgets. These cloud effects must necessarily be parameterized in numerical models of the large-scale circulation in terms of the observed or predicted large-scale parameters.

We also consider the dynamical structure of the observed disturbances in order to determine which large-scale dynamic processes are effective in producing changes of vorticity and momentum. Specifically, we investigate the individual terms of the large-scale budget equations and look for dominant terms or balances. For successful prediction, large-scale models should then simulate the observed dynamics. This type of approach in midlatitude meteorology led to the development of the quasi-geostrophic system.

PRE-GATE RESULTS: VORTICITY

Riehl and Pierce (1968), Williams and Gray (1973), Reed and Johnson (1974), and Ruprecht and Gray (1976) all derived vorticity budgets for tropical disturbances in the western Atlantic and western Pacific. In general, they found that the divergence term, $(\zeta + f)\nabla \cdot \vec{V}$, dominated the large-scale terms. For balance in the large-scale vorticity budget, an apparent source was required that opposed this vorticity production term and therefore acted to reduce the vorticity changes being produced by the large-scale motions. Furthermore, since the relative vorticity and convergence were generally well correlated (i.e., low-level positive vorticity was associated with convergence and upper-level negative vorticity with divergence in the disturbances) the apparent source tended to act in a "down-gradient" fashion, decreasing the positive vorticity at low levels and increasing the negative vorticity at upper levels.

GATE RESULTS: VORTICITY

Shapiro (1978) studied the vorticity budget of the African easterly wave as composited by Reed *et al.* (1977) from GATE data collected at both land and ocean stations. He found that the local vorticity change was balanced quite well by horizontal advection in all phases of the wave at 11° N, the approximate latitude of typical disturbance center at 700 mbar. At all latitudes for which the vorticity budget was evaluated (7° N, 11° N, 15° N), the wave disturbances were governed by linear dynamics.

The other large-scale terms were dominated by the divergence term, so that again the residual imbalance, or apparent vorticity source, strongly resembled the divergence term. Because of the greater amount of vertical structure in the divergence pattern, the apparent vorticity source (Figure 1) also displayed more structure: in particular, a large source was found just ahead of the trough in the middle troposphere, where the relative vorticity is strongly cyclonic. Shapiro was able to account successfully for this complex apparent source with a parameterization based on a one-dimensional cloud model.

Stevens (1979) calculated the vorticity budget for the wave composite of Thompson *et al.* (1979) over the GATE ship array centered at 8.4° N and 23.6° W, using both B and A/B wind data. Again, it was found that the linear terms dominated the large-scale nonlinear terms. However, the vorticity tendency and horizontal advection terms did not balance, their sum having about the same magnitude as each term individually (30×10^{-11} sec^{-2}). As a result, the apparent vorticity source (Figure 2) did not resemble the divergence term, which nonetheless was still a significant term in the budget. Somewhat surprisingly, the midtropospheric apparent source turned out to be less than half of the magnitude of individual terms, indicating a greater degree of balance among the large-scale terms. Assuming that the residual is a real effect of cumulus convection, its detailed, multilayered structure poses a rather severe test of a cumulus parameterization scheme. The apparent sink in the trough near the surface (in both Figures 1 and 2) is consistent with frictional dissipation by surface drag. The large apparent vorticity source at 200 mbar in

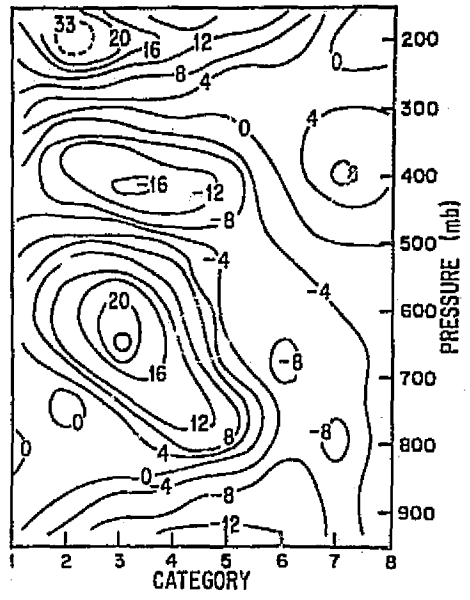

FIGURE 1 Apparent vorticity source Z (10^{-11} sec^{-2}) at 11° N (from Shapiro, 1978).

category 1 is similar between these two GATE wave studies, but Stevens (1979) found a second upper-level source in categories 5 and 6 just after trough passage.

Reeves *et al.* (1979) have recently called into question some of the results of other vorticity studies. They analyzed the mean vorticity budget for each of the three phases of GATE, as well as the budget for disturbed and undisturbed situations defined by precipitation rate. In contrast with the previous studies, they computed values of the twisting term that were comparable in magnitude to the divergence term and therefore

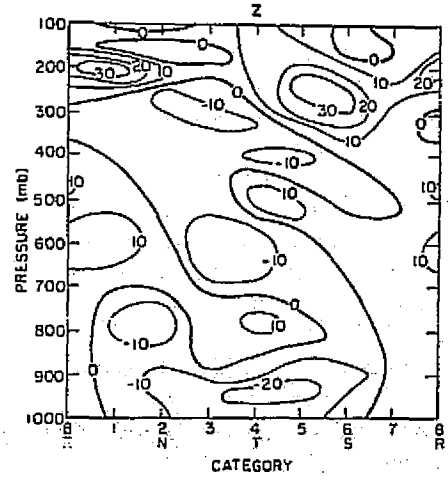

FIGURE 2 Apparent vorticity source Z (10^{-11} sec^{-2}) for GATE ship array (from Stevens, 1979).

a significant component of the mean vorticity budget. Their vertical profile of the mean twisting term is similar to that calculated by Stevens (1979) but has an amplitude four to five times greater. Because this term depends on the second horizontal derivative of the smoothed large-scale wind field (through $\nabla\omega$, where ω is determined kinematically), it may be sensitive to small variations in the analysis scheme.

Even with this difference in individual terms, Reeves *et al.* (1979) obtained an apparent mean vorticity source for Phase III that is qualitatively similar to the result of averaging across the wave in Figure 2; viz., an apparent sink below 800 mbar and an apparent source at 200 mbar, with a negligible residual in the middle troposphere. The upper-level source prevailed throughout all three phases. In fact, consistent with Figure 2, this apparent source of vorticity was present during both disturbed (trough) *and* undisturbed (ridge) situations. Because the upper-level source was found when deep cumulonimbus activity is presumably absent, Reeves *et al.* (1979) pointed out that this "finding then casts some doubt on attributing the upper tropospheric vorticity source during the disturbed state to cumulonimbus activity."

Cho *et al.* (1979) calculated a vorticity budget for a single disturbed day (September 9) during GATE Phase III from A/B data. This day was atypical of most disturbances in that the low-level vorticity was anticyclonic. They also found the twisting term to be a significant component of the vorticity budget.

GATE RESULTS: MOMENTUM

Stevens (1979) calculated horizontal momentum budgets for the wave disturbances, following the general methodology of the vorticity budget studies. Because of data inconsistencies in the observed thermodynamic variables, Phase III means were subtracted off before considering the wave budgets, in order to optimize the reliability of the pressure gradient estimates.

Figure 3 shows the momentum budget for the time-dependent zonal flow. It is immediately apparent that the quasi-geostrophic approximation is not appropriate for the waves, although the Coriolis force and pressure gradient are almost exactly out of phase in the vicinity of the low-level easterly jet. This implies qualitative (but not quantitative) thermal wind balance for the wave disturbances in accord with Reed and Recker's (1971) finding for western Pacific waves. The advective terms are self-canceling to a first approximation, so that the acceleration is very similar to the local tendency of the zonal momentum. As in the vorticity budget, nonlinear advective terms are generally smaller than corresponding linear terms, indicating that linear dynamics are appropriate at this stage of wave development.

Even though the pressure gradient term is somewhat larger than other large-scale terms, the apparent momentum source X', which is just the sum of the large scale terms, has only half of the amplitude of the other terms. This unexpected result suggests that (1) the diagnosed pressure gradient term is probably a realistic estimate, and (2) the effect of cumulus transports of zonal momentum is relatively weak but not negligible. The residual X' has more vertical structure than the

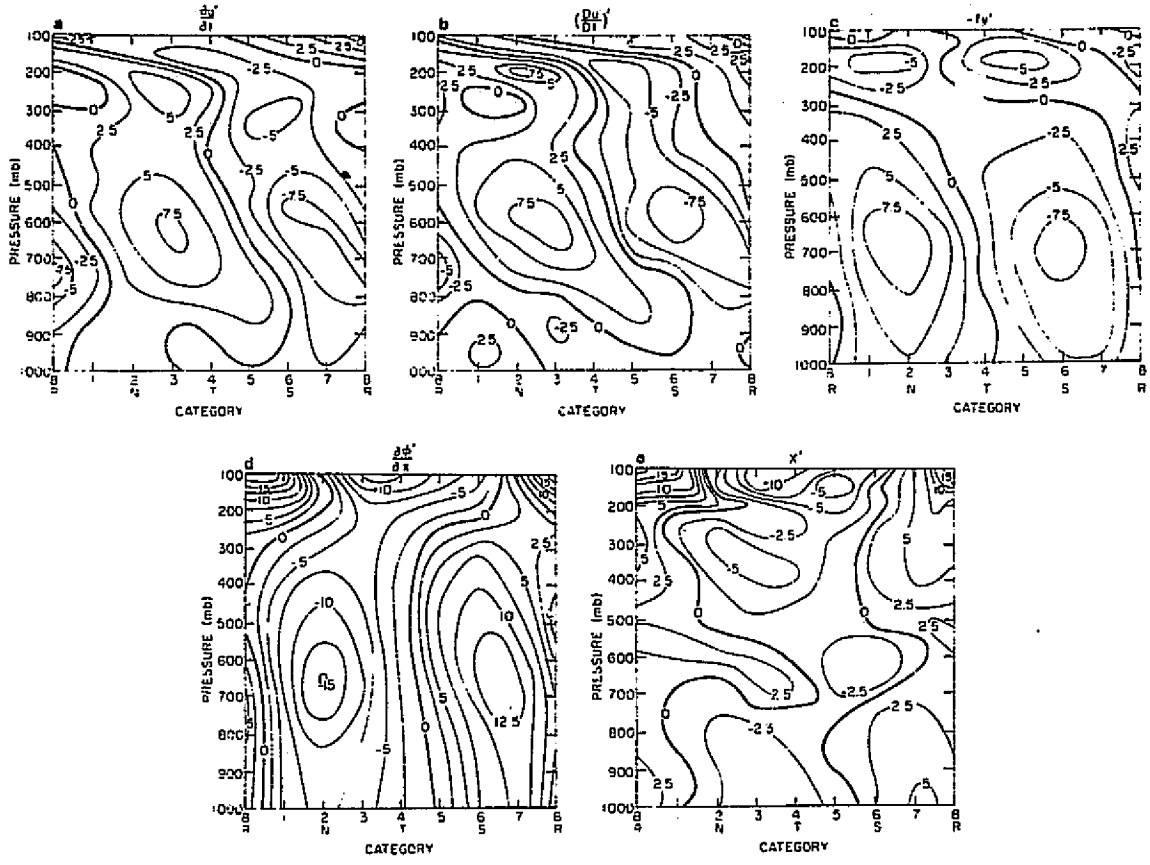

FIGURE 3 Perturbation zonal momentum budget (10^{-5} m sec^{-2}) (from Stevens, 1979).

Coriolis or pressure-gradient terms. Somewhat surprisingly, in the trough it is a sink of westerly momentum at all levels except for a shallow layer at 600-700 mbar; in the ridge, it is a source of westerly momentum at all heights. Therefore the cumulus clouds apparently are not simply removing momentum from one level and transporting it to another; rather, "cumulus friction" provides a vertically integrated net source/sink of westerly momentum for different wave categories. Comparing the structure of X' with that of u' (cf. Figure 4c), it is apparent that this term dissipates zonal kinetic energy between 250 and 750 mbar since u' and X' are 180° out of phase.

Figure 4 displays the wave budget for meridional momentum. The advection of wave momentum by the mean zonal flow dominates the other advective effects, so that in this direction the amplitude of the wave acceleration is 30 percent smaller than the local tendency. Again the Coriolis force has approximately the same amplitude as the local tendency, so that quasi-geostrophy is not a good approximation for the meridional momentum budget. Nevertheless, it is remarkable that the pressure gradient force has not only the appropriate phase relationship with the Coriolis term for

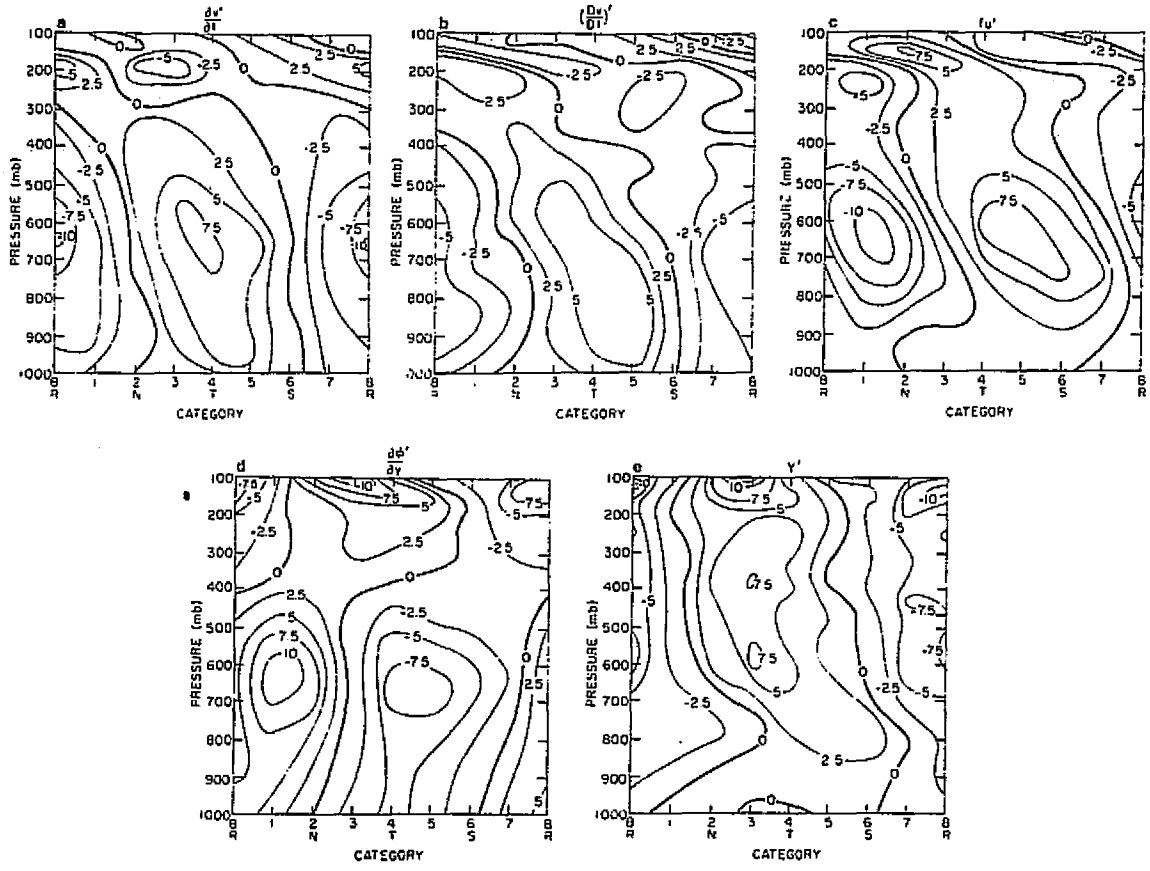

FIGURE 4 Perturbation meridional momentum budget (10^{-5} m sec^{-2}) (from Stevens, 1979).

geostrophy at the easterly jet level but also the same amplitude. Above 400 mbar, the phase relationship reverses.

The apparent source of meridional wave momentum Y' is similar to X' in that there are no broad reversals between upper and lower troposphere. Unlike X', the amplitude of Y' is comparable with other terms in the budget, indicating a relatively more important role for subgrid-scale effects. Y' and v' (cf. Figure 3c) are generally in quadrature through most of the troposphere (up to 350 mbar), suggesting internal transports of meridional momentum without much generation or dissipation of meridional kinetic energy by the clouds. Clearly, cumulus transports are an important part of the momentum budgets for the waves; equally clearly, their parameterization has no simple solution.

The primary result of a consideration of the mean momentum budgets is that thermal wind balance is a good approximation for the mean zonal flow.

REFERENCES

Cho, H.-R., L. Cheng, and R. M. Bloxam (1979). The representation of cumulus cloud effects in the large-scale vorticity equation. *J. Atmos. Sci. 36*, 127-139.

Reed, R. J., and R. H. Johnson (1974). The vorticity budget of synoptic-scale wave disturbances in the tropical western Pacific. *J. Atmos. Sci. 31*, 1784-1790.

Reed, R. J., D. C. Norquist, and E. E. Recker (1977). The structure and properties of African wave disturbances as observed during Phase III of GATE. *Mon. Wea. Rev. 105*, 317-333.

Reed, R. J., and E. E. Recker (1971). Structure and properties of synoptic-scale wave disturbances in the equatorial western Pacific. *J. Atmos. Sci. 28*, 1117-1133.

Reeves, R. W., C. F. Ropelewski, and M. D. Hudlow (1979). Relationships between large scale motion and convective precipitation during GATE. *Mon. Wea. Rev.*, to be published.

Riehl, H., and R. P. Pearce (1968). Studies on the interaction between synoptic and mesoscale weather elements in the tropics, Part II: Vorticity budgets derived from Caribbean data. *Atmos. Sci. Paper No. 126*, Colorado State U., Ft. Collins, Colo., 32 pp.

Ruprecht, E., and W. M. Gray (1976). Analysis of satellite-observed tropical cloud clusters. I. Wind and dynamic fields. *Tellus 28*, 391-413.

Shapiro, L. J. (1978). The vorticity budget of a composite African tropical wave disturbance. *Mon. Wea. Rev. 106*, 806-817.

Stevens, D. E. (1979). Vorticity, momentum, and divergence budgets of synoptic-scale wave disturbances in the tropical eastern Atlantic. *Mon. Wea. Rev. 107*, 535-550.

Thompson, R. M., S. W. Payne, E. E. Recker, and R. J. Reed (1979). Structure and properties of synoptic-scale wave disturbances in the Intertropical Convergence Zone of the eastern Atlantic. *J. Atmos. Sci. 36*, 53-72.

Williams, K. T., and W. M. Gray (1973). Statistical analysis of satellite-observed trade wind cloud clusters in the western North Pacific. *Tellus 25*, 313-336.

DISCUSSION

M. Rennick, *Rapporteur*

Comments and discussion concerned four general areas.

There was considerable discussion as to the reliability of the computation of the individual terms in the vorticity and momentum budget equations. Average values of vorticity and divergence can be computed on the scale of the observations, but it is not clear that further derived quantities, such as advection and twisting terms, can be accurately computed by taking derivatives of these data. This is because the regions of strong updrafts and cumulus activity occur on scales of 100-200 km. The actual gradients of vorticity may be significantly different from those computed in this study. The problem is only partially eliminated

by the linear in time, quadratic in space polynomial fit. In particular, it was pointed out that when vorticity and divergence are well correlated on the small scale, their product may be difficult to compute with confidence.

Further discussion addressed the question of whether, in spite of the possible shortcomings of the budget computations, the results indicate a scheme by which sources of vorticity and/or momentum may be parameterized in terms of the large-scale flow. It was suggested that a simple eddy diffusivity formulation could be used to obtain the zonal momentum budget but not the meridional budget. Some of the results seem to indicate that sources of vorticity could be parameterized in terms of a down-gradient transport, proportional to the divergence. However, this result was not so simple for the case of the B-scale composite wave.

Closely related to this was a discussion of the consistency of these results with those of other studies. Similar work in the Pacific suggests that the divergence term in the vorticity equation is only about a factor of 2 larger than the twisting term, upsetting the apparent balance between the divergence and the small-scale forcing. This difference may be due simply to differences between the two types of systems studied. The differences in the vorticity budgets computed by Stevens and Shapiro for waves in the GATE area are attributed to Shapiro's assumptions of a zonally uniform mean jet and a constant phase speed for the waves. Stevens avoided these assumptions.

Several questions were raised as to whether there exist cloud data that indicate that cumulus activity actually accomplishes the transports of vorticity and momentum required by the budget computations. Aircraft data present a rather confused picture of the momentum transport by the clouds, since values of w are generally small, and u varies over a wide range. It was pointed out that the question is more complex than simply a determination of $\overline{u'w'}$. Since the active systems were usually short lived, there are sampling problems in the data. Mesoscale organization may result in larger transports than the cloud data indicate. Some cloud parameterizations indicate that convection can accomplish some of the required momentum transports, particularly at low levels. This will be discussed further in a later presentation.

GATE RADIATION SUBPROGRAM RESULTS OF SIGNIFICANCE TO NUMERICAL MODELING

Stephen K. Cox
Colorado State University

In this paper I point out specific atmospheric radiation research results from GATE that may have an impact on future numerical modeling efforts. Some of the relationships between the researches and numerical modeling are more direct than others; I take a broad perspective of this relationship and assume that any basic understanding or insight into an unresolved or heretofore unrecognized problem does have a potential impact on future tropical numerical modeling studies.

Smith *et al.* (1977) reported radiance observations in several spectral bandpasses that closely match those bandpasses used in calculating irradiances and divergence values. In essence, these observations allow one to estimate the change of transmissivity with height in these bandpasses. This is a significant contribution in that it is precisely this transmissivity function that is then used to calculate flux divergence in many numerical model radiation algorithms.

Elllingson (1977) reported a set of observations similar to those of Smith *et al.*, with special emphasis on the lowest several kilometers of the atmosphere.

The effects of clouds on the tropospheric radiation budget has been recognized for decades but has received only scant attention because of the difficulty in making the complex computations of the radiative characteristics of specific clouds and the lack of adequate descriptions of the temporal and spatial distributions of clouds. GATE, with its extensive observational network of ship, rawinsonde, radar, aircraft, and satellite systems, together with powerful computational tools, has enabled us to construct four-dimensional representations of the tropospheric radiation budgets for the GATE A/B array. Figure 1 shows aircraft observations of the infrared heating rate for three different days during GATE when cirrus clouds were present. Clearly, these upper-tropospheric clouds dominate the radiative characteristics of an area when they are present. A number of insights into the interplay between clouds and radiation in cluster and synoptic-scale systems are apparent in the following analyses. Figure 2 illustrates the variability in 6-h average values of the long-wave and long-wave plus shortwave tropospheric radiative convergence. The variability is caused by clouds and is much greater in the long-wave component alone than in the total (shortwave plus long wave). The excursions in the long-wave values are clearly associated with cloud and cloud-free areas affecting the B array. On a

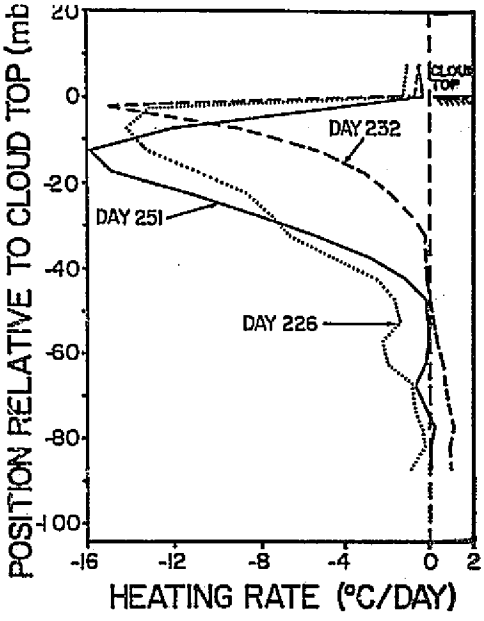

FIGURE 1 Day 251 irradiance profiles.

much smaller time and space scale, Figure 3 shows a N-S cross section of radiative convergence through a disturbance located with the B-scale array. The area of extensive cloudiness is located between 8.5 and 10° N latitude. Both parts of Figure 3 illustrate the magnitudes and spatial gradients to be expected in the radiative convergence values; they also show the magnitude of the diurnal variation in the radiative terms.

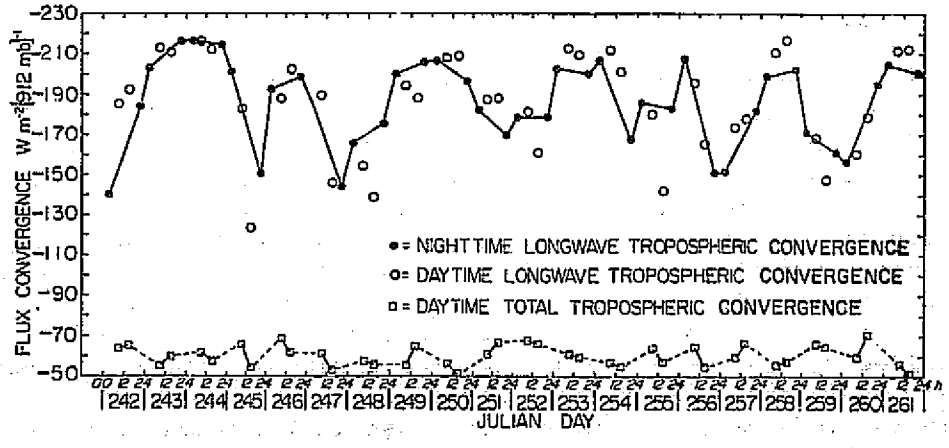

FIGURE 2 GATE Phase III B-scale array tropospheric (100-1012 mbar) LW convergence and daytime total convergence (SW plus LW) as a function of time.

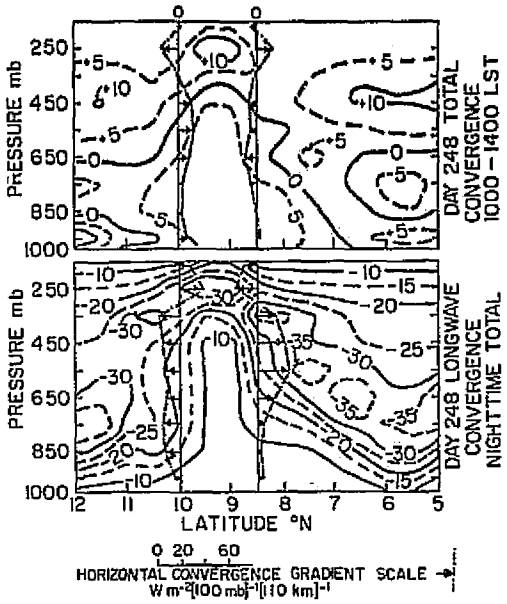

FIGURE 3 A pressure versus latitude (at 23.5° W longitude) cross section of the radiative convergence for the 0600-1800 LST period of Day 248. The top portion of the figure depicts the 1000-1400 LST total (SW plus LW) radiative convergence, and the bottom portion depicts the LW component only (nighttime total). Also shown is the magnitude and direction (arrows point toward regions of greater convergence) of the horizontal radiative convergence gradient (bottom scale) at two points.

Table 1 shows hour-by-hour B-scale average total (SW plus LW) radiative divergence profiles for the 5-day disturbed composite case. In contrast to the suppressed case, near local noon the disturbed case shows only ~45 percent of the troposphere being radiatively heated and the total tropospheric divergence (TTD) is -5.8 W m^{-2} (912 mbar)$^{-1}$. In the periods 0800-0900 and 1500-1600 the TTD values are nearly equal, i.e., -65.6 versus 65.5 W m^{-2} (912 mbar)$^{-1}$. However, the nighttime loss from the disturbed composite is -171.6 W m^{-2} (912 mbar)$^{-1}$, ~15 percent less than for the suppressed case.

If maritime disturbed and undisturbed regions are located adjacent to one another, it is most likely that any diurnal variability in the dynamics of the disturbed area will result from a variation in the horizontal gradients of the radiative divergence. The positive entries in Table 2 (italicized values) represent the condition for which the disturbed region is gaining more (or losing less) power per unit area per pressure interval by radiative processes than the suppressed region, and vice versa for the negative entries. These data show a significant diurnal variation in the difference between the disturbed and suppressed cases. Indeed, the difference changes sign for all layers except 300-400 mbar, where the suppressed region consistently gains energy relative to the disturbed region through the 24-h period. Solar absorption by high clouds accounts for the region of positive values for pressures <300 mbar between the hours of 0800 and 1600. In the disturbed region, these same clouds act as a veil and shade the lower troposphere from shortwave heating, thereby resulting in an effective cooling of the middle and lower troposphere. The positive values indicated for pressures >400 mbar are a result of stronger long-wave cooling of the suppressed area associated with its predominantly clear areas and lower tropospheric clouds. The negative values in these

TABLE 1 Vertical Profiles of the Nighttime and the *Hour* by *Hour* Daytime B-Scale Array Total Divergence (SW plus LW) for the Five-Day *Disturbed Composite Case*[a]

Pressure (mbar)	Local Time 1100–1200 and 1200–1300	1000–1100 and 1300–1400	0900–1000 and 1400–1500	0800–0900 and 1500–1600	0700–0800 and 1600–1700	0600–0700 and 1700–1800	1800–0600 Night
100							
200	*4.0*	*2.8*	*0.5*	-2.7	-6.7	-11.1	-11.1
300	*7.5*	*5.5*	*1.5*	-4.1	-11.0	-18.6	-21.3
400	*5.1*	*3.1*	-0.8	-6.2	-12.8	-20.2	-26.5
500	*1.0*	-0.6	-3.6	-8.0	-13.3	-19.3	-26.8
600	-1.1	-2.5	-5.1	-8.9	-13.5	-18.7	-24.9
700	-2.5	-3.5	-5.5	-8.2	-11.6	-15.4	-19.2
800	-5.8	-6.5	-7.8	-9.6	-11.8	-14.3	-16.3
900	-5.9	-6.4	-7.2	-8.4	-9.8	-11.5	-12.9
1000	-4.3	-4.5	-5.0	-5.6	-6.4	-7.3	-8.6
1012	-3.8	-3.9	-3.9	-3.9	-3.9	-4.0	-4.0
TTD	-5.8	-16.5	-36.9	-65.6	-100.8	-140.4	-171.6

[a] Italicized areas indicate regions of actual radiative heating; units are watts per square meter per pressure interval.

TABLE 2 Vertical Profiles of the *Difference* in B-Scale Total Divergence, Nighttime and *Hour* by *Hour* Daytime, from the Disturbed Composite to the Suppressed Composite Case[a]

Pressure (mbar)	Local Time 1100–1200 and 1200–1300	1000–1100 and 1300–1400	0900–1000 and 1400–1500	0800–0900 and 1500–1600	0700–0800 and 1600–1700	0600–0700 and 1700–1800	1800–0600 Night
100	*1.3*	*0.7*	-0.5	-2.0	-4.1	-6.3	-4.9
200	*5.0*	*4.2*	*2.6*	*0.4*	-2.3	-5.2	-4.5
300	-4.8	-4.5	-4.0	-3.1	-2.0	-0.9	-0.9
400	-8.2	-7.4	-5.7	-3.5	-0.7	*2.3*	*2.0*
500	-5.3	-4.2	-2.0	*1.0*	*4.7*	*8.7*	*9.0*
600	-4.6	-3.4	-1.1	*2.2*	*6.1*	*10.5*	*8.8*
700	-2.2	-1.1	*0.9*	*3.9*	*7.5*	*11.4*	*8.2*
800	-2.3	-1.4	*0.4*	*2.9*	*6.0*	*9.4*	*7.2*
900	-6.2	-5.3	-3.8	-1.5	*1.2*	*4.2*	*4.3*
1000	-0.6	-0.6	-0.5	-0.4	-0.2	-0.1	*0.1*
1012							
TTD	-22.9	-23.0	-13.7	-0.1	*16.2*	*34.0*	*29.3*

[a]Italicized areas indicate regions where the disturbed case is gaining more (or losing less) energy than the suppressed area. Units are watts per square meter per pressure interval.

lower layers around local noon are caused by solar heating in the suppressed area compensating for the larger long-wave losses. Note that no negative values are found for the nighttime case for pressures >400 mbar. At higher levels, however, the sign of the nighttime differences reverses. This is caused by the large long-wave losses from high clouds in the disturbed area. These losses are overpowered by solar heating for only a relatively few hours surrounding local noon. It is important to note that both the area average and the composite presentations smooth the actual magnitudes of these horizontal gradients.

Figure 4 shows extreme values in the TTD and each of its components for the B-scale array for different averaging periods during Phase III. Only the TTD will be discussed, although the reader may find it useful to refer to the individual components in interpreting the TTD envelope of values. The maximum range of extreme values is for the 12-h averaging interval, the shortest averaging period considered; the difference between maximum and minimum values is ~40 W m^{-2} (912 mbar)$^{-1}$. This range decreases to ~12 and 5 W m^{-2}(912 mbar)$^{-1}$ for three-day and six-day averaging periods, respectively, with the rate of decrease beyond six days becoming very small. In essence, this six-day period corresponds approximately to the passage-time of two easterly waves through the B-scale array; after two complete cycles have been sampled, additional cycles disturb the average very little.

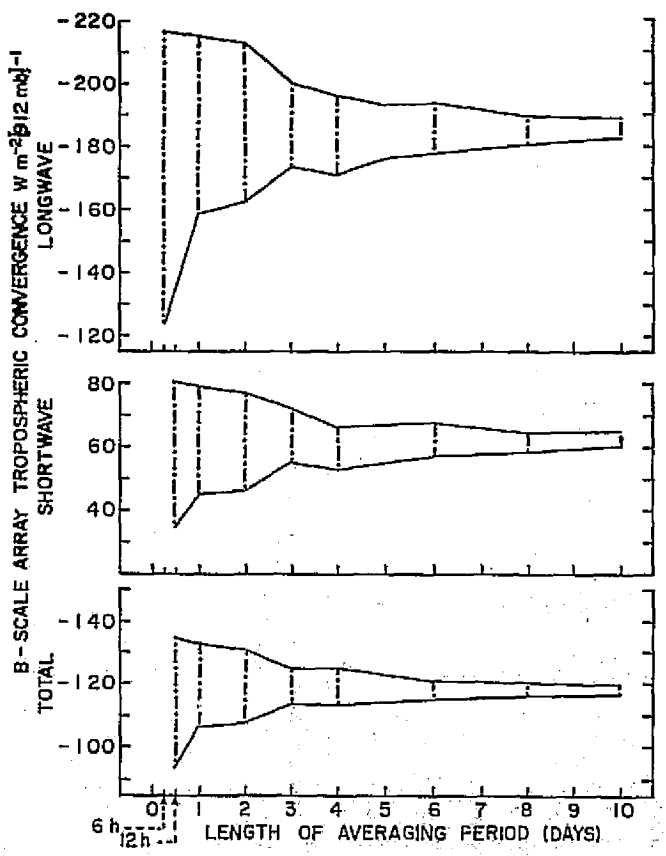

FIGURE 4 Extreme values of the B-scale array tropospheric convergence for the LW, SW, and total components for different temporal averaging periods.

In a recent presentation at the 1979 annual meeting of the American Meteorological Society in Reno, Nevada, Hay and Hanson presented results of constructing a surface solar irradiance budget for the GATE A/B array from a combination of satellite and ship data. The success of this technique and an extension to the total surface radiation budget was independently predicted by Cox and Griffith (1979) from the results shown in Figure 2.

The constancy of the long-wave net irradiance (~ ±10 to 20 W m^{-2}) at the surface in the presence of a large water-vapor overburden (~5 pr cm) and small temperature excursions allows one to relate variations in the infrared atmospheric radiative divergence to the outgoing infrared irradiance at the top of the atmosphere; the latter variable is directly observable and, therefore, represents a direct check of the infrared component of the model's computation. In the daytime the shortwave component may also be checked in one or more of the following modes: constancy of the total tropospheric convergence may be inspected (see Figure 2); the inverse correlation between observations of SW↑ at the top of the atmosphere with the calculated surface shortwave budget may be analyzed. In short, there are a number of ways to use the peculiar characteristics of the tropical atmosphere to check and perhaps simplify model radiation calculations.

The work of Carlson (1977) and Prospero (1977) has significantly increased our awareness of the potential effects that airborne dust may have on the radiative characteristics of the atmosphere. The most intense dust outbreaks were well north of the GATE A/B array during GATE. Had they occurred farther south within the GATE observation network, more definitive information might be available; however, at present we can only say that this topic needs additional investigation.

REFERENCES

Carlson, T. N. (1977). Report of the U.S. GATE Central Program Workshop. National Center for Atmospheric Research, Boulder, Colo., July 25-August 12, 1977.

Cox, S. K., and K. T. Griffith (1979). Estimates of radiative divergence during Phase III of the GARP Atlantic Tropical Experiment, Part II. Analysis of Phase III results. *J. Atmos. Sci. 36*, 586-601.

Ellingson, R. G. (1977). A summary of longwave cooling in the sub-cloud layer during GATE observation periods I and II. Personal Communication.

Griffith, K. T., and S. K. Cox (1977). Infrared radiative properties of tropical cirrus clouds inferred from broadband measurements. *Atmos. Sci. Paper 269*, Colo. State U., Ft. Collins, Colo., 102 pp. (NTIS #PB 268 834).

Prospero, J. (1977). Report of the U.S. GATE Central Program Workshop. National Center for Atmospheric Research, Boulder, Colo., July 25-August 12, 1977.

Smith, W. L., W. C. Shen, and H. B. Howell (1977). A radiative heating model derived from the GATE MSR Experiment. *J. Appl. Meteorol. 16*, 384-392.

DISCUSSION
M. Rennick, *Rapporteur*

Before the general discussion on Cox's talk, Carlson presented some results of his investigations of the dust layer in the northern part of the GATE area. Warm air carries dust aloft in a layer from 900 to 500 mbar off the coast of Africa. Its optical depth is a maximum at about 19° N. The maximum excess heating rate, averaged over a 24-h day, is about 2°C/day at 650 mbar. This is computed as an excess over the dust-free case. The excess long-wave cooling is greatest near 600 mbar, with warming below 900 mbar. The total effect of the dust layer is to produce net excess warming at low levels with a (perhaps artificial) relative minimum near 900 mbar. The overall effect of the dust layer seems to be to enhance the subsidence at night and to suppress it during the day. It helps to preserve the north-south temperature gradient in the oceanic region, and thereby to maintain the easterly jet.

Questions on Cox's talk concerned the implications of his results for the type of mesoscale systems observed in GATE. For cloud base at about 5 km the results suggest a thin layer of cooling of about 20°C/day near cloud top at night and a somewhat deeper layer of warming at about 5°C/day in the afternoon. The suggested low-level profiles are quite similar for day and night, with slight warming just below cloud base and cooling in the lowest 2 km. This profile below cloud base is probably highly dependent on the moisture profile. These radiation profiles would suggest that mesoscale differences between cloud and cloud-free areas would give a daytime maximum in upward motion in the anvil area. This would act in the same direction as condensation in the anvil. At night the radiatively forced circulation would be reversed.

THE GATE FAIR-WEATHER BOUNDARY LAYER

Margaret A. LeMone
National Center for Atmospheric Research

INTRODUCTION

The GATE fair-weather boundary layer has very low turbulence energies. Air-sea temperature contrasts are small, so buoyancy forces are considerably less than in over midlatitude oceans or land. Winds are typically about 3 m/sec. Thus, mixing is even less vigorous than in the trades, where buoyancy forces are comparable. As in most marine boundary layers, water vapor is an important contributor to the buoyancy force. The well-mixed layer, which extends roughly to cloud base, is about 550 m deep, a factor of 3 less than the typical afternoon land value.

Being over the ocean, the air has uniform fetch for hundreds of miles. The diurnal variation is small, yet nonuniformities exist in the mesoscale (10-100 km) even under the most suppressed conditions.

Seven fair-weather days in GATE are analyzed to show the typical structure of the mixed layer. Mean profile and wind, temperature (θ and θ_v), and mixing ratio q are presented. Fluxes of θ and q are shown to be related to cloudiness in such a way that the θ_v flux profile is nearly invariant, if normalized by its surface value. Eddy size is found frequently to exceed the expected $2h$ (h = subcloud layer depth), except for vertical velocity. However, the smaller scales ($<2h$) account for most of the transport. A few examples of mesoscale structures are presented, and their origins discussed. Although these structures are revealed in the cloud field, we shall see that the reverse is not necessarily true. That is, patches of clouds can be maintained for several hours without supporting mesoscale circulation.

Much of the work here is based on gust probe data from three aircraft: the U.S. DC-6 (Bean *et al.*, 1976), the UK-C130 (Nicholls, 1978), and the U.S./NCAR L-188 (e.g., Pennell and LeMone, 1978).

MEAN STRUCTURE

We define the atmospheric boundary layer as that part through which the effect of the surface friction and heating are directly felt. It is generally divided into three parts: the *mixed layer*, which has a nearly constant virtual potential temperature θ_v with height, and a nearly constant, slowly decreasing mixing ratio, q. If there are clouds, the

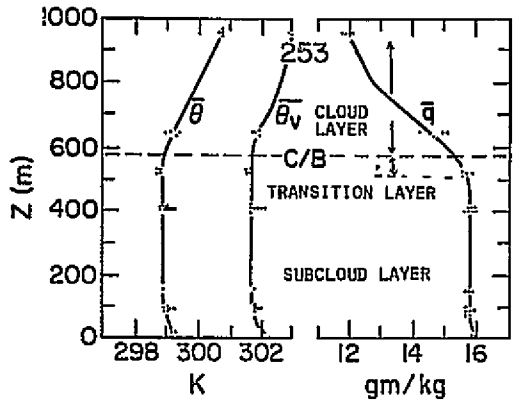

FIGURE 1 Profiles of θ, θ_v, and q for Day 253 (September 10), which had 10 percent Cu from 600 to 1100 m.

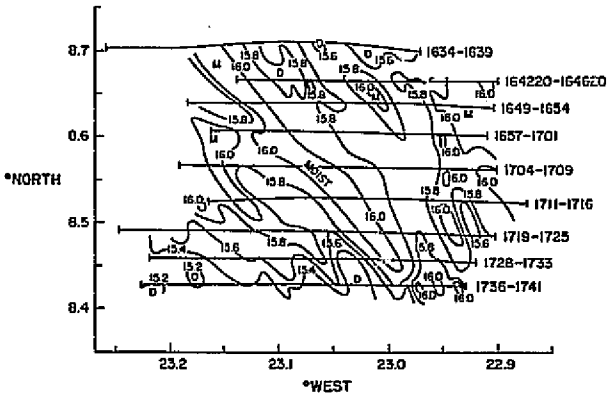

FIGURE 2 q field at 150 m on Day 253, from UK-C130 data. Numbers at ends of legs denote times (GMT).

cloud layer extends from cloud base to cloud top and has a q falloff and θ_v rise intermediate between the mixed layer and the atmosphere above. The *transition layer*, being occupied by both cloud layer (or free atmosphere) and mixed layer air, has intermediate properties. For the days examined, the mixed-layer depth is typically 500 m, and the cloud layer extends to 1-1.5 km. The transition layer, *as we define it here*, is about 50-100 m thick. We shall see below, however, that fluctuations in mixed-layer height are rather large, so this is a conservative estimate. For analysis, we choose here to use the subcloud layer depth h. Figure 1, showing the profiles for a typical fair-weather GATE day (Day 253), illustrates well the three layers. Winds are light, generally less than 4 m sec^{-1}.

Examination of sea-surface mapping missions of the UK-C130 shows the horizontal fields to have structure on the 10-50 km scale. Figure 2 shows the q field at 150 m on Day 253. The structure is normal to the shear (see Figure 3) through the transition level, suggesting an origin from shear gravity waves. Structure on this scale is common and possibly accounts for the variation in mixed-layer height seen in the tethered balloon data (NSF/NCAR, 1976). Examination of spectra suggests also that it can account in part for the large increase in q variance with height in the upper half of the mixed layer. (Clouds, as we shall see, are also important.)

FLUX PROFILES

The vertical flux profiles for θ and q for fair-weather days in GATE are illustrated by the schematic in Figure 4 (left). The profiles marked "1" are for a virtually clear day (258); those labeled "2" are for a day (253) with scattered clouds (10 percent) to 1100 m; and the "3" profiles depict fluxes on a day with scattered to broken cloud, some with tops to 3 km, and showers. Most notable is the extreme sensitivity of the humidity flux profile to cloudiness overhead, with large increase in fluxes at cloud base with relatively small increase in cloudiness. This is offset by more negative temperature fluxes at cloud base, in such a way that the surface-normalized virtual temperature flux is nearly invariant [Figure 4 (right)], decreasing linearly with height to a value of -1/5

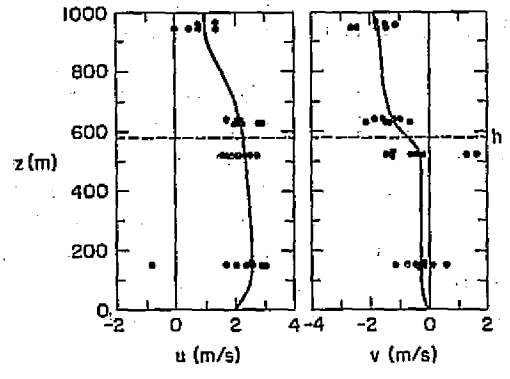

FIGURE 3 Profiles of u (positive east) and v (positive north), for Day 253.

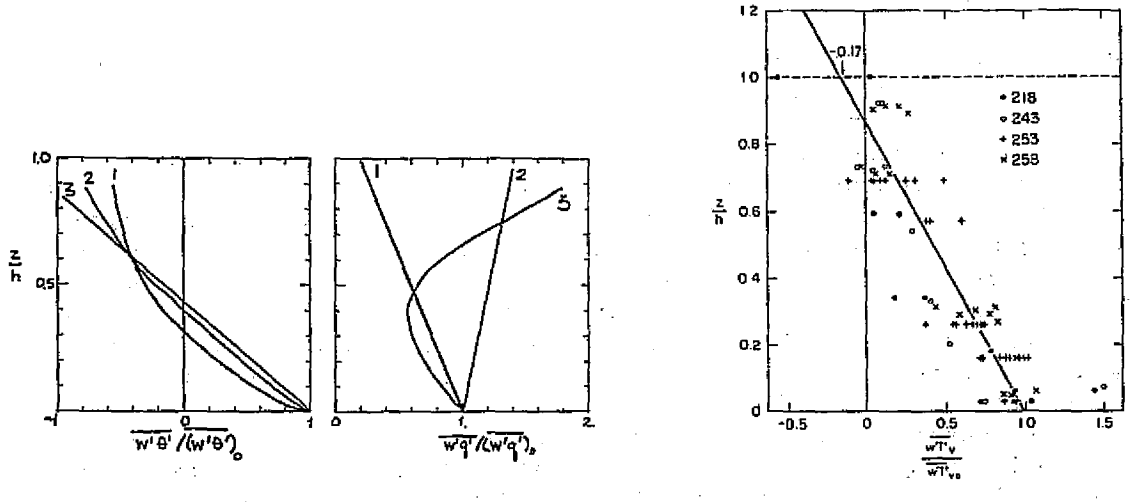

FIGURE 4 (Left) Schematic of flux profiles for $\overline{w'\theta'}$ and $\overline{w'q'}$ for 1, Day 258 (nearly clear); 2, Day 253 (10 percent Cu, from 600 to 1100 m); 3, Day 243 (10-50 percent Cu from 450 to 3000 m in spots), isolated showers. All profiles are normalized by their surface values. (Right) Surface-normalized profile of $\overline{w'\theta_v'}$ for four days, including 243, 253, and 258.

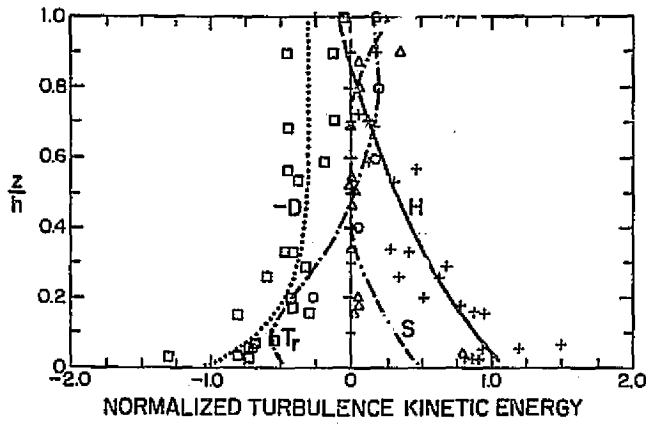

FIGURE 5 Composite turbulence kinetic energy budget for several GATE fair-weather days. The plus symbols denote buoyancy production (H); the triangles, shear production (S); the squares, dissipation ($-D$); and the circles, vertical turbulence transport of turbulence kinetic energy (Tr). The dot-dash curve is the residual after summing paired curves through H, S, and $-D$.

times the surface flux. For the cases studied, the temperature flux is balanced (within experimental accuracy) with net radiation flux divergence.

Momentum fluxes are small, barely resolvable by aircraft measurements. However, it can be said that, for all cases examined, they were almost exclusively down the gradient, even in the cloud layer. Thus clouds, like subcloud layer eddies, were acting as mixers. This is in contrast to the locally countergradient momentum flux found in the trade wind mixed layer by Pennell and LeMone (1974).

Surface fluxes of temperature and humidity found from downward extrapolation aircraft flux profiles matched closely those determined using bulk formulas on ship boom data.

TURBULENCE KINETIC ENERGY BUDGETS

The composite turbulence kinetic energy budget for four fair-weather days appears in Figure 5. All values are normalized by the value of the buoyancy production term, H, at the surface. The remaining terms are S, shear production; D, dissipation; and Tr, transport of turbulence kinetic energy. Transport of pressure cannot be determined from aircraft data. However, if we fit curves through all terms but Tr, we find that the residual assuming that transport is balanced by dissipation and production follows well the circles representing kinetic energy transport. This suggests that pressure transport is small within the subcloud layer. (This may not be true at the surface.) The normalized turbulence kinetic energy budget is quite similar to that measured over eastern Colorado by Lenschow (1970), with buoyancy the dominant production term.

The temperature variance budget (not shown) has dissipations that are "too small" compared with those over land. This *may* be related to the 10-km scale structures such as those in Figure 2, for which attenuation due to radiation may be important. Indeed, using the simple radiation formulation of André *et al.* (1978), the radiation dissipation is of the same order of magnitude as thermal dissipation. This is still under investigation.

EDDY STRUCTURE

The scale of maximum energy for vertical velocity, w, is shown as a function of height in Figure 6, for alongwind (top) and crosswind (bottom) aircraft tracks. Wavelength λ, is normalized by h. In the lowest 200 m, the scale of w eddies increases approximately linearly with height, with alongwind axes 2-3 times the cross wind axes. Maximum eddy size is 1.5-2 h. In the upper subcloud layer, the alongwind eddies scale with h in a similar manner to those measured over land in the Minnesota experiment (Kaimal *et al.*, 1976); lower, the eddies in GATE are 2-3 times too large. Since h for the land data were 2-3 times h for GATE, the actual eddy sizes are the same, suggesting that a scaling with z would be more appropriate.

Spectra for T, q, u, and v (not shown) are often dominated by mesoscale motion such as that shown in Figure 2. Figure 7 shows the energy peaks of the q-w cospectrum as a function of height. The plots, like those for w, show behavior reminiscent of a classical fair-weather boundary layer, with eddies reaching about $2h$ in horizontal extent. The 10-km mesoscale motions, in fact, seem to contribute 20 percent or less to all fluxes but temperature, where it is occasionally larger. The smaller ($<2h$) eddies'

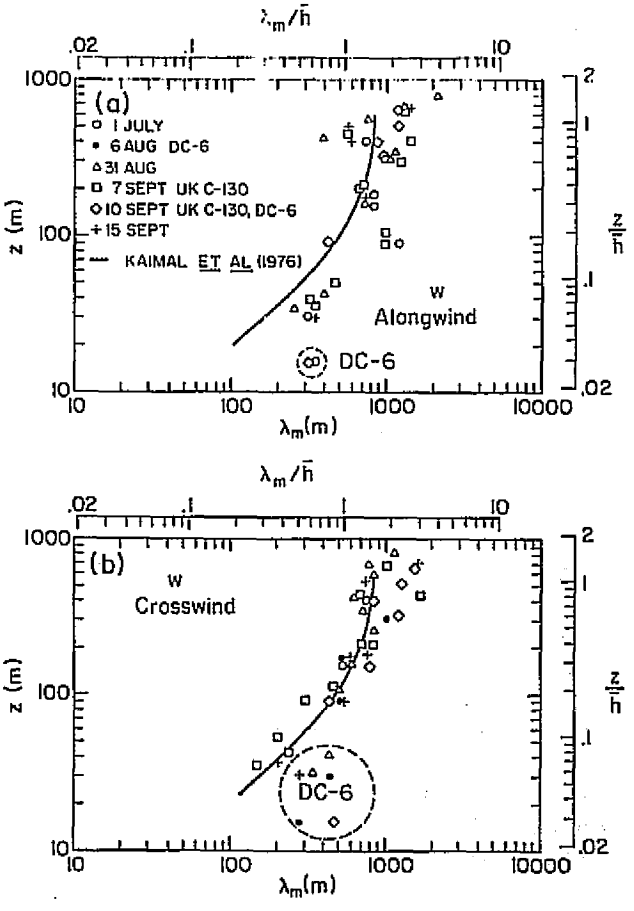

FIGURE 6 Scale of maximum energy in w eddies, normalized by h (cloud base height).

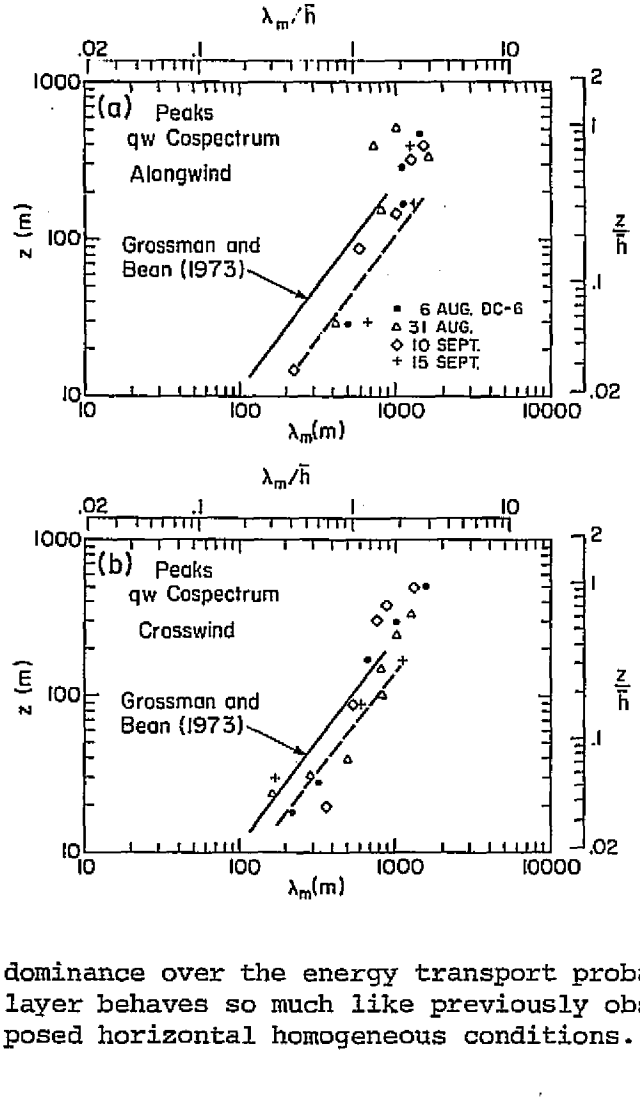

FIGURE 7 Scale of maximum energy *for* w-q covariance, normalized by h.

dominance over the energy transport probably explains why the subcloud layer behaves so much like previously observed boundary layers with supposed horizontal homogeneous conditions.

CLOUD-SUBCLOUD LAYER INTERACTION

Barnes *et al.* (1979) found significant local modification of the subcloud layer by cumulus convection on day 253. However, it was difficult, statistically, to find warm (or cool) moist cloud "roots" from aircraft data. This could be because the "roots" did not consistently intercept the aircraft path before or after observation of cloud overhead or because the cloud "root" had risen out of the subcloud layer to form the cloud, and there is no "root" in the classical sense. However, there is other evidence of the interaction in the GATE data (other than the already mentioned moisture flux). The mesoscale structures such as those in Figure 2 seem related to cloudiness. Also, the variation of humidity variance, like the flux, is sensitive to cloudiness. Figure 8 shows mixing ratio variance $\overline{q'^2}$ as a function of height for two flight legs on Day 243. On the west leg, which had slight convection, the humidity variance shows

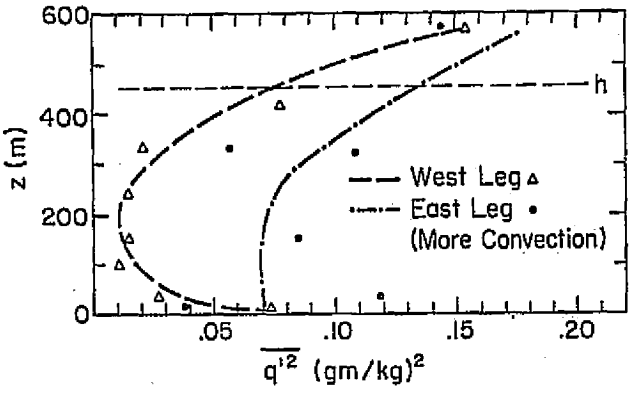

FIGURE 8 Mixing ratio variance, $\overline{q'^2}$ as a function of height for Day 243. The east leg has some Cu to 3 km and showers. The west is more suppressed.

an increase with height from about $\frac{1}{2}h$; but for the last leg, which was flown beneath deeper convection, variance increased from the surface.

Cloud patchiness in fair weather was observed in GATE, as for other tropical areas, on scales of the order of tens to hundreds of kilometers. Based on the humidity flux profiles presented earlier, and accounting for temperature flux profiles (a relatively minor effect) by assuming "invariant virtual temperature flux profiles," one can calculate how long it would take for cloudier areas to "dry up" and turn "clear" (lifting condensation level greater than 650 m). It turns out that GATE patches observed can exist for >20 h without mesoscale support from moisture advection. Hence it is not surprising that one could not observe a complete "cycle" for a large group of cumuli.

DIURNAL VARIATION

The diurnal variation of the 10-m temperature (~0.5°C) and moisture (~0.5 g/kg) is small (LeMone, 1980), a consequence again of the slowly responding sea-surface temperature (0.5°C range). The stratification in the surface layer is nearly always unstable. The surface layer (and perhaps the entire mixed layer) seems most unstable in the early morning. A morning maximum in thunderstorm initiation observed by Gray and Jacobson (1977) supports this. The variation of the tropical marine surface layer winds is dominated by the semidiurnal pressure wave.

CONCLUSION

Certain aspects of the fair-weather boundary layer observed in GATE are similar to the daytime boundary layer over land, if we account for the great difference in buoyancy forcing. Examples are flux profiles, the budget of turbulence kinetic energy, and the scale of w eddies and of vertical transport. On the other hand, perhaps because of smaller turbulence energies, mesoscale structures are often readily visible, as are the effects of clouds. Further, the diurnal cycle is smaller, with perhaps the most unstable time in the early morning.

REFERENCES

André, J. C., G. DeMoor, P. LaCarrère, G. Therry, and R. de Vachet (1978). Modeling the 24-hour evolution of the mean and turbulent structures of the planetary boundary layer. *J. Atmos. Sci. 35*, 1861-1883.

Barnes, G., G. D. Emmitt, B. Brummer, M. A. LeMone, and S. Nicholls (1979). The effect of different observational techniques on the perceived structure of the fair weather boundary layer. Submitted to *Mon. Wea. Rev.*

Bean, B. R., R. O. Gilmer, R. G. Hartmann, R. E. McGavin, and R. F. Reinking (1976). Airborne measurement of vertical boundary layer fluxes of water vapor, sensible heat, and momentum during GATE. *NOAA Tech. Memo.* ERL-WMPO-36, 83 pp.

Gray, W. M., and R. W. Jacobson (1977). Diurnal variation of deep cumulus convection. *Mon. Wea. Rev. 105*, 1171-1188.

Kaimal, J. C., J. C. Wyngaard, D. A. Haugen, O. R. Coté, Y. Izumi, S. J. Caughey, and C. J. Readings (1976). Turbulence structure in the convective boundary layer. *J. Atmos. Sci. 33*, 2152-2169.

LeMone, M. A. (1980). The marine boundary layer. PBL Workshop report. Am. Meteorol. Soc., Boston, Mass. (to be published).

Lenschow, D. H. (1970). Airplane measurements of planetary boundary layer structure. *J. Appl. Meteorol. 9*, 874-884.

NSF/NCAR (1978). National Science Foundation and National Center for Atmospheric Research, Report of the U.S. GATE Central Program Workshop. May be obtained from Publications Office, NCAR, P.O. Box 3000, Boulder, Colo. 80307.

Nicholls, S. (1978). Measurements of convective boundary layer turbulence made by an aircraft over the sea. *Quart. J. R. Meteorol. Soc. 104*, 653-676.

Pennell, W. T., and M. A. LeMone (1974). An experimental study of turbulence structure in the fair weather trade wind boundary layer. *J. Atmos. Sci. 31*, 1308-1323.

Pennell, W. T., and M. A. LeMone (1978). An intercomparison of turbulence measurements from aircraft. Submitted to *J. Appl. Meteorol.*

DISCUSSION

S. Esbensen, *Rapporteur*

The discussion centered on the mesoscale structures of the GATE fair-weather boundary layer, the validity of eddy-flux estimates from bulk aerodynamic formulas, diurnal variations in the undisturbed boundary layer, and the quality of boundary-layer humidity data from the B-scale radiosonde data set.

Participants felt that the significance of the mesoscale boundary features for the large-scale structure of the boundary layer needs to be assessed. Dynamical characteristics of the mesoscale features such as the propagation speed, generation mechanisms, and characteristic time scales were mentioned as potential areas for investigation. Also

mentioned were the vertical transports of heat, moisture, and momentum and the relationship, if any, of the mesoscale structure in the undisturbed boundary layer to vigorous mesoscale structure in the undisturbed boundary layer to vigorous mesoscale cloud systems. P. LeMone mentioned that second-order closure models of the atmospheric boundary layer are having difficulty simulating the mean wind and pressure fields. There is a growing realization that the failure to account for mesoscale structures may be responsible for the discrepancy in the model results.

Questions were raised concerning the reliability of estimates of surface boundary-layer fluxes using bulk aerodynamic formulas under undisturbed conditions during GATE. P. LeMone felt that the estimates should be within 30 percent of the true value if the surface meteorological variables were averaged over a sufficient period of time. Garstang suggested that the averaging time should be on the order of 1 h. Also, Holland suggested that the usefulness of constant transfer coefficients over oceanic regions during GATE undisturbed periods is primarily due to the near-neutral stratification of the surface boundary layer. It was also pointed out that the unusual $w'T'$ found during BOMEX was due to instrumental error.

It was noted that the maximum air-sea temperature differences presented by P. LeMone occur in the morning, rather than in the afternoon when deep convective activity is at a maximum. Albrecht showed evidence from the cloud observations at the *Charterer* to support the hypothesis that the early morning maximum in the air-sea temperature difference is related to cloudiness. However, it was agreed that the diurnal variations in deep convection are probably not related to the small changes in heat flux implied by the diurnal variations of the air-sea temperature difference.

An inquiry was made concerning the validity of an increase in specific humidity from the surface to the first 5-mbar level in the final B-scale radiosonde data set. Betts suggested that the cause of the unreasonable increase is the time-lag correction, but sensitivity tests performed by Reeves while at CEDDA did not support this hypothesis. The reported surface values are apparently of reasonable quality, however.

THE DISTURBED TROPICAL ATMOSPHERIC BOUNDARY LAYER

Michael Garstang
University of Virginia

I. THE DISTURBED BOUNDARY LAYER

Disturbed conditions are defined in terms of the time rate of change of variables of state (primarily temperature) at 10 m above the sea surface.

Figure 1 shows a complex and simple temperature signal at 10 m and the accompanying undisturbed, disturbed, and wake regions. In the undisturbed state, as described by LeMone in the preceding paper, the well-mixed layer (ML) is about 550 m deep, the transition layer about 50-100 m thick, with convective cloud base near 600-650 m. In the presence of active precipitating convective clouds (Figure 2) the ML can essentially disappear, and significant drying and cooling can take place resulting in marked stratification of the boundary layer. Fourteen pairs of soundings, where each

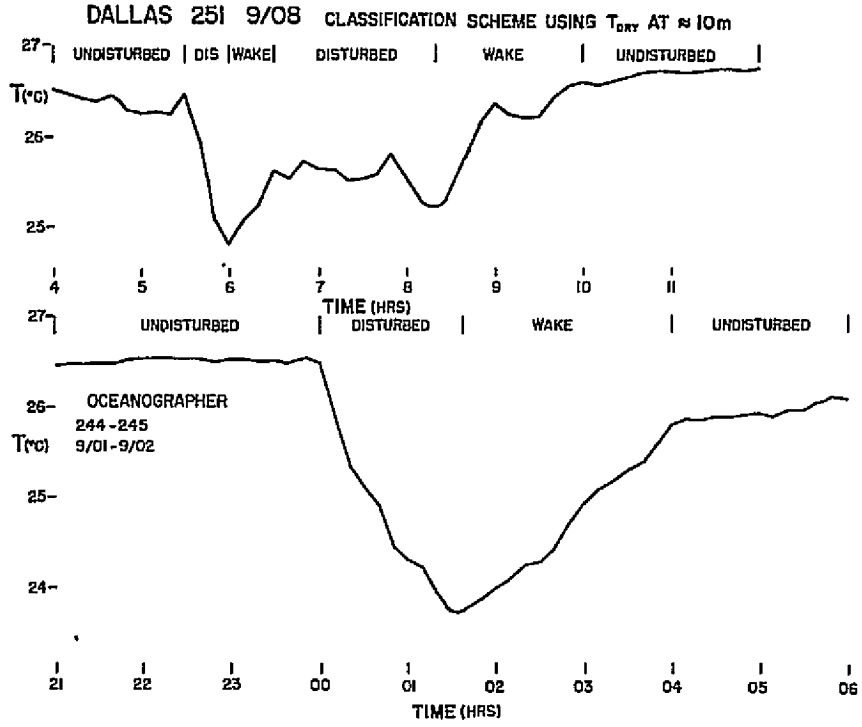

FIGURE 1 Temperature records from the *Oceanographer* and *Dallas*.

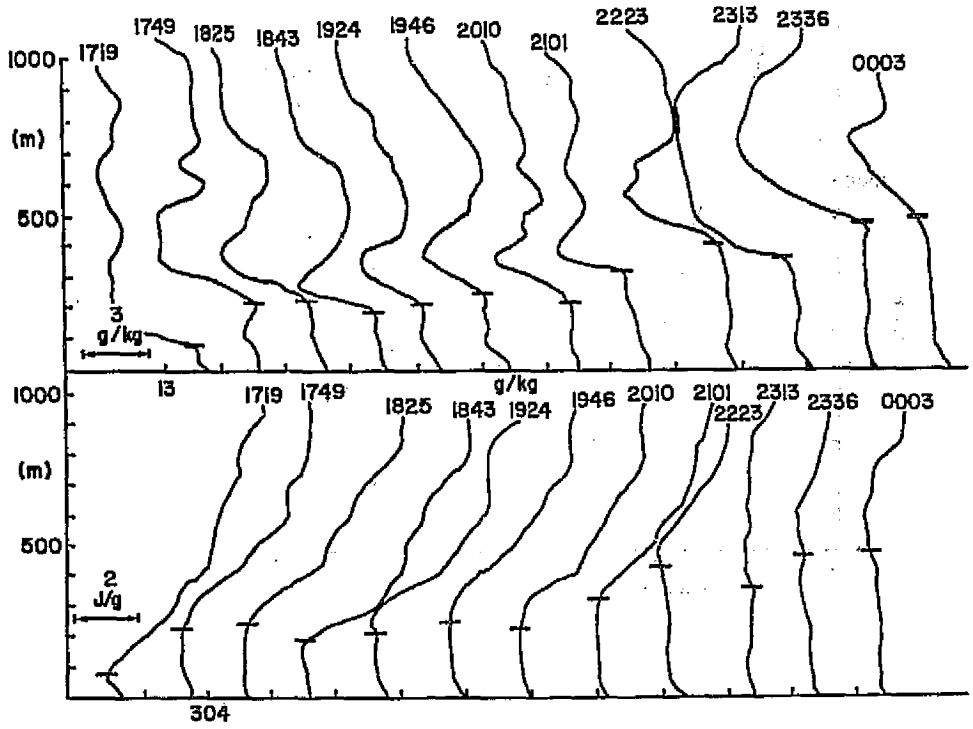

FIGURE 2 Sequence of BLIS profiles of (a) specific humidity and (b) dry static energy during the wake period following a storm made at the *Dallas* on 9/12/74.

pair consists of a "before" undisturbed sounding and an "after" the passage of the disturbance disturbed sounding, are shown in Figure 3. Mixed-layer height (Tables 1 and 2) changes from a mean of 520 ± 110 m to a mean of 163 ± 130 m in the "disturbed" area and a mean of 227 ± 115 m in the "wake." Mean maximum cooling of the layer is 2.0°C, mean cooling 1.2°C, mean maximum drying 1.4 g kg^{-1}, and mean drying 0.9 g kg^{-1}, where the average depth of the cooling extends to at least 850 m and for the drying to 620 m. Drying does not always take place.

II. TIME AND SPACE DISTRIBUTIONS

Table 1 shows the time distribution of undisturbed, disturbed, and wake conditions based on the surface temperature signal at the *Dallas*, *Oceanographer*, *Meteor*, and *Planet* for all of Phase III. Conditions were either disturbed or under a wake for 39 percent of the time. Gaynor (1977) using acoustic sounder records concluded that disturbed/wake conditions occurred at the *Oceanographer* 33 percent of the time. It would appear safe to conclude that for the GATE region under the influence of the equatorial trough, the atmosphere is subject to the influence of active convection one third of the time.

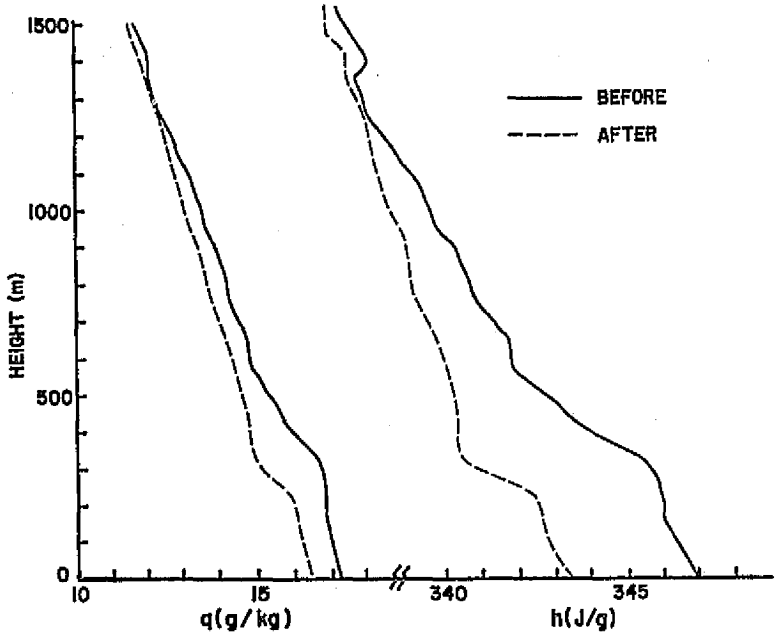

FIGURE 3 Mean profiles of specific humidity, q, and moist static energy, h, for the single-event composite from structure sonde data; the mean profiles before (after) are designated by solid (dashed) lines.

When a band 10 km wide is orientated along the wind and centered over the ship, we find that 70 to 85 percent of all echoes occurring within 30 km of the ship produce a temperature drop of 0.3°C or greater at the ship. In the wake of a disturbance, the effects of the convection are seen for distances up to 100 km from the leading edge of the system.

While the estimate of area or volume of air modified by cloud layer-subcloud layer interaction remains uncertain, it seems clear that substantial regions around active convection are modified by the action of the convection.

TABLE 1 Percentage Occurrence of Disturbances and Mixed-Layer Height: *Dallas*, *Oceanographer*, *Meteor*, and *Researcher*, Phase III Only

	Percentage of Time (%)		MLZ (m)	
Undisturbed	61		520 ± 110	
Disturbed	14	39%	163 ± 130	205 ± 120
Wake	25		227 ± 115	

TABLE 2 Boundary-Layer Mean Results for Light and Heavy Precipitation

Statistic	Precipitation Rate >3 mm h^{-1} (Mass Transport)	Precipitation Rate ≤3 mm h^{-1} (Evaporation)
Mean maximum cooling	2.0°C	1.1°C
Mean cooling	1.2°C	.7°C
Mean maximum drying	1.4 g kg^{-1} (q)	0
Mean drying	0.9 g kg^{-1}	0
Average depth of cooling	850 m to top of P.O.P at least	650 m
Average depth of drying	620 m	0
Average depth of moistening	--	540 m
Mean moistening	--	0.5 g kg^{-1}

III. TRANSPORTS THROUGH THE SUBCLOUD LAYER AND LOWER CLOUD LAYER

The draft structure of the subcloud layer and lower cloud layer has been described by Emmitt (1978). Subsequent work extending the original sample of 19 clouds by an additional 60 cases has substantially confirmed the original results. Figure 4 summarizes these earlier results from which we may conclude the following:

- Coherent updrafts and downdrafts are found from close to or at the sea surface through cloud base. Extension into the subcloud layer and coupling between the cloud and subcloud layers is clearly occurring.
- The ratio of updrafts to downdrafts is ~2:1; both updrafts and downdrafts lasted for approximately same time.
- 81 percent of all drafts were either warm/moist or cold/dry.
- Energy and mass fluxes associated with cold/dry downdrafts are of the same order as those associated with warm/moist updrafts.

The draft measurements allow us to estimate the cloud draft transports and to compare these cloud draft transports with separate budget (Brummer, 1978) estimates of the subgrid scale transports. Table 3 shows the results for a range of active cloud fractions and environmental mass flux. Updrafts and downdrafts in clouds may contribute between 62 and 82 percent of the subgrid scale energy fluxes at 500 m and between 47 and 74 percent at 1000 m.

If we multiply $\overline{M}$ (columns 4 and 5, where $M_c + M_e = \overline{M}$) by $\overline{h}$ (column 8) in Table 3 we obtain a grid scale flux of moist static energy of 11×10^3 W m^{-2} at 500 m. If we further assume $M_e = 0$, then this grid scale energy flux through 500 m must go through the individual cloud bases. Using 5.3 percent coverage by active cloud, we find that 208,905 W m^{-2} passes

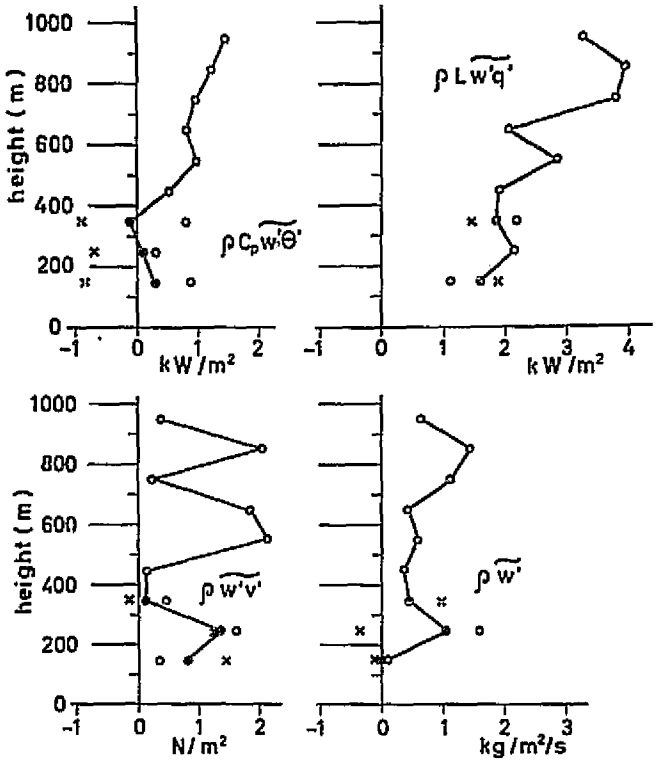

FIGURE 4 Total sensible heat, latent heat, momentum, and mass fluxes for the updrafts and downdrafts as measured by the tethered balloon system: X, nonbuoyant fluxes; 0, buoyant fluxes; 0, average fluxes where applicable.

through the cloud bases. With a mean vertical velocity of 0.50 m sec^{-1} (column 2 divided by ρ), this mean transport of total static energy is ≈2 orders of magnitude greater than the subgrid scale fluxes through cloud base. But with respect to three-dimensional divergence of the energy transports, the latter are at least of equal importance.

The individual clouds in the ITCZ consequently have a "conduit" behavior as proposed earlier by Riehl and Malkus (1958). Here we have more direct evidence that the deep convection is in fact capable of transporting the entire static energy upward, necessary for export to the higher latitudes in the upper troposphere.

The integrated result of the updraft and downdraft transports, as well as the role of any mesoscale circulation, may be reflected in the temperature and moisture changes at the surface. Figure 5 shows a relationship between precipitation amount and temperature change at 10 m. Depending on the organization, intensity, and stage in the life cycle of the convection, the effect on temperature may be marked (growing stage, operating on an undisturbed atmosphere) or weakened as the system decays or operates on a modified atmosphere. Changes in total static energy (Δh) (Figure 6) show that light rainfall events can produce no or weak + and - changes in total static energy. Heavy rainfall events show clear decrease in moist static energy. Table 2 illustrates the differences. The changes clearly indicate that under light precipitation evaporative cooling is occurring with little or no change in total static energy, suggesting no mass transport or overturning. The contrary is true for heavy rainfall: cooling and drying occur with a consequent drop in h and the requirement of mass transport.

TABLE 3 Vertical Flux of Total Static Energy at 500 m and 1000 m due to Cloud Convection in the Disturbed ITCZ[a]

Height (m)	σ (%)	$\overline{(\rho w)_c}$ (g m^{-2} sec^{-1})	M_c (g m^{-2} sec^{-1})	M_e	$\bar{h}_c - \bar{h}$ (J/g)	$M_c(\bar{h}_c - \bar{h})$ (W/m^2)	$\bar{h}$ (J/g)	$\bar{h}_e$ (J/g)	$\bar{h}_e - \bar{h}$ (J/g)	$M_e(\bar{h}_e - \bar{h})$ (W/m^2)	$\sigma\overline{\rho w_c' h_c'} + (1-\sigma)\overline{\rho w_e' h_e'}$ (W/m^2)	$\frac{\sigma\overline{\rho w_c' h_c'}}{\overline{\rho w' h'}}$ (%)
500	5.3	600	32.0	0.0	1.0	32	346	345.94	-0.06	0.00	148.00	82
500	6.6	600	40.0	-8.0	1.0	40	346	345.93	-0.07	0.56	139.44	77
500	8.0	600	48.0	-16.0	1.0	48	346	345.91	-0.09	1.39	130.61	73
500	10.6	600	64.0	-32.0	1.0	64	346	345.88	-0.12	3.81	112.19	62
1000	4.8	800	38.8	0.0	1.8	70	343.5	343.41	-0.09	0.00	195.0	74
1000	6.1	800	48.5	-9.7	1.8	87	343.5	343.38	-0.12	1.16	176.76	67
1000	7.3	800	58.2	-19.4	1.8	105	343.5	343.36	-0.14	2.72	157.28	60
1000	9.7	800	77.6	-38.8	1.8	140	343.5	343.31	-0.19	7.37	117.63	47

[a] At each of these heights computations are carried out for four different σ's (% area covered by active moist convection). Explanations of the column contents are included in Section IV of the text.

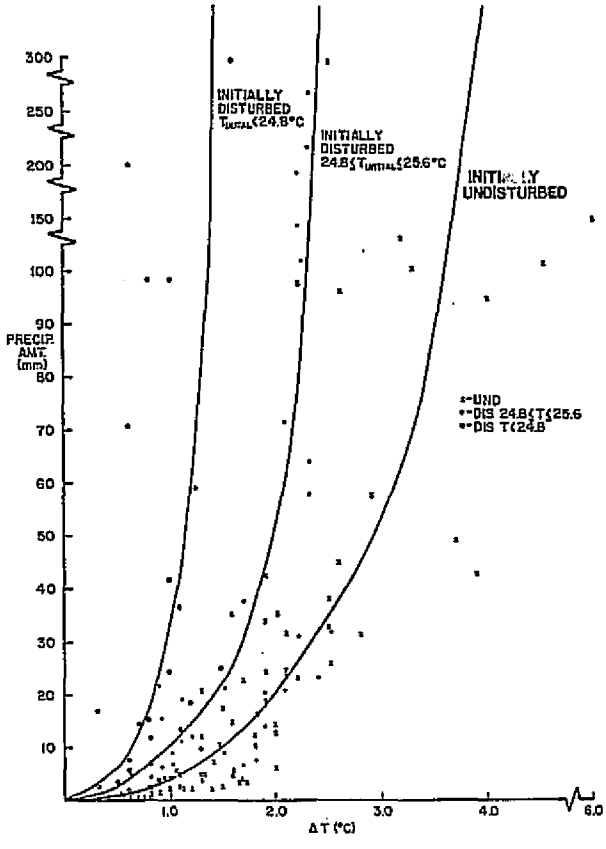

FIGURE 5 Curves describing the relationship between precipitation amount and temperature change ΔT, for each of the three initial conditions.

From these results it would appear that significant overturning or mass transport occurs only in the regions of heavy precipitation. Light precipitation does not result in mass transport, and postulates of anvil rain driving mesoscale circulations that penetrates the mixed layer are not supported by these data. The overturning postulated by Betts (1976) based on traveling Venezuelan disturbances is supported by our observations.

It may be possible to conclude from the results of the temperature and moisture changes as a function of precipitation rates and the overturning calculations that

1. The most intense mixing occurs in the core of the convective system coincident with the heavy rainfall. Here, vertical transfer of mass and significant changes in state occur.
2. Modification of the boundary layer is predominantly due to the mass transfer occurring in the core of the system.
3. No significant transfer of mass occurs outside of the core. Evaporative cooling in the light-rainfall areas changes temperature but not total static energy, and little or no mass exchange occurs. The mesoscale sinking commonly associated with anvil precipitation does not play any significant role in maintaining the modified temperatures and humidities of the boundary layer. On the contrary, increased mesoscale

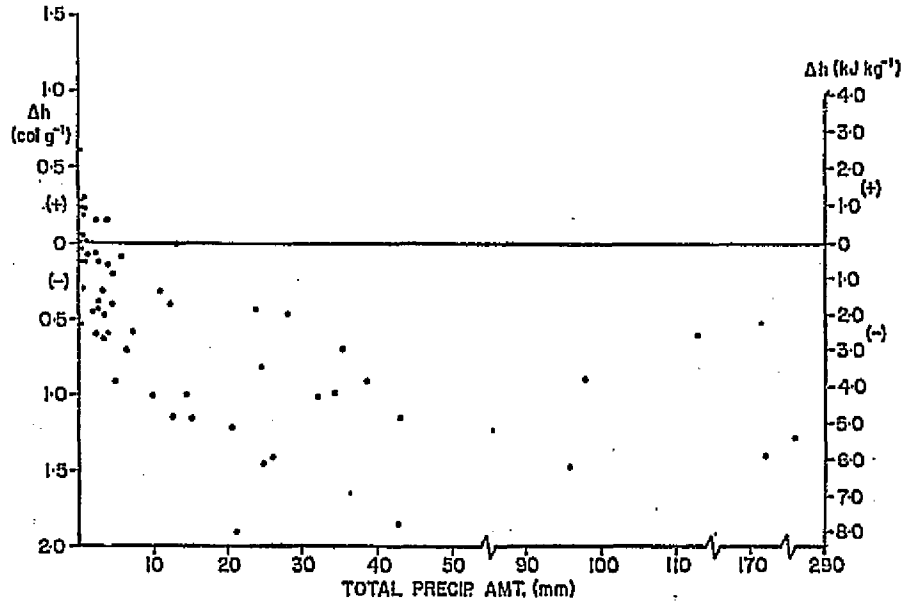

FIGURE 6 Scattergram of changes in total static energy, Δh, showing that light rainfall events can produce no or weak ± changes in total static energy.

circulation would serve to suppress the mixed layer and increase the temperatures and humidities of that layer.

IV. RECOVERY OF THE MIXED LAYER

A one-dimensional model of the boundary layer following Tennekes (1973) is used to test the sensitivity of the boundary recovery to various model conditions. Figure 7(a) shows the growth of the boundary layer when a surface wind of 3 m/sec (solid), 10 m/sec (dashed), and an environmental sinking of 0.01 m/sec is assumed. The model allows various assumptions on the form of the environmental divergence profile. For example, we may take (a) the vertical velocity constant above the ML, (b) constant divergence in the ML, (c) constant divergence in the ML and the layer above the ML. Results are

1. The entrainment velocity (w_{en}) peaks at t = 0.5 h during the period of maximum dH/dt and approaches approximately steady state at the environmental subsidence value of -0.01 m/sec after 8 h.
2. Specific humidity decreases and reaches a minimum after 2 h and increases thereafter.
3. The virtual potential temperature at the top of the ML θ_{vH} and the virtual potential temperature θ_{vm} in the ML initially approach each other, then diverge and become parallel after 5 h.
4. The mixed layer thickness H grows to an approximately steady state value of 360 m, 160 m below the LCL, reaching 80 percent of its final value in the first 3 h.

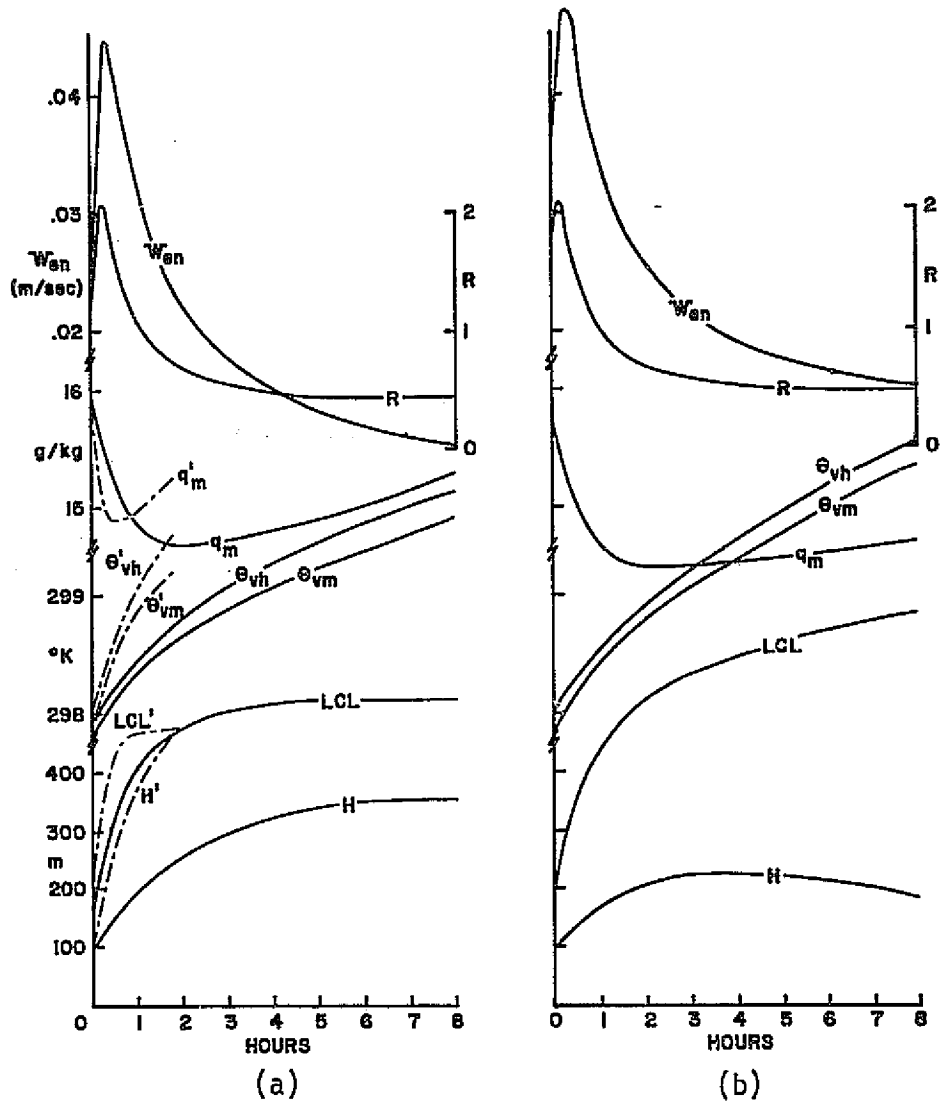

FIGURE 7 Results of a one-dimensional mixed-layer model. Variables plotted against the time are w_{en}, the entrainment velocity; θ_{vm}, the mixed-layer specific humidity; q_m, the mixed layer virtual potential temperature; H, the mixed layer thickness; LCL, the mean-mixed-layer lifting condensation level. The external specified parameters were Γ = 3.5 K/km; Γ_q = -3 g kg^{-1} km^{-1}, θ_v at the sea surface = 302 k; k = 0.25. The uniform vertical velocity was w = -0.01 m/sec. All divergence was assumed to occur within the mixed layer. The diabatic term, $Q_{\theta m}$ = 0, for (a) wind-speed sensitivity: model results with wind speeds of 3 m/sec and 10 m/sec are shown with solid lines, respectively; (b) same as (a) except subsidence is 2 cm/sec.

5. After 8 h the ML is warming and moistening at rates that keep the LCL nearly constant.

When the wind speed is increased to 10 m/sec,

6. The ML is saturated in ~2 h,

and we conclude that the recovery of the ML is very sensitive to the surface fluxes, which, in the model, are controlled by wind speed.

During the early stages of growth it appears that an initially shallow ML may entrain dry air at the top at a rate greatly exceeding the ability of the surface fluxes to moisten the layer. Thus the observed drying is a result of both the rapid growth and the entrainment of subsiding dry air above the ML. When environmental sinking increases, dH/dt is slowed and the drying increased.

In Figure 7(b) all conditions are the same except that subsidence w is doubled to -0.02 m/sec.

7. The mixed layer now grows to a maximum of 227 m in 3-5 h then *shrinks* slightly.

8. Specific humidity falls from 16 g/kg to 147 g/kg in 2 h then increases very slowly.

When the lapse rates of θ are changed, however, regrowth of the ML is also affected. In Figure 8 a Gaussian increase of the lapse rate of 4.0 K/km to 8.1 K/km over a 7-h period is specified.

9. The ML growing into an environment of increasing stability ends up *shallower* and *moister* than an environment of constant lapse rate. This is obtained when $\Gamma_q = 0$ above the ML.

Thus increasing subsidence, increasing the lapse rate, and stabilizing the environment will have the effect not of drying the ML but of moistening the ML.

We conclude that

- Any process that will promote rapid growth of the ML will cause an initial drop in specific humidity.
- Any process that maintains the ML low and in approximate equilibrium will tend to make it moist.
- A low ML is maintained by increased subsidence both by entrainment of dry air across the boundary (drying) and by increasing the stability (moistening).
- ML properties are not a simple consequence of entrainment of sinking environmental air when the ML depth is changing appreciably.
- If evaporative cooling is a function of anvil precipitation and is called upon to increase mesoscale subsidence, Γ_q is likely to equal zero or become positive (increase with height), and stratification will increase both factors, resulting in moistening of the mixed layer and not, as increased subsidence would intuitively suggest, drying.

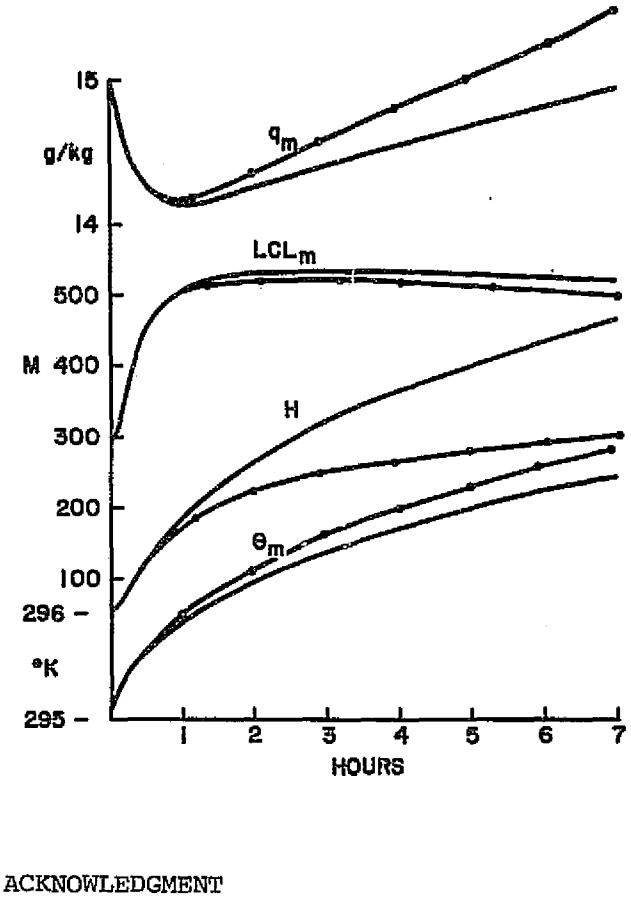

FIGURE 8 Results of the one-dimensional mixed-layer model with variable lapse rates. The time constant, T_f, was 8 h. Note that θ not θ_v is plotted. q_H was 13 g/kg; $\Gamma_q = 0$; Γ_o is 4 K/km; Γ increased to 8.1 K/km after 7 h.

ACKNOWLEDGMENT

The work in this paper has been supported by a grant from the Global Atmospheric Research Program, National Science Foundation, and the U.S. GATE Project Office, National Oceanic and Atmospheric Administration grant ATM74-21701. The work reported in this paper is substantially due to David Fitzjarrald and Gary Barnes. Assistance and results from G. D. Emmitt are also gratefully acknowledged.

REFERENCES

Betts, A. K. (1976). The thermodynamic transformation of the tropical subcloud layer by precipitation and downdrafts. *J. Atmos. Sci. 33*, 1008-1020.

Brummer, B. (1978). Mass and energy budgets of a 1 km high atmospheric box over the GATE C-scale triangle during undisturbed and disturbed weather conditions. *J. Atmos. Sci. 35*, 997-1011.

Emmitt, G. D. (1978). Tropical cumulus interaction with and modification of the subcloud layer. *J. Atmos. Sci. 35*, 1485-1502.

Gaynor, J. (1977). U.S. GATE Central Program Workshop. Sponsored by the National Science Foundation and the National Oceanic and Atmospheric Administration, July 25-August 12, Boulder, Colo.

Riehl, H., and J. S. Malkus (1958). On the heat balance in the equatorial trough zone. *Geophysica 6*, 503-538.

Tennekes, H. (1973). A model for the dynamics of the inversion above a convective boundary layer. *J. Atmos. Sci. 30*, 558-567.

DISCUSSION

S. Esbensen, *Rapporteur*

The discussion centered on the nature of the boundary layer during its recovery from disturbed conditions, the applicability of the bulk aerodynamic formulas under disturbed conditions, the heat balance of the GATE boundary layer, and the structure of the wind profiles from tethered-balloon systems.

The long recovery time of the boundary layer in the wake of disturbances was discussed. It was agreed that the contributing factors to the slow recovery are the low wind speeds, the mesoscale subsidence, the increase of gravitational stability of the transition layer at the top of the boundary layer, and the free atmospheric stratification in the wake of disturbances.

The reliability of heat and moisture flux estimates from bulk aerodynamic formulas was questioned. It was suggested that the enhancement of eddy fluxes in disturbed conditions might lead to a twofold or threefold increase in fluxes over what would be calculated using large-scale area-averaged wind speeds and air-sea temperature and humidity differences. It was agreed that the reliability of such flux estimates is in need of further investigation.

It was pointed out that the sensible heat-flux convergence in the boundary layer was large and that this fact is consistent with the results of Cox, which show a large radiative cooling of the boundary layer in the presence of small local changes and advections of temperature.

It was also noted that the wind profiles from tethered-balloon systems showed no systematic veering or backing with height at individual times. Gray stated that systematic turning of the wind appears only when large numbers of soundings are composited.

7. Theoretical Concepts of Tropical Circulation

Organizer ..... R. Reed

Speakers ..... J. Charney
R. Lindzen

Session Chairman ..... R. Reed

Rapporteur ..... D. Stevens

A PERSONAL RETROSPECT OF LARGE-SCALE TROPICAL DYNAMICS IN THE LAST FIFTEEN YEARS

Summary of J. Charney's Lecture prepared by J. Shukla from notes taken during the lecture

Charney's interest in tropical meteorology was triggered by Hurricane Carol (1954), which hit Woods Hole when Charney was lecturing there and von Neumann was visiting. After going back to Princeton, Charney was able to predict with some success using the Institute for Advance Study barotropic model, the acceleration of this hurricane, which caught the Cape Codders unaware, because the steering field was well defined.

Interest developed in understanding the growth and maintenance of the hurricane. It was natural to think that this must be due to some instability mechanism because anything that does not have the shape of boundaries is most likely to grow because of some sort of hydrodynamical instability. Syono had already published a paper considering a hurricane to be a single large moist convective element and had found, as Bjerknes had shown earlier, that the preferred scale of growth is the shortest scale. Therefore, in the competition between a cloud and a hurricane the cloud must win. This suggested that there should be "cooperation" (rather than "competition") between the synoptic-scale disturbance and the clouds. The next question was to understand the exact mechanism of the cooperation. If a hurricane or a prehurricane depression is assumed to be a symmetric vortex, and if it is in a balanced state, one needs a mechanism to generate vertical velocity. Frictional boundary-layer convergence seemed to be an obvious choice. Holton later worked on the role of Ekman pumping in connection with the dissipation of baroclinic Gulf stream rings. The limited penetration of the pumping H for limited horizontal scale L [$H \sim f(L/N)$] was later used by Williams and Chang to give a lower boundary to the size of the convection area.

Ooyama was also independently investigating the mechanisms of hurricane growth, and his work demonstrated convincingly that hurricanes cannot grow as a single moist convective element because the mean hurricane atmosphere is not moist enough.

Charney and Eliassen presented a mechanism for the growth of the hurricane depression in which they considered the combined role of low-level moisture convergence and frictional convergence. The role of frictional convergence was considered important only for the growth of the prehurricane depression, and it was never intended to explain the growth of tropical lows and weak waves. Their definition of the Conditional Instability of the Second Kind (CISK) was intended to explain the Cooperative Instability effects in the tropical Atmosphere (CIA).

CISK as a mechanism for the formation of the ITCZ was suggested by several factors. The ITCZ was found to have the cyclonic vorticity needed for the Ekman pumping to operate. It was also seen that the ITCZ never forms at the equator where Ekman pumping does not exist. If we go too far away from the equator, the static stability is not favorable. It was therefore hypothesized that the location of the ITCZ is governed by the combined effects of Ekman pumping and static stability. It was subsequently pointed out by Lindzen and Schneider that the Ekman pumping argument at the equator is not correct since because of stratification the pressure does not "boundary layer."

There was an alternative suggestion that the ITCZ forms wherever the sea-surface temperature (SST) is a maximum. Pike had done some numerical experiments to demonstrate this. While it is true that the ITCZ is observed to be where the SST is approximately a maximum, it is likely that the SST is a maximum under the ITCZ because the ITCZ is there. Location of the ITCZ away from the equator can be understood as a combined air-sea instability mechanism. Let us assume that the SST is a maximum at the equator and the ITCZ is at the equator. If we displace the ITCZ northward, will it come back to the equator, or will it tend to move further away from the equator? When the ITCZ is displaced northward from the equator, conservation of angular momentum produces southeasterlies at the equator, which become less easterly as they penetrate northward, and northeasterlies north of the ITCZ. There are thus two effects. The southeasterlies at the equator will cause upwelling at the equator and lower the SST. The weakened easterly component of the southern branch gives rise to an enhanced cyclonic shear in the ITCZ. It can therefore be argued that the equatorial SST is low and the ITCZ is more intense when it is located away from the equator. Several numerical experiments with a symmetric version of the GLAS (Goddard Laboratory for Atmospheric Sciences) model and a symmetric ocean model of Rivas have confirmed this idea.

Much progress has been made in our understanding of the mechanism of Hadley circulation. Schneider and Lindzen have shown the importance of momentum mixing and moist convective heating in the ascending branch of the Hadley cell. Numerical experiments with symmetric models can be useful in understanding the instability of cross equatorial flow. For example, if the southern hemisphere flow with its negative potential vorticity crosses the equator, it becomes unstable and may give rise to cloud bands. Cloud bands associated with the Somali jet may be due to inertial instability of the cross equatorial flow.

But how symmetric is the Hadley circulation? Mintz has shown from the satellite pictures and it is already known from the global rainfall maps that most of the latent heat release takes place over separate continental areas and the strong meridional circulation at upper levels is mostly confined to narrow geographical regions. We should therefore be careful in approximating such a nonsymmetric flow pattern by its zonal average. There remain open questions regarding the role of tropical disturbances in the general circulation of the atmosphere.

It has been shown that barotropic instability may be an important mechanism for the scale selection of easterly waves. Gray has said

that CISK is dead as far as tropical waves are concerned. We have yet to understand what maintains these waves as they propagate across the Atlantic and sometimes intensify into hurricanes. Is it possible that frictional dissipation is not large because their amplitudes are a maximum near 700 mbar? What is the role of cumulus convection in maintaining these waves? Wave-CISK as it is employed is a linear concept, and it is questionable because of its assumptions of positive and negative precipitation. Real waves have their precipitation confined to a particular phase of the wave, and most of the precipitation comes from the mesoscale and cluster scale. For these reasons it is questionable whether it is meaningful to composite the precipitation in these waves as done by Reed and others. Compositing cannot resolve the most interesting scales at which most of the action takes place. In order to understand the role of small scale in maintaining the wave scale, we should be able to look at the correct relations between the cloud cluster and synoptic scales, and compositing does not give this.

Since the easterly waves and the clouds are so widely separated in scale, it is hard to understand the interaction mechanism. The mechanisms for rain bands and squall lines have also to be understood. Instabilities can sometimes provide understanding. For example, Fung has shown that hurricane rain bands can be explained as Ekman-layer instabilities. Emanuel has shown that midlatitude squall lines can be ascribed to inertial instability. Even Gray's diurnal variation of the vertical velocity can be regarded as a kind of instability due to the cloud-radiation feedback.

Numerical experiments by Charney *et al.* have shown that if land surface evaporation is very large over Africa, there is more precipitation but the kinematics of the easterly waves is not well defined. If the land surface evaporation is negligible (the only moisture source being evaporation from the ocean), the easterly waves are well defined and realistic. Several results of this study highlight the important role of soil moisture in tropical continental rainfall.

Finally, it is too early to assess the significance of GATE. We should, perhaps, meet again ten years from now and examine the impact and significance of GATE. There are still basic unsolved problems. For example, how are weak easterly waves and depressions driven, and what is the mechanism? How are mesoscales driven, and how do they interact with the synoptic scale. How does Hadley-scale circulation interact with the synoptic scales? We still have to understand how hurricanes form. Data by themselves are not sufficient. Nor is mind. We need a combination of both.

DISCUSSION
D. Stevens, *Rapporteur*

Much of the discussion following Charney's lecture focused on the long-standing problem of understanding the complex interactions between the synoptic-scale waves and smaller-scale circulations. For example, since the waves seem to modulate the statistical behavior of precipitation on

the 1000-km trough-ridge scale, why is rainfall limited to regions no larger than the 100-200 km mesoscale? It was pointed out that even with the large-scale influence, convection starts from the smallest scales (individual cells) and apparently finds a scale limitation at the mesoscale. When asked about his view of the parameterization effort, Charney affirmed the importance of the work initiated by the groundbreaking ideas of Ooyama and Arakawa. But with GATE has come a realization that the mesoscale link between the cumulus and large scale cannot be neglected and requires more consideration. It was also noted in discussion that the structure and dynamics of the precipating systems are intimately related to the fact that the boundary layer is very effectively suppressed for a relatively long period of time, thus acting to shut off the moisture supply before the systems can attain a large scale.

EASTERLY WAVES, WAVE CISK, AND PARAMETERIZATION OF CUMULUS HEAT AND MOMENTUM TRANSPORTS

Richard S. Lindzen
Harvard University

The present paper is based primarily on work reported in the following papers: Schneider and Lindzen (1976), Stevens *et al.* (1977), Stevens and Lindzen (1978), and Lindzen *et al.* (1979). Details of many things discussed here can be found in these papers.

Recent studies of African easterly waves (see Mass, 1979, and references therein) have convincingly argued that scale selection arises from conventional barotropic instability. This is consistent with the paper by Stevens and Lindzen (1978), which shows that CISK, itself, produces little scale selection. The paper by Lindzen *et al.* (1979) presents a new unified approach to baroclinic and barotropic instability wherein these instabilities are explained as interactions between internal Rossby waves and the mean flow. Wave-CISK deals with the interaction of internal waves with the tropical moisture field. The introduction of CISK concepts into the description by Lindzen *et al.* (1979) of baroclinic and barotropic instability is conceptually straightforward and leads to a comprehensive qualitative description of the mechanics of various tropical waves.

In addition to the application of the theory of Lindzen *et al.* (1979) to tropical waves, certain aspects of the earlier papers of Stevens *et al.* (1977) and Stevens and Lindzen (1978) warrant review--especially in the light of GATE. In the paper by Stevens *et al.* (1977), it was shown that in waves forces by latent heat release, gross inconsistencies with data would result in the absence of some form of strong momentum transport. For example, temperature perturbations would be too large and vorticity perturbations would be 5-10 times divergent. In observed waves, temperature perturbations are small and vorticity ~0 (divergence). These inconsistencies are based on very general scaling arguments and not on specific models. Allowing clouds to transport momentum as well as heat eliminates these basic inconsistencies. It also leads to a relative independence of wave amplitude (for temperature and horizontal velocity fields) on rainfall rates for a large range of rainfalls. In this range of rainfalls (~0.15 cm/day to 10 cm/day), friction tends to counteract thermal forcing--both of which are proportional to rainfall. Stevens and Lindzen (1978) investigated the consequences of cumulus friction for CISK. It was discovered that CISK required finite but sufficiently *small* precipitation rates and/or high wave frequences (as are found in squalls and clusters). For regions of substantial precipitation rates, one found approximate neutrality rather than growth or decay,

regardless of whether one expected either growth or decay in the absence of cumulus momentum exchange. Squalls and clusters remain as prime candidates for CISK instabilities.

Certain other specific points in the papers by Stevens *et al.* (1977) and Stevens and Lindzen (1978) related to the above general features, should be emphasized:

1. It is found in Stevens and Lindzen (1978) that for CISK results to be meaningful, cumulus heating must be parameterized in a thermodynamically consistent manner. When heating is taken to be proportional to low-level convergence, the coefficient of proportionality cannot be chosen arbitrarily. If it is, then spurious instability and/or instability is produced.
2. Based on Stevens and Lindzen's (1978) findings, it seems possible that in regions of substantial precipitation, a primary balance in easterly waves is between cumulus heating and cumulus "friction" leading to neutrality (i.e., little apparent generation of wave energy), and that those terms that appear to generate wave energy may, in fact, be part of a secondary and less important balance.
3. In regions of significant precipitation, the details of cumulus heating and friction (apart from the satisfaction of certain gross budgets) do not appear important for disturbances with the time and space scales of easterly waves. This lends some hope to the possibility of a simple cumulus parameterization, which is still thermodynamically consistent in the manner mentioned in item 1 above. A brief description of such a parameterization will be presented. In this parameterization, precipitation is taken to be some fraction of the moisture converged below the minimum of the moist static-energy profile (and evaporation). This fraction depends on the height of the tallest clouds and upper-level humidity. In regions of well-developed easterly waves, this fraction is essentially one. The vertical distribution of heating is determined by allowing air originating with a particular moist static energy to detrain where it sees the same environmental moist static energy. This parameterization quantitatively reproduces existing data for large-scale waves--in contrast to other parameterizations.
4. Stevens and Lindzen (1978) find that CISK always exists for internal gravity waves with the time and space scales of squalls and clusters. Such waves generally do not involve the vertical component of vorticity; however, such waves can have Reynolds stresses involving horizontal momentum--quite apart from those momentum transports associated with the clouds themselves. This may account for certain problems in the observational analysis of cumulus momentum transports. These problems are discussed in the paper by Shapiro.

REFERENCES

Lindzen, R. S., B. Farrell, and K.-K. Tung (1979). The concept of wave overreflection and its application to baroclinic instability. Submitted to *J. Atmos. Sci.*

Mass, C. (1979). A linear primitive equation model of the African wave disturbance, *J. Atmos. Sci.*, to be published.

Schneider, E. K., and R. S. Lindzen (1976). A discussion of the parameterization of momentum exchange by cumulus convection. *J. Geophys. Res. 81*, 3158-3160.

Stevens, D. E., and R. S. Lindzen (1978). Tropical wave-CISK with a moisture budget and cumulus friction. *J. Atmos. Sci. 35*, 940-961.

Stevens, D. E., R. S. Lindzen, and L. J. Shapiro (1977). A new model of tropical waves incorporating momentum mixing by cumulus convection. *Dyn. Atmos. Oceans 1*, 365-425.

DISCUSSION

D. Stevens, *Rapporteur*

Following Lindzen's presentation, Betts presented results from a recent Ph.D. dissertation by Maria Silva Dias at Colorado State University. Silva Dias investigated mesoscale circulations using the linear wave-CISK formulation described by Lindzen. She found that with a parameterization of mountain transfer by cumulonimbus clouds as well as latent heat release, several aspects of mesoscale squall lines could be simulated: the sloping structure, deep tropospheric circulation, and rapid propagation. The mean wind shear proved to be an important parameter for the instability characteristics of the modeled squall line.

In the model of synoptic-scale easterly waves described by Lindzen, vertical shear of the mean zonal wind was not included, although it could be important. It was pointed out in discussion that a recent wave-CISK model of Davies (1978), in which the heating by condensation lagged the low-level convergence, produced no intensification of the small-scale gravity waves; Lindzen believed the gravity waves should intensify as in the usual formulations.

A question was raised regarding the role of the Reynolds stress $\overline{\rho u'w'}$ due to cloud-scale circulation in causing the large-scale temperature changes to be small. Lindzen reiterated that the stress term (mixing of momentum by the clouds) was the crucial element in keeping temperature changes small, through a dynamic interaction between the equations of horizontal motion and the heat equation. Other participants expressed a difference in interpretation of the small temperature changes and the dynamics that cause the observed result.

It was pointed out that Lindzen's results depended on a particular cloud parameterization and that generalization to other schemes was unwarranted. Lindzen responded that the essential assumption is the satisfaction of a moisture budget, which determines precipitation and therefore net release of latent heat. There was no consensus on the importance of large-scale vertical velocity above the low-level region of significant moisture convergence.

Concern was expressed that wave-model results would change with an explicit treatment of the mesoscale features, which contain the bulk of the rainfall. Lindzen believes that the large-scale dynamics have been correctly treated by using a simple moisture budget parameterization.

8. Parameterization Studies

Organizer ..... W. Schubert

Speakers..... Y. Ogura
S. Lord
L. Shapiro
D. Rodenhuis
D. Randall
H. R. Cho
K. Ooyama
S. Soong
T. Nitta

Session Chairmen ..... W. Schubert
D. Rodenhuis
H. R. Cho

Rapporteurs ..... H. R. Cho
S. Soong
L. Shapiro

RELATIONSHIP BETWEEN LARGE-SCALE FORCING AND PRECIPITATION OBSERVED IN GATE

Yoshi Ogura and Yi-Leng Chen
University of Illinois

INTRODUCTION

Several authors have shown convincingly that deep cumulus convection observed during GATE Phase III was strongly modulated by traveling easterly waves (Burpee and Dugdale, 1975; Aspliden *et al.*, 1976; Reed *et al.*, 1977; Payne and McGarry, 1977; Thompson *et al.*, 1979; and others). There are other forcing mechanisms that determine the location and intensity of cumulus convection (Gray, 1978). One of them is the low-level convergence associated with the surface confluence line, which was located inside or near the GATE A/B array during the entire GATE period. Analyzing pre-GATE data, Sadler (1975) found that the maximum cloudiness was embedded in the westerly flow south of the equatorial trough. Estoque and Douglas (1978) composited 25 cases during GATE Phase II referring to the surface confluence line and found that the maximum of cloudiness or measured precipitation was located about 1° S of the surface confluence axis. It is known that the easterly wave activity was strongest in Phase III. Easterly waves were identified also in Phase I and II, even though they were less regular (Burpee and Dugdale, 1975). In the first two phases, convective systems were more frequently organized into the line structure rather than into blob-type clusters in comparison to cloud systems observed in Phase III. The phase mean precipitation patterns within the B array estimated by Hudlow and Patterson (1979) from radar data show that heavy precipitation areas were concentrated in a narrow band oriented in the northeast-southwest direction in Phase I and II, whereas precipitation was spread more widely in Phase III. Further, the total precipitation amount in Phase II was notably smaller than that in Phase I or III.

Ogura *et al.* (1979) analyzed GATE surface and rawinsonde data from the A/B array for two selected periods: August 11-12 in Phase II and September 3-6 in Phase III. The result of analysis reveals good correlation between the vertical velocity field and the development of organized convective systems. In all cases considered, low-level convergence and, consequently, upward motion was present or enhanced prior to the development or organized convective systems. A low-level inversion was absent in the area of subsequent convective development in contrast to other areas having no organized convective activity.

The objective of this work is to correlate the aforementioned precipitation characteristics in each phase of GATE to large-scale circulations

characterized by easterly waves, surface confluence line, and the cross-equatorial flow, by analyzing surface and upper-air sounding data within the A/B array for the entire GATE period.

COMPOSITE-OBJECTIVE ANALYSIS OF WIND DATA

The data used were the Convective Subprogram Data Center (CSDC) hourly surface meteorological data set and CSDC final basic upper-air sounding data set. All ship data within the A/B array were used in this study.

The first task in this analysis was to identify traveling easterly waves (if there were any) and to assign each observation time (3-h or 6-h interval) to one of eight wave categories introduced by Reed and Recker (1971) at the center of the A/B array. For this purpose, the time series of the meridional wind component (v) observed at each ship at 700 mbar was bandpass-filtered to isolate wave-related fluctuations. The filter used was the same as that used by Payne and McGarry (1977), which exhibits a peak response at a period of 3 days. An objective analysis scheme used in Ogura *et al.* (1979) was then applied to the resulting v field at each observation time to generate values of v at regularly spaced grid points inside the A/B array. The result of the analysis is shown in Figure 1 in the form of time-longitude sections at 8.5° N (figure for Phase III is not shown), which were then used to assign one of eight wave categories to each observation time at the center of the A/B array (23.5° W). The chronology of wave categories presented by Thompson *et al.* (1979) was used for Phase III.

Next, all surface and upper-air data were stratified according to the wave category thus assigned. An objective analysis scheme was again applied to the composited wind data on selected constant pressure surfaces. The horizontal divergence and vertical component of vorticity were then computed from the wind data thus generated at regularly spaced grid points in a fashion similar to that of Ogura *et al.* (1979). The vertical p-velocity (ω) was then computed kinematically. Figure 2 is an example of the results of our analysis, which shows the surface streamlines and the surface divergence for wave category 2. Here wave category 1 represents

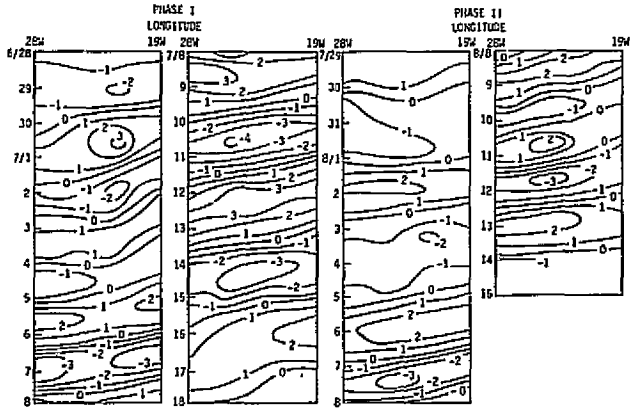

FIGURE 1 Time-longitude sections for the north-south wind component (in units of m/sec) at 8.5° N and at 700 mbar for GATE Phase I and Phase II. The positive value indicates the southerly wind.

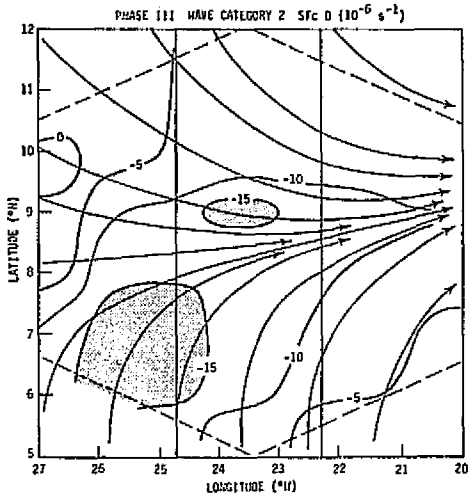

FIGURE 2 The surface streamlines and the surface divergence in units of 10^{-6} sec^{-1} composited for wave category 2 in Phase III.

the 700-mbar trough, category 8 marks the 700-mbar ridge, and categories 2 and 6 are the maximum northerly and southerly wind components, respectively. The intermediate regions of the waves are designated by categories 1, 3, 5, and 7. We note in Figure 2 that there are two local maxima of the surface divergence; one is located over the surface confluence line and the other over the area south of the surface confluence line, where the surface streamlines exhibit an anticyclonic curvature. The latter maximum of convergence is apparently caused by the wind change, which occurs in association with the rapid variations of the Cariolis parameter when the air flow coming from the southern hemisphere crosses the equator, in a manner similar to that described by Mart (1972).

The final step of the analysis was to take averages of the variables along the east-west direction from 22.25° W to 24.75° W, that is, 1.25° each side of the central longitude in the A/B array, as shown in Figure 2. The results of the analysis are interpreted to represent the latitudinal distribution of the variables for each wave category assigned. The resulting fields were also decomposited into the phase means and deviations from them. The latter quantities, denoted by the prime in this paper, represent fluctuations caused by synoptic-scale disturbances.

PRECIPITATION IN RELATION TO EASTERLY WAVES AND THE SURFACE CONFLUENCE LINE

Figure 3 shows the modulation of deep cumulus convection by the composited easterly wave and the surface confluence line in Phase III. We note in Figure 3(a) that the position of the surface confluence line, defined as the line of $v = 0$, undergoes substantial fluctuations with the wave passage. It moves rapidly southward in wave categories 1 through 2 and gradually moves northward during the passage of the 700-mbar trough. Figure 3(b) shows that the precipitation rate, estimated from radar data by Hudlow and Patterson (1979), has a local maximum just south of the

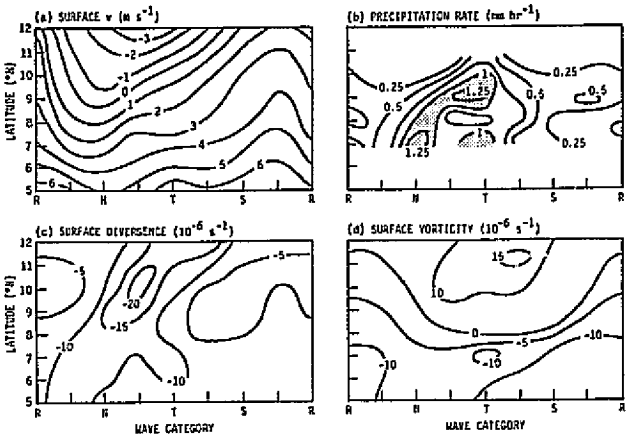

FIGURE 3 (a) North-south wind component (v) at the ocean surface in units of m/sec, (b) precipitation rate estimated from radar data by Hudlow and Patterson (1979) in units of mm/h, (c) surface divergence in units of 10^{-6}/sec, (d) vertical component of surface vorticity in units of 10^{-6}/sec in Phase III.

surface confluence line, as shown earlier by Estoque and Douglas (1978) and that heavy precipitation occurs in wave categories 2-4, as shown earlier by Reed *et al.* (1977) and others. The surface convergence field shown in Figure 3(c) agrees remarkably well with the precipitation field shown in Figure 3(b). The agreement is better when the surface convergence field is shifted about a half-wave category length, indicating a time lag of about 5-10 h between the maxima of the surface convergence and the precipitation rate. This is consistent with the earlier finding of Cho and Ogura (1974) and Johnson (1978). Both a local maximum of the precipitation rate in wave category 2 and a secondary maximum in wave category 4 are located a few degrees south of the surface confluence line, in agreement with Sadler (1975). An example of the events that contributed to the former maximum is a cloud cluster formed on September 4, which was designated as cluster A in Ogura *et al.* (1979). An example of the events for the latter secondary maximum is cluster F in Ogura *et al.* (1979), which developed on September 6.

As shown in Figure 4, wave categories 6-8 are the segments of the wave where the descending motion prevails. Nevertheless the ascending motion associated with the low-level convergence in the cross-equatorial flow was strong enough to overcome the wave-induced descending motion and produced some rain.

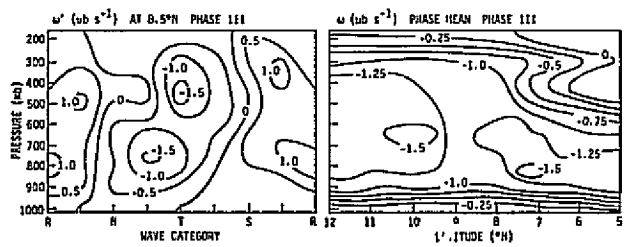

FIGURE 4 Wave-related vertical p-velocity (ω') in units of μbar/sec at 8.5° N and the meridional cross section for phase mean vertical p-velocity (ω) at 23.5° W for Phase III.

On the other hand, Figure 3(d) shows that the pattern of the vertical component of surface vorticity does not resemble the precipitation pattern. In fact, the airflow south of the surface confluence line is anticyclonic, indicating that the boundary-layer pumping plays very little role in producing precipitation in that area.

We note in Figure 4 that the phase mean ω at 23.5° W has two local maxima in Phase III. One is located at 7° N and associated with the low-level convergence in the cross-equatorial flow. The other is located at 10° N, approximately the location of the phase mean surface confluence line. Because the latter ascending motion is supported by easterly waves, the deep convective activity was stronger and the level of the maximum ω is higher in comparison with the ω maximum located south of the surface confluence line. The distribution of wave-related ω shown in Figure 4 is quite similar to that determined earlier by Reed *et al.* (1977) and Thompson *et al.* (1979) from a somewhat different composite technique. We also note that the magnitude of the phase mean ω is about that same as that associated with easterly waves.

In sharp constrast to Phase III, the surface confluence line hardly moved in Phase I and II, as shown in Figure 5. A partial answer to a question why it behaved so differently is given in Figure 6. We note that the amplitude of the composited easterly wave measured by v' (wave-related v component) at 700 mbar was largest in Phase III, with the amplitude of ±5 m/sec; Phase I was the second with the amplitude of

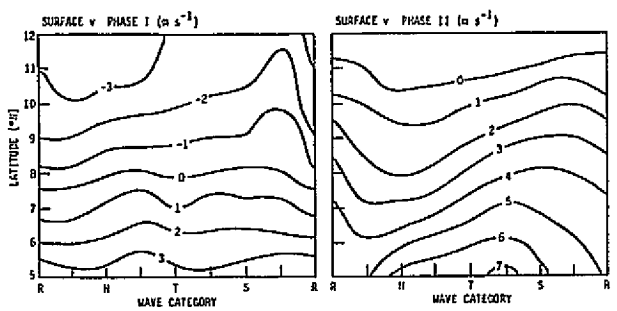

FIGURE 5 North-south wind component at the ocean surface for Phase I and II in units of m/sec.

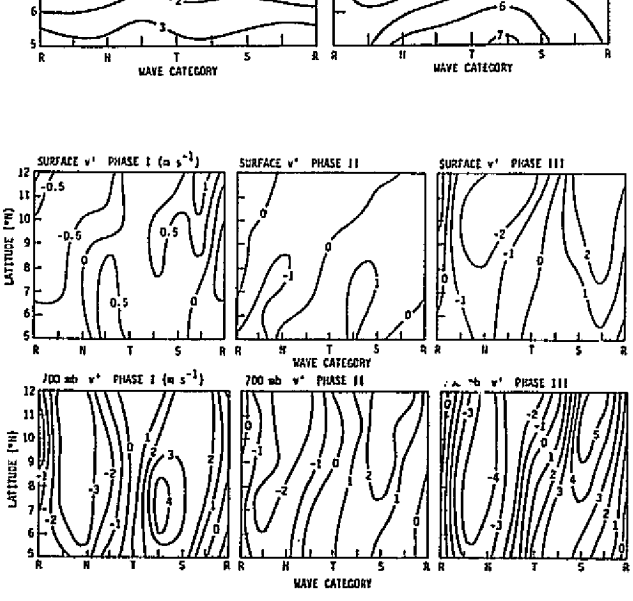

FIGURE 6 Latitudinal distributions of meridional wind component at the ocean surface and 700 mbar as functions of wave categories in units of m/sec for three GATE phases. The values have been subtracted from the phase means to show wave-related patterns.

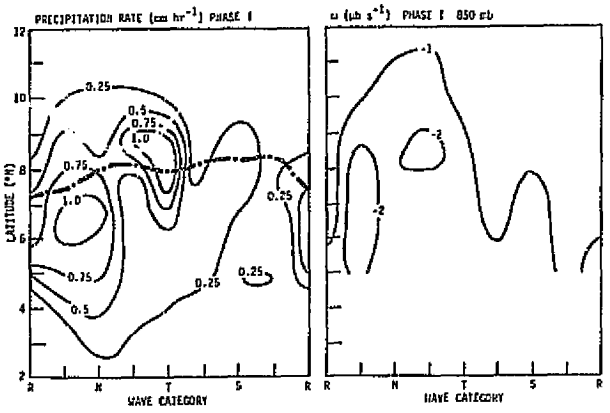

FIGURE 7 Satellite-estimated precipitation rate as a function of latitude and wave category based on Woodley *et al.*'s data (1980) and the vertical *p*-velocity in units of μbar/sec for Phase I.

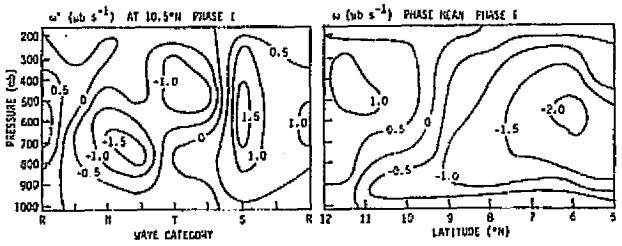

FIGURE 8 Wave-related vertical *p*-velocity (ω') in units of μbar/sec at 10.5° N and the meridional cross section for phase mean vertical *p*-velocity (ω) at 23.5° W for Phase I.

±4 m/sec; the amplitude was very small in Phase II, only ±2 m/sec. However, the situation is significantly different in v' at the ocean surface. v' fluctuations have an amplitude of only ±0.5 m/sec in Phase I in contrast to ±2 m/sec in Phase III. Thus the coupling between the surface and 700-mbar flows was extremely weak in Phase I, and consequently easterly waves did not modulate the position of the surface confluence line significantly in Phase I. This may account for, at least partially, frequent formation of line-structured cloud systems in Phase I. Nevertheless, easterly waves modulated precipitation also in Phase I in that heavy precipitation occurred in wave categories 2-4, as shown in Figure 7. The distribution of ω at 850 mbar again agrees well with the precipitation distribution. The structure of the wave shown in Figure 8 is remarkably similar to that in Phase III shown in Figure 4. On the other hand, the phase mean ω distribution in the meridional cross section in Phase I shown in Figure 8 is markedly different from that in Phase III.

Finally, we note that, as shown in Figure 5, v' at the ocean surface was strong in Phase II in comparison with Phase I. In contrast, as shown in Figure 6, the amplitudes of the composited 700-mbar and surface waves were very weak in Phase II, and the precipitation amount was also low in Phase II. Thus the sequence of events from Phase I through Phase III does not seem to be a smooth gradual transition.

Most of the materials presented in this paper will appear in Yi-Leng Chen's Ph.D. thesis.

REFERENCES

Aspliden, C. I., Y. Tourre, and J. B. Sabine (1976). Some climatological aspects of West African disturbance lines during GATE. *Mon. Wea. Rev. 104*, 1029-1035.

Burpee, R. W., and G. Dugdale (1975). A summary of weather systems affecting western Africa and eastern Atlantic during GATE. GATE Report No. 16, ICSU/WMO, Geneva, Switzerland, pp. 2.1-2.42.

Cho, H.-R., and Y. Ogura (1974). A relationship between the cloud activity and the low-level convergence as observed in Reed-Recker's composite easterly waves. *J. Atmos. Sci. 31*, 2058-2065.

Estoque, M. A., and M. Douglas (1978). Structure of the Intertropical Convergence Zone over the GATE area. *Tellus 30*, 55-61.

Gray, W. M. (1978). Large scale controls on convection. Atmos. Sci. Paper No. 259, Dept. Atmos. Sci., Colorado State Univ. US ISSN 0067-0340.

Hudlow, M. D., and V. L. Patterson (1979). GATE radar rainfall atlas. NOAA Special Report. 155 pp.

Johnson, R. H. (1978). Cumulus transports in a tropical wave composite for Phase III of GATE. *J. Atmos. Sci. 35*, 484-494.

Mart, L. J. (1972). A numerical study of the influence of advective accelerations in an idealized, low-latitude, planetary boundary layer. *J. Atmos. Sci. 29*, 1477-1484.

Ogura, Y., Y.-L. Chen, J. Russell, and S.-T. Soong (1979). On the formation of organized convective systems observed over the eastern Atlantic. *Mon. Wea. Rev. 107*, 426-441.

Payne, S. W., and M. W. McGarry (1977). The relationship of satellite inferred convective activity to easterly waves over West African and the adjacent ocean during phase III of GATE. *Mon. Wea. Rev. 105*, 413-420.

Reed, R. J., and E. E. Recker (1971). Structure and properties of synoptic-scale wave disturbances in the equatorial western Pacific. *J. Atmos. Sci. 28*, 1117-1133.

Reed, R. J., D. C. Norquist, and E. E. Recker (1977). The structure and properties of African wave disturbances as observed during Phase III of GATE. *Mon. Wea. Rev. 103*, 317-333.

Sadler, J. C. (1975). The monsoon circulation and cloudiness over the GATE area. *Mon. Wea. Rev. 103*, 369-387.

Thompson, R. M., S. W. Payne, E. E. Recker, and R. J. Reed (1979). Structure and properties of synoptic-scale wave disturbances in the Intertropical Convergence Zone of the eastern Atlantic. *J. Atmos. Sci. 36*, 53-72.

DISCUSSION

H. R. Cho, *Rapporteur*

The paper discussed the relationship between the observed precipitation patterns and the positions of surface confluence lines for the entire three GATE phases. It brought the study of precipitation distributions into a larger context. The effect of cross-equatorial flow was particularly noted.

The lack of modulation of surface confluence lines by easterly waves during Phases I and II of GATE was suggested as an indication of the change in vertical linkage of the waves during the three phases of the experiment. The inability of quadratic surface fits of wind data to resolve the double maxima of vertical velocity in the latitudinal cross section obtained in the composite analysis was also discussed. It was suggested that the northern maximum was perhaps caused by confluence convergence, while the southern maximum was caused by speed convergence.

The validity of the composite method in general was another focal point of discussions. Possible problems with composite analysis include (1) elimination of mesoscale features that might provide the dynamic link between convective-scale and large-scale motions and (2) tendency to eliminate geographic features. The general opinion appears to be that the validity of compositing depends on the particular phenomena under investigation. With a proper composite criterion, the method is a very good way to enhance signal-to-noise ratio.

Vincent presented a comparison of Phase III mean precipitation distributions over Western Africa and the Eastern Atlantic obtained from satellite observations and from Kuo's parameterization scheme. While there is an agreement in overall broad features, the two distributions differ in detail. Several causes for the discrepancy have been suggested: (1) the low data density over Western Africa, (2) the quality of precipitation rate deduced from satellite data, and (3) deficiency in the Kuo scheme.

VERIFICATIONS OF CUMULUS PARAMETERIZATIONS USING GATE DATA

Stephen Lord
University of California, Los Angeles

The purpose of this paper is to evaluate several cumulus parameterization schemes designed for large-scale numerical weather-prediction models. The first scheme, that of Arakawa and Schubert (1974), will be evaluated in some detail by first presenting some supporting evidence for the closure assumption, the cloud work-function quasi-equilibrium. Then the Arakawa-Schubert scheme, the moist convective adjustment scheme (Manabe *et al.*, 1965), and Kuo's (1965) scheme will be evaluated by comparing the precipitation rates and the cumulus warming and drying predicted by the parameterizations with observed estimates over the same time period during Phase III of GATE.

Before proceeding, however, let us present some basic principles concerning the parameterization of cumulus convection:

1. The goal of a cumulus parameterization is to predict the changes in grid-scale variables (assumed to be due to subgrid-scale cumulus convection) from the given large-scale variables.
2. To achieve this goal, the collective effects of a cloud ensemble, or large group of clouds imbedded within the grid box, must be predicted.
3. The closure assumption must relate the properties of the ensemble to the grid-scale variables. The assumption must be in the form of a quasi-equilibrium between the ensemble properties and the grid-scale variables. Without any quasi-equilibrium, it is in principle impossible to parameterize.
4. The quasi-equilibrium condition should not cause the loss of predictability of the large-scale variables. For example, we cannot use steadiness in the large-scale temperature or moisture in the quasi-equilibrium condition because these variables must be predicted. Although observations show these variables to be approximately steady in some situations, the cumulus parameterization must reproduce this fact without *a priori* assumptions.

The implementation of the Arakawa-Schubert scheme has been described in detail by Lord (1978). In this scheme, the distribution of cloud base mass flux into a spectrum of subensembles is determined by assuming the quasi-constancy of the cloud work function for each subensemble. The cloud work function is defined by

$$A(\lambda) = g\int_{z_B}^{\hat{z}(\lambda)} \frac{\eta(z,\lambda)}{\overline{T}} \left[(T_v)_c - \overline{T}_v\right] dz, \tag{1}$$

where λ is a parameter that characterizes the subensemble, $\eta(z,\lambda)$ is the subensemble mass flux normalized at cloud base, $(T_v)_c$ and $\overline{T}_v$ are, respectively, the subensemble and large-scale virtual temperatures, and z_B and $\hat{z}(\lambda)$ are the heights of cloud base and cloud top.

The cloud work function may, in general, be modified by large-scale processes and cumulus processes. Therefore the total change of $A(\lambda)$ may formally be written as

$$\frac{dA(\lambda)}{dt} = \left[\frac{dA(\lambda)}{dt}\right]_{LS} + \left[\frac{dA(\lambda)}{dt}\right]_{CU}, \tag{2}$$

where the subscripts LS and CU refer to large-scale and cumulus processes, respectively. The change of $A(\lambda)$ by cumulus processes is a linear function of the cloud-base cumulus mass flux, $M_B(\lambda)$ of all cloud types, so that we can write

$$\left[\frac{dA(\lambda)}{dt}\right]_{CU} = \int_0^{\lambda_{max}} K(\lambda,\lambda')\, M_B(\lambda')d\lambda'. \tag{3}$$

The large-scale forcing is defined by

$$F(\lambda) = \left[\frac{dA(\lambda)}{dt}\right]_{LS}. \tag{4}$$

$F(\lambda) > 0$ indicates growth of the cloud work function due to large-scale processes.

The closure assumption for this parameterization is that the destabilization by the large-scale processes is approximately balanced with the self-stabilization by clouds. This approximate balance is expressed in terms of the cloud work function change is

$$\frac{dA(\lambda)}{dt} << F(\lambda). \tag{5}$$

We now present some evidence from the GATE supporting this assumption.

Figure 1 is a time series of $F(\lambda)$ estimated from GATE Phase III B- and A/B-scale data. The data were provided by R. J. Reed and are described in Thompson *et al.* (1979). The abscissa is the time, September 1-18, and the ordinate is the cloud-top pressure, $\hat{p}$, for each subensemble. The maxima on September 2, 4, and 9 correspond to the large-scale easterly wave troughs passing over the GATE area.

Figure 2 is a time series of the observed time change of the cloud work function for each subensemble. It is clear that $dA/dt << F$, at least for disturbed conditions.

In addition to the GATE data, the following data have been used to calculate the cloud work function: Marshall Islands (Yanai *et al.*, 1973), VIMHEX (Betts and Miller, 1975), West Indies (Jordan, 1958), AMTEX (Nitta,

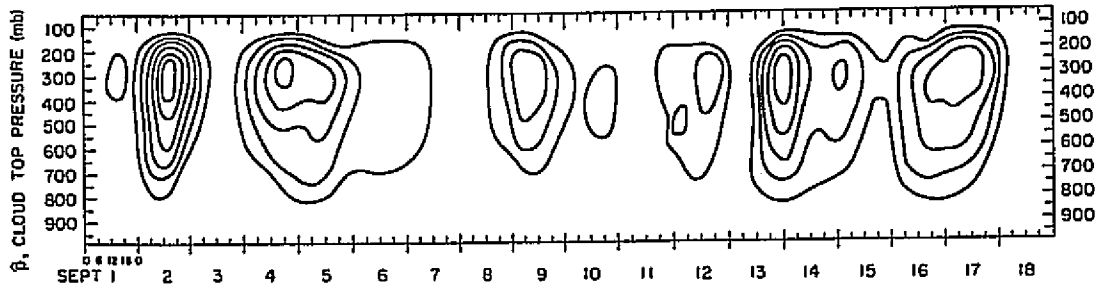

FIGURE 1 A time series of the large-scale forcing for each subensemble, September 1-18. The ordinate is the cloud-top pressure, $\hat{p}$, and contour lines indicate equal values of the large-scale forcing (kJ kg^{-1} day^{-1}).

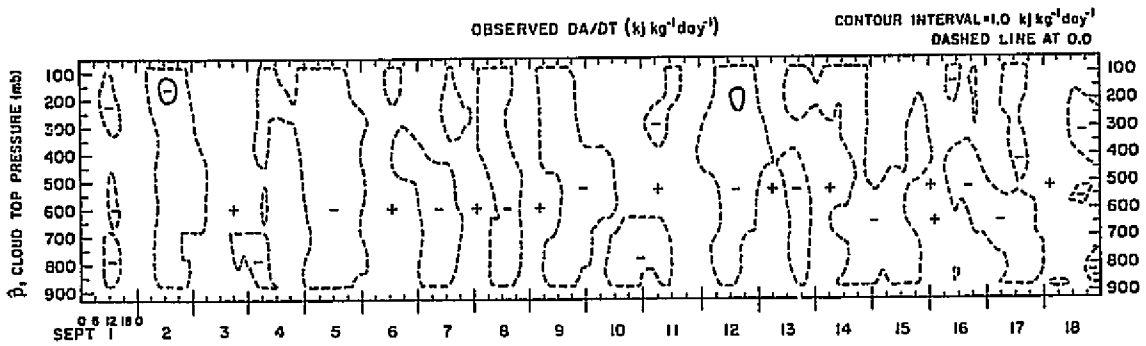

FIGURE 2 A time series of the observed time change dA/dt(kJ kg^{-1} day^{-1}) of the cloud work function for each subensemble. The contour lines are identical to Figure 1, and the dashed line indicates the zero line.

1976), and composited soundings from West Pacific Tropical Cyclones and West Indies Hurricanes (Frank, 1977). These data represent a wide variety of synoptic conditions since both undisturbed and high disturbed conditions are included. Figure 3, for example, shows the cloud work function for each $\hat{p}$ calculated from GATE and the composite tropical cyclone and hurricane data. The error bars for the GATE results indicate one standard deviation. The radius, R, is in degrees latitude from the center of the cyclones.

We can estimate the order of magnitude of dA/dt in Eq. (2) using typical variations of A, δA, in Figure 3. For example, let us assume that the change of A from $R = 2°$ to $R = 6°$ in the hurricane takes place over a period of $\tau = 1$ day. For cloud with $\hat{p} = 350$ mbar, $dA/dt \sim \delta A/\tau \sim 0.14$ kJ kg^{-1} day^{-1}. Figure 1, on the other hand, shows $F \sim 4$ kJ kg^{-1} day^{-1} for the same cloud type. This value of F is clearly a conservative estimate of F in tropical cyclones, and, therefore, the inequality (5) holds to a very good approximation.

These results are supporting evidence for the cloud work function quasi-equilibrium. The complete parameterization will now be evaluated by

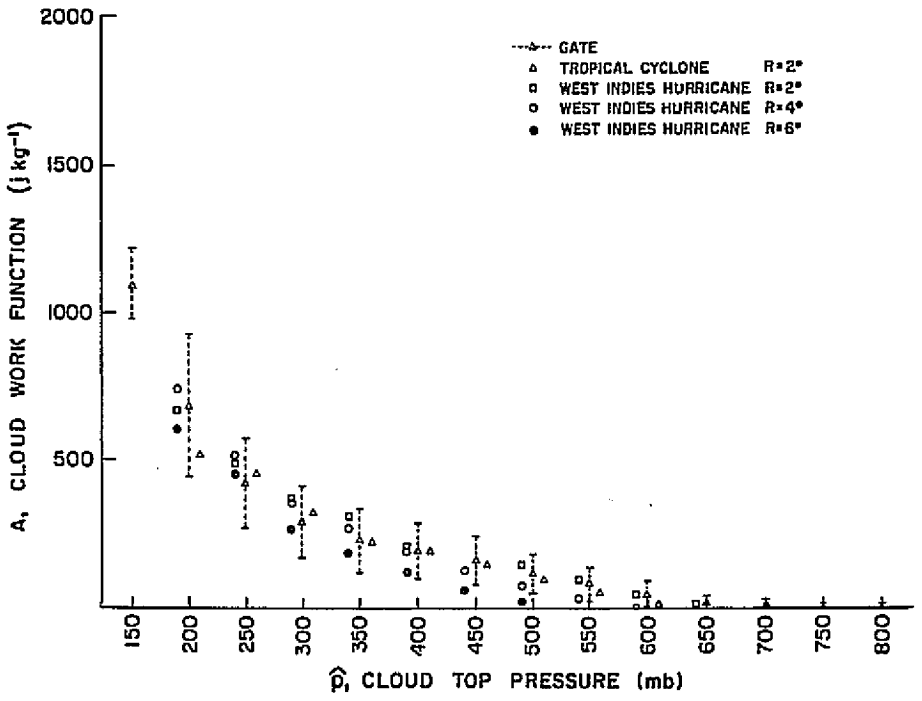

FIGURE 3 Cloud work function (J kg^{-1}) versus $\hat{p}$ for GATE and composite tropical cyclone and hurricane data.

comparing predictions of precipitation rates and cumulus warming and drying effects with observed rainfall estimates and residuals in the observed heat and moisture budgets, $Q_1 - Q_R$ and Q_2. The following results were obtained from the cumulus cloud-base mass-flux spectrum determined by Eq. (2) using estimates of the large-scale forcing shown in Figure 2. From the distribution of cloud-base mass flux, instantaneous values of the precipitation rate and the cumulus warming and drying were calculated at each observation time.

Figure 4 shows a time series of the calculated precipitation rate (mm day^{-1}) from September 1 to September 18 and the rates estimated by the observed moisture budget and radar measurements. The estimate from the observed moisture budget, P_{Q2}, was obtained from

$$P_{Q2} = \int_{100}^{p_S} \frac{Q_2}{L} \frac{dp}{g} + E_S \ , \qquad (6)$$

where p_S is the surface pressure, Q_2 is given at 3-h intervals by the observations, and E_S is an estimated surface evaporation rate.

The precipitation rate derived from radar estimates, P_{RA}, shown in Figure 4 is a time-smoothed version of the hourly rainfall data over 1/4° × 1/4° latitude-longitude squares as described in Hudlow and

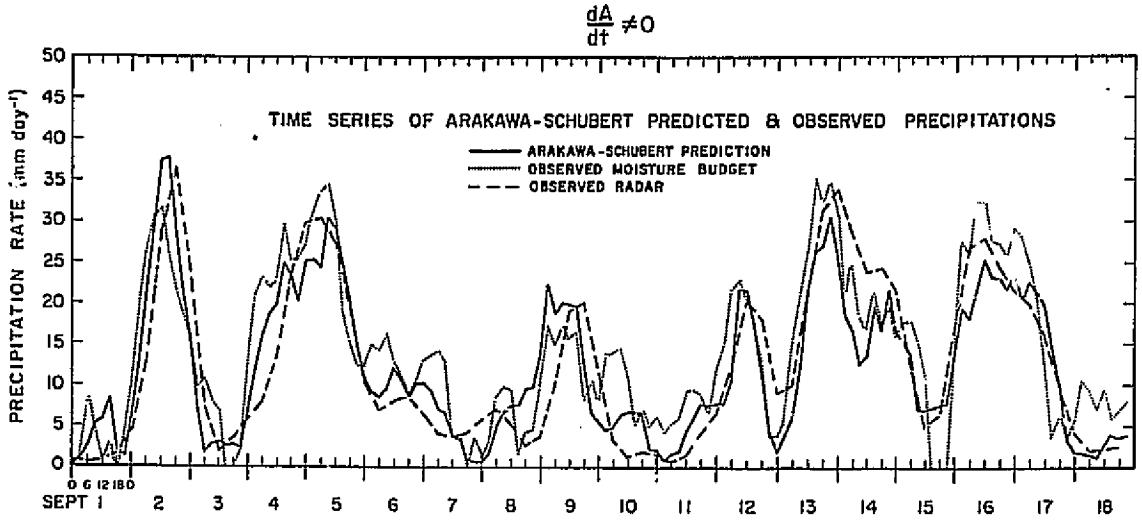

FIGURE 4 Time series of precipitation rates (mm day^{-1}) calculated from the mass-flux distribution function determined by Eq. (2), the observed moisture budget and observed radar measurements.

Patterson (1978). This smoothing does not, of course, alter the mean precipitation rate. The mean precipitation rates over this period are P_{Q2} = 14.3 mm day^{-1} and P_{RA} = 12.4 mm day^{-1}.

The calculated precipitation rate, P_{AS}, shown in Figure 4 was obtained from the cloud mass-flux spectrum determined by Eq. (2) using the observed values of dA/dt on the left-hand side. The values of this P_{AS} for each observation time agree closely in both magnitude and phase with the two independently derived observed estimates, P_{Q2} and P_{RA}, in both disturbed and undisturbed conditions. The mean P_{AS} is 12.3 mm day^{-1}. The correlations between the time series are as follows: P_{AS} and P_{RA}, 0.868; P_{AS} and P_{Q2}, 0.877; P_{Q2} and P_{RA}, 0.817.

We now compare a similar time series (Figure 5) of calculated precipitation rates obtained from Eq. (2) *but with* dA/dt *neglected*, i.e., using the cloud-work-function quasi-equilibrium hypothesis. Comparing Figures 5 and 4, we see that the precipitation rates differ by less than 10 percent in almost all instances. P_{AS} in this case is 12.2 mm day^{-1}, only 0.1 mm day^{-1} smaller than the case in which the quasi-equilibrium hypothesis was not used. This result is strong supporting evidence for the cloud-work-function quasi-equilibrium hypothesis.

Let us define calculated values of the large-scale heat source and moisture sink as

$$(Q_1 - Q_R)_{AS} \equiv c_p \left(\frac{\partial \bar{T}}{\partial t}\right)_{CU} \tag{7}$$

and

$$(Q_2)_{AS} \equiv -L\left(\frac{\partial \bar{q}_v}{\partial t}\right)_{CU}, \tag{8}$$

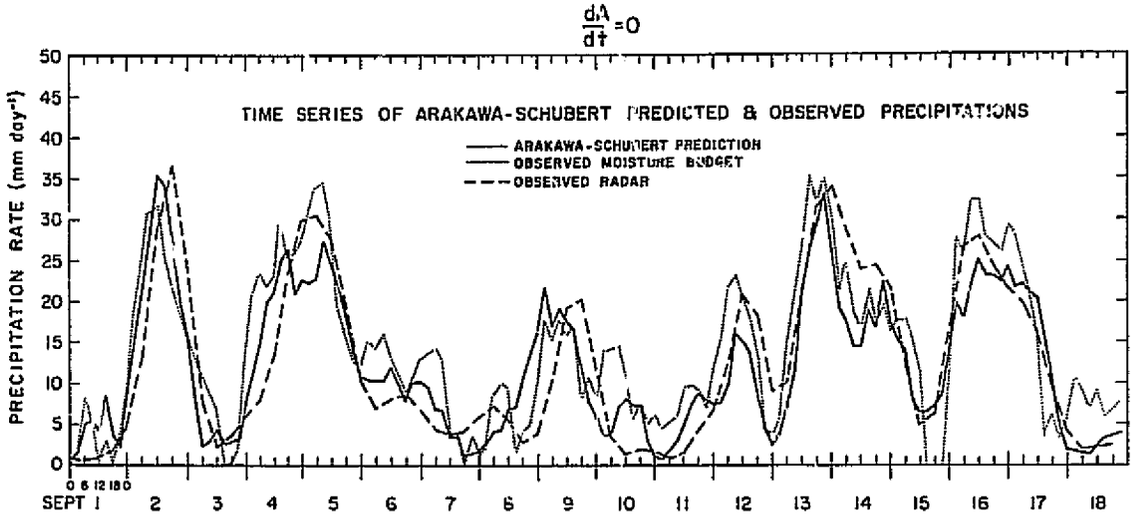

FIGURE 5 Same as Figure 4 but with $dA/dt = 0$ in Eq. (2).

where $(\partial\overline{T}/\partial t)_{CU}$ and $(\partial\overline{q}_v/\partial t)_{CU}$ are the calculated warming and drying by cumulus clouds. Figures 6 and 7 show the mean calculated and observed $Q_1 - Q_R$ and Q_2. We see that there is net cooling due to cumulus clouds above 300 mbar and net moistening above 400 mbar. Between 300 and 600 mbar, the warming is underestimated, and below 650 mbar it is overestimated. The drying predicted by the parameterization is underestimated above 700 mbar and overestimated below 750 mbar. These results show that the time changes in temperature and moisture due to clouds calculated by the parameterization are not well simulated level by level, although the vertically integrated changes are close to observations.

The dashed lines in Figures 6 and 7 represent a modification of the above calculation, by allowing the detrained liquid water at cloud-top levels above the freezing level to precipitate and evaporate into the large-scale environment below the freezing level. This modification produces a noticeable redistribution of the heating and moistening in the vertical air column. Overprediction of cooling and moistening in the upper layers is reduced, as is the overprediction of warming and drying in the lower layers.

We have performed similar calculations of precipitation rates and cumulus warming and drying using the moist convective adjustment scheme of Manabe *et al.* (1965) and the parameterization of Kuo (1965). Table 1 shows the mean precipitation rates P_{Q_2} and P_{AS}, and those using Kuo's scheme, P_{KUO} and the moist convective adjustment, P_{MCA}. P_{MCA} depends on the critical relative humidity, $(RH)_C$, which must be exceeded for adjustment to occur. We see that the precipitation rates predicted by Kuo's scheme and the moist convective adjustment scheme for $(RH)_C \geq 80$ percent are considerably smaller than observed estimates.

Table 2 summarizes the correlation coefficients between the various schemes for predicting cumulus precipitation discussed in this paper. $(RH)_C = 70$ percent is used for P_{MCA}. There is a large, though not

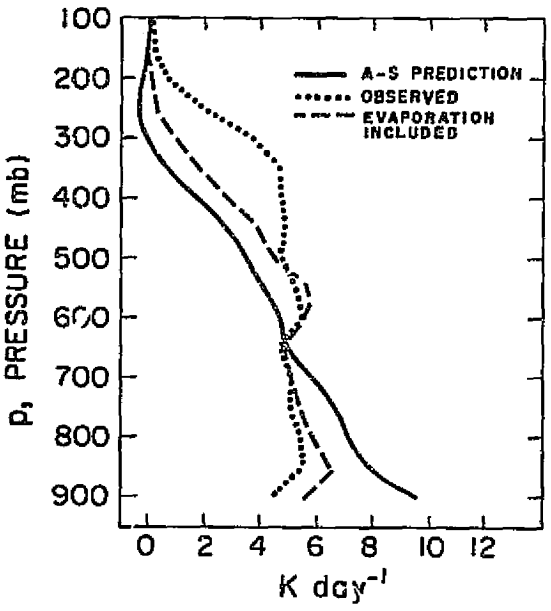

FIGURE 6 The time-averaged vertical distribution of the calculated and observed heat source due to clouds, $Q_1 - Q_R$.

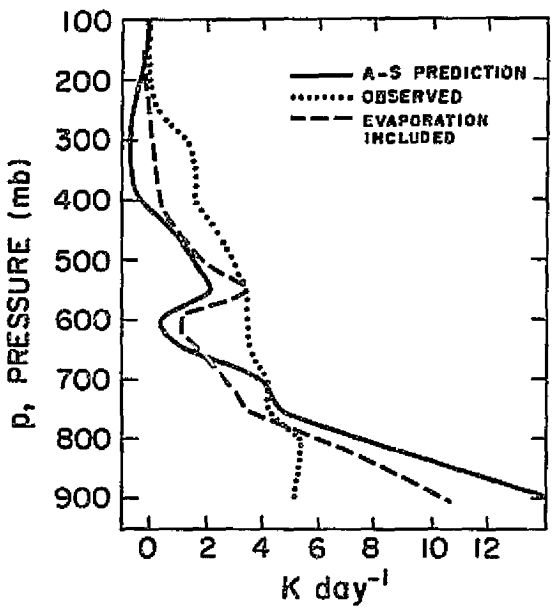

FIGURE 7 The time-averaged vertical distribution of the calculated and observed moisture sink due to clouds, Q_2.

frequent, noise in P_{MCA} due to the use of the critical relative humidity. This noise is largely responsible for the low correlations of P_{MCA} with P_Q and P_{RA}. P_{KUO} is highly correlated with P_{Q2}. This high correlation is not surprising, because P_{KUO} strongly depends on the large-scale moisture convergence.

Comparison of the vertical distributions of cumulus warming and drying with Kuo's scheme and the moist convective adjustment reveals the following: Kuo's scheme predicts a monotonic increase in warming with height up to a maximum value at 350 mbar. The drying predicted by Kuo's scheme resembles the observed Q_2 but is underpredicted. The warming and drying predicted by the moist convective adjustment is characterized by large noise due to the use of the critical relative humidity.

From the results presented above, we conclude that the Arakawa-Schubert cumulus parameterization is very successful in predicting the precipitation rates over the GATE area during Phase III. The precipitation rates are not changed substantially by the inclusion of the dA/dt term in Eq. (2), thereby proving a strong verification of the cloud-work-function quasi-equilibrium. There are, however, discrepancies with observations in the predicted vertical distributions of warming and drying due to cumulus clouds. Kuo's scheme and the moist convective adjustment are less successful in predicting precipitation and cumulus warming and drying.

TABLE 1 Mean Precipitation Rates Calculated by the Arakawa-Schubert Parameterization, Kuo's Scheme, and the Moist Convective Adjustment for Different Values of $(RH)_C$

Method		Time-Averaged Precipitation Rate (mm day^{-1})
P_{Q2}		14.3
P_{AS}		12.1
P_{KUO}		6.63
P_{MCA}	60%	11.86
$(RH)_C$	70%	11.40
	80%	7.75
	90%	2.63

TABLE 2 Correlation Coefficients for Precipitation Rates

	P_{AS}	P_{Q2}	P_{RA}	P_{MCA}	P_{KUO}
P_{AS}	1.000	0.877	0.868	0.413	0.947
P_{Q2}	0.877	1.000	0.817	0.429	0.901
P_{RA}	0.868	0.817	1.000	0.472	0.850
P_{MCA}	0.413	0.429	0.472	1.000	0.435
P_{KUO}	0.947	0.901	0.850	0.435	1.000

REFERENCES

Arakawa, A. (1974). Modeling clouds and cloud processes for use in climate models. *Report of the International Study Conference on the Physical Basis of Climate Modeling in Stockholm, 29 July-10 August 1974*. GARP Publication Series No. 16.

Arakawa, A., and W. H. Schubert (1974). Interaction of a cumulus cloud ensemble with the large-scale environment, Part 1. *J. Atmos. Sci. 31*, 674-701.

Betts, A. K., and R. D. Miller (1975). VIMHEX-1972 rawinsonde data. Atmos. Sci. Research Report, Colorado State U., Ft. Collins, Colo.

Frank, W. M. (1977). The structure and energetics of the tropical cyclone, Paper I: Storm structure. *Mon. Wea. Rev. 105*, 1119-1135.

Hudlow, M. D., and V. L. Patterson (1978). GATE Radar Rainfall Atlas. NOAA Special Report, Center for Environmental Assessment Services, National Oceanic and Atmospheric Administration. 162 pp.

Jordan, C. L. (1958). Mean soundings for the West Indies area. *J. Meteorol. 15*, 91-97.

Kuo, H. L. (1965). On the formation and intensification of tropical cyclones through latent heat release by cumulus convection. *J. Atmos. Sci. 22*, 40-63.

Lord, S. J. (1978). Development and observational verification of a cumulus cloud parameterization. Ph.D. thesis, UCLA, 359 pp.

Manabe, S., J. Smagorinsky, and R. Strickler (1965). Simulated climatology of a general circulation model with hydrological cycle. *Mon. Wea. Rev. 93*, 769-798.

Nitta, T. (1976). Large-scale heat and moisture budgets for the Air Mass Transformation Experiment. *J. Meteorol. Soc. Jpn. 54*, 1-14.

Thompson, R. M., S. W. Payne, E. E. Recker, and R. J. Reed (1979). Structure and properties of synoptic-scale wave disturbances in the Intertropical Convergence Zone of the eastern Atlantic. *J. Atmos. Sci. 36*, 53-72.

Yanai, M., S. K. Esbensen, and J.-H. Chu (1973). Determination of bulk properties of tropical cloud clusters from large-scale heat and moisture budgets. *J. Atmos. Sci. 30*, 611-627.

DISCUSSION

H. R. Cho, *Rapporteur*

The discussions were focused mainly on the possible causes for discrepancies between the mean apparent heat sources observed in Phase III of GATE and those predicted by the Arakawa-Schubert scheme. The Arakawa-Schubert scheme underpredicts the heat source in the upper troposphere and overpredicts it in the lower troposphere.

One problem of the scheme appears to be the simple cloud ensemble model used to represent cloud processes. The model does not include evaporation-induced cloud downdrafts. It also does not describe observed features of the organized mesoscale circulations. The predicted rainfall rate, however, appears rather insensitive to the microphysics parameterization used in the model.

This parameterization attempts to connect forcing over a large-scale area directly to cloud-scale processes. This could be another problem. The large-scale averaged forcing mechanism applied to individual clouds might be quite different from the forcing felt by organized mesoscale cloud clusters. It is not yet clear how the cloud work function quasi-equilibrium hypothesis may be formulated to include mesoscale systems, and it is not known whether the hypothesis will hold within a mesoscale system.

The theory has now been implemented in several large-scale numerical models. The results are somewhat mixed. Testing results from the GFDL

GCM seem to suggest that it works better than most of the other models. Despite its apparent complexity, the scheme takes only a relatively small fraction (~5 percent) of the total computer time used by these models.

Schubert presented a few hypothetical cloud mass-flux distributions predicted according to the Arakawa-Schubert parameterization, illustrating how a cloud population responds to changes of mean vertical velocities at the upper levels. According to these predictions, a deep cloud population is determined by the mean convergence field at all levels not merely by the low-level convergence.

Krishnamurti presented rainfall rates predicted according to Kuo's 1974 scheme and the moist adjustment scheme, using GATE data. The performance of the 1974 version of Kuo's scheme was found to be generally very good.

PARAMETERIZATION OF CONVECTIVE EFFECTS ON THE MOMENTUM AND VORTICITY BUDGETS

Lloyd J. Shapiro
National Hurricane and Experimental Meteorology Laboratory, NOAA

If large-scale observations are used to evaluate all the terms in the dynamic budget equations, large residual imbalances not attributable to error will be found. These "apparent sources" of vorticity and momentum represent the effect of subgrid-scale processes on the large-scale dynamics. The significant of cumulus-associated transports of vorticity and momentum in the GATE region is discussed in the paper by Stevens. The importance of the inclusion of cumulus-associated momentum transports in the modeling of synoptic-scale disturbances is discussed in the presentations of Lindzen and of Mass.

Thermodynamic budgets and simple cloud models (spectral, bulk, and single-cloud) have been used extensively to diagnose average cloud properties, including mass flux, moisture, and energy. The same models have been used to diagnose the average dynamic properties of the idealized clouds. For example, single-cloud models were used by Austin and Houze (1973) to diagnose cloud momentum, and by Reed and Johnson (1974) to diagnose cloud mass flux and vorticity.

It is difficult to relate cloud parameters diagnosed from these models to directly observable quantities. Convection is not simply a random distribution of isolated cumuli but is characteristically organized on the mesoscale into transient clusters or squalls. However, the diagnosed parameters (mass flux, moisture, and momentum, for example) have been used to interpret the interaction between the cumulus scale and the large scale. The simple cloud models have also been used in analytic and numerical models to parameterize the feedback between cumulus-scale and large-scale dynamics. A complete independent verification of the models used is not possible. But an *a posteriori* test may be made of the consistency of the models with the apparent sources, which are observable.

The studies to be discussed in this presentation have addressed the particular problem of establishing the degree of consistency between the diagnosed residuals obtained from the large-scale dynamic budgets, representative of the effect of cumulus transports, and simple parameterized forms of the cumulus transports determined from *independently* derived cloud mass fluxes and budgets. This method has been used in Shapiro (1978), Cho, *et al.* (1979), and Cheng, *et al.* (1979) for vorticity and Shapiro and Stevens (1979) for vorticity and momentum. All these studies have used GATE data for the large-scale observations. The results and

implications of these studies will be discussed below. Cheng *et al.* (1978), and Cheng (1979) have also used this method for potential vorticity.

If the subgrid processes that account for the large-scale imbalances above the boundary layer are associated with cumulus-scale motion, the apparent sources of vorticity (Z) and zonal and meridional momentum (X and Y) may be parameterized in terms of cloud and large-scale quantities. Paralleling the spectral models used in thermodynamic budgets, the dynamic sources may be parameterized by

$$X \equiv (X,Y) \approx \left[\sum_i m_i \, (\vec{u}_{ci} - \vec{u})\right]_p ,$$

$$Z \approx \sum_i \delta_i \, (f + \zeta)_{ci} - \varepsilon(f + \zeta) - M_c \zeta_p - \vec{k} \cdot \nabla M_c \times \vec{u}_p .$$

The notation is the same as that used by Yanai *et al.*, (1973). The summation is taken over all cloud types in the spectral ensemble. m_i is the mass flux in each cloud type, and M_c is the total mass flux. A subscript c represents a cloud-averaged value. δ_i is the rate of cloud detrainment of mass for each cloud type, and ε is the total rate of cloud entrainment. A steady-state one-dimensional cloud model has been used. The horizontal eddy transports have been neglected. Evaluating the cloud budget of momentum and vorticity for each cloud type,

$$-m_i \, (\vec{u}_{ci})_p - \varepsilon_i (\vec{u} - \vec{u}_{ci}) = -\sigma_i (\nabla\phi)_{ci} ,$$

$$\delta_i (f + \zeta)_{ci} - \varepsilon_i (f + \zeta) = -\sigma_i \omega_i^B (\zeta_{ci})_p \approx \tfrac{1}{2} m_i \, (\zeta_{ci})_p ,$$

where σ_i is the fractional area covered by each cloud type (taken here to be constant and $<<1$) and ω_i^B, the cloud boundary value of ω is taken to be the average of the cloud and environmental values ($\approx \frac{1}{2}\omega_{ci}$). $(\nabla\phi)_{ci}$ is the pressure force of the environment on the cloud momentum. With cloud-base values of cloud vorticity specified, the cloud budget equations provide values of cloud vorticity and momentum at all levels once m_i is known.

Alternate bulk forms may be derived for the momentum budgets, using a mass flux-weighted average cloud momentum and assuming that this momentum is detrained by each cloud type at its level of detrainment [cf., Yanai *et al.* (1973)]. Although no corresponding system may be directly derived for the vorticity budget, the analogous bulk relation may still be evaluated in an *ad hoc* manner. The bulk relations are identically the spectral model equations evaluated for one cloud type. In the single-cloud model (e.g., Reed and Johnson, 1974), the total mass flux M_c is used directly to derive entrainment and detrainment rates.

In Shapiro (1978) the vorticity budget of a composite synoptic-scale African wave was analyzed using the velocity, vorticity, and divergence fields analyzed by Reed *et al.* (1977) during Phase III of GATE. The apparent vorticity source Z diagnosed at the reference latitude (near 11° N) is shown in Figure 1. The cloud model used was the same single-cloud model as that used by Reed and Johnson (1974). The total mass fluxes M_c were obtained by R. Johnson, based on thermodynamic budgets, using a spectral cloud model without downdrafts and the standard global radiative cooling profile of Dopplick (1972). The inclusion of downdrafts would affect the total mass flux only at low levels. Since shallow trade cumulus are not expected to contribute significantly to the net vertical vorticity transport, only clouds detraining above 750 mbar were included. Cloud-base values of vorticity were assumed equal to environmental values at that level. The twisting-like term in the parameterized vorticity source was evaluated and found to be very small. The parameterized form of the vorticity source due to cumulus found in Shapiro (1978) is shown in Figure 2. Almost all features of the observed source (Figure 1) are reflected, with a smaller magnitude, in the parameterized source. The absence of negative values near the surface is due to the omission of boundary-layer dissipation in the parameterized form.

In recent analyses (Shapiro and Stevens, 1979), large-scale residuals based on dynamic budgets of momentum as well as vorticity have been derived, and the cloud models have been extended to include spectral and

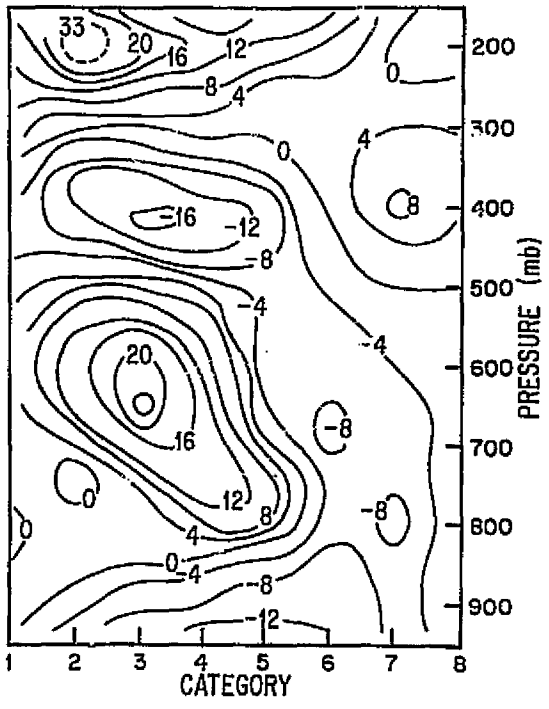

FIGURE 1 Apparent vorticity source Z ($\times 10^{-11}$ sec^{-2}) at reference latitude for African wave.

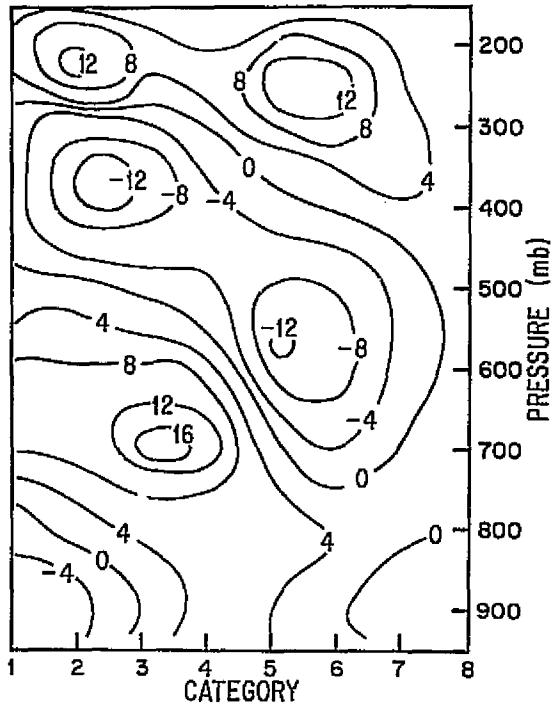

FIGURE 2 Parameterized vorticity source ($\times 10^{-11}$ sec^{-2}) at reference latitude for African wave.

bulk, as well as single-cloud models. The large-scale residuals are those derived by Stevens (1978) and described by him in his presentation, based on the average synoptic-scale wave composited by Thompson *et al.* (1979) from GATE Phase III A/B-scale data. The cumulus mass fluxes have been derived thermodynamically by D. Stevens, using Johnson's (1978) algorithm including only updrafts. In order to test the sensitivity of the parameterized sources to the assumed radiative cooling profiles, two radiative rates have been used. The first are those derived by Thompson *et al.* (1979) based on rates given by Gray and Jacobson (1977). The second are those derived by Johnson (1979) based on profiles of Cox and Griffith (1978). First, results using Gray and Jacobson's profiles will be discussed. There are difficulties with the diagnosed mass fluxes outside of the wave trough. In the following discussion only results from the most convectively active trough region, category 4, are considered.

Figure 3 shows the apparent vorticity source Z in category 4 as a solid line. Virtually all the features of the apparent source derived from the large-scale variables are mirrored, both qualitatively and quantitatively, in the parameterized source derived from the single-cloud model (dashed line). The same computation was made using the bulk model and was found very close to that of the single-cloud model. The parameterized vorticity source derived from the spectral model (dotted line) gives values far in excess of those observed. The strongly nonconservative nature of cloud vorticity for each member of the cloud spectrum, due to entrainment and resulting vortex stretching, makes the use of the spectral model unsuitable for vorticity studies. With the Cox and Griffith profile of radiative cooling, the quantitative agreement between the apparent and parameterized source is less than with the Gray and Jacobson profile, especially in the lower troposphere. Thus the ability of the simple cloud model to account for the observed vorticity source is sensitive to the specified radiative profile.

A parallel analysis to vorticity was made with both zonal and meridional momentum. The cloud values of u were derived assuming zero pressure drag on the clouds. Both the single-cloud model and the spectral model produce profiles of cloud momentum with values very close to the cloud-base value. In fact, the parameterized momentum sources derived from these cloud models were not significantly different from those found from a model in which the cloud momentum was taken as constant with height, as proposed by Schneider and Lindzen (1976). The solid line in Figure 4 shows X', the deviation from a time-averaged value of the zonal momentum source derived by Stevens (1978). The very simple cloud model with cloud momentum constant with height (dashed line) agrees quite well with the apparent source up to 500 mbar. Above 500 mbar, where the wind is highly baroclinic, it is likely that the pressure force term, which is omitted here, contributes to the cloud momentum profile. The inclusion of a quadratic drag law, representing the force of the environmental flow on the cloud momentum [as proposed by Malkus (1952) and used by Austin and Houze (1973)] does not, however, improve the agreement between the observed and parameterized profiles of X'. To the extent that the disagreement between the observed and parameterized momentum sources cannot

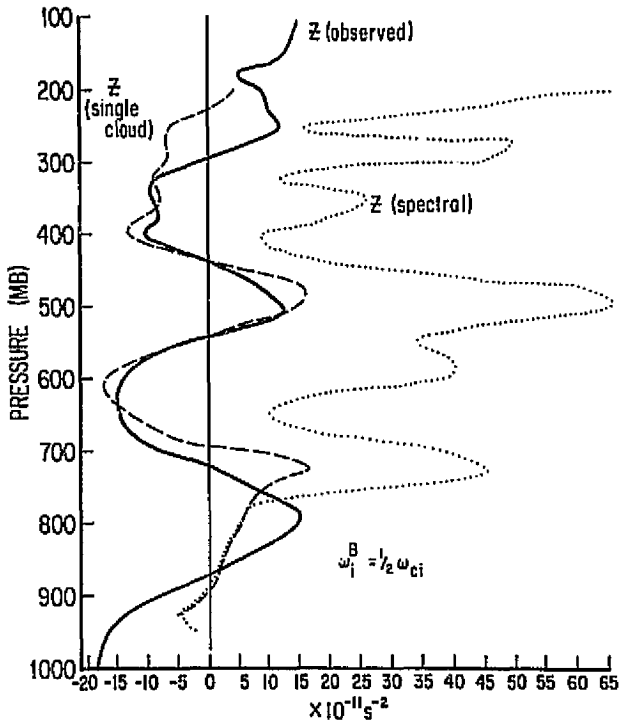

FIGURE 3 Vorticity source in category 4 (trough) of Atlantic wave ($\times 10^{-11}$ sec^{-2}).

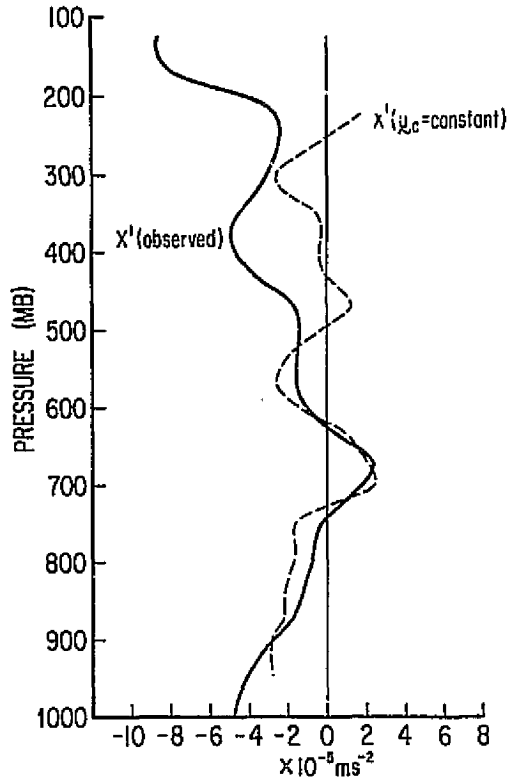

FIGURE 4 Deviation from time mean of zonal momentum source in category 4 (trough) of Atlantic wave ($\times 10^{-5}$ msec^{-2}).

be explained by data errors (most likely in the geopotential gradient), the drag law may not simply account for the pressure force of the environment on the cloud air.

Cho *et al.* (1979) have presented results from an alternate cloud model to represent the effects of cumulus transports on the large-scale vorticity budget. Cho in another paper in this volume presents results from his formulation, including effects neglected in Cho *et al.* (1979). The important difference from the model I have described is the use of a cloud model in which updrafts and downdrafts are implicitly included by defining the cloud boundary to be where the cloud vertical velocity matches smoothly onto the environment (instead of a tophat profile). Neglecting the horizontal eddy flux of vorticity, Cho's parameterized form for Z [Eq. (30) of Cho *et al.* (1979)] is found to omit the terms in the formulation that I have presented that account for the entrainment and detrainment of cloud vorticity. Since the parameterized vorticity source is then decoupled from the production of cloud vorticity by vortex stretching, there is no term that can account for a strong large-scale production of vorticity by

convergence. Cho *et al.* (1979) compared the parameterized and apparent vorticity sources for the GATE A/B-scale array during September 9 and found good agreement. The large-scale convergence production term was not large during this day, except near 300 mbar. More recently, Cheng *et al.* (1979) have presented results from September 2, a day for which the large-scale convergence production term was more significant, as it was for the composite wave studies that I have described. In this case, less-favorable agreement with the observed source was found. Cho will relate results that account for the differences by inclusion of the horizontal eddy-flux term previously neglected. With the eddy-flux term included, Cho's formulation becomes equivalent to what I have presented.

The agreement between the parameterized vorticity source derived from the single-cloud model and the apparent vorticity source, within the error implied by the assumed radiative profile, provides verification of the consistency between the parameterization and the large-scale observations. Although this *a posteriori* consistency check does not verify the model in any absolute sense, it does provide additional confidence for its use in theoretical or numerical simulations.

The consistency tests were found to be useful in rejecting inconsistent parameterizations, in particular, the spectral formulation for vorticity and a parameterized vorticity source that omits the effect of the production of vorticity by vortex stretching.

Although the details of cloud-environment dynamic interactions are complex, a simple, one-dimensional single-cloud model appears to account adequately for the net effect of the cumulus transport and production of vorticity. The generation of horizontal cloud momentum from vertical momentum due to cloud outflow, however, cannot be accounted for in a one-dimensional cloud model. Such generation may account for the diagnosed zonal momentum sink found for the Atlantic wave in the upper-tropospheric easterly wind. The implication is that the net effect of the cumulus transport and production of vorticity on the synoptic scale may depend less on the detailed internal dynamics of the convective system (e.g., whether the mesoscale organization is in squall lines or clusters) than does the net transport and production of momentum. The difficulties found with the cumulus mass flux in the Atlantic wave outside the trough, and the sensitivity of the parameterized source to the radiative cooling profile, highlight the strong coupling between the dynamic and thermodynamic parameterizations.

REFERENCES

Austin, P., and R. Houze (1973). A technique for computing vertical transports by precipitating cumuli. *J. Atmos. Sci. 30*, 1100-1111.

Cheng, L. (1979). The determination of mean cloud vorticity from the potential vorticity budget and its application. Presented at 12th Technical Conf. on Hurricanes and Tropical Meteorology, New Orleans.

Cheng, L., T. Yip, and H. Cho (1978). Dynamic effects of cumulus clouds as observed in large-scale potential vorticity budget. Preprint, 11th Technical Conf. on Hurricanes and Tropical Meteorology, Miami.

Cheng, L., R. Bloxam, and H. Cho (1979). The parameterization of cumulus effects in the large-scale voritcity equation. Presented at 12th Technical Conf. on Hurricanes and Tropical Meteorology, New Orleans.

Cho, H., L. Cheng, and R. Bloxam (1979). The representation of cumulus cloud effects in the large-scale vorticity equation. *J. Atmos. Sci. 36*, 127-139.

Cox, S., and K. Griffith (1978). Tropospheric radiative divergence during Phase III of the GARP Atlantic Tropical Experiment (GATE). *J. Atmos. Sci. 35*, 586-601.

Dopplick, T. (1972). Radiative heating of the global atmosphere. *J. Atmos. Sci. 29*, 1278-1294.

Gray, W., and R. Jacobson (1977). Diurnal variation of deep cumulus convection. *Mon. Wea. Rev. 105*, 1171-1188.

Johnson, R. (1978). Cumulus transports and their meridionally varying response to large-scale forcing in an African tropical wave disturbance composite for Phase III of GATE. *J. Atmos. Sci. 35*, 484-494.

Johnson, R. (1979). A diagnostic model for cloud population properties that includes effects of convective-scale and mesoscale downdrafts. Submitted to *J. Atmos. Sci.*

Malkus, J. (1952). The slopes of cumulus clouds in relation to external wind shear. *Quart. J. R. Meteorol. Soc. 78*, 530-542.

Reed, R., and R. Johnson (1974). The vorticity budget of synoptic-scale wave disturbances in the tropical western Pacific. *J. Atmos. Sci. 31*, 1784-1790.

Reed, R., D. Norquist, and E. Recker (1977). The structure and properties of African wave disturbances as observed during Phase III of GATE, *Mon. Wea. Rev. 105*, 317-333.

Schneider, E., and R. Lindzen (1976). A discussion of the parameterization of momentum exchange by cumulus convection. *J. Geophys. Res. 81*, 3158-3160.

Shapiro, L. (1978). The vorticity budget of a composite African tropical wave disturbance. *Mon. Wea. Rev. 106*, 806-817.

Shapiro, L., and D. Stevens (1979). Cumulus transports of vorticity and momentum in GATE Phase III wave disturbances. Presented at 12th Technical Conf. on Hurricanes and Tropical Meteorology, New Orleans.

Stevens, D. (1978). Vorticity, momentum and divergence budgets of synoptic-scale wave disturbances in the tropical eastern Atlantic. *Mon. Wea. Rev. 106*, 535-550.

Thompson, R., S. Payne, and E. Recker (1979). Structure and properties of synoptic-scale wave disturbances in the Intertropical Convergence Zone of the eastern Atlantic. *J. Atmos. Sci. 36*, 53-72.

Yanai, M., S. Esbensen, and J.-H. Chu (1973). Determination of bulk properties of tropical and cloud clusters from large-scale heat and moisture budgets. *J. Atmos. Sci. 30*, 611-627.

DISCUSSION

S. Soong, *Rapporteur*

Since ζ is not a conservative quantity, the formulation of cloud-scale transport of ζ in a way analogous to the conservative quantities such

as h may not be adequate. The potential vorticity, which is conservative, could be a better variable to use. The computation of the ζ budget using the averaged wave properties instead of the average of individual vorticity budgets may also produce differences in the interpretation of the ζ budget. However, the good agreement between the predicted cloud effect on ζ and the observed budget provides a verification of the current approach.

Since primitive equation models do not predict ζ, the parameterization of ζ cannot directly be used in these numerical models. The parameterization of momentum, which can be used in models, involves the difficulty of determining the pressure gradient force. A trade-off exists no matter which variable we are looking at. But the study of the ζ budget and its parameterization certainly adds to our understanding of dynamic processes. Since vorticity may be the dynamically important quantity for easterly waves, the correct prediction of subgrid vorticity transports should aid in their prediction.

EXPERIMENTS WITH IMAGINARY CONVECTION

David R. Rodenhuis
University of Maryland

INTRODUCTION

A comparison of four different parameterization models has been made using identical data input. The composite data set for September 6, 1974, constructed by Nitta (1977) has been used. The models that are tested are different versions of the entraining jet model (Arakawa and Schubert, 1974; Nitta, 1977) and an ensemble cellular model of Rodenhuis and Cheng (1979).

The purpose of these studies is to discover real physical differences in the models that will limit their application.

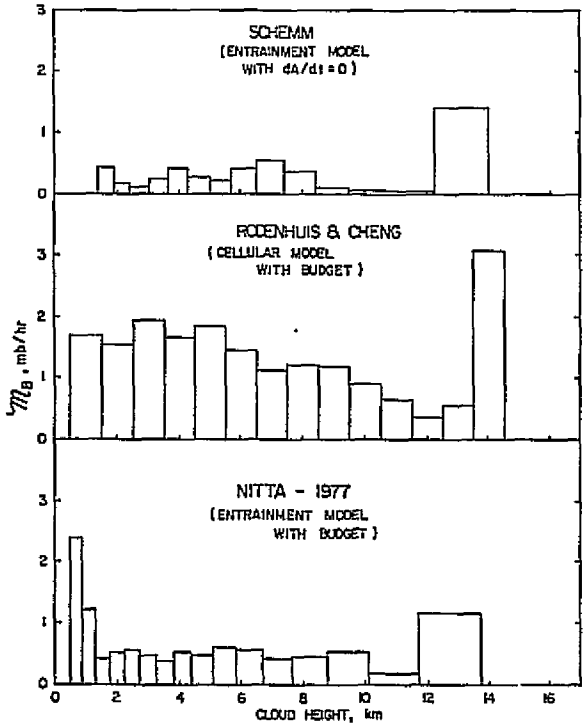

FIGURE 1 A comparison of mass-flux spectra using identical data (September 6, 1974) for three different parameterization models.

TABLE 1 Results of Analysis from Several Different Parameterization Models[a]

	Boundary-Layer Mass Flux, M_B(mbar/h)	Precipitation, R (mm/day)	Convective Cloud Coverage (%)	Precipitation Efficiency, η(%)
Predictive extrainment model (Schemm)	4.7	41.54	--	77.96
Diagnostic cellular model (Rodenhuis and Cheng)	19.0	10.21	13.55	67.9
Diagnostic entrainment model (Nitta, 1977)	11.5	(?)	--	(?)
Comparison	2.3[1]	10[3]	80 (total)[6]	74[1]
		6.87[4]	12[7]	60[2]
			26.4 (total)[4]	
			11.2[5]	

[a]Data are September 6, 1974, composite for A/B area.
[1]Houze and Leary, 1976 (Pacific data).
[2]Reed and Johnson, 1974 (Pacific composite).
[3]McGarry and Reed, 1978 (GATE ship reports).
[4]GATE radar Atlas, 24-h average precipitation (GATE Master Array, 131,000 km^2).
[5]GATE radar Atlas, 24-h echo coverage with precipitation ≥0.5 mm/mr.
[6]SMS-IR cloud cover of A/B array (total cloud coverage).
[7]SMS-IR cloud cover of A/B array (brightest 1/3 of cloud coverage).

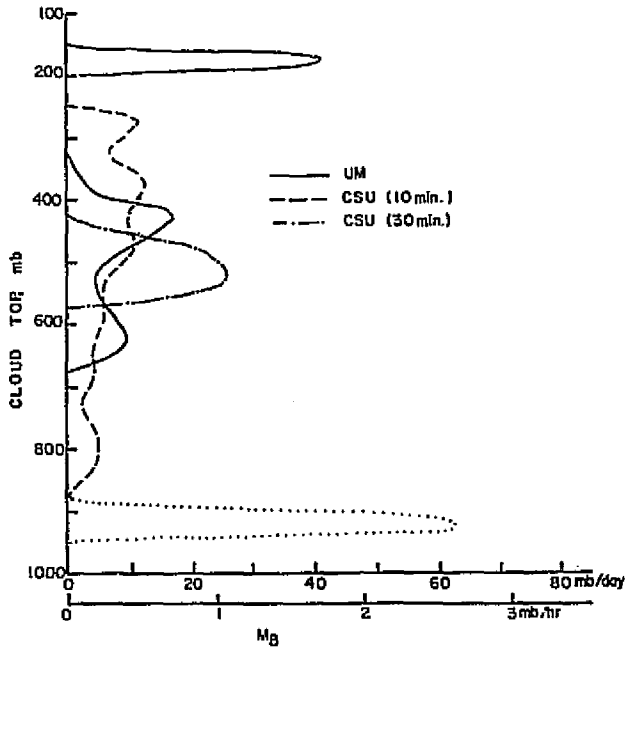

FIGURE 2 A comparison of the CSU and UM versions of the entrainment parameterization model (prediction application). Left: detrainment level as a function of entrainment parameter. Right: cloud mass-flux spectra.

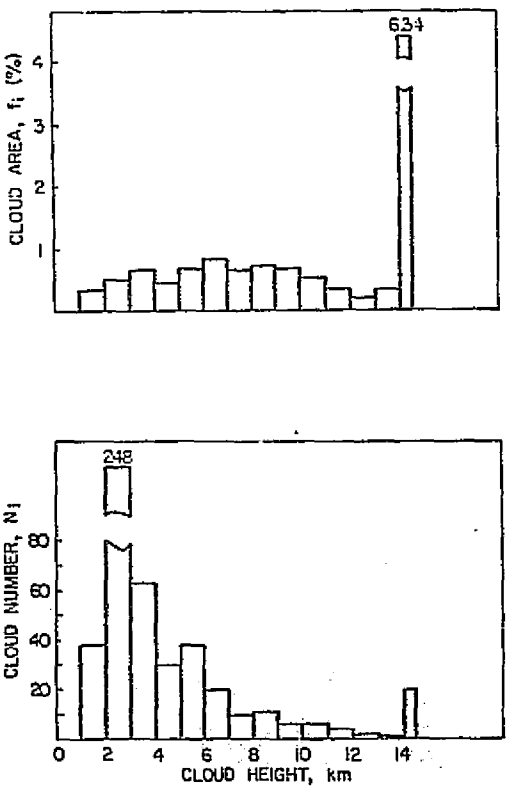

FIGURE 3 Cloud spectra for area fraction (upper) and number density (per 100,000 km^2).

RESULTS

Figure 1 presents the different cloud spectra in terms of cloud-base mass flux for several different models. The upper figure (Schemm) are the results using a predictive version of the entrainment parameterization model. The middle figure (Rodenhuis and Cheng) shows the results with the cellular model. A strong bimodal structure is absent from both results. However, the entrainment model generally produces a much weaker mass flux than the ensemble cellular model.

These results can be compared with those of Nitta (1977), who also used an entrainment model but applied it in a diagnostic sense. In these results the bimodal structure is clearly evident.

Table 1 summarizes some additional characteristics of these models. In the lower part of the table several results from independent studies are presented. The differences in results are due in part to the different energetic levels of cumulus activity that each model selects to represent the individual cumulus elements.

DISCUSSION

In order to investigate some of the variations in these results due to our application of the entrainment model, we performed a series of tests in collaboration with W. Schubert at Colorado State University (CSU) (Figure 2). In these experiments identical data were used; however, $Q_R = 0$. Both the CSU and University of Maryland (UM) results are obtained from an entraining cloud model. However, the models use different methods to enforce the condition that (i) cloud work function (A) be constant, and (ii) the boundary-layer mass flux (M_B) be positive.

Taken all together, there appears to be a large variation in the application of the entraining cloud model, and this may overwhelm physical differences between models, which are apparent in Figure 1.

Furthermore, the mass flux is not the only variable that describes the cloud spectra. Figure 3 shows the cloud spectra from the cellular model in terms of a real cloud fraction and cloud number density function. This description gives a superior physical view of the cloud population.

ACKNOWLEDGMENTS

The contributions of W. Schubert, P. Silva-Diaz, and J. Schemm are gratefully acknowledged.

REFERENCES

Arakawa, A., and W. H. Schubert (1974). Interaction of a cloud ensemble with the large-scale environment, Part I. *J. Atmos. Sci. 31*, 674-701.

Nitta, T. (1977). Response of cumulus updraft and downdraft to GATE A/B-scale motion systems. *J. Atmos. Sci. 34*, 1163-1186.

Rodenhuis, D., and C-S. Cheng (1979). An ensemble model of cellular convective elements. M.S. in preparation from Ph.D. dissertation of C-S. Cheng.

DISCUSSION

S. Soong, *Rapporteur*.

The implementation of the Arakawa and Schubert (A&S) parameterization scheme by Schemm produced a predicted precipitation rate may times larger than that measured by ship rain gauges or that estimated from radar data. On the other hand, Lord reported earlier a good agreement between the predicted rainfall by the same A&S scheme and that estimated from either the moisture budget or radar data.

A comparison between the results of Schemm's implementation of the A&S scheme with the diagnostic cellular model of Rodenhuis and Cheng (R&C) shows that the R&C model produces four times as much M_B as the A&S scheme. The precipitation rate diagnosed by the R&C model, however, is only one fourth of that of the A&S scheme. The explanation of these differences is at present unknown. There are also differences between A&S's cloud spectrum and that of Nitta. Since Nitta's model contains downdraft and the A&S scheme does not, some difference between the computed spectrum is expected.

A STOCHASTIC MODEL OF CUMULUS CLUMPING

David A. Randall
and
George J. Huffman
Massachusetts Institute of Technology

I. INTRODUCTION

There exist in cumulus-cloud fields a great variety of features with spatial scales in the range 10-100 km and temporal scales in the range 2-10 h. The most familiar of these "mesoscale" structures are squall lines and nonsquall bands, and open cells and cloud streets. Their sheer ubiquity, revealed by satellite photographs, suggests that they act as important mediators of the interactions between the cumulus and synoptic scales. Cumulus parameterization theories should therefore take their influence into account, but to date none does. The prerequisite theoretical understanding of the mesoscale has, so far, eluded us; in mesoscale meteorology, observations are far ahead of theory. This may be largely due to the baffling variety of mesoscale phenomenology. It seems that, at this point, theoretical progress may best be achieved by focusing on a single, particularly simple form of mesoscale structure. The GATE data set is ideally suited to guide us in our selection.

II. REVIEW OF OBSERVATIONS

In an interesting study of GATE radar data, López (1978) investigated local groups of cumulus cells, which he called composite echoes. He reported that "... at the start of a composite echo, a few cells are observed to occur together. With time, new cells form next to the old ones. The old ones may decay while the newer ones grow and develop. During the lifetime of the composite echo, many cells can go through their cycle of growth and decay." The individual cells that were members of composite echoes lasted longer, and rained more copiously, than isolated cells of the same cross-sectional area. They also achieved larger cross-sectional areas, on the average, than did their isolated counterparts. We shall refer to these local cloud groups as cumulus "clumps."* More precisely, we define a clump as a group of cumulus clouds the members of which are much more closely spaced than the average spacing over the

*We prefer "clump" to "cluster" because the term "cloud cluster" has been widely used to refer to the satellite-observed cloud features, of small synoptic scale, that are associated with tropical waves.

population and that maintains its identity over many cloud lifetimes. This is somewhat similar, but not identical, to Cho's (1978) concept of the independent cloud group.

A search of the observational literature reveals that clumps have been reported by many investigators. In an aircraft photographic survey of summertime Florida cumulus populations, Plank (1965, pp. 63-66; 1969) found that clumps developed in virtually all of the cloud populations, whether or not the clouds were organized into streets or bands. In a typical diurnal cycle, clumping was most noticeable between 1030 and 1300 EST; it was also especially pronounced in disturbed weather. Plank (1969) reported that the onset of clumping was associated with a shift in the population from a unimodal distribution (morning) to a bimodal distribution (afternoon). The largest clouds of the populations were found in clumps. Many clumps occurred within a population, and Plank (1965) reported that their distribution and spacing was "geometrically regular and seemingly systematic." Their sizes ranged from roughly that of the largest individual member cloud to one order of magnitude larger. The largest clumps occurred on disturbed days. Large clear "holes" in the cloud field were sometimes observed in the vicinity of the clumps.

Browning and Harrold (1969), Kreitzberg and Brown (1970), Harrold and Browning (1971), and Hill and Browning (1979) observed clumps in the convective regions of extratropical cyclones. They reported that the clumps include numerous cumulus congestus elements, are typically 50 km across, have been observed to persist for up to 8 h, appear to be advected by the mean wind in the convective layer, and are often aligned in bands.

Although chance groupings will occur even in a completely random cloud field, both the observed persistence of clumps over many individual cloud lifetimes and the observed tendency for the most vigorous clouds to occur preferentially in clumps strongly suggest that there exists a dynamical mechanism that favors the formation of clumps and tends to maintain them through time. Since clumping is a very widespread phenomenon, the mechanism must be rather fundamental, in the sense that no special circumstances are required to trigger it.

III. A SURVEY OF HYPOTHESES

Perhaps the simplest possibility is that clumps are directly forced by hot spots, orography, or other surface features. Malkus (1957) reported that trade cumulus cloud groups were associated with mesoscale sea-surface temperature anomalies. But although surface features can undoubtedly force the formation of local cloud groups, this idea cannot account for the observed persistence of clumps as they drift with the wind over synoptic distances.

A second possibility is that latent heat release in clumps forces a mesoscale circulation, which, in turn, tends to support the clump. Although we do not discount this CISK hypothesis, we shall not discuss it further in this paper; other possibilities exist.

One of these, discussed by López (1978), is that clumping occurs because gust fronts from existing clouds trigger the formation of new

clouds nearby. Another hypothesis, which also involves direct mechanical interactions between the clouds, is that cloud-induced circulations, like vortex rings, tend to organize themselves into groups by mutual advection. Hill (1974) noticed such a tendency in his numerical results. But it is not clear how either of these two ideas can explain López's observation that clouds in clumps are the largest, longest-lasting, and most heavily precipitating members of the population.

Finally, there is the possibility that clumps occur because, by the shedding of evaporatively cooled, moist wakes, cumulus clouds can tend to create, in their near environments, relatively favorable conditions for the development of succeeding clouds. This is actually an old idea, first advanced by Scorer and Ludlam (1953), and resurrected by López (1978). Although modern studies (e.g., Arakawa and Schubert, 1974) have emphasized that cumulus clouds are self-stabilizing, in the sense that they tend to relieve the conditional instability of their environment, the *distribution* of the rate of stabilization over the volume around the cloud has not been discussed in the literature. As is well known, clouds tend to modify their environments by the two very different mechanisms of induced subsidence and detrainment. The former tends strongly to stabilize by warming and drying, but the latter can actually tend to destabilize by moistening and by cooling at the upper levels. A third factor that may matter is radiative cooling, which can be strong near the cloud-top level and so tends to destabilize cloudy regions more rapidly than clear regions. These considerations suggest that, close to a cloud, detrainment and radiative cooling may combine to effectively weaken or even overpower the stabilizing effects of induced subsidence (see, e.g., Gray, 1973; López, 1973). At intermediate distances from the cloud, detrainment and radiative cooling do not operate, so that the stabilizing effects of induced subsidence are unopposed. Of course, at great distances, the influence of the cloud is hardly felt at all. The net effect, then, is that the rate of stabilization is strongest at an intermediate distance from the cloud, so that new clouds that happen to arise nearby will develop more vigorously than others that arise at intermediate distance. Through a stochastic process, local clumps of clouds will arise spontaneously, even though the spatial distribution of the triggering of cloud "seeds" may be quite random.

In the next section, we describe a simple model designed to test this idea that clouds band together for mutual protection from the environment.

IV. MODEL FORMULATION

Consider a square grid of points. In practice, we use a grid 50 points on a side. Each point represents a vertical column that may or may not contain a cloud. We define over the grid a prognostic variable J, which represents the degree of conditional instability; clouds are permitted if J is positive. The prognostic equation for J is

$$\dot{J}_{ij} = \alpha_{ij} - \sum_{i',j'} \beta\, C_{ij,i'j'} I_{i'j'} \,, \qquad (1)$$

where subscripts i and j denote a particular point, α_{ij} is a prescribed forcing, as explained further below, and the summation represents the tendency of nearby clouds to reduce J_{ij}, i.e., to "stabilize." The rate of stabilization, at a given point, is determined by the prescribed coefficient β, the stabilization profile $C_{i'j',ij'}$, which satisfies

$$\sum_{i'j'} C_{i'j',ij} = 1 \quad , \tag{2}$$

and $I_{i'j'}$, which is a measure of the intensity of convection at point $i'j'$. The value of I_{ij} is determined from

$$I_{ij} = \begin{cases} 0, \text{ if } J_{ij} \leq 0 \text{ or } r_{ij} > \tau \\ \gamma J_{ij}, \text{ otherwise.} \end{cases} \tag{3}$$

Here r_{ij} is a random number between zero and 1, and τ is prescribed.

The model works as follows: The distribution of J_{ij} is initialized to zero at all points. The forcing α_{ij} is given a uniform and time-independent value, so that J_{ij} tends to increase with time. On each iteration, at each point, I_{ij} will be positive only if the random number generator selects the point to receive a "subcloud layer perturbation suitable for triggering a cloud," *and* if J_{ij} is positive, i.e., if the column is conditionally unstable. Once the distribution of I_{ij} has been determined, the new distribution of J_{ij} is predicted using Eq. (1). The rate at which point ij is stabilized by cloud activity at point $i'j'$, for a given value of $I_{i'j'}$, is controlled by the stabilization profile $C_{ij,i'j'}$. We have performed experiments using the stabilization profiles shown in Figure 1. In each case, point ij is influenced only by those neighbor points that lie within a circle of radius of 10 points. In order to evaluate the summation in Eq. (1) for points near the grid boundary, we use cyclic boundary conditions in the i and j directions.

If we ignore the stochastic forcing of the model, then Eqs. (1) and (3) have the steady, homogeneous solution

$$J = \frac{\alpha}{\beta\gamma} \quad , \quad I = \frac{\alpha}{\beta} \, . \tag{4}$$

This shows that increasing the forcing increases both the degree of conditional instability and the level of cloud activity but that the ratio of α to β is more important than either separately.

V. RESULTS

Figures 2 and 3 show the predicted distribution of J after 125 iterations, for the "peak" and "dip" stabilization profiles, respectively. As shown

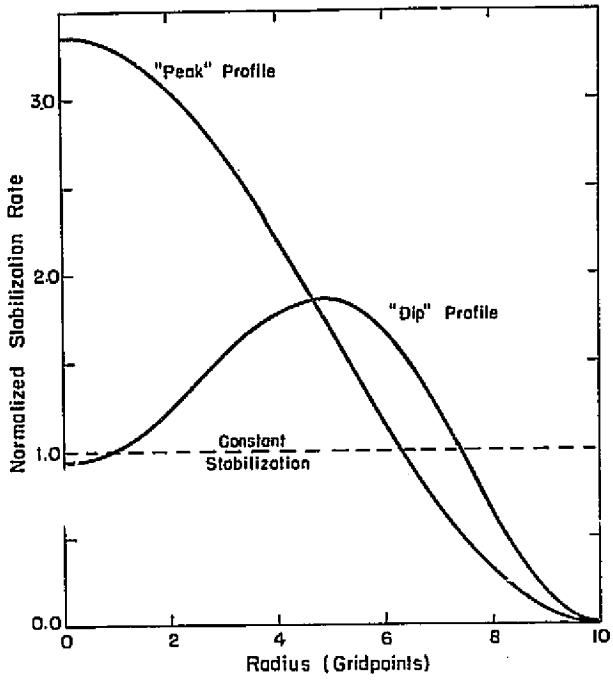

FIGURE 1 Stabilization profiles plotted against radius in points.

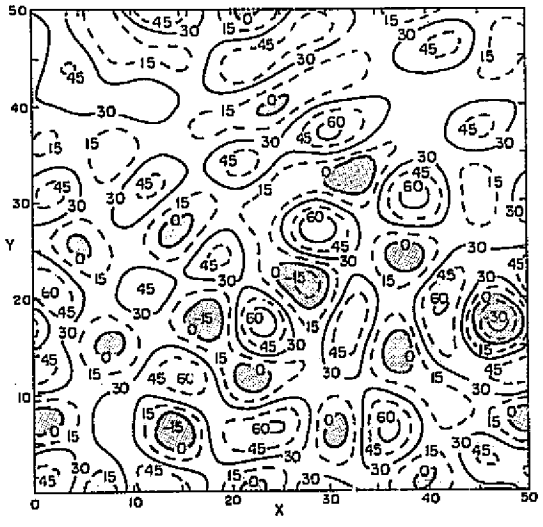

FIGURE 2 Map of J after 150 iterations, for the "peak" stabilization profile. (The domain is actually square, not rectangular.) The contour interval is 15.

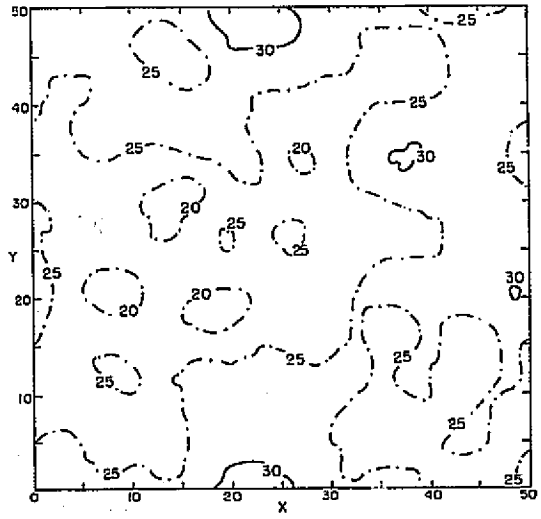

FIGURE 3 Same as Figure 2, but for the "dip" stabilization profile.

in Figure 1, the "peak" stabilization profile decreases monotonically with radius, while the "dip" profile has a local minimum on the cloud, which is interpreted as a consequence of cooling and moistening due to detrainment. All other parameters are identical in the two runs. There are three main differences in the results. First, for the dip there is more power at small scales. This simply reflects the introduction of a radius of maximum stabilization. The second, more spectacular difference is that the range of values of J for the dip greatly exceeds that for the peak. Of course, the range of values of I (not shown) is similarly increased. The third difference, which cannot be shown without including more figures than space permits, is that the sharp maxima and minima of Figure 3 (dip) maintain their identities over many time steps, while the weaker features of Figure 2 (peak) show no tendency to persist and so appear to be mere statistical fluctuations.

Regardless of the choice of stabilization profile, the time- and domain-averaged values of J and I agree well with the values predicted by Eq. (4). Also, it is of some interest that as the "seeding rate" is decreased [by decreasing τ; see Eq. (3)] the average of I over those points, where $I \neq 0$ increases, i.e., the clouds become more vigorous. But because the number of active points is smaller, the area-averaged value of I is not changed. This suggests that the rate at which subcloud layer perturbations trigger new clouds influences the intensity of individual clouds more than it influences the overall level of convective activity.

VI. DISCUSSION AND CONCLUSIONS

Although the model studied here is obviously too schematic to provide conclusive proof that the mutual protection mechanism accounts for clumping, our results are highly suggestive, and certainly warrant further research. Perhaps the first step should be the use of a time-dependent, axisymmetric cloud model, of good radial resolution, to study the shape of the stabilization profile of an isolated cloud. Next, we must clarify the way in which the stabilization profiles of neighboring clouds interact with each other; the superposition principle adopted here is probably an oversimplification. It would be of some interest to study the stabilization surface set up in the presence of shear.

Extension of the model should begin with the introduction of the third dimension and the use of predicted temperature and moisture fields with a more explicit cloud model. The present model includes no "smoothing" processes, such as gravity wave dispersion, to oppose the formation of unreasonably sharp features; this deficiency must be corrected. It will be a challenge to generalize the model in these ways without making it prohibitively complicated and expensive.

Some of the other hypotheses listed in Section III deserve theoretical attention as well.

Observational studies of clumping should focus on the distributions of heating and moistening around both individual clouds and clumps. Grube (1979) has recently reported interesting results along these lines.

Finally, the analogies between cloud populations and biological populations, some of which are suggested by this study, should be exploited,

not ignored. For example, Hubbell (1979) has discussed clumping in tropical tree populations, and the statistical methods employed in his and similar studies could well prove useful in the study of cumulus clumping.

ACKNOWLEDGMENTS

This research has been supported by NSF grant no. 77-12534. The comments of Fred Sanders and the other members of the MIT Convection Club were very helpful.

REFERENCES

Arakawa, A., and W. H. Schubert (1974). The interaction of a cumulus cloud ensemble with the large-scale environment, Part I. *J. Atmos. Sci. 31*, 674-701.

Browning, K. A., and T. W. Harrold (1969). Air motion and precipitation growth in a wave depression. *Quart. J. R. Meteorol. Soc. 95*, 288-309.

Cho, H-R. (1978). Some statistical properties of a homogeneous and stationary shallow cumulus cloud field. *J. Atmos. Sci. 35*, 125-138.

Gray, W. M. (1973). Cumulus convection and larger scale circulations: I. Broadscale and mesoscale considerations. *Mon. Wea. Rev. 101*, 839-855.

Grube, P. G. (1979). Convection induced temperature change in GATE. Dept. of Atmos. Sci. Paper No. 305, Colorado State U., Ft. Collins, Colo., 128 pp.

Harrold, T. W., and K. A. Browning (1971). Identification of preferred areas of shower development by means of high power radar. *Quart. J. R. Meteorol. Soc. 97*, 330-339.

Hill, F. F., and K. A. Browning (1979). Persistence and orographic modulation of mesoscale precipitation areas in a potentially unstable warm sector. *Quart. J. R. Meteorol. Soc. 105*, 57-70.

Hill, G. E. (1974). Factors revealing the size and spacing of cumulus clouds as revealed by numerical experiments. *J. Atmos. Sci. 31*, 646-673.

Hubbell, S. P. (1979). Tree dispersion, abundance, and diversity in a tropical dry forest. *Science 203*, 1299-1309.

Kreitzburg, C. W., and H. A. Brown (1970). Mesoscale weather systems within an occlusion. *J. Appl. Meteorol. 9*, 417-432.

López, R. E. (1973). Cumulus convection and larger scale circulations: II. Cumulus and mesoscale interactions. *Mon. Wea. Rev. 101*, 856-870.

López, R. E. (1978). Internal structure and development processes of C-scale aggregates of cumulus clouds. *Mon. Wea. Rev. 106*, 1488-1494.

Malkus, J. S. (1957). Trade cumulus cloud groups: Some observations suggesting a mechanism of their origin. *Tellus 9*, 33-44.

Plank, V. G. (1965). The cumulus and meteorological events of the Florida peninsula during a particular summertime period. Environmental Res. Paper No. 151, Air Force Cambridge Res. Labs., 146 pp.

Plank, V. G. (1969). The size distribution of cumulus populations. *J. Appl. Meteorol. 8*, 46-67.

Scorer, R. S., and F. H. Ludlam (1953). Bubble theory of penetrative convection. *Quart. J. R. Meteorol. Soc. 79*, 94-103.

DISCUSSION
L. Shapiro, *Rapporteur*

It was emphasized that the model is at this stage purely thermodynamic. Questions were raised as to the importance of dynamic forcing by one cloud favoring the development of neighboring clouds. Although this effect may be important, it was not included in the simple model presented. The dynamics of the interaction between clouds is only included implicitly: the subsidence that stabilizes the environment is associated with the dispersion of gravity waves that are "frozen" in time. In the future the model may be generalized to include heat and moisture budgets, as well as explicit gravity-wave dispersion. The model does not have any vertical structure. The inclusion of vertical shear could organize the convection into lines. In response to a question, Randall showed a figure of the distribution of convective intensity diagnosed from a model integration. The distribution is neither demonstrably normal nor log normal.

HORIZONTAL TRANSPORT OF VORTICITY BY CUMULUS CONVECTION

Han-Ru Cho
University of Toronto

INTRODUCTION

In theories of cumulus parameterization, horizontal transports of air properties by cumulus convection are usually neglected. A straightforward order-of-magnitude estimate of the horizontal eddy fluxes due to cumulus clouds will show that the assumption should usually be correct:

$$\overline{\vec{v}'\alpha'} \sim \Sigma(\vec{v}_c - \bar{\vec{v}})(\alpha_c - \bar{\alpha}) \ . \qquad (1)$$

Here, α is a meteorological variable, $\vec{v}$ is the horizontal wind vector. Subscript c is used to denote properties of clouds. Σ is the fractional cloud coverage. Usually $\vec{v}_c$ and $\vec{v}$ are comparable in magnitude. Since Σ is only of the order of 10^{-2}-10^{-1}, horizontal eddy flux $\overline{\vec{v}'\alpha'}$ should be much smaller in magnitude than the horizontal flux due to the mean flow, $\bar{\vec{v}}\ \bar{\alpha}$, provided that a_c and $\bar{\alpha}$ are comparable in magnitude. If one lets α be temperature (T) or water-vapor mixing ratio (q), he concludes readily that $\overline{\vec{v}'T'}$ and $\overline{\vec{v}'q'}$ are negligibly small.

In this paper, we shall examine the possibility of significant horizontal transport of vorticity by cumulus convection. The ability of clouds to transport vertical component of absolute vorticity, as I shall attempt to demonstrate, depends critically on the structure of cloud-scale vorticity fields.

CLOUD-SCALE VORTICITY FIELD

Results from recent Doppler radar observations (Ray 1976; Kropfli and Miller, 1976) indicate that the magnitude of the vorticity field in a cumulus cloud or a mesoscale cloud system could be one to two orders larger than that of the large-scale mean flow in which they are embedded. A typical cloud vorticity field obtained in these studies shows the presence of a cyclonic-anticyclonic vortex couplet, with magnitude of vorticities as large as $\pm 10^{-2}$ sec^{-1}.

Similar results have also been obtained in three-dimensional numerical modeling of cumulus convection (Schlesinger 1978; Klemp and Wilhelmson, 1978a, 1978b). Typically, a vortex couplet develops within a cumulus

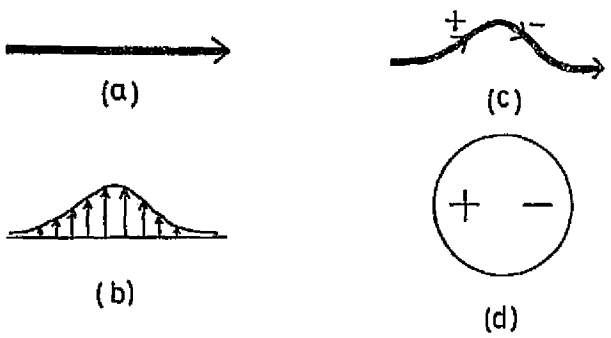

FIGURE 1 Generation of cyclonic-anticyclonic vortex couplet.

cloud embedded in an environment with vertical wind shear. Looking downward, pronounced cyclonic and anticyclonic vorticities appear in the respective left and right flanks, with maximum magnitude of $\sim 10^{-2}$ sec^{-1}. The vortex couplet appears to be able to develop independent of either the earth rotation or the presence of large-scale vorticity at the time of storm initiation.

A simple scale analysis of the vorticity equation will be able to show that the initiation of the strong vortex couplet is caused by the tilting of horizontal vortex tubes into the vertical direction. This generation process is illustrated schematically in Figure 1. In the presence of vertical wind shear, the vortex tubes of the mean airflow lie approximately on a horizontal plane. The horizontal components of vorticity due to vertical wind shear are usually two orders of magnitude larger than its vertical component. This is shown in Figure 1(a). When a vertical velocity field as shown in Figure 1(b) is induced by a cumulus cloud, the essentially horizontal vortex tube is distorted because of the combined actions of vertical advection and tilting processes. A vortex couplet is thus generated, as shown in Figure 1(c). The distribution of vorticity on a horizontal plane is illustrated schematically in Figure 1(d). Pronounced cyclonic and anticyclonic regions appear on the respective left and right flanks of the vertical wind shear vector.

If the vertical velocities in the cloud environment are very weak, the vertical displacement and tilting of vorticity in the cyclonic region should be approximately equal in magnitude to the vertical displacement and tilting in the anticyclonic region. The vertical advection and tilting effects, when averaged over the entire cloud area, should approximately balance each other. The area averaged cloud vorticity $\overline{\eta}_c$, satisfies a simple equation.

$$\frac{\partial \overline{\eta}_c}{\partial t} + \frac{1}{a} \oint \eta_c \vec{v}_c \cdot \hat{n} \, dl = 0 \, . \qquad (2)$$

Here, the line integral is performed around the boundary of the cloud region. $\hat{n}$ is the unit vector normal to the cloud boundary and a is the cloud cross-sectional area. The proof of Eq. (2) has been given by Cho *et al.* (1979).

HORIZONTAL EDDY FLUX OF VORTICITY

Since the local values of vorticity inside a cumulus cloud may be $10\text{-}10^2$ times that of the mean flow, the importance of eddy flux of vorticity by cumulus clouds cannot be ruled out by a simple order-of-magnitude estimate according to Eq. (1). On the other hand, the magnitude estimate alone is not sufficient to establish the ability of clouds to transport vorticity in a horizontal direction either. Some insights are needed to understand the basic dynamic processes by which clouds may transport vorticity in a horizontal direction.

To begin with, we have the following theorem:

Theorem: If $\vec{v}'$ and η' are the perturbations in the horizontal wind vectors and the vertical component of absolute vorticity, and $\vec{v}' = \vec{v}'_\delta + \vec{v}'_\chi$, where $\vec{v}'_\delta$ and $\vec{v}'_\chi$ are the irrotational and solenoidal components of $\vec{v}'$, then

$$\overline{\vec{v}'_\chi \eta'} \equiv 0 \ , \tag{3}$$

or in other words

$$\overline{\vec{v}'\eta'} = \overline{\vec{v}'_\delta \eta'} \ . \tag{4}$$

The theorem will not be proved here for lack of space. It states that the horizontal eddy flux of vorticity is associated entirely with the irrotational component of the wind. To illustrate how winds associated with the divergence fields of clouds may transport vorticity, let us consider in Figure 2(a), a typical cloud vorticity field. The vorticity field is characterized by regions of strong cyclonic and anticyclonic vorticities. For the purpose of this discussion, let us assume that the vertical wind-shear vector is directed toward the east. Since the vortex couplet is initiated by the tilting of vortex tubes, it should be oriented in the north-south direction. Superimposed on the vorticity field is a wind field associated with a symmetric cloud convergence field. With the configuration shown, the wind field transports negative vorticity southward in the anticyclonic region and transports positive vorticity northward in the cyclonic region. The net result is a northward eddy transport

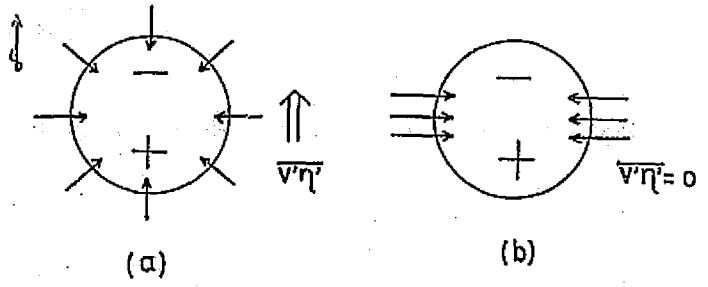

FIGURE 2 Horizontal eddy transport of vorticity.

of vorticity. Because of the orientation of the vortex couplet, this vorticity flux should be roughly perpendicular to the vector of vertical wind shear.

Of course, it is possible to construct a convergence field that produces no net eddy vorticity flux. One example is shown in Figure 2(b). This, however, appears to be only a very special case. There is no reason for us to believe that the cloud convergence field is always such that the irrotational wind vectors are perpendicular to the axis of the vortex couplet.

THE APPARENT VORTICITY SOURCE

To parameterize fully the cumulus effects on the large-scale vorticity field, all the eddy terms on the mean vorticity equation must be expressed in terms of cloud ensemble properties. The net effect of cumulus clouds is usually referred to as the apparent vorticity source and is defined as

$$Z = \frac{\partial \bar{\eta}}{\partial t} + \bar{\vec{v}} \cdot \vec{\nabla}\bar{\eta} + \bar{\omega}\,\frac{\partial \eta}{\partial p} + \bar{\eta}\vec{\nabla} \cdot \bar{v} + \hat{k} \cdot \vec{\nabla}\omega \times \frac{\partial \vec{v}}{\partial p}$$

$$= - \vec{\nabla} \cdot \overline{\vec{v}'\eta'} - \overline{\omega' \frac{\partial \eta'}{\partial p}} - \hat{k} \cdot \overline{\vec{\nabla}\omega' \times \frac{\partial \vec{v}'}{\partial p}} \quad . \tag{5}$$

Cho *et al.* (1979) have shown that the eddy advection and eddy tilting processes can be parameterized in terms of the total cloud mass flux M_c:

$$- \overline{\omega' \frac{\partial \eta'}{\partial p}} - \hat{k} \cdot \overline{\vec{\nabla}\omega' \times \frac{\partial \vec{v}'}{\partial p}} = - M_c \frac{\partial \bar{\eta}}{\partial p} - \hat{k} \cdot \vec{\nabla} M_c \times \frac{\partial \bar{\vec{v}}}{\partial p} \quad . \tag{6}$$

It can be shown by straightforward calculations that

$$\vec{\nabla} \cdot \overline{\vec{v}'\eta'} = \frac{\partial M_c}{\partial p} (\bar{\eta}_{cB} - \bar{\eta}) \quad , \tag{7}$$

where $\bar{\eta}_{cB}$ is the mean cloud boundary vorticity defined by

$$\frac{\partial M_c}{\partial p} \bar{\eta}_{cB} = \frac{1}{A} \sum_i \oint \vec{v}_c \eta_c \cdot \hat{n} \, dl \quad . \tag{8}$$

The apparent vorticity source can be then expressed as

$$Z = -\frac{\partial M_c}{\partial p} (\bar{\eta}_{cB} - \bar{\eta}) - M_c \frac{\partial \bar{\eta}}{\partial p} - \hat{k} \cdot \vec{\nabla} M_c \times \frac{\partial \bar{\vec{v}}}{\partial p} \tag{9}$$

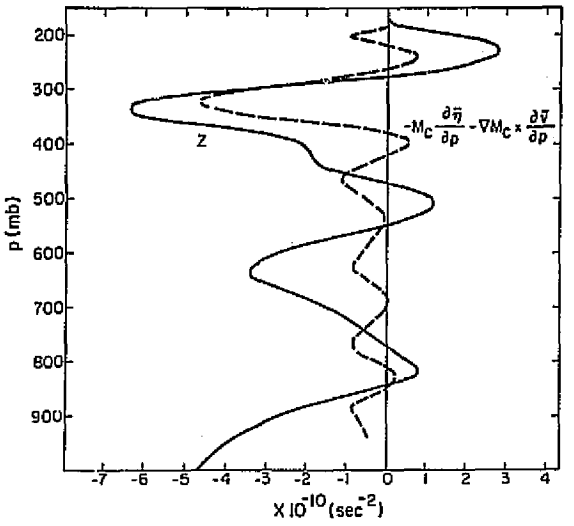

(a)

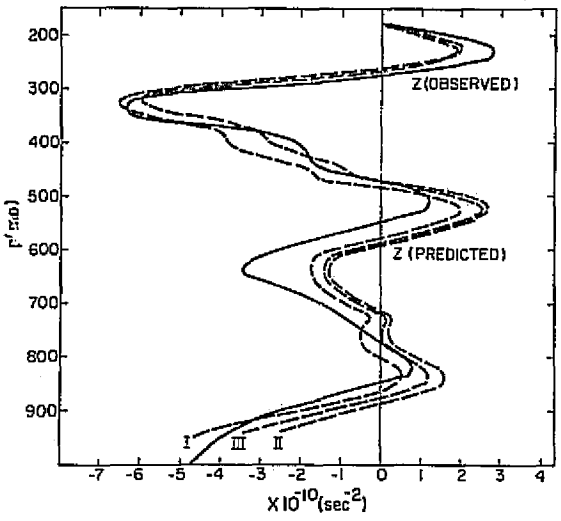

(b)

FIGURE 3 Observed and predicted A/B-scale vorticity sources for a one-day period (00-24 GMT, September 2) during Phase III of GATE. (a) Z predicted by neglecting horizontal eddy transport of vorticity. (b) Z predicted including horizontal eddy transport of vorticity.

or

$$Z = \int \frac{\sigma}{\tau p'} dp' \ (\bar{\eta}_c - \bar{\eta}) + \frac{\partial M_c}{\partial p} \bar{\eta} - M_c \frac{\partial \bar{\eta}}{\partial p} - \hat{k} \cdot \vec{\nabla} M_c \times \frac{\partial \vec{v}}{\partial p} . \qquad (10)$$

The second form is obtained by combining Eq. (9) with Eq. (2). The first term on the right-hand side of Eq. (10) represents the cloud life-cycle effect discussed in Cho (1977).

The simple parameterization theory given by Eq. (9) or (10) has been verified (in the sense discussed in the paper by Shapiro) by comparing the (so-called predicted) Z profile calculated using Eq. (12) with the

(so-called observed) Z profile determined from large-scale mean wind and vorticity data. The M_c and $\bar{\eta}_c$ profiles used in computing Z through Eq. (10) are derived from the large-scale heat, moisture, and potential vorticity budgets.

The observed mean A/B-scale vorticity source Z for a one-day period (00-24 GMT, September 2, 1974) during Phase III of GATE is shown in Figure 3(a) as the solid line. The dashed line shows the cloud effects due to vertical eddy advection and eddy tilting processes only. A comparison between the two profiles shows that the apparent vorticity source predicted by neglecting the horizontal eddy vorticity flux does not adequately explain the observed apparent vorticity source.

The apparent vorticity source predicted by including the effects of horizontal eddy transport of vorticity is shown in Figure 3(b). The three dashed lines correspond to three different boundary conditions used in determining the mean cloud vorticity profile $\bar{\eta}_c$. The differences between the three profiles are rather small. For all practical purposes they can be considered identical. The observed and predicted Z profiles have now very good agreement. It appears to suggest that one cannot neglect the horizontal eddy flux of vorticity in parameterizing cloud effects on the large-scale vorticity field.

REFERENCES

Cho, H. R. (1977). Contribution of cumulus cloud life-cycle effects to the large-scale heat and moisture budget equations. *J. Atmos. Sci. 34*, 87-97.

Cho, H. R., L. Cheng, and R. M. Bloxam (1979). The representation of cumulus cloud effects in the large-scale vorticity equation. *J. Atmos. Sci. 36*, 127-139.

Klemp, J. B., and R. B. Wilhelmson (1978a). The simulation of three-dimensional convective storm dynamics. *J. Atmos. Sci. 35*, 1070-1096.

Klemp, J. B., and R. B. Wilhelmson (1978b). Simulations of right- and left-moving storms produced through storm splitting. *J. Atmos. Sci. 35*, 1097-1110.

Kropfli, R. A., and L. J. Miller (1976). Kinematic structure and flux quantities in a convective storm from dual-Doppler radar observations. *J. Atmos. Sci. 33*, 520-529.

Ray, P. S. (1976). Vorticity and divergence fields within tornadic storms from dual-Doppler observations. *J. Appl. Meteorol. 15*, 879-890.

Schlesinger, R. E. (1978). A three-dimensional numerical model of an isolated thunderstorm: Part I. Comparative experiments for variable ambient wind shear. *J. Atmos. Sci. 35*, 690-713.

DISCUSSION

L. Shapiro, *Rapporteur*

Following Cho's talk, Yanai presented results from the Marshall Islands based on averages of individual budgets derived from 100 days of four

times daily observations. He emphasized that the results could be different from the budget derived from a composite wave because of the deviations of individual cases from the composite, which modify the nonlinear terms. He found that all terms in the large-scale vorticity budgets are significant, including horizontal advection and twisting terms. The vertical profile of the apparent vorticity source showed more complexity than the simple lower-level sink and upper-level source found by Reed and Johnson and others for the same region. Yanai maintained, additionally, that since values of vorticity inside the clouds can be more than an order of magnitude larger than environmental values, the assumptions implicit in Shapiro's and Cho's formulations may not be justified. In reply, Cho reiterated his result from scaling analysis that although point values inside the cloud may be much larger than environmental values, the average over the cloud is of the same order as environmental values. Yanai also gave the opinion that the agreement between the observed and parameterized sources is no proof of the validity of the parameterization and that the approximate balance between the large-scale vertical velocity and the cloud mass flux predetermines agreement. Cho agreed that the agreement is not a proof of the validity of the parameterization but only a consistency check. The omission of the horizontal eddy transport of vorticity, however, leads to an inconsistency between the observed and parameterized sources, which must be accounted for.

Shapiro emphasized the equivalence between his and Cho's parameterization, with the detrainment of cloud vorticity in the steady-state cloud model corresponding to the recycling term in the model that includes life-cycle effects. Although the formulations are different, their net effect on the large scale is the same.

The question was raised as to the applicability of the model to squall systems, and Cho stated that the results were independent of the structure on that scale.

SOME COMMENTS ON CUMULUS PARAMETERIZATION AND ITS PURPOSE

Katsuyuki V. Ooyama
National Center for Atmospheric Research

The parameterization of moist convection in the tropics has been a subject of interest for nearly two decades. In the hurricane models, in which the present subject has a historical origin, the parameterization of whole clouds has already become a burdensome relic of the past, as discussed in the paper by Rosenthal. In the light of the recent work by Rosenthal (1978) and Yamasaki (1977), one may wonder if all the exercises with parameterized convection were an unfortunate detour in the history of hurricane modeling. In technical terms of the modeling, probably they were. However, the real value of my original contribution (Ooyama, 1963; 1969) was in the conceptual change in our perception of the hurricane as a cooperative dynamical process between the cumulus convection and the cyclone-scale vortex. The simple parameterization of convection based on the energy budget and the frictional convergence in the boundary layer was a distillation of observationally known facts of the hurricanes.

Philosophically, it was not the parameterization that changed the course of hurricane modeling efforts, but it was the change in our perception of the problem and the rearrangement of priorities that made the parameterization a tolerable substitute for real clouds for the purpose of understanding the basic mechanisms of hurricane intensification and maintenance. Once this was done and the goal of models shifted toward the quantitative accuracy, the parameterization of whole clouds became an albatross around the modeler's neck and was to be cast off sooner or later. I foresaw this coming and discussed it with Rosenthal in 1974, although the realization of my prophecy is, of course, entirely his work. Nevertheless, the conceptual understanding of the hurricane as an intense storm as we derived from parameterized models is still valid, independent of the question how, or whether, to parameterize cumulus convection in the models.

The understanding of the tropical cyclogenesis is still an open question. Synoptic circumstances favoring the tropical cyclogenesis has become better known through a large number of diagnostic studies (e.g., Gray, 1968) and more recently by a unique contribution by Shapiro (1977), but a further understanding of organized convection in the tropics is also needed in order to formulate a dynamically coherent and model-testable idea. Although the motivation of my theory on cumulus parameterization (Ooyama, 1971) was primarily on the question of tropical cyclogenesis, I think that it was rather a naive hope in the light of what I have learned since then.

Convective activities in the tropics are organized in subsynoptic and mesoscale systems. For such a system of deep convective clouds to remain active for more than a few hours, the unstable moist air must be supplied advectively to the system. The eyewall convection of a hurricane is a very special case of mesoscale systems in which the supply is secured by frictionally induced convergence over the supporting area of several hundred kilometers across. In more general states of the tropics, the large-scale frictional convergence is not a dominant factor in maintaining mesoscale systems. In the case of squall lines, the advective supply is relative to the system's motion against the boundary-layer air, and mesoscale circulations, especially the vertical circulation, are essential parts of the self-supporting mechanism. The parameterization scheme on the basis of postulated cloud elements becomes a difficult proposition because what we assume and what we deduce from it begin to impinge on each other. Besides, there are more parameters to consider than the currently prevailing basis of parameterization, the one-parametric cloud ensemble, could possible handle. It is to say that the purpose of parameterizing whole clouds is obscure in the study of mesoscale convective systems.

I am not certain that the mesoscale systems themselves could be parameterized on a different basis. However, a conceptual understanding of the essential parameters that control the organization and aggregate behavior of these convective systems is desirable even if a numerical model explicitly calculates convective elements. To obtain such is, of course, part of the purpose of model experiments, but diagnostic studies of real data should also help. (In this regard, the quality of wind observations by the GATE B- and C-scale ships was regrettable.)

The purpose of cumulus parameterization in large-scale numerical models is different, unless such a model aims at explicit replication of subsynoptic details and occasional tropical cyclones as part of its synoptic-scale simulation. The activity of individual convective systems in an area several hundred kilometers across, or greater, is not directly coupled with the low-level convergence of that scale. The energetic needs of supporting aggregate convective activity is met "locally," and the total energy balance over the area becomes an important controlling factor. The fact that mesoscale dynamics of convective systems has a great influence on the air-sea exchange of heat and moisture does not change by shifting our attention to the synoptic scale. However, the mesoscale details of this account merge with the question of parameterizing the boundary-layer processes in terms of synoptic-scale variables. Thus, I presume, Arakawa's particular emphasis on the boundary layer in cumulus parameterization.

Above the boundary layer, the role of parameterized convection is the vertical redistribution of mass, energy, and momentum toward restoration of certain equilibrium states, in which the primary factor is (moist) static stability. If the convection associated with synoptic-scale tropical waves were responsible for the generation of the waves by instability as some misguided CISK theories asserted, the basic assumption about restoring an equilibrium state would have to be re-examined. I do not believe that this is the case. (On the other hand, there is no

guarantee that a synoptic-scale model would be free of unstable small-scale growths.)

There are differences among specific methods of synoptic-scale cumulus parameterization, such as the convective adjustment (GFDL), the diffusive adjustment (British Meteorological Office), and the convective equilibrium closure (Arkawa and Schubert, 1974), with respect to the postulated equilibrium states and the internal relationships among convectively redistributed, different variables, since the redistribution of moisture or momentum under one primary constraint on static stability requires additional assumptions.

In this regard, the results of momentum (or vorticity) budget analysis of the GATE A/B-scale upper-air data by Shapiro (1978), Cho *et al.* (1979), and Stevens (1979), and a theoretical paper by Schneider and Lindzen (1977), are interesting to compare. The common finding, in my interpretation, is that a dominant contribution to the apparent source of momentum (or vorticity) comes from the virtual source (defined in Ooyama, 1971), which arises from writing the large-scale equations in terms of the total vertical motion rather than in terms of the vertical motion in the environment. In other words, the vertical transport by the cloud mass flux itself is secondary, or obscured by the uncertainty in data. It will be interesting to see if my analysis of the GATE wind data could provide a more definite answer.

REFERENCES

Arakawa, A., and W. H. Schubert (1974). Interaction of cumulus cloud ensemble with the large-scale environment, Part I. *J. Atmos. Sci. 31*, 674-701.

Cho, H.-R., L. Chen, and R. M. Bloxam (1979). The representation of cumulus cloud effects in large-scale vorticity equation. *J. Atmos. Sci. 36*, 127-139.

Gray, W. M. (1968). Global view of the origin of tropical disturbances and storms. *Mon. Wea. Rev 95*, 669-700.

Ooyama, K. (1963). A dynamical model for the study of tropical cyclone development. (Unpublished report, Dept. of Meteorol. and Oceanog., New York University.)

Ooyama, K. (1971). A theory on parameterization of cumulus convection. *J. Meteorol. Soc. Jpn. 49*, 744-756.

Ooyama, K. (1969). Numerical simulation of the life cycle of tropical cyclones. *J. Atmos. Sci. 26*, 3-40.

Rosenthal, S. L. (1978). Numerical simulation of tropical cyclone development with latent heat release by the resolvable scales I: Model description and preliminary results. *J. Atmos. Sci. 35*, 258-271.

Schneider, E. K., and R. S. Lindzen (1977). Axially symmetric steady-state models of the basic state for instability and climatic studies. Part I: Linearized calculations. *J. Atmos. Sci. 34*, 263-279.

Shapiro, L. J. (1977). Tropical storm formation from easterly waves: a criterion for development. *J. Atmos. Sci. 34*, 1007-1021.

Shapiro, L. J. (1978). The vorticity budget of a composite African tropical wave disturbance. *Mon. Wea. Rev. 106*, 806-817.

Stevens, D. (1979). Vorticity, momentum and divergence budgets of synoptic-scale wave disturbances in the tropical eastern Atlantic. *Mon. Wea. Rev. 107*, 535-550.

Yamasaki, M. (1977). A preliminary experiment of the tropical cyclone without parameterizing the effects of cumulus convection. *J. Meteorol. Soc. Jpn. 55*, 11-30.

DISCUSSION

D. Rodenhuis, *Rapporteur*

Ooyama presented the following page as a summary of the development of ideas in the understanding of the theory of tropical cyclones (A) and tropical waves (B). In these tables the "O" or "X" generally represent a sense of "success" or "failure," respectively, in the application of a particular theory or model listed in the left-hand column. The meaning of other notations in the table and the cryptic remarks in the last column are intentionally left for deciphering by the reader.

In the subsequent discussion there was some rebuttal of the assertion that there was no scale selection by the CISK hypothesis. Also, "WAVE-CISK" dynamics were defended as simply a requirement to explain the small temperature fluctuations and the observed vorticity changes observed in an easterly wave. Yet, Atlantic easterly waves do not seem to be driven by a CISK mechanism or cumulus friction.

Hurricane formation should be viewed as a problem of mesoscale convection with support from a large-scale moisture source. Although the importance of *parameterized* cumulus convection has been challenged in this case, there are many occasions when the concept is of great practical importance. There was some conjecture concerning the need for convection to sustain the African wave during its passage across the Atlantic, but certainly tropical disturbances of the Western Pacific and monsoon depressions require parameterized convection. In any case, the prediction of convective precipitation of the ground is an extremely important and practical objective, even without a strong dynamic interaction with the synoptic-scale circulation.

For the future, spectral parameterization models seem to hold the most promise. Since the GATE experiment, we now have extensive observations of convection to guide model development and testing. However, it is *also* necessary to account for true nonlinearities which exist in nature--both in the convective processes (e.g., mesoscale organization) and in the large-scale flow. In a simple example, major errors have been made when attempting to represent a quadratic wind profile accurately.

Therefore, in conclusion, some discretion is required in the use and application of parametric convection models. However, it is quite clear that their use is justified and highly desirable in, for example, general circulation models.

	Convection		Cyclone		Remarks(*)
	L.I.	N.-L.	L.I.	N.-L.	
C.I. (First kind)	O	X			
Cloud model	O	O(*)			Not well developed in early 1960's.
Early P.E. model	O	X(*)			Not formulated for fully non-linear stage.
(Intent was)	→	→	→	→	
I.I. theory	*		X		Implied, though not included.
Param. Cu *					Coupling by frictional convergence
Balanced. Lin.	Implicitly included		O	X	
" N.L.	"	" (*)	O	O	stabilization in the inner core
P.E. Lin.	O	X	? (*)		Too "cloudy" to see
" N.L	O	O(*)	O	O	Barely making through in earlier attempts
P.E. with explicit Cu(*)	O	O	O	O	Cloud physics parameterized

	Convection		Wave		*Various kinds.
	L.I.	N.-L.	L.I.	N.-L.	
Param. Cu*					Cu coupling in the wave scale (linear theory) is dubious. Results of L.I. theories too arbitrary.
Balanced "CISK"	Implicit		? (*)		
P.E. CISK (mod)	O	X	? (*)		
? ⟸ The "WAVE CISK"	*				CISK without clouds ?
I.I. theory	*		O*	?	Convection N/A. Basic state ?
GCM	Adjustment / Equilib. conv. *		O	O	Not guaranteed to be trouble free
Diagnostic theories	External		?	O*	Specialized interests

THE NUMERICAL SIMULATION OF DEEP AND SHALLOW CLOUD ENSEMBLES IN THE TROPICS

Su-Tzai Soong
University of Illinois

INTRODUCTION

The major factors controlling the static stability of the tropical atmosphere are large-scale vertical motion, differential horizontal advection, radiative cooling, and evaporation from the ocean surface. When some of these large-scale forcing effects act continuously over a certain period of time, the atmosphere may be sufficiently destabilized, and convective clouds will then start developing to release the potential instability. The response of shallow and deep convective clouds to large-scale destabilizing processes has been investigated using a two-dimensional slab-symmetric cumulus cloud ensemble model. The model domain is assumed to correspond to the resolution of observational data or a grid area in a large-scale numerical weather-prediction model. In contrast to many other cloud-simulation studies, which only simulate an isolated convective cloud, this study allows several clouds of various sizes to develop simultaneously in the domain. The input to the model includes the vertical velocity and the horizontal advections of temperature and mixing ratio due to large-scale or mesoscale motion as well as radiative cooling and sea-surface temperature. Clouds are generated in the model by introducing random perturbations of small amplitude at low levels, and the intensity of cloud activity is controlled by the large-scale forcing effects. The cloud ensemble feedback effects due to the condensation and evaporation of cloud liquid drops and vertical fluxes of heat and moisture, which are needed for cumulus parameterization, are computed.

SHALLOW CLOUD SIMULATIONS

During the two-day period of June 22-23, 1969, a typical trade wind inversion dominated the BOMEX area with no major change in the large-scale circulation. Figure 1 shows the composite temperature and mixing ratio sounding during these two days. The reference points used for compositing are the heights of the transition layer and the inversion layer in each of the individual temperature profiles. The large-scale vertical velocity is negative in the entire vertical domain. The maximum downward velocity is 0.76 cm sec^{-1} located just at the top of the inversion. This value translates to a downward movement just at the inversion layer at a rate of 65 mbar day^{-1} in the absence of convective activity.

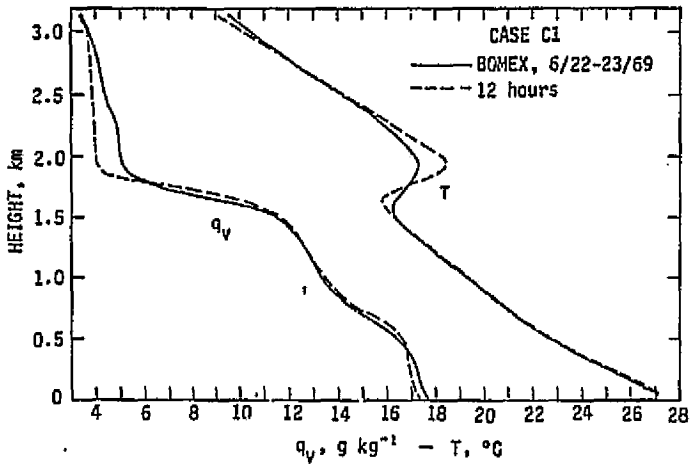

FIGURE 1 The composite sounding during June 22-23, 1969, of BOMEX and the simulated sounding in the control experiment.

Figure 2 shows the changes of $\bar{\theta}$ and $\bar{q}_v$ due to large-scale horizontal advection and vertical motion. The large warming and drying effects in the inversion layer are the dominant large-scale processes. The Q_R profile is the radiative cooling rate adopted for the shallow cloud experiments.

A 12-h simulation is made in the control experiment using the observed large-scale variables. At the end of the 12-h simulation, the horizontally averaged temperature and mixing ratio profiles remain very close to the initial temperature profile (Figure 1). The computed fluxes of

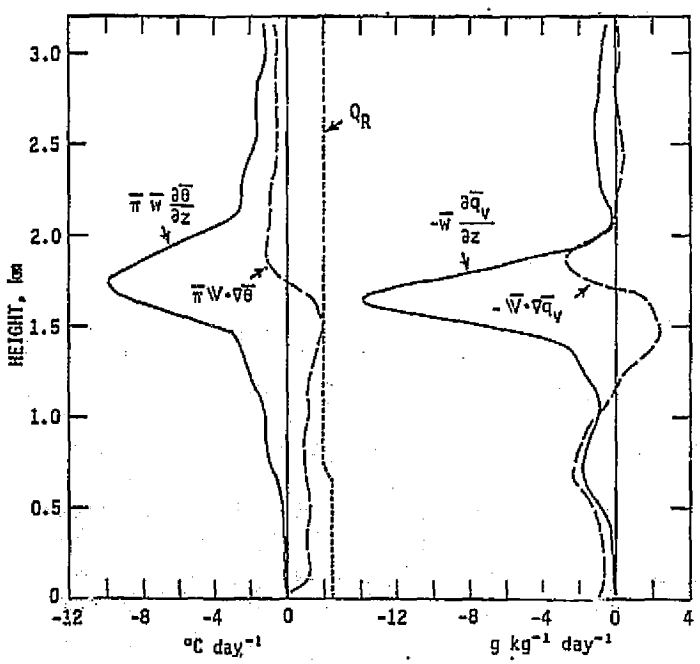

FIGURE 2 The large-scale effects on temperature and humidity during June 22-23, 1969, of BOMEX. The Q_R profile is the radiative cooling rate used in the model.

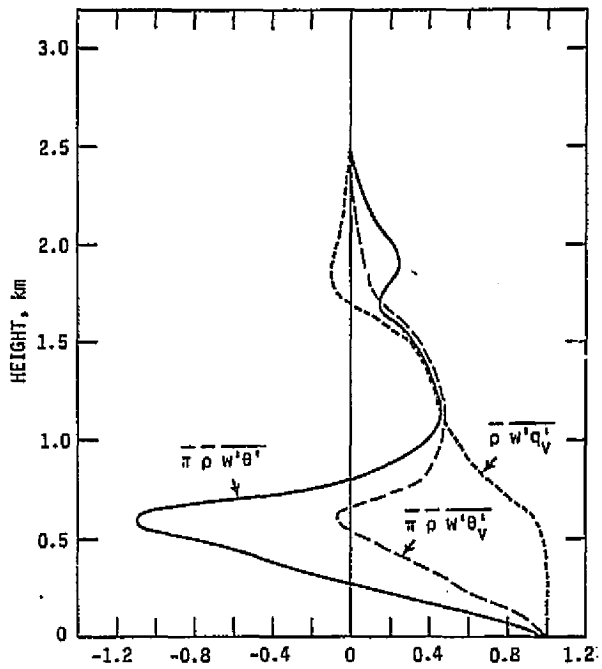

FIGURE 3 The normalized vertical fluxes of temperature, virtual temperature, and mixing ratios.

θ, θ_v, and q_v due to grid scale and subgrid scale motions are shown in Figure 3. All values are normalized to their respective surface values. The vertical flux of θ decreases very rapidly with height, reaching a minimum -1.2 times the surface heat-flux value at the cloud-base level. This large downward heat transport signifies a cold cloud base. The heat flux becomes positive again above 0.9 km, indicating that the clouds attain a warm core structure above that level due to condensation.

The vertical flux of q_v is almost constant in the subcloud layer. Above the cloud base, the q_v flux decreases rapidly with height to a slightly negative value near the top of the inversion layer. The θ_v flux, which indicates the buoyancy of clouds, decreases to a slightly negative value at the cloud base. It is positive again in the cloud layer, with rapid decrease in magnitude above the inversion base level.

The effects of condensation, evaporation of cloud droplets and rain drops, and divergence of vertical fluxes of θ and q_v due to cloud and turbulence are shown in Figure 4. The condensation produces a heating maximum close to 15°C day^{-1} just above the cloud-base level. The corresponding drying effect is about 6 g kg^{-1} day^{-1}. The condensation rate remains large in the entire cloud layer, but it decreases rapidly in the inversion layer. The vertical variation of the evaporation rate in the cloud layer is small. The maximum evaporation occurs in the lower part of the inversion layer, where there is a cooling rate of 14°C day^{-1} and a corresponding moistening rate of 5.5 g kg^{-1} day^{-1}. Slight evaporation of rainwater in the subcloud layer produces a cooling of less than 1°C day^{-1}. Most of the heat produced by excess condensation over evaporation

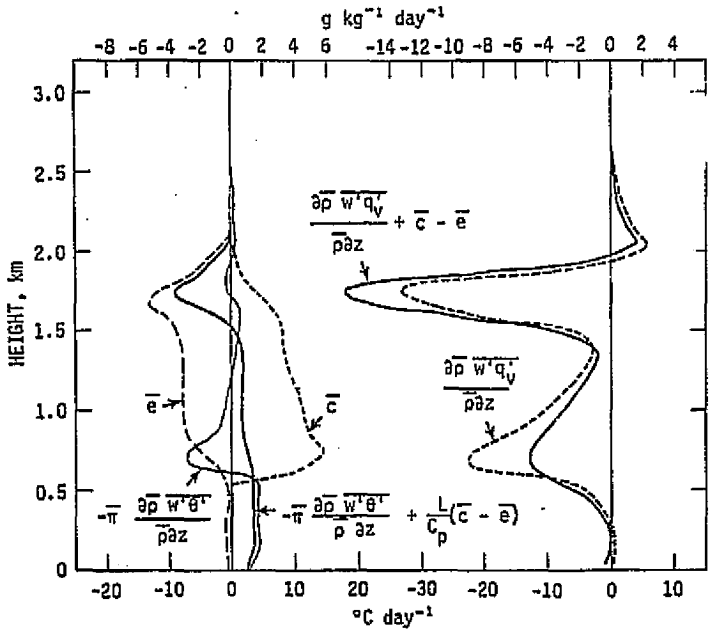

FIGURE 4 The simulated cloud ensemble effects in the control experiment.

in the lower part of the cloud layer is transported downward to the subcloud layer, resulting in a cooling just above the cloud base of 7°C day^{-1} and a warming in the subcloud layer of 4°C day^{-1}. The divergence of heat flux also warms the lower part and cools the upper part of the inversion layer slightly. The total cloud effect is, therefore, a strong cooling in the inversion layer with a maximum cooling rate of 9°C day^{-1}, a heating in the cloud layer of slightly more than 2°C day^{-1}, and a heating in the subcloud layer of 3.5°C day^{-1}.

The vertical transport of q_v brings moisture from the ocean surface to the cloud layer, producing a maximum moisture convergence just above the cloud-base level and another maximum in the inversion layer. Part of the moisture transported to the cloud layer condenses and then is transported to the inversion layer, where is evaporates. The net effect is a maximum moistening due to clouds and turbulence in the inversion layer reaching 17 g kg^{-1} day^{-1} and a lesser maximum of 5 g kg^{-1} day^{-1} above the cloud-base level.

Sensitivity tests of the model are made for different magnitudes of the large-scale vertical velocity. The most striking result is that the temperature and humidity in the cloud layer below the inversion do not change significantly in spite of a relatively large variation in height and intensity of the tradewind inversion when the vertical velocity is doubled or reduced to half. This may indicate that cumulus clouds respond quickly to the large-scale forcing and adjust their own transport properties to maintain the observed large-scale thermodynamic fields whose variation has a much longer time scale. Sensitivity tests on varying sea-surface temperature indicate that a ±1°C change in the sea-surface temperature does not change the height of the inversion significantly during a 6-h simulation period.

DEEP CLOUD SIMULATIONS

A well-defined Intertropical Convergence Zone (ITCZ) rainband formed on August 12, 1974, over the GATE A/B-scale area. The explosive development of the ITCZ rainband started at 0600 GMT from a cloud band that was first observed at 0000 GMT August 12. This rainband gradually dissipated from 1800 to 2400 GMT, August 12. This case has been analyzed by Ogura *et al.* (1979) using an objective analysis scheme to interpolate the data onto a 25 × 25 grid array. The evolution of ω near the ship *Researcher*, where the rainband intensified during the period 0000-2400 GMT August 12, shows that upward motion of -2 μbar sec^{-2} had already dominated the lower levels by 0000 GMT. This upward motion increased to -4 μbar sec^{-1} at 0600 GMT and extended to the entire atmosphere. During the period of 0600-1500 GMT, when the rainband was developing explosively, the level of the maximum upward motion shifted from the lower level (~850 mbar) to the upper level (~400 mbar). The magnitude of the upward motion also increased to -11 μbar sec^{-1}. Thereafter, the upper maximum decreased in magnitude, becoming -3 μbar sec^{-1} by 2400 GMT, at which time the low-level upward motion had nearly disappeared.

The effects of mesoscale advections on θ and q_v as well as the time tendency terms at 0600 GMT near the *Researcher* are shown in Figure 5. The mesoscale vertical advection caused a cooling of about 1°C h^{-1} over a deep layer between 900 and 300 mbar. The moistening effect due to mesoscale vertical advection was also large, with the maximum located around the 775-mbar level. Horizontal advection and time tendency terms were generally small.

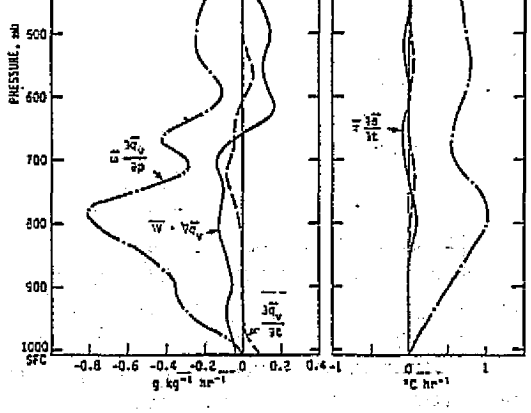

FIGURE 5 The mesoscale advection of temperature and humidity at 0600 GMT. Solid line is temperature and dotted line is humidity advection.

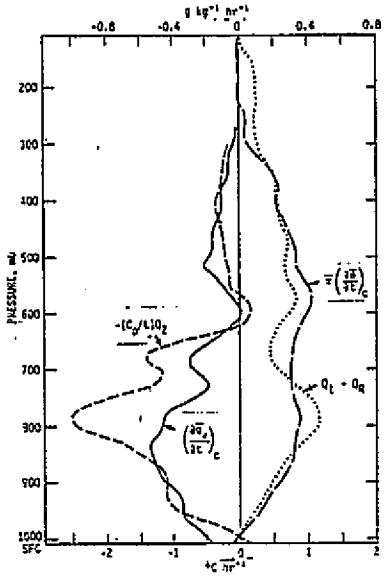

FIGURE 6 The simulated cloud heating and moistening effects. The corresponding profiles of $Q_1 - Q_R$ and $-(c_p/L)Q_2$ are computed from GATE data.

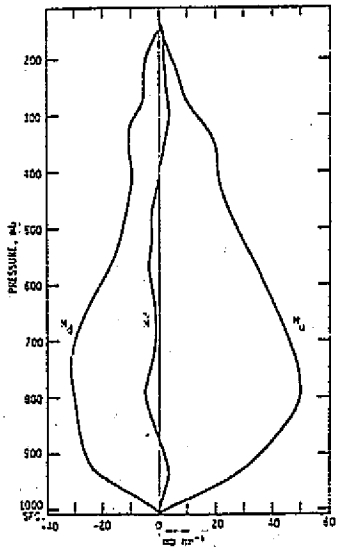

FIGURE 7 The simulated vertical cloud-mass fluxes: Mu, Upward mass flux inside clouds; Md, downward mass flux inside clouds; $\tilde{M}$, mass flux outside clouds.

The profile of radiative heating rate (Q_R) used in the deep cloud simulations is the weighted mean of typical Q_R profiles of a cloud cluster area and a clear area used by Frank (1977). The weights are 0.3 for the cluster profile and 0.7 for the clear area profile, since the computed cloud area coverage is about 30 percent. The response of deep cloud convection to a fixed mesoscale $\bar{w}$, $\bar{u}$, horizontal advection of $\bar{\theta}$ and $\bar{q}_v$ and sea-surface temperature was first simulated for 6 h using the mesoscale data at 0600 GMT, August 12. Figure 6 compares the vertical profiles of the simulated cloud heating effect, $\bar{\pi}(\partial\bar{\theta}/\partial t)_c$, and cloud moistening effect, $(\partial\bar{q}_v/\partial t)_c$, with the profiles of $Q_1 - Q_R$ and $-(c_p/L)Q_2$, respectively. The simulated cloud heating and moistening effect discussed here represent values that have been averaged over the 6-h period. These effects agree rather well with the estimated value from the rawinsonde data except that the clouds in the simulation removed less water vapor in the layer of 850–600 mbar. Caution should be made in this comparison because the profiles of $\bar{\theta}$ and $\bar{q}_v$ in the model changed with time. As a consequence, the vertical advection of $\bar{\theta}$ and $\bar{q}_v$ by $\bar{w}$ computed in the model would be different from the profiles in Figure 5.

The integrated upward mass flux inside clouds, downward mass flux inside clouds, and mass flux outside clouds during the 6-h simulation time are shown in Figure 7. A grid point is considered to be cloud area if the liquid-water mixing ratio at that point is larger than 10^{-2} g kg^{-1}. The sum of the three profiles will equal the mesoscale mass flux corresponding to the ω profile at 0600 GMT. The upward mass flux inside clouds had a maximum of 50 mbar h^{-1} around 775 mbar. The downdraft mass flux had a magnitude approximately three fifths of the updraft mass flux in the cloud layer. The updraft and downdraft mass fluxes had the same

magnitude near the cloud base and in the subcloud layer. The mass flux outside the clouds was actually small, and it had a general downward motion in the layer of 850-400 mbar. Slight upward motion was found in the subcloud layer and in the upper troposphere.

In order to examine whether different mesoscale forcings result in different cloud ensembles or different cloud heating and moistening profiles, another simulation was made in which the magnitudes of the mean vertical velocity was doubled without changing other input variables. The cloud heating and moistening effects computed from the model became almost twice as large as the corresponding $Q_1 - Q_R$ and $-(c_p/L)Q_2$ profiles. This result indicated that the effects of cloud convection follow closely the mesoscale effects.

In a third simulation all the mesoscale terms were set to zero except the surface heat flux, evaporation, and radiative cooling. The purpose of this simulation is to investigate the cloud development without the mean vertical velocity. No cloud developed to a height greater than 600 mbar, and the width of the clouds was only 2-3 grid points.

An experiment of 24-h cloud simulation is performed in order to encompass the developing, mature, and decaying stages. In this simulation, the radiative cooling, sea-surface temperature, and horizontal mean wind were kept fixed with time. However, the mean vertical velocity and mesoscale horizontal advections of $\bar{\theta}$ and $\bar{q}_v$ were changed at every time step. These data were obtained by a linear interpolation in time of the computed mesoscale variables, which had a time resolution of 3 h. The simulated cloud effects on θ and $\bar{q}_v$ and the profiles of $Q_1 - Q_R$ and $-(c_p/L)Q_2$ averaged over each 6-h period are shown in Figure 8. It can be seen that there was close agreement between $Q_1 - Q_R$ and $\bar{\pi}(\partial\bar{\theta}/\partial t)c$ and between $(c_p/L)Q_2$ and $(\partial\bar{q}_v/\partial t)c$ at every stage of cloud development. It also gives an indication that the cloud ensemble model presented here is capable of adequately reproducing the cloud convection under larger-scale lifting.

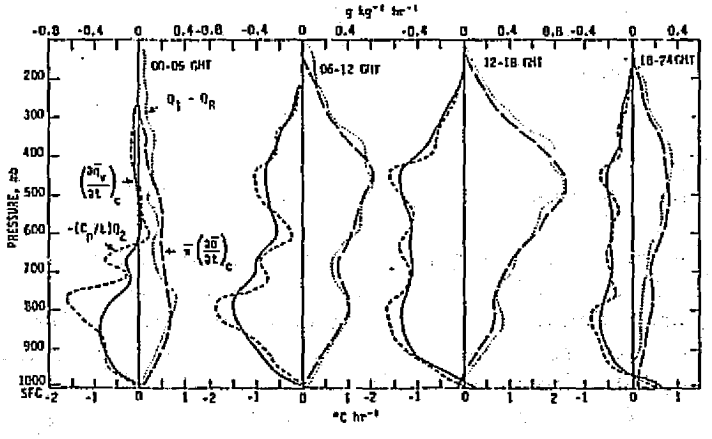

FIGURE 8 The simulated cloud heating and moistening effects for each 6 h during 0000-2400 GMT, August 12, 1974. The corresponding profiles of $Q_1 - Q_R$ and $-(c_p/L)Q_2$ are presented for comparison.

CONCLUDING REMARKS

A two-dimensional cloud ensemble model was used to study the controlling effects of the larger-scale environment on the initiation and development of deep and shallow cumulus clouds as well as the feedback effects of cumulus on the large-scale environment. In the shallow cloud simulations, the simulated vertical fluxes of heat and moisture compare reasonably well with observations. The convection will also respond to the changes in large-scale downward motion rather quickly to raise or lower the inversion height. However, the temperature and mixing ratio profiles above and below the inversion do not change appreciably during the simulations of 6-12 h when the large-scale downward motion is changed.

The results of deep cloud simulation indicated that differences in the mean vertical velocity caused the generation of different sizes of clouds as well as different cloud heating and moistening effects. Without the mean vertical motion, the clouds were much narrower and the cloud tops reached a much lower level. The simulated feedback effects of the cumulus ensemble on the mean temperature and moisture fields agreed fairly well with those estimated from rawinsonde observations.

ACKNOWLEDGMENT

This work was done in cooperation with Y. Ogura and W.-K. Tao. The work is supported by the National Science Foundation and the National Oceanic and Atmospheric Administration under Grant Nos. ATM 73-00238 and ATM78-11642. National Center for Atmospheric Research (NCAR) supported the major part of the computing time for this research. NCAR is supported by the University Corporation for Atmospheric Research under sponsorship of the National Science Foundation. The Research Board of the University of Illinois also provided computer support.

REFERENCES

Frank, W. M. (1977). Convective fluxes in tropical cyclones. *J. Atmos. Sci. 34*, 1554-1568.

Ogura, Y., Y. L. Chen, J. Russell, and S. T. Soong (1979). On the formation of organized convective systems observed over the GATE A/B array. *Mon. Wea. Rev. 107*, 426-441.

DISCUSSION

D. Rodenhuis, *Rapporteur*

A pair of experiments were discussed in which the simulated convection was allowed to respond to a specified large-scale forcing. It was noted that about 3 h is necessary for convection to reach quasi-equilibrium. Of course, feedback of convection to the large-scale field cannot be ascertained.

The random forcing at the lower boundary is not a crucial feature of

the convection since the cloud elements develop on quite a different scale. However, slab-symmetric cloud models are known to produce different results than axisymmetric or fully three-dimensional models. Nevertheless, Soong asserts that the *statistical* results of the convection are unlikely to change significantly; in any case, even the current results are quite satisfactory.

The results of these tests are important in that they show a development to quasi-equilibrium between large-scale forcing and simulated convection. There was some discussion concerning the question of whether any other result was possible, given the imposed conditions and transports at the boundaries. Apparently, changes in stability caused by the imposed large-scale flow were compensated by the convection so that a quasi-equilibrium could be obtained. These experiments are the first in a series that will examine the response of convection to different mean flow conditions.

ON THE COMPARISON OF COMPUTED CLOUD MASS FLUXES WITH OBSERVATIONS OVER THE GATE AREA

Tsuyoshi Nitta
University of Tokyo

INTRODUCTION

In recent years computations of the cloud mass fluxes based on large-scale heat and moisture budgets and parameterized cloud models have been performed by many authors to study the interaction between cumulus convection and its environment (Yanai *et al.*, 1973; Ogura and Cho, 1973; Nitta, 1975; Johnson, 1976; and others). Using observations from the GARP Atlantic Tropical Experiment (GATE), Nitta (1977; 1978) and Johnson (1978) made similar computations, including both convective updrafts and downdrafts.

While these diagnostic studies clarified the important role of the cumulus cloud in the large-scale field, the results of the cloud mass flux computations are dependent on the adopted cloud models and should be verified by other independent observations for clouds. However, comparison between computed cloud mass fluxes and other directly observed cloud parameters has not been thoroughly made mainly because of the lack of direct observations for cumulus clouds.

The GATE observation systems have been planned to provide the data for estimating the effects of the smaller-scale systems on the large-scale fields in the tropics, and a variety of observations have been carried out to measure different scales of meteorological phenomena. Therefore it is possible to test the computed cloud mass fluxes by different types of observation data obtained in GATE.

This study is an extension of the previous study by Nitta (1978) in which the cloud mass fluxes were computed using the GATE A/B-scale upper-air observations for Phase III. The purpose of this study is to compare the computed cloud mass fluxes with the observed convective activity based on the satellite and radar observations and to verify the cloud mass flux computations.

DATA

The results of the cloud mass fluxes obtained by Nitta (1978) are used in this study. The cloud mass flux computations have been carried out for each 6-h observation time using upper-air observations over the GATE A/B-scale area during Phase III (August 31-September 18, 1974). Figure 1

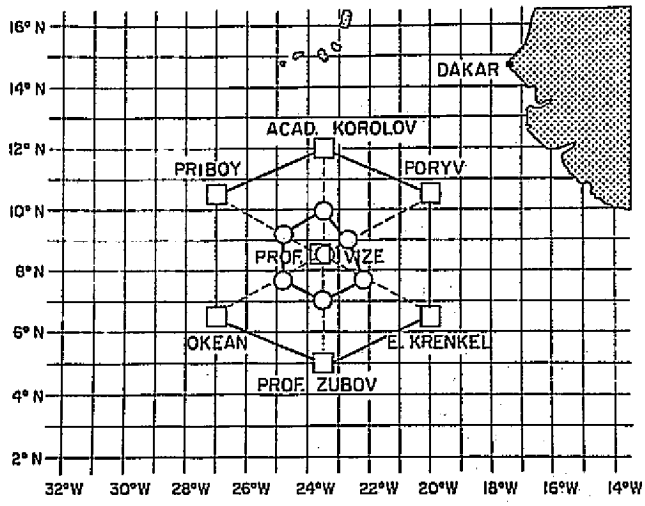

FIGURE 1 Observation networks for Phase III of GATE. Larger hexagonal area enclosed by solid lines is the A/B-scale area, and smaller hexagonal area is the B-scale area.

shows observation networks for A/B- and B-scale areas in GATE. The reader is referred to Nitta (1978) for further details of the computation method.

Digital SMS-1 IR brightness data and precipitation calculated from radar measurements are used for comparison with the cloud mass flux. Three-hour IR brightness data averaged over the A/B-scale area were kindly supplied by M. Murakami of the Meteorological Research Institute of Japan. Additional details of the data processing are described by Murakami (1979). Short-period variations less than 1 day are filtered out in order to make comparison with 6-h cloud mass fluxes whose short period fluctuations are also eliminated.

Six-hour precipitation described by Thompson *et al.* (1979) is used. The precipitation was calculated from radar measurements and averaged over the B-scale area. Although the B-scale area is much smaller than the A/B-scale area as shown in Figure 1, the former is located near the center of the latter, and most active cloud clusters move along the longitudinal belt crossing the B-scale area, and hence comparison between the cloud mass flux for the A/B area and the precipitation for the B-area could be justified.

Since IR brightness data mostly measure the deep convective activity, the cloud base mass flux due to deep clouds with tops above 400 mbar is used for comparison.

TIME VARIATIONS OF DEEP CLOUD MASS FLUXES, IR BRIGHTNESS, AND PRECIPITATION

Figure 2 shows time variations of the IF brightness, precipitation, and cloud base mass fluxes for deep clouds during Phase III of GATE. It is found that large mass fluxes for deep clouds correspond quite well to high IR brightness and heavy precipitation. Especially, similar time variations with a period of about 2-4 days, which would be associated with the African wave disturbances, can be seen in all three parameters.

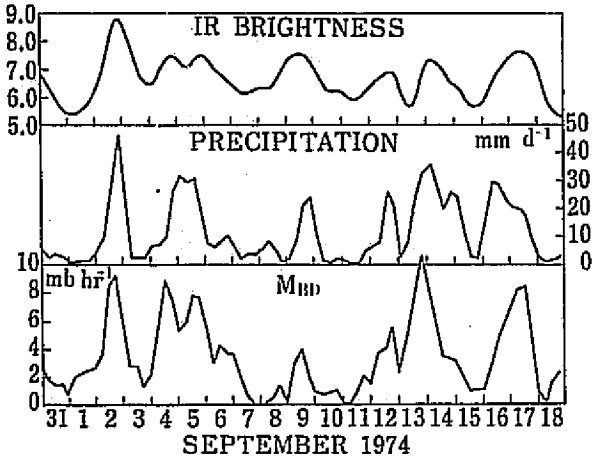

FIGURE 2 Time variations of IR brightness, precipitation, and cloud mass fluxes due to deep clouds.

We compute the correlation coefficients between the deep cloud mass flux and the other two parameters with different time lags to examine more detailed relationships (Figure 3). The result shows that the deep cloud mass flux M_{BD} correlates very well with both IR brightness B and precipitation P. While there is no time lag between M_{BD} and P, the curve of the correlation coefficient between M_{BD} and B is slightly shifted to the positive time lag ($\Delta t > 0$) indicating that IR brightness has its maximum a few hours after the peak of the deep cloud mass flux. This is likely due to the fact that the area of upper-level cirrus canopy would expand even after the development of cumulonimbus clouds had ceased.

If we parameterize the conversion from cloud droplets to raindrops in the cloud model, we can estimate the precipitation rate in the updraft as well as the cloud mass flux (see Nitta, 1977). In the diagnostic cloud model developed by Nitta (1977), it is assumed that the air inside convective downdrafts is saturated and maintained by evaporation from the

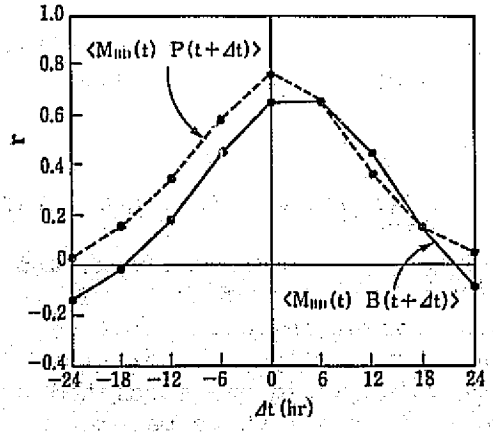

FIGURE 3 Correlation coefficients between the cloud mass flux for deep clouds M_{BD} and IR brightness B (solid line) and those between M_{BD} and the observed precipitation P (dashed line) for different time shifts (Δt).

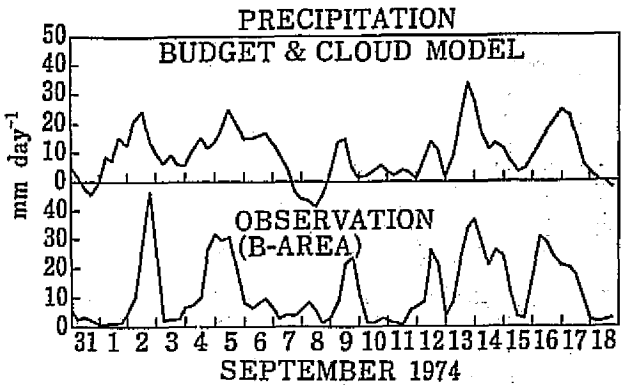

FIGURE 4 Time variations of computed (upper) and observed (lower) precipitation rates.

falling raindrops. By taking into account generation of raindrops in updrafts and evaporation in downdrafts, we can calculate net precipitation rate falling on the sea surface. Figure 4 shows the time variations of calculated and observed precipitation, respectively. Though the areas used for taking the average of precipitation are different between the model computations and observations, both variations of precipitation generally agree well with each other, especially for the latter half of GATE Phase III.

Negative precipitation found on September 7 and 8 resulted from overestimation of evaporation in the downdraft. It is assumed in the model that the air in the downdraft is saturated and maintained by the evaporation from the falling raindrops. However, nonsaturated downdrafts are frequently observed as well as saturated downdrafts in GATE (Houze, 1977; Zipser, 1977), and the above saturation condition would lead to overestimation of evaporation.

The mean value of the computed precipitation for the whole period is 9.1 mm day^{-1}, which is 2.8 mm day^{-1} smaller than that observed. Since the convective activity has its maximum along the longitudinal belt where the B-scale area is located as mentioned previously, it is expected that the amount of precipitation averaged over the B-scale area is greater than that averaged over the A/B-scale area, where regions with small rainfalls are also included. It is also probable that the saturation assumption in the downdraft would result in underestimation of the net precipitation, as discussed previously.

RELATIONSHIP BETWEEN CUMULUS CONVECTION AND AFRICAN WAVE DISTURBANCES

The GATE area is largely affected by the passage of the African wave disturbances, which propagate westward with an average period of 3.5 days and an average wavelength of approximately 2500 km. The relationship of convection and precipitation to the African wave disturbance has been extensively studied by Reed *et al.* (1977) and that between waves and cloud mass fluxes computed by the diagnostic cloud models has been examined

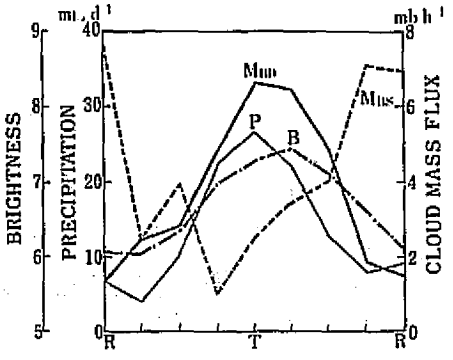

FIGURE 5 The IR brightness B, observed precipitation rate P, cloud mass flux M_{BD} due to deep clouds, and cloud mass flux M_{BS} due to shallow clouds for the composite wave. T and R denote wave trough and ridge, respectively. The phase on the left leads to that on the right.

by Johnson (1978) and Nitta (1978). Here we re-examine the relationship between cumulus cloud activity and the African wave disturbance using observed precipitation, SMS-1 IR brightness, and computed cloud mass fluxes.

The same compositing method as that in Nitta (1978) is used. Figure 5 shows variations of B, P, M_{BD}, and M_{BS} (cloud base mass fluxes due to shallow clouds with tops below 700 mbar) relative to the phase of the wave disturbance. All parameters except M_{BS} have maximum values around the wave trough and minimum around the wave ridge. While M_{BD} and P have their peaks at the wave trough, the maximum IR brightness occurs just behind the trough. This is consistent with the previous result of the time lag between M_{BD} and B.

The phase relationship of M_{BS} to the wave disturbance is opposite to that of other parameters, i.e., shallow cloud mass fluxes are small near the trough but large near the ridge. It is not easy to detect the activity of shallow clouds, which have short lifetime and small horizontal scales, and there is no direct observational support indicating modulations of shallow clouds by the wave disturbance. However, it is likely that the shallow clouds would be suppressed by the strong stabilization due to active deep clouds as discussed by Johnson (1978) and Nitta (1978). Recently, Ninomiya and Yamazaki (1979) have found in their analysis in Asian subtropical humid region that weak radar echoes tend to be suppressed when extremely strong echoes develop.

CONCLUSIONS AND REMARKS

The cloud mass flux due to deep clouds computed by the diagnostic cloud model is tested by using SMS-1 IR brightness and the precipitation calculated from radar measurements. The cloud mass flux for deep clouds correlate quite well with both IR brightness and precipitation. The IR brightness has its peak a few hours after the maximum deep cloud activity. This may be due to the horizontal expansion of the upper-level cirrus canopy after the cessation of cumulus development.

The precipitation computed by the model is compared with that observed. Time variations of both precipitation are quite similar to each other, although the mean value of the former is smaller than that of the latter.

Relationships between the African wave disturbance and the IR brightness, precipitation, and cloud mass fluxes are examined by using a compositing method. The maximum precipitation and the greatest cloud mass flux for deep clouds occur at the wave trough, but the IR brightness has its peak just behind the wave trough. Cloud mass fluxes for shallow clouds are small around the wave trough but large around the wave ridge. The weak shallow cloud activity near the wave trough may result from the stabilization effect by intense deep clouds, but further studies about the variation of the shallow cloud activity are needed in the future.

Although it is concluded in this study that the cloud mass flux for deep clouds computed by the diagnostic cloud model represents well the activity of deep clouds in the real tropical atmosphere in the qualitative sense, more quantitative verification is desired in the future. For that purpose we may have to develop techniques to obtain more quantitative data for cumulus clouds such as mass fluxes inside clouds and precise areas covered by cumulus clouds.

ACKNOWLEDGMENTS

The author would like to express his thanks to M. Murakami, who kindly supplied the IR brightness data averaged over the A/B-scale area. Thanks are also due to K. Kudo for typing the manuscript.

REFERENCES

Houze, R. A. (1977). Structure and dynamics of a tropical squall-line system. *Mon. Wea. Rev. 105*, 1540-1567.

Johnson, R. H. (1976). The role of convective-scale precipitation downdrafts in cumulus and synoptic-scale interactions. *J. Atmos. Sci. 33*, 1890-1910.

Johnson, R H. (1978). Cumulus transports in a tropical wave composite for Phase III of GATE. *J. Atmos. Sci. 35*, 484-494.

Murakami, M. (1979). Large-scale aspect of cumulus convective activity over the GATE area. *Mon. Wea. Rev. 106* (in press).

Ninomiya, K., and K. Yamazaki (1979). Heavy rainfalls associated with frontal depression in Asian subtropical humid region (II). Submitted to *J. of Meteorol. Soc. Japan*.

Nitta, T. (1975). Observational determination of cloud mass flux distributions. *J. Atmos. Sci. 32*, 73-91.

Nitta, T. (1977). Response of cumulus updraft and downdraft to GATE A/B-scale motion systems. *J. Atmos. Sci. 34*, 1163-1186.

Nitta, T. (1978). A diagnostic study of interaction of cumulus updrafts and downdrafts with large-scale motions in GATE. *J. Meteorol. Soc. Jpn. 56*, 232-242.

Ogura, Y. and H.-R. Cho (1973). Diagnostic determination of cumulus cloud populations from observed large-scale variables. *J. Atmos. Sci. 30*, 1276-1286.

Reed, R. J., D. C. Norquist, and E. E. Recker (1977). The structure and properties of African wave disturbances as observed during Phase III of GATE. *Mon. Wea. Rev. 105*, 317-333.

Thompson, R. M., S. W. Rayne, E. E. Recker, and R. J. Reed (1979). Structure and properties of synoptic-scale wave disturbances in the Intertropical Convergence Zone of the Eastern Atlantic. *J. Atmos. Sci. 36*, 53-72.

Yanai, M., S. Esbensen, and J.-H. Chu (1973). Determination of bulk properties of tropical cloud clusters from large-scale heat and moisture budgets. *J. Atmos. Sci. 30*, 611-627.

Zipser, E. J. (1977). Mesoscale and convective-scale downdrafts as distinct components of squall-line structure. *Mon. Wea. Rev. 105*, 1568-1589.

DISCUSSION

D. Rodenhuis, *Rapporteur*

The rather high correlation between cloud-base mass flux (M_B) determined from A/B-scale budgets and rainfall estimates from B-scale radar observations drew a great deal of attention. Apparently, the boundaries of the budget volume do sense the influence of mesoscale convection within the boundaries. However, M_B and rainfall are not shifted in phase as determined by earlier studies. This point needs further study.

The out-of-phase relationship between shallow cloud population and those of deep clouds was also of interest. Although there was not immediate observational evidence to support this result, it was recognized that mass flux cannot be directly interpreted as cloud number density. Furthermore, the imposed condition of saturation on downdrafts of all model clouds (which sometimes produces negative precipitation) may contribute to this strong difference in variation between deep and shallow clouds.

9. Large-Scale Modeling Studies

Organizer ..... R. Anthes

Speakers ..... S. Rosenthal*
Y. Hayashi
C. Mass
A. Gilchrist
K. Miyakoda

Session Chairmen ..... R. Anthes
V. Pandolfo

Rapporteurs ..... D. Randall
M. Rennick
C. Mass

*Scheduled but unable to be present

CUMULUS EFFECTS IN HURRICANE MODELS--
TO PARAMETERIZE OR NOT TO PARAMETERIZE?

Stanley L. Rosenthal
National Hurricane and Experimental Meteorology Laboratory, NOAA
(author not present)

INTRODUCTION

The first attempts at numerical simulation (Kasahara, 1961, 1962; Syono, 1962) included only latent heat release in large moist convective elements that were explicitly resolved on grids with horizontal resolutions of a few tens of kilometers. Small-scale features in the vertical motion field grew rapidly and obscured the vortex-scale motions. Since this was consistent with the linear theory of small-amplitude disturbances in a conditionally unstable, saturated, atmosphere, many investigators concluded that the direct, or explicit, approach to latent heat release could not be used to simulate the growth of "larger-scale" systems such as hurricanes.

In early discussions of *parameterized* cumulus convection, the main thrust was not the "subgrid" nature of the cumulus. The motivating factor seemed to be a desire to separate the dynamics of the buoyant moist convection from those of the larger-scale systems (hurricanes) to avoid results of the type described above. Spar (1964), in a review paper, wrote "...the mean circulation must not itself be energy producing through condensation, for if this is permitted the computations of the mean motion will give rise to dominating small scale cumulus convection cells." Charney and Eliassen (1964), in their classic paper, wrote, "Thus, if one applies perturbation techniques to the study of small-amplitude perturbations of a conditionally unstable saturated atmosphere, one finds, not surprisingly, that the smallest scale modes grow at the greatest rate and ultimately predominate. Similarly, if one resorts to numerical integration, the large-scale motions are found to be obscured by the 'noise' of the unstable small-scale motions."

More recent numerical experiments by Yamasaki (1975; 1977), Jones (1979) and Rosenthal (1978) have shown that the pessimism regarding the direct (explicit) calculation was largely unfounded. The lack of success in the early models, in retrospect, is not difficult to understand since these models contained quasi-linearizations of the moist static stability that eliminated the nonlinear feedback of the convection onto the vertical stratification.* Saturated (but otherwise adiabatic) motions in a

*Syono's (1962, p. 416) model also contained a numerical instability in the condensation heating term that could only be eliminated by reducing the time step to economically unfeasible values.

hydrostatic atmosphere obey the approximate form of the first law of thermodynamics:

$$\frac{\partial T}{\partial t} = - \vec{V} \cdot \nabla T + \frac{\omega}{\rho g} (\gamma_s - \gamma). \qquad (1)$$

Here, ω is the p-system vertical velocity, γ_s is the moist adiabatic lapse rate, γ is the actual lapse, and the other symbols are standard. For a conditionally unstable atmosphere ($\gamma > \gamma_s$), saturated upward vertical motion produces a positive temperature tendency. As γ and γ_s approach each other, the temperature tendency produced by upward saturated vertical motion should approach zero but, in the early hurricane models ($\gamma_s - \gamma$), or equivalent expressions, was replaced by a constant "climatological" value. This appears to have been the cause of the unlimited linear growth of small-scale features. When stability is treated in a self-determining fashion, as is the case with more recent numerical models, the smaller scales are less of a problem, and this has been demonstrated in axisymmetric models (Rosenthal, 1978), as well as fully three-dimensional models (Jones, 1979).

In the 1960's, investigators, convinced that explicit calculations were doomed to fail, vigorously (and with reasonable success) pursued numerical hurricane modeling with parameterized cumulus convection. The cumulus parameterizations used in these hurricane models were largely intuitive and empirical (Ooyama, 1964; Kuo, 1965), but they did work rather well in highly idealized models (e.g., Yamasaki, 1968; Rosenthal, 1970; Ooyama, 1969; Sundqvist, 1970). Later Ooyama (1971) and Arakawa and Schubert (1974) developed more physically based parameterizations, but these have not led to any substantial advantages in hurricane modeling.

AN UNRESOLVED PROBLEM

To address the question posed by the title of this paper, we should look back at the array of hurricane modeling results obtained with cumulus parameterization and attempt to identify those aspects of the hurricane problem that have not been significantly addressed. Tropical cyclone numerical modeling studies with parameterized cumulus convection seem to have provided a body of information that has substantially improved our understanding of the dynamics and energetics of the mature state of the tropical cyclone. Models that have been developed for operational prediction of hurricane tracks have also been reasonably successful (Elsberry, 1979; Simpson and Pielke, 1976) with only the crudest of cumulus parameterizations. However, in the opinion of this author, the parameterized models have failed to provide significant insight into the problem of tropical cyclogenesis. Given that the sea-surface temperature is sufficiently warm, and given that the parameterization provides an appropriate distribution of heating between the upper and lower troposphere (Koss, 1976), these models, for the most part, will develop hurricane-like vortices. In the real atmosphere, however, only a few percent of tropical disturbances attain hurricane intensity despite the fact that many encounter favorable sea-surface temperatures (Simpson and Pielke, 1976).

MODES OF INTERACTION

The essence of a meaningful definition of Conditional Instability of the Second Kind (CISK), as emphasized by Charney and Eliassen (1964), is the *cooperative interaction* of the cumulus clouds and a larger scale. Observational studies of cumulus convection over the tropical oceans, however, indicate that not all moist convection is cooperative in this sense. In certain situations, weak synoptic-scale systems trigger cumulus convection that takes on a squall-line mesoscale organization and overwhelms the synoptic scale (Zipser, 1977; Frank, 1977; Lilly, 1975). When this occurs, despite the organization of the cumulus convection, and despite reasonably large amounts of precipitation, the synoptic system does not grow (e.g., Ruprecht and Gray, 1976).

Zipser (1971) pointed out that tropical oceanic squall lines tend to propagate at 12-15 m sec^{-1}, whereas the typical synoptic system over the tropical oceans moves at speeds of 6-8 m sec^{-1}. He questioned how the squall line could remain coupled with the synoptic system as would be necessary if the statistical effect of the cumulus activity is to provide an energy source for development of the synoptic scale. Also, this type of organized cumulus convection would not readily be parameterized from knowledge of the synoptic scale, since it is not coupled to the synoptic scale.

Zipser (1971) also pointed out that some disturbances, particularly tropical disturbances that are attempting to develop, seem to carry their cloud systems with them for longer periods of time than would be reasonable for the squall systems. He presented observational evidence to show that a distinguishing feature of these systems, in comparison to the squall type, was a lack of downdraft air at low levels and proposed that interactions between the convective scale and the synoptic scale over the tropical oceans could, perhaps, be classified into two modes.

Squall type: The synoptic-scale disturbance develops zones of boundary-layer convergence that produce organized cumulus convection. Zones of strong, cool and/or dry downdrafts develop that destroy new convection near the center of the synoptic system and force new convection to develop and propagate ahead of the original convection. The cumulus convection does not remain coupled to the large-scale forcing. There is a destructive feedback on the large scale.

Tropical cyclogenesis type: The synoptic-scale disturbance develops zones of boundary-layer convergence that produce organized cumulus convection. The zones of convection remain closely coupled to the large-scale forcing. No strong, cool, or dry downdrafts form near the center of the convective region. Heating due to the release of latent heat remains coupled to the large-scale forcing. There is a direct feedback, in a positive (cooperative) sense, on the synoptic-scale system.

This second mode of interaction is like CISK. Since the convection is closely coupled to the larger-scale system, it would seem that cumulus parameterization would have a better chance of succeeding here.

The key to the mode of interaction that will occur appears to be whether organized, strong downdrafts develop with thermodynamic properties that are significantly different from unprocessed low-level air (Zipser and Gautier, 1978). Data from GATE, as well as from other sources,

support the contention that those modes of interaction do indeed occur over the tropical oceans (Zipser, 1977; Zipser and Gautier, 1978; Houze, 1977). It appears to be more than a coincidence that the conditions that favor Zipser's squall-type interaction (vertical shear and a dry middle troposphere) have long been recognized as inhibitors to tropical storm development (Simpson and Pielke, 1976).

MODELING THE INTERACTIONS

To parameterize cumulus convection, it is essential that the large-scale control be so strong that the statistical properties of the cumulus can be deduced from knowledge of the large scale alone. In view of Zipser's (1971) ideas, parameterization would seem to bias the mode of interaction toward the tropical cyclogenesis type (cooperative type or CISK type), since the properties of the convective ensemble in the squall type are not coupled to the large-scale system. Furthermore, the effects of downdrafts have not, to this writer's knowledge, been incorporated into any of the *prognostic* schemes of cumulus parameterization (some *diagnostic* schemes do represent downdrafts), and this would seem to limit severely the ability of existing parameterizations to generate Zipser's squall-type (noncooperative, non-CISK) interaction.

In contrast, axisymmetric simulations carried out by the author with direct calculations of latent heat release (with 20-km horizontal resolution) have resulted in solutions that resemble both of Zipser's modes and even transitions from dominance of one mode to dominance of the other (Rosenthal, 1978).

In the experiment reported on by Rosenthal (1978), the initial conditions were obtained by perturbing a thermodynamic base-state similar to Jordan's (1958) mean hurricane season sounding. The perturbation was a weak vortex in gradient balance. Jordan's mean atmosphere has a relatively dry middle troposphere (500-mbar relative humidity is 42 percent) and provides a thermodynamic structure appropriate for squall-like convection to develop. The model solutions, in the early portions of the integration, show a convective system that strongly resembles Zipser's (1969; 1977) and Houze's (1977) tropical squall lines. It develops in a region of Ekman pumping and propagates radially outward through a generation-decay process. New convective elements (explicitly represented in the 20-km grid) form at low levels radially outward from old ones. Through strong nonlinear processes, these elements rise as bubbles and are detached from the low-level energy source. Below the rising convective element, a region of absolutely stable air forms. Continued ascent in this region leads to cooling. Below cloud base, cooling is aided by evaporation of rain falling from the convective element. This cooling leads to a hydrostatic rise of pressure at low levels beneath the convective element, and a downdraft forms. The downdraft builds upward from the lowest levels to the convective element aloft. Precipitation evaporation is insufficient to maintain saturation in the downdraft, and warming and drying occur within it. The propagating convective system is the dominant motion in this period. Its formation is a result of the vortex-scale frictional inflow. However, once the squall system

is formed, the vortex scale appears to exert little control on the convection for a period of several tens of hours. While the convection significantly modifies the vortex, there is no important intensification of the latter. This convection is noncooperative in the CISK sense.

In the real atmosphere, stabilization of the low troposphere, particularly the subcloud layer, in the wake of squall systems, results from precipitation evaporation, convective-scale (cold and saturated) downdrafts, and mesoscale (warm and unsaturated) downdrafts (Zipser, 1969, 1977; Betts 1976; Miller and Betts, 1977). While the author's model does not simulate the cold, saturated convective-scale downdraft, the downdrafts that are simulated, together with precipitation evaporation, do a reasonably good job of providing the observed type of stabilization.

In a subsequent experiment, the initial state was changed such that the relative humidity was everywhere 100 percent. This provides for a significant increase of the moist static energy in the middle troposphere and a smaller vertical gradient of moist static energy in the lower troposphere. The vertical motions in this calculation reveal deep plume-like convection without downdrafts. This resembles the type of convection that comprises hurricane eyewalls in numerical experiments. These plumes do not propagate and are cooperative. Hence, the explicit calculation is capable of differentiating between different modes of moist convection when initial conditions are varied. The calculation was also capable of making this transition within a given numerical experiment as various processes altered the static stability of the system. A plume-like cloud, in the original experiment, which developed in the vortex interior, was the first evidence of an eyewall feature. The moist static energy in the vicinity of this feature more closely resembled that associated with the plumes of the saturated atmosphere than the earlier squall-like convection that appeared in this calculation.

These results strongly argue for continued hurricane modeling with the explicit (nonparameterized) representation of convective clouds. This is particularly true if one clue to tropical cyclogenesis is indeed the type of cumulus convection that is triggered by the larger-scale system.

REFERENCES

Arakawa, A., and W. H. Schubert (1974). Interaction of a cumulus cloud ensemble with the large-scale environment, Part I. *J. Atmos. Sci. 31*, 675-701.

Betts, A. K. (1976). The thermodynamic transformation of the tropical subcloud layer by precipitation downdrafts, *J. Atmos. Sci. 33*, 1008-1020.

Charney, J. G., and A. Eliassen (1964). On the growth of the hurricane depression. *J. Atmos. Sci. 21*, 68-74.

Elsberry, R. L. (1979). Applications of tropical cyclone models. *Bull. Am. Meteorol. Soc.*, to be published.

Frank, W. M. (1977). The life-cycle of GATE convective system. Paper presented at the NCAR GATE Workshop, August 1977.

Houze, R. A. (1977). Structure and dynamics of a tropical squall-line system. *Mon. Wea. Rev. 105*, 1540-1567.

Jones, J. W. (1979). A three-dimensional tropical cyclone model with release of latent heat by the resolvable scales. Submitted to *J. Atmos. Sci.*

Jordan, C. L. (1958). Mean soundings for the West Indies area. *J. Meteorol. 15*, 91-97.

Kasahara, A. (1961). A numerical experiment on the development of a tropical cyclone. *J. Meteorol. 18*, 259-282.

Kasahara, A. (1962). The development of forced convection caused by the release of latent heat of condensation in a hydrostatic atmosphere. *Proc. Int. Symp. Numerical Weather Predictions in Tokyo*, S. Syono, ed., Meteorol. Soc. Japan, pp. 387-404.

Koss, W. J. (1976). Linear stability of CISK-induced low latitude disturbances. NOAA Tech. Memo. ERL WMPO-24, 167 pp.

Kuo, H. L. (1965). On the formation and intensification of tropical cyclones through latent heat release by cumulus convection. *J. Atmos. Sci. 22*, 40-63.

Lilly, D, K. (1975). Severe storms and storm systems: scientific background, methods, and critical questions. *Pure Appl. Geophys. 133*, 713-734.

Miller, M. J., and A. K. Betts (1977). Traveling convective storms over Venezuela. *Mon. Wea. Rev. 105*, 833-848.

Ooyama, K. (1964). A dynamical model for the study of tropical cyclone development. *Geofis. Int. 4*, 187-198.

Ooyama, K. (1969). Numerical simulation of the life cycle of tropical cyclones. *J. Atmos. Sci. 26*, 3-40.

Ooyama, K. (1971). A theory of parameterization of cumulus convection. *J. Meteorol. Soc. Jpn. 49*, 744-756.

Rosenthal, S. L. (1970). A circulatory symmetric primitive equation model of tropical cyclone development containing an explicit water vapor cycle. *Mon. Wea. Rev. 98*, 643-663.

Rosenthal, S. L. (1978). Numerical simulation of tropical cyclone development with latent heat release by the resolvable scales. I: Model description and preliminary results. *J. Atmos. Sci. 35*, 258-271.

Ruprecht, E., and W. M. Gray (1976). Analysis of satellite-observed tropical cloud clusters II. Thermal, moisture and precipitation. *Tellus 28*, 415-425.

Simpson, R. H., and R. A. Pielke (1976). Hurricane development and movement. *Appl. Mech. Rev.* 601-609.

Spar, J. (1964). A survey of hurricane development, *Geofis. Int. 4*, 169-178.

Sundqvist, H. (1970). Numerical simulation of the development of tropical cyclones with a 10-level model, Part I. *Tellus 22*, 359-390.

Syono, S. (1962). A numerical experiment of the formation of tropical cyclones. *Proc. Int. Symp. Numerical Weather Prediction in Tokyo*, Syono, ed., Meteorol. Soc. Japan, pp. 405-418.

Yamasaki, M. (1968). Detailed analysis of a tropical cyclone simulated with a 13-layer model. *Pap. Meteor. Geophys. 19*, 559-585.

Yamasaki, M. (1975). A numerical experiment of the interaction between cumulus convection and larger-scale motion. *Pap. Meteor. Geophys. 26*, 63-91.

Yamasaki, M. (1977). A preliminary experiment of the tropical cyclone without parameterizing the effects of cumulus convection. *J. Meteorol. Soc. Jpn. 55*, 11-31.

Zipser, E. J. (1969). The role of organized unsaturated downdrafts in the structure and rapid decay of an equatorial disturbance. *J. Appl. Meteorol. 8*, 799-814.

Zipser, E. J. (1971). Internal structure of cloud clusters. *GATE Experimental Design Proposal, Interim Scientific Management Group*, Vol. 2, Annex VII, WMO-ICSU, Geneva.

Zipser, E. J. (1977). Mesoscale and convective-scale downdrafts as distinct components of a squall line structure. *Mon. Wea. Rev. 105* 1568-1589.

Zipser, E. J., and C. Gautier (1978). Mesoscale events within a GATE tropical depression. *Mon. Wea. Rev. 106*, 789-805.

STUDIES OF THE TROPICAL GENERAL CIRCULATION WITH A GLOBAL MODEL OF THE ATMOSPHERE

Y. Hayashi
Geophysical Fluid Dynamics Laboratory/NOAA, Princeton University

INTRODUCTION

Some highlights are given of the tropical general circulation simulated by GFDL general circulation models (Manabe *et al.*, 1970, 1974; Hayashi, 1974; Manabe and Mahlman, 1976; Hayashi and Golder, 1978, 1979). The present report is based mainly on an 11-layer 2.4° mesh grid model (Manabe *et al.*, 1974) with moist convective adjustment and seasonal variation, while some improved results from a current 30-wavenumber spectral model (Manabe *et al.* 1979) are shown for comparison. These models not only simulate the geographical and seasonal variation of the tropical circulation reasonably well but can also be used to study the generation of tropical planetary waves by eliminating, one by one, their possible causes (Hayashi and Golder, 1978).

TIME MEAN STREAMLINES

In Figure 1, July mean streamlines simulated by the grid (top, 190 mbar) and spectral (middle, 205 mbar) models are compared with those observed (bottom 200 mbar). The spectral model is superior to the grid model in simulating the primary features such as the Tibetan and Mexican highs, the mid-Pacific and mid-Atlantic troughs, and the easterly jet of southern Asia. The shortcoming of the grid model is the intense upper-level high-pressure belt over the western Pacific, which results from the unusually frequent occurrence of typhoons. This defect has not appeared in the spectral model, although the reason for this is not known.

TRANSIENT WAVES

The transient eddy kinetic energy in the equatorial model stratosphere is mostly accounted for by eastward moving Kelvin waves, consisting of wavenumbers 1-2 and periods of 10-20 days, which were observed by Wallace and Kousky (1968), and westward moving mixed Rossby gravity waves with wavenumbers 3-5 and periods of 4-6 days, observed by Yanai and Maruyama (1966), as well as transient planetary waves extending from midlatitudes. As illustrated by Figure 2, Kelvin waves in the grid model attain their

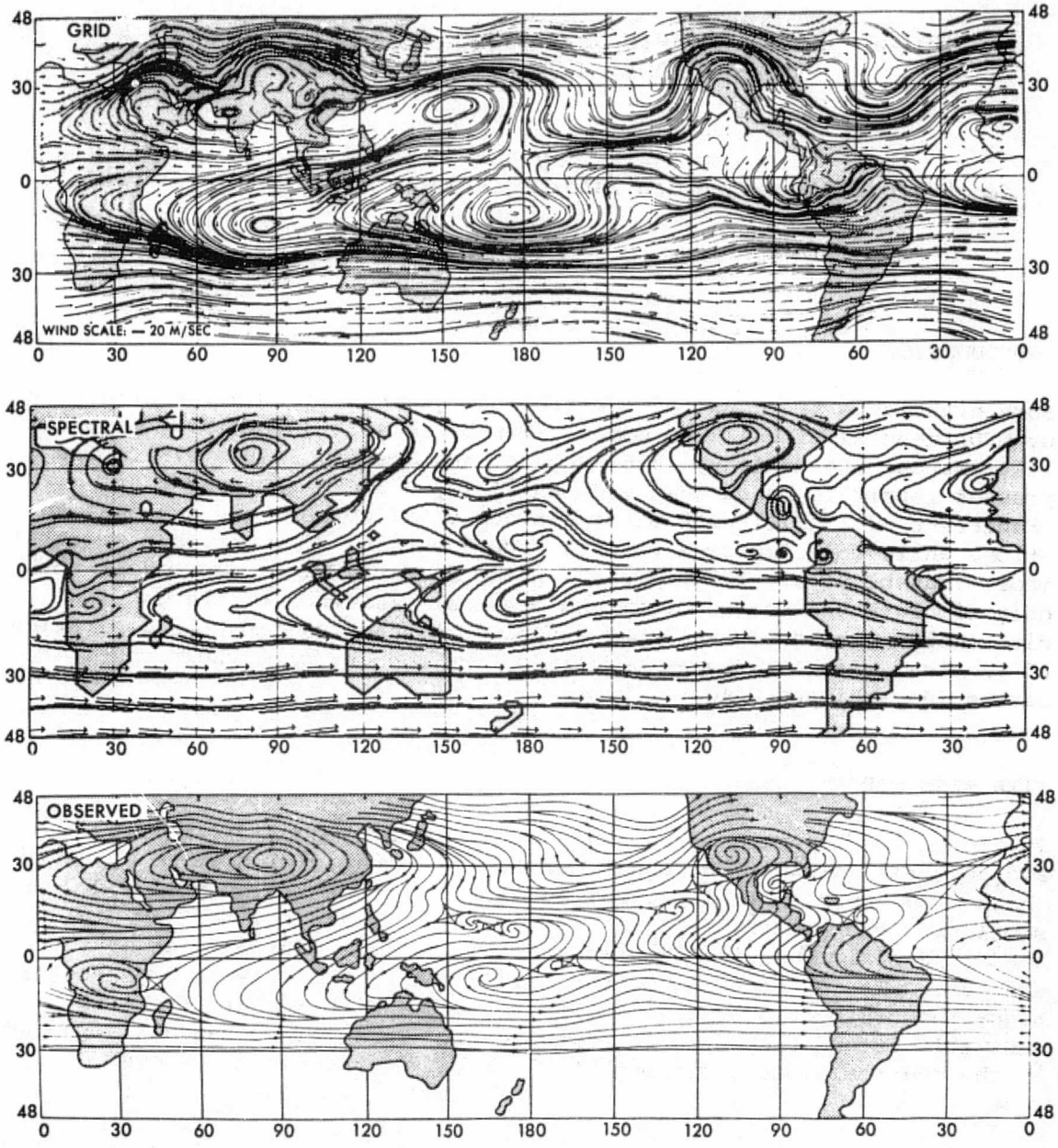

FIGURE 1 *Top*: computed (grid model, Manabe *et al.*, 1974) July mean streamlines at 190 mbar. *Middle*: computed (spectral model, Manabe *et al.*, 1979) July mean streamlines at 205 mbar. *Bottom*: observed (Sadler, 1972) July mean streamlines at 200 mbar.

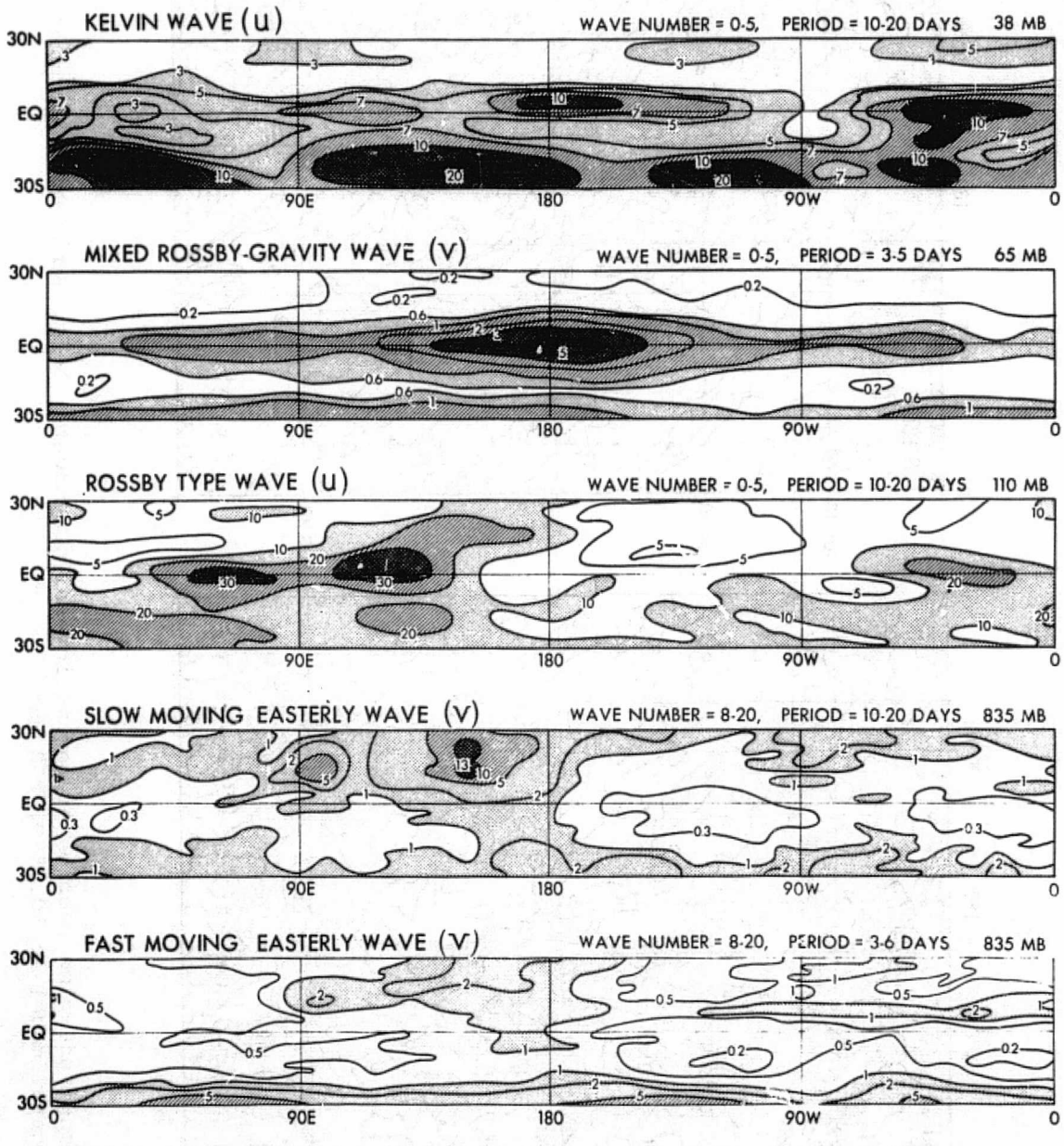

FIGURE 2 Longitude-latitude section of time-power spectra (m^2 sec^{-2}) of wavenumber-filtered winds (Hayashi, 1974) in the grid model.

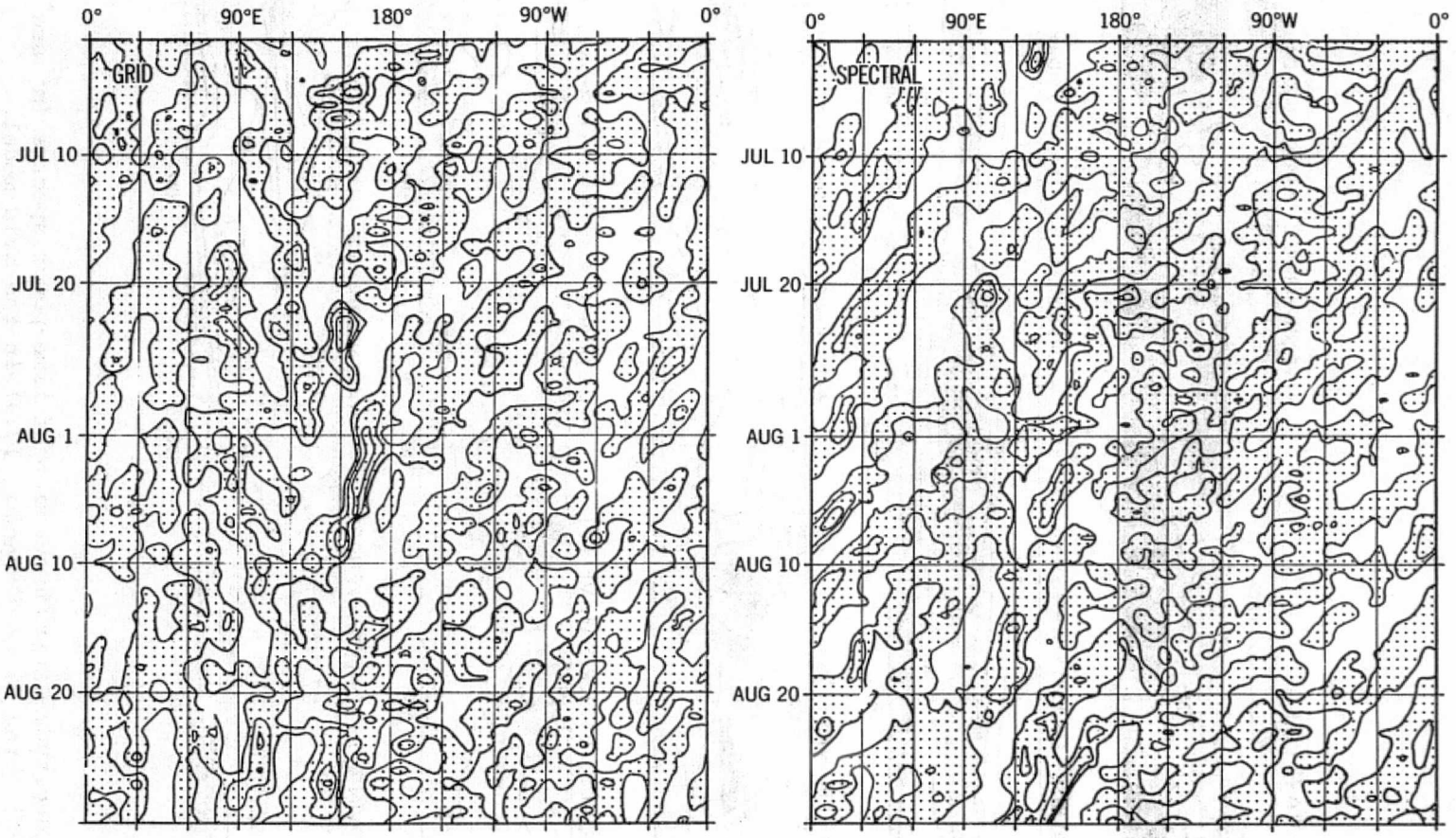

FIGURE 3 Longitude-time section of the meridional component. *Left*: grid model at 9.6° N, 835 mbar. *Right*: spectral model at 10.1° N, 830 mbar.

maximum over the equatorial Pacific and Atlantic, while mixed Rossby-gravity waves attain their maximum in the Pacific and can also be detected in the Atlantic.

Tropical transient disturbances in the model troposphere are more complex than those in the stratosphere. Some of them can be interpreted as westward moving planetary-scale equatorial Rossby waves, synoptic-scale easterly waves, and monsoon disturbances.

As illustrated by Figure 2, Rossby-type waves consisting of wavenumbers 0-5 and periods of 10-20 days, attain their maxima in the western Pacific, the Indian monsoon region, and also the Atlantic. Easterly waves consisting of wavenumbers 8-10 and periods of 3-6 days, are found only in the Atlantic in the grid model. These waves move slowly westward with periods of 10-20 days in the western Pacific (Figure 3, left), contrary to those observed. The spectral model is free from this defect as seen in Figure 3 (right). This is probably because the basic current is more realistic in the spectral model.

GENERATION OF TRANSIENT PLANETARY WAVES

In order to study the generation of tropical transient planetary waves, the effects of topography, midlatitude disturbances, and condensational heat have been eliminated one by one from a 13-layer grid model during the period June and July (Hayashi and Golder, 1978).

It was concluded that the kinetic energy of equatorial transient disturbances as a whole is generated primarily as the result of latent heat release in the tropics, while that of subtropical transient disturbances is reduced significantly in the absence of midlatitude disturbances. This conclusion is consistent with that by Manabe *et al.* (1970; 1974). It was also found that the characteristic scale and period of Kelvin and mixed Rossby gravity waves do not depend on land-sea contrast or on the zonal variation of sea-surface temperature. Even if midlatitude disturbances are eliminated, both of these waves appear in the stratosphere because of the effect of latent heat release in the troposphere. In contrast to Kelvin waves, however, mixed Rossby gravity waves can be significantly enhanced by the westward moving component of midlatitude disturbances, which are found to propagate intermittently toward the equator.

REFERENCES

Hayashi, Y. (1974). Spectral analysis of tropical disturbances appearing in a GFDL general circulation model. *J. Atmos. Sci. 31*, 180-218.

Hayashi, Y., and D. G. Golder (1978). The generation of equatorial transient planetary waves: Control experiments with a GFDL general circulation model. *J. Atmos. Sci. 35*, 2068-2082.

Hayashi, Y., and D. G. Golder (1979). The seasonal variation of tropical transient planetary waves appearing in a GFDL general circulation model. Submitted to *J. Atmos. Sci.*

Manabe, S., and J. D. Mahlman (1976). Simulation of seasonal and interhemispheric variations in the stratospheric circulation. *J. Atmos. Sci. 33*, 2185-2217.

Manabe, S., J. L. Holloway, Jr., and H. M. Stone (1970). Tropical circulation in a time integration of a global model of the atmosphere. *J. Atmos. Sci. 27*, 580-613.

Manabe, S., D. G. Hahn, and J. L. Holloway, Jr. (1974). The seasonal variation of the tropical circulation as simulated by a global model of the atmosphere. *J. Atmos. Sci. 31*, 43-83.

Manabe, S., D. G. Hahn, and J. L. Holloway, Jr. (1979). Climate simulations with GFDL spectral models of the atmosphere: effect of truncation. GARP Publications (in press).

Wallace, J. M., and V. E. Kousky (1968). Observational evidence of Kelvin waves in the tropical stratosphere, *J. Atmos. Sci. 25*, 900-907.

Yanai, M., and T. Maruyama (1966). Stratospheric and wave disturbances propagating over the equatorial Pacific. *J. Meteorol. Soc. Jpn. 44*, 291-294.

DISCUSSION

D. Randall, *Rapporteur*

Hayashi showed a film of a numerical simulation of summer weather over the GATE area. Depicted in the film were surface wind vectors and precipitation. In the discussion period, it was pointed out that it was difficult to detect the waves in the simulated surface wind field. They are also difficult to detect in the observed surface wind field unless a sufficient number of wind vectors are plotted. Hayashi described plans to construct composite waves from model data, for comparison with those obtained from observations. He reported that studies of the momentum budget for the 200-mbar winds gave unsatisfactory results with the grid point model but that the analysis will be repeated for the spectral model, with the expectation of better results.

The results of the grid point and spectral models differed in several noticeable respects. The 200-mbar wind field was significantly better in the spectral model. False hurricanelike disturbances, which were very prominent in the results of the grid point model, were absent in those of the spectral model. For the spectral model only, very regular wave disturbances were seen near Ethiopia. Several questions prompted Hayashi to elaborate on the design of the spectral model. He explained that it employs a biharmonic friction with a small constant coefficient instead of nonlinear viscosity. This is why spectral models give good results even if the horizontal resolution is coarse.

THE EFFECTS OF CUMULUS PARAMETERIZATIONS IN LINEAR MODELS

Clifford Mass
University of Maryland

INTRODUCTION

The effects of cumulus clouds have generally been absent or simply parameterized in the linear models that have been developed to study tropical waves in the troposphere. Of the studies that have included convective effects, Rennick (1976) only included latent heating, while Stevens *et al.* (1977) and Mass (1979) parameterized cumulus momentum mixing as well. This paper will briefly outline the convective parameterizations used in the above studies and their influence on model results.

RENNICK MODEL

In order to study initial disturbance growth and development, Rennick (1976) made use of a five-level channel model with a mean state based on the August mean zonal winds at 5° E from Burpee (1972) and the specific humidity field from Newell *et al.* (1972).

Rennick parameterized convection by assuming that all the moisture converged into a column rained out. The resultant latent heating was distributed in the vertical using the observed profile of Reed and Recker (1971), which possessed a maximum near 400 mbar.

The propagation parameters and disturbance fields were nearly unchanged by the inclusion of convective heating. For an unusually intense jet with a maximum of 23 $msec^{-1}$ the most unstable mode of both dry and moist cases had a wavelength of 3000 km, a period of 2.2 days, a phase speed of 16 $msec^{-1}$, and a growth rate of approximately 0.35 day^{-1}. The wave axis correctly tilted southwest-northeast up to about 12° N, but then precipitously changed its slope to southeast-northwest, whereas all observations indicate a continuous southwest-northeast slope equatorward of the jet axis (≈15° N) with either no slope or a very slight southeast-northwest orientation on the poleward side of the jet. Also in contrast to observations, this model field had minimal disturbance amplitude south of 10° N. The vertical motion field of the Rennick model at 800 mbar, the level of its maximum amplitude, had an upward maximum of 0.90 mbar h^{-1} west of the trough axis at 13° N; in constrast, the Reed *et al.* (1977) land and ocean composites attained maxima of 3 mbar h^{-1}. The energetics in this model were dominated by the horizontal barotropic conversion from mean to eddy

kinetic energy. However, with its southeast-northwest slope south of the jet core, Rennick's disturbance actually lost energy by the barotropic conversion between 11° N and 14° N, where Norquist *et al.* (1977) and Burpee (1972) found strong positive contributions. Eddy energy and temperature perturbations were only slightly enhanced by the model's maximum rainfall rate of 2.5 mm day^{-1}.

STEVENS/LINDZEN/SHAPIRO MODEL

This linear model (Stevens *et al.*, 1977) was applied on a "midlatitude" beta plane with the x, y, and t dependencies represented by single Fourier components. The mean wind field did not possess vertical or horizontal shears. Cumulus momentum exchange was parameterized by the method of Schneider and Lindzen (1976). This "cumulus friction" was found to be essential in reducing the model's perturbation fields to observed amplitudes. Furthermore, the disturbance response was rather insensitive to the shape of the perturbation heating and the shape of the mean cloud mass flux.

MASS MODEL

A ten-level, linear, primitive equation channel (0-30° N) model was used in the Mass (1979) study to investigate the instability properties of a realistic mean jet profile that was constructed from a one-week average of a zonal wind at 5° E. The effects of diabatic heating were parameterized by equating the moisture convergence in a vertical column and the rainfall rate; the heating was distributed in the vertical using observed land and ocean heating profiles. Cumulus momentum mixing was parameterized by the use of a linear version of the method of Schneider and Lindzen (1976).

In all the numerical experiments done for Mass (1979), the most unstable modes of a short-term (August 21-28, 1963) averaged jet at 5° E possessed wavelengths, phase speeds, and periods quite close to the frequency quoted observational means of 2500 km, 8 $msec^{-1}$, and 3.5 days. Latent heating, cumulus momentum mixing, boundary-layer friction, and variations in the vertical heating profile had little influence on these propagation parameters. With or without the convective parameterization the model fields possessed structures quite similar to those found by observation. Some examples include the following:

1. The jet-level wind perturbations were greatest just south of the jet core; at this level the trough and ridge axes sloped southwest-northeast. The maximum wind perturbations occurred near the jet level, and, when convective processes were included, secondary maxima appeared in the upper troposphere.
2. The divergence field possessed a complex vertical structure with low-level convergence at and ahead of the jet level trough with two reversals of this horizontal structure aloft.
3. Upward vertical motion was found west of the jet level trough with maximum values (1.8 $mbar^{-1}$) near 700 mbar.

4. The precipitation rate perturbation reached a positive maximum (3 to 4.1 mm day^{-1}) west of the jet level trough near 9° N with the area of positive enhancement sloping to behind the trough to the north.

5. The barotropic conversion from mean to eddy kinetic energy, which dominated the disturbance energetics, reached a maximum at the jet level near 11° N.

The inclusion of latent heating did not significantly alter the propagation characteristics or low-level structure of the disturbances. However, many of the model parameters (e.g., meridional and zonal wind components, divergence) developed reversals near 300 mbar that made them more similar to the composite fields of Reed *et al.* (1977) and Burpee (1974). With the added reversal, upper-level divergence is found west of the 650-mbar trough axis, as is frequently observed. In addition, the wind and divergence perturbations were enhanced at low levels by 30 to 50 percent, while above 300 mbar increases range from 2.5 (winds) to 7 (divergence) times the dry case values. As a result of the new divergence field there is a 25 percent increase in the upward motion maximum at 700 mbar to 1.5 mbar h^{-1} and a weakening of the model's midtropospheric subsidence.

The precipitation rate cross section (Figure 1) has a distinct maximum of 3 mm day^{-1} near 9° N, west of the 650-mbar trough axis, with the area of enhancement sloping behind the trough to the north. The corresponding maxima in the composites of Burpee (1974) and Reed *et al.* (unpublished, GATE final data set) have nearly identical locations with amplitudes of 2 mm day^{-1} and 5 mm day^{-1}, respectively. These composites also possess the model's slope of the precipitation enhancement to behind the trough axis; the areas of enhancement in the IR brightness composites of Payne and McGarry (1977) exhibit a similar orientation.

The addition of the parameterization of cumulus momentum mixing using the land vertical heating profile resulted in less abrupt midlevel slopes and the establishment of secondary wind maxima of over 1 $msec^{-1}$ at 150 mbar; as an illustration, these features can be seen in Figure 2, vertical cross sections of the zonal wind perturbations with and without the convective parameterizations. Upper-tropospheric secondary maxima were also in the composites of Reed *et al.* (1977) and Burpee (1974). The cumulus mixing parameterization decreased the temperature perturbations by over 20 percent but increased the low-level divergence perturbations by 15 percent and lowered the maxima to a more realistic 900 mbar. The 700-mbar vertical motion maximum increases slightly, and a new center was established

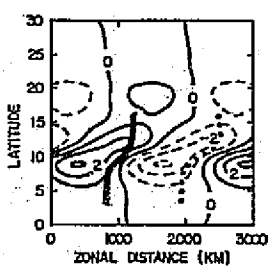

FIGURE 1 Perturbation precipitation rate (mm day^{-1}). The 650-mbar trough (heavy solid) and ridge (dotted) lines are indicated. Thin solid and dashed lines indicate positive and negative perturbations, respectively.

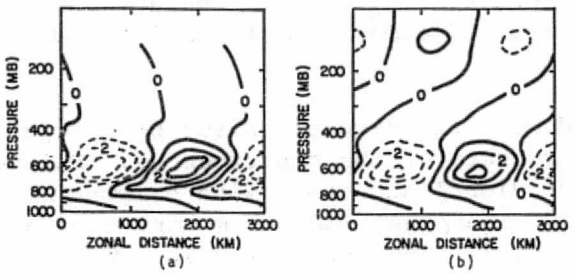

FIGURE 2 Vertical cross sections of the zonal wind perturbations ($msec^{-1}$) at 11.8° N (a) without and (b) with parameterizations of latent heating and cumulus momentum mixing.

near 300 mbar. The corresponding Reed *et al.* (1977) land region composite has similarly placed maxima at 700 and 300 mbar, with lower one twice and the upper one 15 times as intense as the model results.

Cumulus momentum mixing increased the maximum perturbation precipitation rate to 3.5 mm day^{-1}. A vertical cross section of the cumulus mass flux is shown in Figure 3 for 9° N, the latitude of maximum precipitation. The largest upward mass flux occurred west of the 650-mbar trough axis with a primary maximum of 4 mbar h^{-1} near 200 mbar and a secondary maximum of 2 mbar h^{-1} near 700 mbar.

Using the combined region composite disturbance for Phase III of GATE constructed in Reed *et al.* (1977), Shapiro (1978) calculated the cumulus mass flux near 11° N for all clouds detraining above 750 mbar; the greatest perturbation mass flux occurred near 700 mbar, with a magnitude of approximately 2.5 mbar h^{-1}. Although the model produced a secondary maximum of similar amplitude at 700 mbar, the far greatest height of the

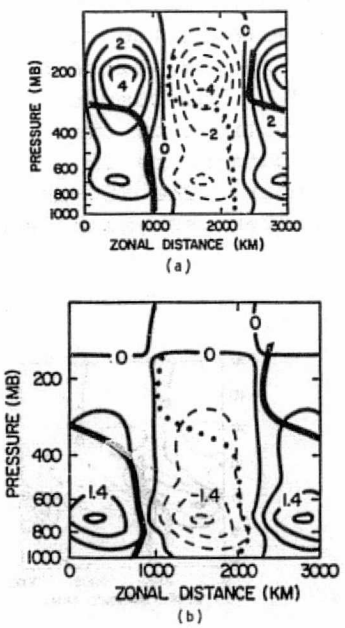

FIGURE 3 Cumulus mass-flux perturbations (mbar h^{-1}) at 9° N using the (a) land and (b) ocean vertical heating profiles. The contour interval is 1 mbar h^{-1}. The solid and dashed lines indicate upward and downward mass fluxes, respectively.

primary maximum is clearly at odds with the Shapiro results. Undoubtedly, this difference can be traced to the land vertical heating profile used in the cloud mass-flux parameterization, which forces most of the precipitation to "rain out" from the upper model levels, thus producing an upper-tropospheric maximum in the moisture flux. A second series of runs with latent heating and cumulus mixing were made with the ocean heating profile with its lower heating maximum. Although the wavelength, period, phase speed, and growth rate of the most unstable mode were nearly unaltered, there is one significant change in the perturbation fields; namely, the amplification of the lower tropospheric values by about 30 percent with a concomitant attenuation of the upper level features. As might be expected from the switch in heating profiles, the cumulus mass-flux perturbations change appreciably (Figure 3); not only did the maximum shift from 200 to 700 mbar but is also weakened appreciably from 4 to just over 2 mbar h^{-1}. This structure is very similar to that of Shapiro (1978), in which the combined region mass-flux results are heavily weighted with oceanic data aloft.

These model results suggest an important role for convection in extending and vertically coupling the disturbance fields away from the jet level, where barotropic instability appears to be the most significant energy source. This is supported by a consideration of previous observational studies. These studies (e.g. Erikson, 1963; Arnold, 1966; Burpee, 1972; Reed *et al.*, 1977) indicate that the domain of disturbance influence expands from the jet level (600-700 mbar) over central Africa, where convection is weak and disorganized, to the entire troposphere over west Africa, where convection becomes more intense and disturbance modulated. It is just in the regions where the disturbances have greatest vertical extent that Carlson (1969a; 1969b) found the environment to be convectively unstable and the wave-modulated convection most intense.

REFERENCES

Arnold, J. E. (1966). Easterly wave activity over Africa and in the Atlantic with a note on the intertropical convergence zone during early July 1961. SMRP Res. Pap. No. 65, Dept. Geophys. Sci., U. of Chicago, 23 pp.

Burpee, R. W. (1972). The origin and structure of easterly waves in the lower troposphere of North Africa. *J. Atmos. Sci. 29*, 77-90.

Burpee, R. W. (1974). Characteristics of North African easterly waves during the summers of 1968 and 1969. *J. Atmos. Sci. 31*, 1556-1570.

Carlson, T. N. (1969a). Synoptic histories of three African disturbances that developed into Atlantic hurricanes. *Mon. Wea. Rev. 97*, 256-276.

Carlson, T. N. (1969b). Some remarks on African disturbances and their progress over the tropical Atlantic. *Mon. Wea. Rev. 97*, 716-726.

Erickson, C. O. (1963). An incipient hurricane near the west African coast. *Mon. Wea. Rev. 91*, 61-68.

Mass, C. F. (1979). A linear primitive equation model of African wave disturbances. Accepted for publication in *J. Atmos. Sci.*

Newell, R. J., J. W. Kidson, D. G. Vincent, and G. J. Boer (1972). *The General Circulation of the Tropical Atmosphere and Interactions with Extratropical Latitudes*. Vol. 1. The MIT Press, 258 pp.

Norquist, D. C., E. E. Recker, and R. J. Reed (1977). The energetics of African wave disturbances as observed during Phase III of GATE. *Mon. Wea. Rev. 105,* 334-342.

Payne, P. W., and M. M. McGarry (1976). The relationship of satellite inferred convective activity to easterly waves over west Africa and the adjacent ocean during Phase III of GATE. *Mon. Wea. Rev. 105,* 414-420.

Reed, R. J., and E. E. Recker (1971). Structure and properties of synoptic-scale wave disturbances in the equatorial western Pacific. *J. Atmos. Sci. 28,* 1117-1133.

Reed, R. J., D. C. Norquist, and E. E. Recker (1977). The structure and properties of African wave disturbances in as observed during Phase III of GATE. *Mon. Wea. Rev. 105,* 317-333.

Rennick, M. A. (1976). The generation of African waves. *J. Atmos. Sci. 33,* 1955-1969.

Schneider, E., and R. Lindzen (1976). A discussion of parameterization of momentum exchange by cumulus convection. *J. Geophys. Res. 81,* 3158-3160.

Shapiro, L. (1978). The vorticity budget of a composite African tropical wave disturbance. *Mon. Wea. Rev. 106,* 806-817.

Stevens, D., R. Lindzen, and L. Shapiro (1977). A new model of tropical waves incorporating momentum mixing by cumulus convection. *Dyn. Atmos. Oceans 1,* 365-425.

DISCUSSION

D. Randall, *Rapporteur*

There were several questions on the formulation of Mass' model, particularly the treatment of cumulus effects. In order to avoid "negative rain" the linear spectral model requires that the heating distribution implied by the convergence of moisture be clipped, and then reduced to its principal Fourier component. This may be interpreted as a wave-induced modulation of a mean heating rate. It was pointed out that the treatment of cumulus friction was different from that of previous studies in that it included shear in the basic state but had no mean cloud mass flux.

Differences between Mass' results and those of Rennick were attributed mainly to differences in the basic states assumed by the two models. Other differences in the formulation of the models include boundary-layer friction, vertical resolution, and slight differences in the treatment of cumulus effects. Studies have shown that the models are most sensitive to the curvature of the mean state zonal wind profile.

Other comments concerned the comparison of the linear model results to observations. The growth rate for the model wave is about 0.5 day^{-1}, which agrees well with estimates made from observations. The ratio of divergence to vorticity generated by the model is about half of that for the observed waves. Disturbances very similar to those generated by the linear model are seen in the Monterey GCM results.

Some questions were raised regarding the appropriateness of using a

linear model to simulate African waves. Particular concern was expressed about the fact that the data indicate that the waves continue to propagate outside of the longitude range for which the zonal flow is approximately uniform. The model cannot reflect the interaction of the waves with a longitude-dependent basic state.

THE IMPACT OF GATE ON LARGE-SCALE NUMERICAL MODELING: THE PERFORMANCE OF THE METEOROLOGICAL OFFICE FORECAST MODEL IN THE TROPICS

A. Gilchrist

The model that has been used for numerical prediction experiments in the tropics is a regional version of an 11-layer general circulation model. Tropical results of experiments with both the global and limited-area versions will be used to illustrate the sensitivity of tropical simulations to aspects of the formulation. Three experiments will be considered in particular.

SENSITIVITY TO MOISTURE

Walker and Rowntree (1977) have demonstrated that the structure of tropical traveling disturbances over regions like West Africa is affected by the ground wetness and the availability of soil moisture. An experiment with an 11-layer global circulation model indicates additionally a sensitivity to the initial moisture content of the atmosphere. A persistent feature of Meteorological Office general circulation models has been the northward spread of rainfall from the moist coastal region of Africa into what ought to be desert areas. Two integrations that differed only with respect to the initial atmospheric humidities show marked differences during a 20-day integration. In the "dry" integration, the rainfall did not spread northward. Also the easterly flow of regions at about 700 mbar and features that appear to have some similarity to observed easterly waves were simulated more realistically.

SENSITIVITY TO VARIATIONS IN CLOUDINESS

Most of the integrations over West Africa carried out by the Meteorological Office Tropical Group have assumed fixed cloudiness. A cloud parametrization that allows cloud amounts to be determined internally within the forecast model has been developed by Slingo (1978a; 1978b). GATE observations, satellite pictures of the GATE area, and simultaneous forecasts with the limited-area model were used to investigate the relations between cloud amounts at high, medium, and low levels with (1) relative humidity; (2) the mass of air taking part in convective motions as indicated by the convective parametrization; (3) the change of potential temperature with pressure, i.e., the presence of inversions. The cloud

scheme allows four types of cloud; viz., convective (amount determined from the convective parametrization) and stratiform high, medium, and low. The amount of the last depends on the presence of a low-level inversion as well as on relative humidity. Stratiform cloud of one type may occupy one of a number of layers in the model at any one time.

Two integrations, one with fixed cloud, the other with the cloud parametrization scheme and starting from the GATE analysis for 1200 GMT, September 4, 1974, have been compared. The inclusion of time-dependent clouds had a considerable effect on the rainfall and synoptic developments during the forecast run. There was more development over the sea, whereas over land the rain decreased and the disturbances were less intense. Cloud increased over land, leading to reduced solar fluxes, and hence reduced evaporation and sensible heat exchange. Over the sea, the surface temperatures are fixed, and the difference appears therefore to be due to differences in radiative cooling rates.

SENSITIVITY TO CONVECTIVE PARAMETRIZATIONS

Gilchrist (1979) has discussed the simulation of the Asian southwest monsoon by two Meteorological Office general circulation models: a 5-layer model with 330-km resolution and a fixed ground wetness and the 11-layer model with 220-km resolution and an interactive ground hydrology. He showed that differences in the simulations arose from the sensitivity of the monsoon circulation to the diabatic heating in the region over and around the Indian subcontinent. The monsoon simulations of the 11-layer model incorporating a penetrative convective parametrization (Lyne and Rowntree, 1976) can be compared with these earlier simulations. There are significant changes particularly with regard to the strength of the surface trough and the rainfall and low-level flow over the Bay of Bengal. The structure and development of Bay of Bengal depressions are being further investigated using data and analyses for the second Special Observing Period of the FGGE.

REFERENCES

Gilchrist, A. (1979). A comparison of Asian southwest monsoon simulation by two general circulation models presented at joint IUTAM/IUGG International Symposium on Monsoon Dynamics, Delhi, Dec. 1977. Cambridge U. Press, Cambridge, England, to be published.

Lyne, W. H., and P. R. Rowntree (1976). Development of a convective parameterization using GATE data. Met.0.20. Tech. Note. II/70. (Unpublished, available on request.)

Slingo, J. (1978a). Interactive cloud and radiation in the 11-layer model. Part II: Cloud scheme. Met.0.20. Tech. Note. II/122. (Unpublished, available on request.)

Slingo, J. (1978b). The effect of interactive clouds and radiation on convective activity in a numerical model of the tropics. Met.0.20. Tech. Note. II/130.

Walker, J., and P. R. Rowntree (1977). The effects of soil moisture on circulation and rainfall in a tropical model. *Quart. J. R. Meteorol. Soc. 103*, 29-46.

DISCUSSION
M. Rennick, *Rapporteur*

Several comments were made concerning the sensitivity of the model to the initial atmospheric conditions. The GFDL model requires four months of simulation for the hydrologic cycle to adjust to the initial conditions. The easterly waves generated by the GLAS model are also sensitive to hydrology. The waves are better defined under dry conditions. This may be a result of the response of the jet structure to the moisture field rather than a direct dependence of the waves on the moisture budget. It was suggested that the presence of soil moisture in the model acts to maintain a sufficiently high humidity field to allow for the formation of clouds and subsequent enhancement of precipitation.

The treatment of radiation in the model is somewhat similar to that proposed by Cox. High cirrus is treated as a blackbody to IR, and the transmissivity of high cloud to solar radiation is about 0.75. No attempt was made to consider diurnal variations. When the clouds were allowed to interact with the model, the waves were enhanced over oceanic regions and damped over land, bringing them into better agreement with observations.

The simulation of the westward propagation of the wave at 700 mbar in the absence of cumulus friction questions the importance of this effect. Apparently, for short-term integrations cumulus friction is not required, but for longer integrations the model waves take on the characteristics of the dry shear instabilities. It was also suggested that some sort of cumulus friction may be implicitly included in the convective adjustment scheme.

Techniques for testing different parameterization schemes were discussed. Both diagnostic and prognostic tests are possible. Diagnostic studies attempt to isolate the problems of parameterization from other model features. However, these do not test the feedback to the large-scale variables. Also, because of the different input parameters required by different types of parameterization schemes, these tests may be somewhat biased. Prognostic testing is difficult because it requires that each scheme be used in otherwise identical models for a large number of cases so that the results can be compared. The type of large-scale system in which a parameterization scheme should be tested was also questioned. In a region such as the GATE area the easterly waves are of obvious importance so that convective effects do not dominate the forcing. This can be a help or a hindrance, depending on the principal objective of the parameterization. In regions with less-distinct large-scale forcing the vertical structure of the fluxes implied by a parameterization scheme may require more initial testing.

THE FOUR-DIMENSIONAL ANALYSIS AND FORECAST EXPERIMENT WITH GATE DATA

K. Miyakoda, J. Sirutis, and J. Sheldon
Geophysical Fluid Dynamics Laboratory/NOAA
Princeton University

FOUR-DIMENSIONAL ANALYSIS OF THE 1978 VERSION

The 101-day sequential map analysis of the GATE data in the GFDL was first conducted in 1974 on a near-real-time basis, using the four-dimensional analysis method (Miyakoda *et al.*, 1976). In 1978-1979, we repeated the GATE analysis with a revised analysis system, using the full GATE data set, which includes the supplemental data.

The four-dimensional analysis used for the 1978 version consists of three steps, i.e., preprocessing of input data, dynamical analysis, and static analysis. The dynamical analysis is restarted at 12-h intervals from these static analysis.

The insertion data are determined at the model's grid points, using the optimum interpolation analysis method (OPA) (Gandin, 1963). The data-collection range around a grid point is 250 km in the extratropics and 150 km in the tropics, and the initial guess for OPA is the climatological normal for the respective variable. A spectral model is used for the dynamical data assimilation; the assimilation system was developed primarily by Simmonds (1978). The basic GC model is a global spectral transform model with a spherical harmonic representation in the horizontal and finite difference formulation in the vertical direction (Gordon and Stern, 1974). The spectral resolution of the model is R30L9, which denotes the rhomboidal 30 harmonic truncation and the 9 vertical levels and has the longitudinal grid distance $\Delta\lambda = 3.75$ and the meridional grid distance $\Delta\psi = 2.4°$. After the dynamical assimilation, the global OPA is performed, again using the same data. The static analysis is the final adjustment, eliminating the model's bias and making an optimal fit of the analysis to original observations. In the global OPA, the data collection range is 500 km, and the initial guess fields are the results of the dynamical assimilation.

The differences between the 1978 and 1974 versions are (1) the global OPA was used every 12 h in the 1978 version; (2) the GC model was the R30L9 spectral model instead of the finite-difference model of resolution N48L9; (3) the data were inserted in all layers including the planetary boundary layer, whereas in the 1974 version, the data in the lowest two levels were not used at all; and (4) the moisture data were used this time.

Figure 1 shows an example of analysis for 850-mbar streamlines on September 6, 1974, 00 GMT, based on the 1978 version, and the 1974 version

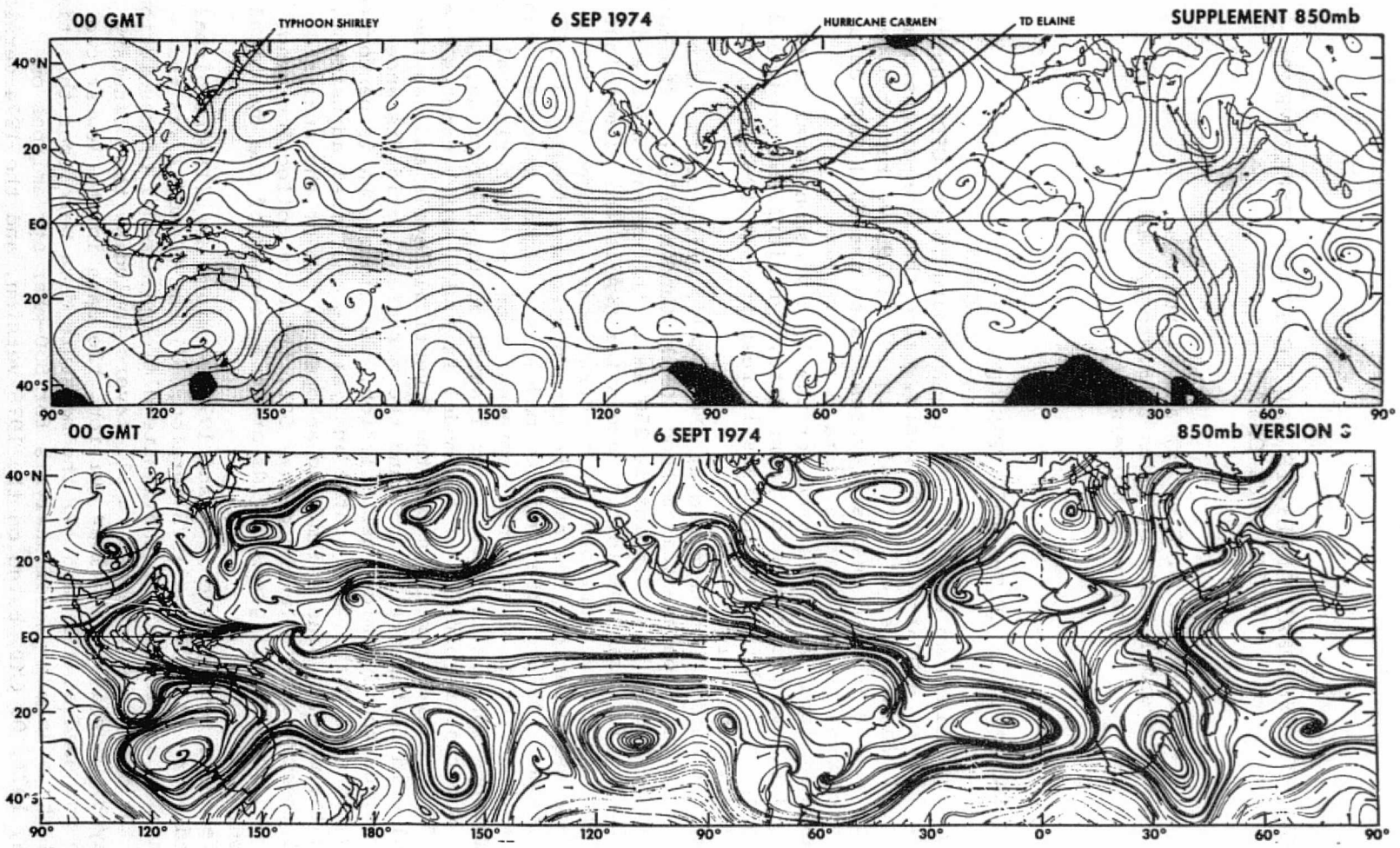

FIGURE 1 850-mbar streamlines on September 6, 1974, 00 GMT. *Top*: the 1978-1979 analysis; *bottom*: the 1974 analysis.

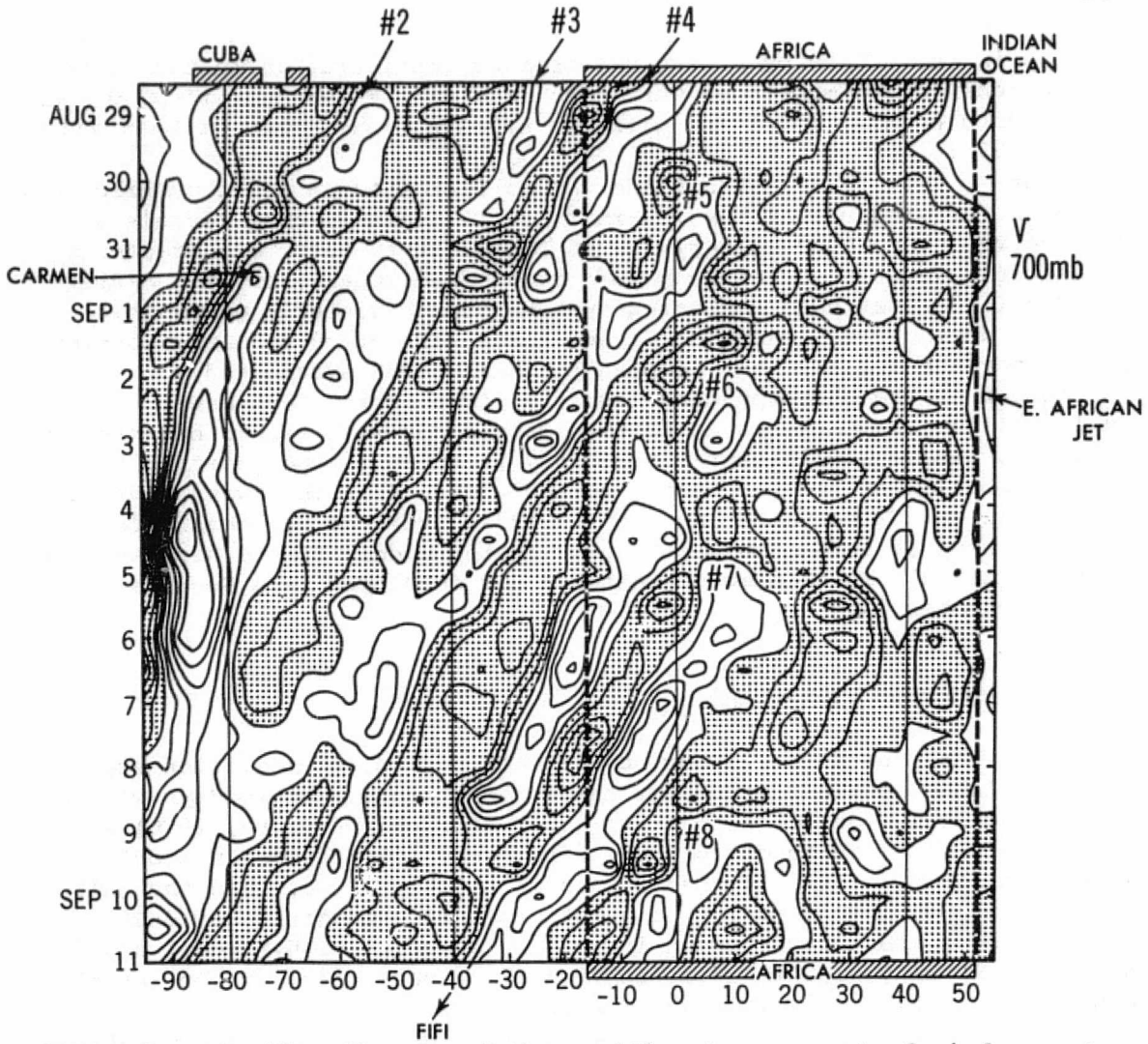

FIGURE 2 Hovmoller diagram of the meridional component of wind, v, at 700-mbar level, derived from the four-dimensional analysis. The shaded areas correspond to the northerlies, and the nonshaded areas to the southerlies. The contour interval is 2 m sec^{-1}

analysis. It is interesting to note that both the maps include Hurricane Carmen, Typhoon Shirley, and Tropical Depression Elaine. Surprisingly, despite the different analysis techniques and different volume of data employed, the two maps display a great deal of resemblance in the overall features. Yet there are also noticeable differences. In the 1979 version maps, easterly waves over the Atlantic Ocean are better represented, and the troughs and ridges in the extratropics are deeper than in the 1974 version maps.

We compared the maps of the GFDL 1978-79 version with those of Sadler and Oda (1978) and recognized a reasonably good agreement for 250 mbar and 1000 mbar. However, in Sadler's hand analyses, the easterly waves at 1000-mbar maps were drawn so as to be confined to a small region,

whereas in the GFDL maps a wave has broader configuration in the west-east extension. Comparisons were also made with Krishnamurti's 250-mbar maps (Pasch *et al.*, 1978) and with the A/B-scale area maps of Dean and Smith (1978).

Figure 2 shows a time-longitude (Hovmöller) diagram for the meridional component of wind, v, at the 700-mbar level. This diagram reveals a systematic movement of easterly waves from east to west, a characteristic of easterly waves that has long been recognized (Chang, 1970). Sadler and Oda (1978) set up a numbering system for the easterly waves that appeared during the pre-Phase III and Phase III period of GATE, ranging from 1 through 10. We have adopted the Sadler-Oda system and plotted the number on the corresponding easterly waves in the GFDL maps. Amazingly, all the easterly waves in both maps agree with each other precisely without a single significant discrepancy in terms of the position and the displacement. Let us look at the easterly wave #2. This wave developed into Hurricane Carmen about August 30, 1974, over the Caribbean area. Easterly wave #7 formed on September 4 in the middle of the African continent (Figure 2); it then moved westward and developed into Hurricane Fifi about September 17.

TROPICAL FORECAST EXPERIMENT

Using the analyzed data set during the GATE period, a prediction experiment is planned and performed for the forecast ranges of 10 days with a spectral global model of resolution R30L9 (Gordon and Stern, 1976) and of 5 days with a finite-difference, fine-mesh, limited-domain model (Mesinger, 1979). This limited domain is slighly larger than the GATE A-scale area as specified by the Joint Organizing Committee of GARP. The fine-mesh model is embedded inside the spectral global model and is nested by specifying all variables from the global model at the interface boundary condition (Miyakoda and Rosati, 1977).

The finite-difference model is called the "HIBU" model, representing the Federal Hydrometeorological Institute and Belgrade University, Yugoslavia. This model has the finite-difference formulation of an entrophy-conserving and energy-conserving scheme and has a resolution of $1° \times 1°$ and nine vertical levels.

In general, there are at least two important aspects that need special care for tropical forecasts, i.e., the initial condition and the treatment of subgrid-scale physics such as ensemble cumulus convection and planetary boundary-layer processes.

Concerning the subgrid-scale physics, we selected three major versions, denoted by A, E, and F physics (Miyakoda and Sirutis, 1977). The A version is a package of "standard" physics, which is similar to that of the 1965 GFDL hemispheric model and almost the same as that in the GC model used in the 1974 GATE implementation. Let us describe the A version briefly. In the interfacial layer, the Prandtl-type aerodynamic drag is used for the wind stress, and also for the sensible and latent heat fluxes. Above the lowest level and up to 3 km, the vertical tranports of momentum and moisture are calculated by the eddy viscosity transfer, using the mixing length method. However, the heat transport is modeled by the

"dry convective adjustment." The cumulus convection effect is simulated by the "moist convective adjustment" (Manabe *et al.*, 1965).

The E-version models were constructed based on the knowledge of turbulent observation and theories achieved in the past two decades. Among all E models, the E2 version model uses the Monin-Obukhov-type process for the interfacial layer, which includes the effect of Richardson number (Delsol *et al.*, 1971). The remaining physics are exactly the same as the A-version physics. On the other hand, the E4 version introduces the approach of turbulent closure hypothesis, in addition to the E2 version, and consequently it eliminates the process of the "dry convective adjustment." In particular, we used the Mellor-Yamada 2½-level hierarchy of turbulent closure theory (Mellor and Yamada, 1974; Yamada and Mellor, 1978).

In the preceding models, the ensemble cumulus convection is parameterized by the "moist convective adjustment." The F-version models, on the other hand, employ the Arakawa-Schubert cumulus convection parameterization (A-S). (Arakawa and Schubert, 1974). The F2 version includes the UCLA-type physics in the important parts of the model, i.e., the A-S cumulus convection as well as Randall's mixed-layer theory (Randall and Arakawa, 1974).

THE GC ONE-MONTH SIMULATION EXPERIMENTS

Apart from the GATE case, results of the simulation studies for one-month range are presented for March 1, 1965, 00 GMT case. In these experiments, the various subgrid-scale parameterizations were included in the GC model and the results were compared with each other. In this regard, the study is very much related to the goal of GATE. The finite-difference global models of resolution N24L18 or N48L18 on the modified Kurihara grid were used, in which the A2, E4, F2, and F3 physics are incorporated.

Figure 3 is one-month average of wind vectors at the 200-mbar level, displayed as streamlines and isotachs. The top panel in the figure is the ensemble mean field for March (close to climatology), obtained by Atkins (1974).

Although it is not shown here, the 1000-mbar flow fields are similar to each other among the A2, E4, F2, and F4 version models, implying that the impact of mixed-layer processes on the GC feature near the surface is not great. In particular, the F2 model includes the most elaborate and refined treatment of the planetary boundary layer, which nevertheless results in flow fields similar to the other formulations.

The difference in flow patterns become more pronounced in the 200-mbar flow fields shown in Figure 3. Overall, the 200-mbar is dominated by the outflows over continents in the summer hemisphere, because the outflows are a consequence of strong cumulus activities over land. While the overall features in various models appear to be similar to each other, differences may be recognized. The flows in the F2 and F3 models are similar to each other, but different from those in the A2 and E4 models, particularly off western edges of continents, such as in the eastern South Pacific. A further investigation has revealed that this is due to the erroneous precipitation in the F2 and F3 models. In this sense, flow

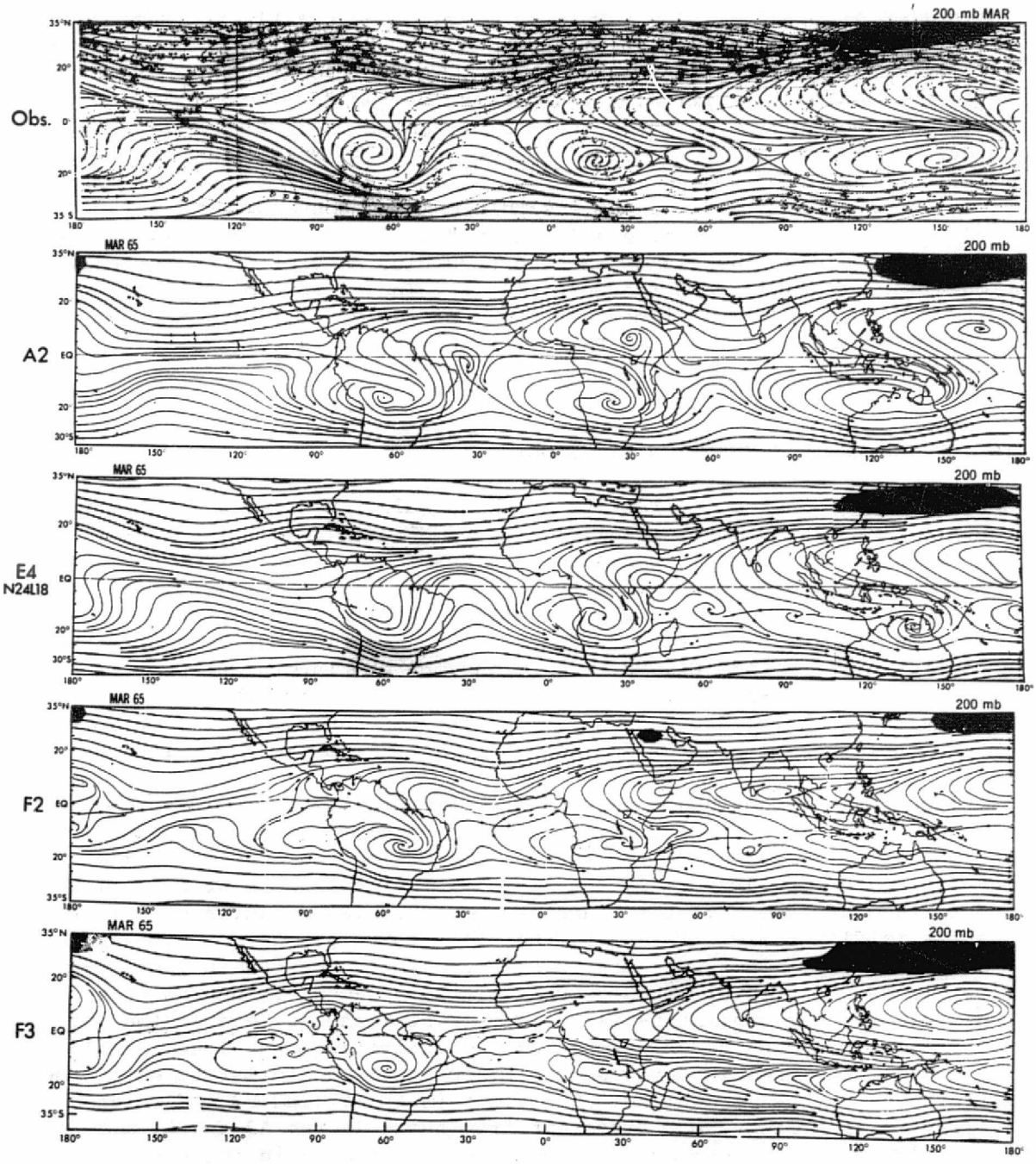

FIGURE 3 Monthly mean flow fields at 200-mbar level.

at upper levels such as 200 mbar is a good indicator of the performance of cumulus convection parameterization.

The deficiencies in the F2 and F3 models may not be of an intrinsic nature. The survey is under way.

REFERENCES

Arakawa, A., and W. H. Schubert (1974). Interaction of cumulus cloud ensemble with the large-scale environment, Part I. *J. Atmos. Sci. 31*, 674-701.

Atkinson, G. D., and J. C. Sadler (1970). *Mean cloudiness and gradient-level-wind charts over the tropics.* AWS. Technical Report 215, Vols. I and II.

Chang, C. P. (1970). Westward propagating cloud patterns in the tropical Pacific as seen from time-composite satellite photographs. *J. Atmos. Sci. 27*, 133-138.

Dean, G., and C. Smith (1977). A study of synoptic and mesoscale interaction over the GATE ship network: September 4-6, 1974. NCAR Technical Note, NCAR/TN-122+STR, Boulder, Colo., p. 95.

Delsol, F., K. Miyakoda, and R. H. Clarke (1971). Parameterized processes in the surface boundary layer of an atmospheric circulation model. *Quart. J. R. Meteorol. Soc. 97*, 181-208.

Gandin, L. S. (1963). *Objective Analysis of Meteorological Fields.* Gidrometeoizdat, Lenningrad.

Manabe, S., J. Smagorinsky, and R. F. Strickler (1965). Simulated climatology of a general circulation model with a hydrological cycle. *Mon. Wea. Rev. 93*, 769-798.

Mesinger, F. (1979). Finite difference schemes of a staggered grid entrophy and energy conserving model (to be submitted to Mon. Wea. Rev.).

Miyakoda, K., L. Umscheid, D. H. Lee, J. Sirutis, R. Lusen, and F. Pratte (1976). The near-real-time, global, four-dimensional analysis experiment during the GATE period, Part I. *J. Atmos. Sci. 33*, 561-591.

Miyakoda, K., and A. Rosati (1977). One-way nested grid models: the interface conditions and the numerical accuracy. *Mon. Wea. Rev. 105*, 1092-1107.

Miyakoda, K., and J. Sirutis (1977). Comparative integrations of global models with various parameterized processes of subgrid-scale vertical transports: description of parameterizations. *Beitr. Phys. Atmos. 50*, 445-447.

Pasch, R., T. N. Krishnamurti, and C. Depradine (1978). An atlas of the motion field over the GATE area, Part II (250 mbs). Report No. 78-3, Dept. Meteorol., Fla. State U., Tallahassee, Fla.

Randall, D. A., and A. Arakawa (1974). A parameterization of the planetary boundary layer for numerical models for the atmosphere. In the UCLA Atmospheric General Circulation Model, notes distributed at the workshop, U. of California, Los Angeles.

Sadler, J. C., and L. K. Oda (1978). The synoptic (A) scale circulations during the third phase of GATE, August 20-September 23, 1974, Dept. of Meteorol. U. of Hawaii, Honolulu, Hawaii.

Simmonds, I. (1978). The application of a multi-level spectral model to data assimilation. *J. Atmos. Sci. 35*, 1321-1339.

Yamada, T. (1977). A numerical experiment on pullutant dispersion in a horizontally homogeneous atmospheric boundary layer. *Atmos. Environ. 11*, 1015-1024.

DISCUSSION

M. Rennick, *Rapporteur*

Miyakoda's claim that some African waves could be traced back toward Egypt was controversial. Reed stated that in a current study he could find no wave-related signal east of 15° E. Mass indicated that he has occasionally seen features such as Miyakoda observes but questioned whether they propagated to W. Africa. The appearance of waves in the Pacific in Miyakoda's analysis were noted. Apparently satellite-derived winds made an important contribution in defining them.

There was much excitement over a Hovmoller diagram at 200 mbar. Apparently a large-scale wave of approximately a 15-day period can coherently propagate over large distances. Shukla indicated that it might be a topographically forced Rossby wave. The proposition that this wave modulates hurricane formation was criticized by Gray, who indicated that such a 15-day periodicity is not observed. Several participants expressed the intent to use the GFDL analyses.

The GFDL analysis scheme appears to be little affected by the inclusion of cumulus momentum mixing. Initial shock of new data appeared minimal with the possible exception of data-rich regions.

Gilchrist registered surprise that two different convective parameterizations resulted in very similar fields in one-month simulation experiments.

THE IMPACT OF GATE ON LARGE-SCALE NUMERICAL MODELING: RESULTS OF EXPERIMENTAL FORECASTS FOR THE GATE AREA

A. Gilchrist

During the intensive observing phases of GATE, a continuous forecast-analysis cycle was run using the Meteorological Office 11-layer limited-area model (Lyne and Rowntree, 1976; Shaw and Rowntree, 1976.) Features of the analysis and forecasting schemes will be reviewed briefly. On the whole, the forecasts treated easterly waves convincingly, and the synoptic developments and rainfall distributions were generally realistic.

The structure of easterly waves, which appear to involve an initial barotropic instability followed by baroclinic development as warm air is drawn in from the north, will be described and illustrated. "Box" diagrams showing the flow of energy at different stages of the wave development will be shown.

New spatial structure functions were produced from the GATE observations and have been incorporated into the analysis scheme. Particularly for the geopotential fields at low levels, these give a wider area of influence and therefore contribute to smoother fields produced in revised analyses.

The third phase of GATE is being re-analyzed using the new structure functions and the more complete observational data set now available.

REFERENCES

Lyne, W. H., and P. R. Rowntree (1976). Development of a convective parameterization using GATE data. Met.0.20. Tech. Note II/70. (Unpublished, available on request.)

Shaw, D. B., and P. R. Rowntree (1976). Tropical model and experiments using GATE data. Met.0.20. Tech. Note II/80. (Unpublished, available on request.)

DISCUSSION

C. Mass, *Rapporteur*

Some concern was expressed over a warm anomaly produced by the model close to the northern boundary. Several differences between the modeled and observed easterly disturbances were discussed. For instance, the wave-related temperature and vertical velocities over land appeared to be

far in excess of the observed. However, Gilchrist indicated that this condition mitigates over the ocean. Several speakers pointed out differences between the model's energetics and that of Norquist *et al.* (1977) and others. For example, the barotropic conversion was in the opposite direction over land and much weaker than "observed" over the ocean. Finally, it was felt that an examination of how the conversions vary with height could yield important physical insight into the maintenance of the modeled disturbances.

APPENDIX A: Attendees

Bruce Albrecht, Pennsylvania State University
Richard A. Anthes, Pennsylvania State University
Akio Arakawa, University of California, Los Angeles
Alan K. Betts, Colorado State University, Retired
Eugene W. Bierly, National Science Foundation
Robert W. Burpee, National Oceanic and Atmospheric Administration
Toby N. Carlson, Pennsylvania State University
Jule G. Charney, Massachusetts Institute of Technology
Han-Ru Cho, University of Toronto
Stephen K. Cox, Colorado State University
Stephen K. Esbensen, Oregon State University
Jay S. Fein, National Science Foundation
William M. Frank, University of Virginia
Michael Garstang, University of Virginia
Andrew Gilchrist, Meteorological Office, U.K.
William M. Gray, Colorado State University
Richard S. Greenfield, National Science Foundation
David Halpern, Pacific Marine Environmental Laboratory
Yoshikazu Hayashi, National Oceanic and Atmospheric Administration
Joshua Z. Holland, National Oceanic and Atmospheric Administration
Robert A. Houze, Jr., University of Washington
John B. Hovermale, National Oceanic and Atmospheric Administration
Richard H. Johnson, University of Wisconsin-Milwaukee
T. N. Krishnamurti, Florida State Univeristy
Joachim Kuettner, National Center for Atmospheric Research
Noel E. LaSeur, Florida State University
Margaret LeMone, National Center for Atmospheric Research
Richard S. Lindzen, Harvard Univeristy
Raul E. López, National Oceanic and Atmospheric Administration
Steven J. Lord, University of California, Los Angeles

APPENDIX A: Attendees

Bruce Albrecht, Pennsylvania State University
Richard A. Anthes, Pennsylvania State University
Akio Arakawa, University of California, Los Angeles
Alan K. Betts, Colorado State University, Retired
Eugene W. Bierly, National Science Foundation
Robert W. Burpee, National Oceanic and Atmospheric Administration
Toby N. Carlson, Pennsylvania State University
Jule G. Charney, Massachusetts Institute of Technology
Han-Ru Cho, University of Toronto
Stephen K. Cox, Colorado State University
Stephen K. Esbensen, Oregon State University
Jay S. Fein, National Science Foundation
William M. Frank, University of Virginia
Michael Garstang, University of Virginia
Andrew Gilchrist, Meteorological Office, U.K.
William M. Gray, Colorado State University
Richard S. Greenfield, National Science Foundation
David Halpern, Pacific Marine Environmental Laboratory
Yoshikazu Hayashi, National Oceanic and Atmospheric Administration
Joshua Z. Holland, National Oceanic and Atmospheric Administration
Robert A. Houze, Jr., University of Washington
John B. Hovermale, National Oceanic and Atmospheric Administration
Richard H. Johnson, University of Wisconsin-Milwaukee
T. N. Krishnamurti, Florida State Univeristy
Joachim Kuettner, National Center for Atmospheric Research
Noel E. LaSeur, Florida State University
Margaret LeMone, National Center for Atmospheric Research
Richard S. Lindzen, Harvard Univeristy
Raul E. López, National Oceanic and Atmospheric Administration
Steven J. Lord, University of California, Los Angeles

Man-Kin Mak, University of Illinois
Clifford F. Mass, University of Maryland
Wayne McGovern, National Oceanic and Atmospheric Administration
Kikuro Miyakoda, National Oceanic and Atmospheric Administration
Tsuyoshi Nitta, University of Tokyo
Yoshimitsu Ogura, University of Illinois
Katsuyuki Ooyama, National Center for Atmospheric Research
Joseph P. Pandolfo, Center for Environment & Man, Inc.
George Philander, Princeton University
David Randall, Massachusetts Institute of Technology
Richard J. Reed, University of Washington
Mary A. Rennick, Florida State University
David R. Rodenhuis, University of Maryland
Thomas Rosmond, Naval Environmental Prediction Research Facility
Wayne Schubert, Colorado State University
L. J. Shapiro, National Oceanic and Atmospheric Administration
Jagadish Shukla, National Aeronautics and Space Administration
Joanne Simpson, University of Virginia
Su-Tzai Soong, University of Illinois-Urbana
Duane E. Stevens, Colorado State University
Dayton G. Vincent, Purdue University
John M. Wallace, University of Washington
Charles Warner, University of Virginia
Michio Yanai, University of California, Los Angeles
Edward J. Zipser, National Center for Atmospheric Research